

# DYNA

Journal of the Facultad de Minas, Universidad Nacional de Colombia - Medellín Campus  
DYNA 92 (238), July - September, 2025 - ISSN 0012-7353

ai

Facultad de Minas  
Sede Medellín



UNIVERSIDAD  
**NACIONAL**  
DE COLOMBIA

DYNA is an international journal published by the Facultad de Minas, Universidad Nacional de Colombia, Medellín Campus since 1933. DYNA publishes peer-reviewed scientific articles covering all aspects of engineering. Our objective is the dissemination of original, useful and relevant research presenting new knowledge about theoretical or practical aspects of methodologies and methods used in engineering or leading to improvements in professional practices. All conclusions presented in the articles must be based on the current state-of-the-art and supported by a rigorous analysis and a balanced appraisal. The journal publishes scientific and technological research articles, review articles and case studies.

DYNA publishes articles in the following areas:

Organizational Engineering  
Civil Engineering  
Materials and Mines Engineering

Geosciences and the Environment  
Systems and Informatics  
Chemistry and Petroleum

Mechatronics  
Bio-engineering  
Other areas related to engineering

## Publication Information

DYNA (ISSN 0012-7353, Printed; 2346-2183, online).

Is published by the Facultad de Minas, Universidad Nacional de Colombia, with a quarterly periodicity (January - March, April - June, July - September and October - December).

Circulation License Resolution 000584 de 1976 from the Ministry of the Government.

### Contact information:

Web page: <https://revistas.unal.edu.co/index.php/dyna>

E-mail: [dyna@unal.edu.co](mailto:dyna@unal.edu.co)

Mail address:

Revista DYNA

Facultad de Minas

Universidad Nacional de Colombia - Medellín Campus

Carrera 80 No. 65-223 Bloque M9 - Of.:107

Telephone: (574) (604) 4255343

Medellín - Colombia

### © Copyright 2025. Universidad Nacional de Colombia

The complete or partial reproduction of texts with educational ends is permitted, granted that the source is duly cited. Unless indicated otherwise.

### Notice

All statements, methods, instructions and ideas are only responsibility of the authors and not necessarily represent the view of the Universidad Nacional de Colombia. The publisher does not accept responsibility for any injury and/or damage for the use of the content of this journal.

The concepts and opinions expressed in the articles are the exclusive responsibility of the authors.

### Institutional Exchange Request

DYNA may be requested as an institutional exchange through the e-mail: [canjebib\\_med@unal.edu.co](mailto:canjebib_med@unal.edu.co) or to the postal address:

Biblioteca Central "Efe Gómez"  
Universidad Nacional de Colombia, Sede Medellín  
Calle 59A No 63-20  
Teléfono: (574) (604) 430 97 86  
Medellín - Colombia

## Indexing and Databases

DYNA is admitted in:

The National System of Indexation and Homologation of Specialized Journals CT+I-PUBLINDEX, Category C

Science Citation Index Expanded

SCImago Journal & Country Rank - SJR

SCOPUS

SciELO Scientific Electronic Library Online

Chemical Abstract - CAS

Scientific Electronic Library on Line - SciELO

GEOREF

PERIÓDICA Data Base

Latindex

Actualidad Iberoamericana

Redalyc - Scientific Information System

Directory of Open Acces Journals - DOAJ

PASCAL

CAPES

UN Digital Library - SINAB

EBSCO Host Research Databases

### Publisher's Office

Luz Alexandra Montoya Restrepo, Director  
Mónica del Pilar Rada T., Editorial Coordinator  
Catalina Cardona A., Editorial Assistant  
Manuela González C., Editorial Assistant

Todograficas Ltda., Diagramming

### Reduced Postal Fee

Tarifa Postal Reducida # 2014-287 4-72.

*La Red Postal de Colombia*, expires Dec. 31<sup>st</sup>, 2025





UNIVERSIDAD  
**NACIONAL**  
DE COLOMBIA

DYNA





## COUNCIL OF THE FACULTAD DE MINAS

### Dean

Eva Cristina Manotas, PhD

### Vice-Dean

Néstor Ricardo Rojas Reyes, PhD

### Vice-Dean of Research and Extension

Jorge Eliécer Córdoba Maquilón, PhD

### Director of University Services

Camilo Alberto Suárez Méndez, PhD

### Academic Secretary

Maria Constanza Torres Madroñero, PhD

### Representative of the Curricular Area Directors

John Robert Ballesteros Parra, PhD

### Representative of the Curricular Area Directors

Claudia Helena Muñoz Hoyos, PhD

### Representative of the Basic Academic Units

Álvaro Jesús Castro Caicedo, PhD

### Representative of the Basic Academic Units

Albeiro Rendón Rivera, PhD

### Professor Representative

Luis Hernán Sánchez Arredondo, PhD

### Student representative at the Faculty Council

BleidysThamara Valderrama Casas

### Student representative at the Faculty Council

Sara Daniela Coronado Maju

## JOURNAL EDITORIAL BOARD

### Editor-in-Chief

Luz Alexandra Montoya Restrepo,  
PhD. Universidad Nacional de Colombia, Colombia

### Editors

Raúl Ocampo Pérez,  
PhD. Universidad Autónoma de San Luis Potosí, Mexico

Vladimir Alvarado,  
PhD. Universidad de Wyoming,  
USA

Francisco Carrasco Marin,  
PhD. Universidad de Granada, Spain

Sergio Velastin,  
PhD, University of London, England

Hans Christian Öttinger,  
PhD. Swiss Federal Institute of Technology (ETH),  
Switzerland

Jordi Payá Bernabeu,  
PhD. Instituto de Ciencia y Tecnología del Hormigón  
(ICITECH), Universitat Politècnica de València, Spain

Javier Belzunce Varela,  
PhD. Universidad de Oviedo, Spain

Henrique Lorenzo Cimadevila,  
PhD. Universidad de Vigo, Spain

Carlos Palacio,  
PhD. Universidad de Antioquia, Colombia

Oscar Jaime Restrepo Baena,  
PhD. Universidad Nacional de Colombia,  
Colombia

## FACULTY EDITORIAL BOARD

### Dean

Eva Cristina Manotas, PhD

### Vice-Dean of Research and Extension

Jorge Eliécer Córdoba Maquilón, PhD

### Members

Luz Alexandra Montoya Restrepo, PhD  
Néstor Ricardo Rojas Reyes, PhD  
Enrique Posada Restrepo, MSc  
Mónica del Pilar Rada Tobón, MSc

### Support members

Francisco Montaña Ibáñez, MSc  
Director Editorial UN  
Diana Carolina Martínez Santos, MSc.  
Directora Nacional de Bibliotecas UN



## CONTENTS

<b>Research on airport reservation bus scheduling.</b>	
Jin Li, Long Chen, Xiaowen Li & Huasheng Liu	9
<b>Enhancing urban E-commerce efficiency: a fleet composition benchmark.</b>	
Mauricio Peña-Acosta, Raúl Fabián Roldán-Nariño & Nicolás Rincón-García	19
<b>Integration of AI, RPA and Big Data in strategic accounting management and consulting: perspectives and challenges.</b>	
William Alberto Guerrero, Stefanny Camacho-Galindo, Laura Estefanía Guerrero-Martin, John Carlos Arévalo & Camilo Andrés Guerrero-Martin	26
<b>Implementation of Google App script for automatic generation of pre-registration form.</b>	
Jorge Lira-Camargo, José Antonio Ogozi-Auqui & Francisca Sonia Vera-Tito	35
<b>A framework for environmental performance evaluation in resource-constrained air navigation services: a Cuban case study.</b>	
Yohana Depestre-Wray, Rosa Mayelin Guerra-Bretaña, Oridayma Tarano-Artigas, Fridel Julio Ramos-Azcuy	39
<b>Classification of pothole distress severity in asphalt pavements using YOLOv8.</b>	
Átila Marconcine de Souza, Vinicius Fier Cestari & Heliana Barbosa Fontenele	47
<b>Agent-Based models for integrated water resource management: quantifying land use changes by integrating economic and social incentives. Case study: Vista Hermosa (Meta).</b>	
Nicol Chicacausa, Martín Otalora-Low, Natalia Carrillo-Acosta, María Cristina Arenas-Bautista & Antonio Preziosi-Ribero	57
<b>The adoption of cutting software in small furniture manufacturers: a survey in Brazil.</b>	
Nádyá Zanin Muzulon, Pedro Rochavetz de Lara Andrade, Rafael Henrique Palma Lima, Juliana Verga Shirabayashi & Gislaine Camila Lapasini Leal	66
<b>Cost analysis of climate change and prevention measures in the Chancay-Lambayeque Valley, Perú.</b>	
Alex Segundino Armas-Blancas, Silvia del Pilar Iglesias-León, Eric Rendón-Schneir, Guillermo Vilchez-Ochoa, Javier Herrera-Espinoza, Leidy Milady Ramos-Alarcón, Jorge Luis Capuñay-Sosa, Hellen Felicia Blancas-Amaya & Rubén Armando Daga-López	76
<b>Analysis of the infrastructure works on accessibility using graph theory: case study "la Línea" tunnel.</b>	
David Fernando López-Patiño & Juan Pablo Londoño-Linares	82



**Microstructure influence on crack propagation behavior of nodular cast iron.**

Carla Tatiana Mota Anflor, José David Hurtado-Agualimpia, Adrián Alberto Betancur-Arroyave, Sergio Henrique da Silva Carneiro and John Nero Vaz Goulart 93

**Structural performance of composite beams using advanced modeling for nonlinear analysis.**

Mazin M. Sarhan & Faiq M.S. Al-Zwainy 103

**Flexible electrode for spinal cord electrostimulation.**

Juan José Melo-Portilla, Luisa Fernanda Puentes-Alzate, Karen Daniela Valencia-Poveda & Angelica María Ramírez-Martínez 111

**Technological characterization of the generation and distribution of electric power in Colombia at the beginning of the 20th century: case Manizales.**

Carolina Salazar-Marulanda, Javier Herrera-Murcia & Camilo Younes-Velosa 120

Our Cover  
 Image created with Artificial Intelligence AI at  
<https://designer.microsoft.com/image-creator>.

Author  
 David Álvarez C., Designer - Todográficas Ltda.



## CONTENIDO

<b>Investigación sobre la programación de autobuses de reserva en aeropuertos.</b>	9
Jin Li, Long Chen, Xiaowen Li & Huasheng Liu	
<b>Mejorando la eficiencia del comercio electrónico urbano: una referencia para la composición de flotas.</b>	19
Mauricio Peña-Acosta, Raúl Fabián Roldán-Nariño & Nicolás Rincón-García	
<b>Integración de IA, RPA y Big Data en la gestión y consultoría estratégica contable: perspectivas y desafíos.</b>	26
William Alberto Guerrero, Stefanny Camacho-Galindo, Laura Estefanía Guerrero-Martin, John Carlos Arévalo & Camilo Andrés Guerrero-Martin	
<b>Implementación de Google app script para la generación automática de la ficha de pre-matricula.</b>	35
Jorge Lira-Camargo, José Antonio Ogozi-Auqui & Francisca Sonia Vera-Tito	
<b>Evaluación del desempeño ambiental en navegación aérea con recursos limitados: estudio de caso en Cuba.</b>	39
Yohana Depestre-Wray, Rosa Mayelin Guerra-Bretaña, Oridayma Tarano-Artigas, Fridel Julio Ramos-Azcuy	
<b>Clasificación de la severidad del deterioro tipo bache en pavimentos asfálticos utilizando YOLOv8.</b>	47
Átila Marconcine de Souza, Vinicius Fier Cestari & Heliana Barbosa Fontenele	
<b>Modelo basado en agentes para la gestión integral del recurso hídrico: cuantificación de los cambios en el uso del suelo mediante la integración de incentivos económicos y sociales. Estudio de caso: Vista Hermosa (Meta).</b>	57
Nicol Chicacausa, Martín Otalora-Low, Natalia Carrillo-Acosta, María Cristina Arenas-Bautista & Antonio Preziosi-Ribero	
<b>Adopción de software de corte en pequeños fabricantes de muebles: una encuesta en Brasil.</b>	66
Nádyá Zanin Muzulon, Pedro Rochavetz de Lara Andrade, Rafael Henrique Palma Lima, Juliana Verga Shirabayashi & Gislaine Camila Lapasini Leal	
<b>Análisis de costos de cambio climático y medidas de prevención en el valle de Chancay-Lambayeque, Per.</b>	76
Alex Segundino Armas-Blancas, Silvia del Pilar Iglesias-León, Eric Rendón-Schneir, Guillermo Vilchez-Ochoa, Javier Herrera-Espinoza, Leidy Milady Ramos-Alarcón, Jorge Luis Capuñay-Sosa, Hellen Felicia Blancas-Amaya & Rubén Armando Daga-López	
<b>Análisis del impacto de obras de infraestructura sobre accesibilidad mediante teoría de grafos: estudio de caso túnel de la Línea.</b>	82
David Fernando López-Patiño & Juan Pablo Londoño-Linares	

**Influencia de la microestructura en el comportamiento de propagación de grietas en fundición nodular.**

Carla Tatiana Mota Anflor, José David Hurtado-Agualimpia, Adrián Alberto Betancur-Arroyave, Sergio Henrique da Silva Carneiro and John Nero Vaz Goulart 93

**Rendimiento estructural de vigas compuestas mediante modelado avanzado para análisis no lineal.**

Mazin M. Sarhan & Faiq M.S. Al-Zwainy 103

**Electrodo flexible para electroestimulación medular.**

Juan José Melo-Portilla, Luisa Fernanda Puentes-Alzate, Karen Daniela Valencia-Poveda & Angelica María Ramírez-Martínez 111

**Caracterización tecnológica de la generación y distribución de energía eléctrica en Colombia en los inicios del siglo XX: caso Manizales.**

Carolina Salazar-Marulanda, Javier Herrera-Murcia & Camilo Younes-Velosa 120

**Nuestra carátula**

Imagen creada con Inteligencia Artificial IA en  
<https://designer.microsoft.com/image-creator>.

**Autor:**

David Álvarez C., Diseñador - Todográficas Ltda.







# Research on airport reservation bus scheduling

Jin Li <sup>a</sup>, Long Chen <sup>a</sup>, Xiaowen Li <sup>b</sup> & Huasheng Liu <sup>a</sup>

<sup>a</sup> Department of Transportation Planning and Management, Jilin University, Institute of Transportation, Chang Chun, China. li\_jin@jlu.edu.cn, 18980546569@163.com, liuhuasheng521@163.com

<sup>b</sup> FAW-Volkswagen Quality Assurance Vehicle Analysis Center, Anqing Road, Green Park, Changchun, Jilin, China. xiaowen.li@faw-vw.com

Received: January 23<sup>rd</sup>, 2025. Received in revised form: June 6<sup>th</sup>, 2025. Accepted: June 16<sup>th</sup>, 2025.

## Abstract

Passengers face high costs or multiple transfers when they arrive or depart from the airport. In addition, most transportation modes in a city typically stop operating from midnight to early morning, making it impossible for passengers to enjoy quality and inexpensive services. Considering the passenger detour and multi-types, this paper sets up the passenger detour rebate mechanism and constructs the Airport Reservation Bus (ARB) scheduling model to maximize the profit of ARB enterprise. Meanwhile, an Improved Adaptive Genetic Algorithm (IAGA) is designed to solve the model, where the crossover and mutation operations are optimized to prevent it from falling into local optimum. Finally, a case study shows that ARB costs at least 39% less than taxis, with slightly longer travel time. Compared to traditional GA, IAGA reduced running time by more than 12%, showing faster convergence.

**Keywords:** airport reservation bus; differential pricing; vehicle scheduling; improved adaptive genetic algorithm.

# Investigación sobre la programación de autobuses de reserva en aeropuertos

## Resumen

Los pasajeros afrontan altos costos o múltiples trasbordos al viajar al aeropuerto. Además, la mayoría de los medios de transporte urbano cesan su operación de medianoche a primera hora, privando a los pasajeros de servicios económicos y de calidad. Considerando desvíos y tipos mixtos de vehículos, se propone un mecanismo de reembolso por desvío y un modelo de programación de autobuses de reserva aeroportuaria (ARB) para maximizar la rentabilidad. Se diseña un Algoritmo Genético Adaptativo Mejorado (IAGA) optimizando cruce y mutación para evitar el óptimo local. Los casos muestran que el ARB cuesta 39% menos que los taxis con un ligero aumento de tiempo. En comparación con el AG tradicional, el IAGA redujo el tiempo de ejecución en más del 12%, lo que demuestra una convergencia más rápida.

**Palabras clave:** autobús con reserva de aeropuerto; tarificación diferencial; programación de vehículos; algoritmo genético adaptativo mejorado.

## 1 Introduction

If the airport connection service is not good enough, it would be inconvenient for passengers. Currently, the public transportation modes from airport to urban area mainly include 'airport bus + bus/subway', 'railway + bus/subway' and cab, etc., which are difficult to balance the convenience, economy and comfort of travel. Nevertheless, the Airport Reservation Bus in this paper strives for a compromise among the three, while reducing the total social cost, easing traffic pressure and improving the efficiency of passenger distribution.

Fare studies are mainly divided into two categories, fixed fare and differential fare. Regarding fixed fare, Zhou (2001) [1] et al developed a bi-level transit fare optimization method based on line capacity constraints. Borndörfer (2012) [2] et al proposed a nonlinear fare optimization method based on a discrete choice model. However, these studies predominantly adopted fixed fares and overlooked the impact of detours on passenger cost. Due to the unfairness of fixed fare, differential pricing is attracting more and more attentions. Emele (2013) [3] et al introduced a variable pricing mechanism into the fare planning for flexible transport

**How to cite:** Li, J., Chen, L., Li, X., and Liu, H., Research on airport reservation bus scheduling. DYNA, (92)238, pp. 9-18, July - September, 2025.



services. Kamel (2020) [4] et al constructed a platform for optimizing time-based transit fares in large multimodal transportation networks. Guo (2021) [5] et al established a time-dependent transit pricing model considering elasticity and time-distributed demand. While these studies explored dynamic pricing mechanisms, they seldom connected fare adjustments with detour distances.

Vehicle scheduling is categorized into single-vehicle type and multiple-vehicle type. Concerning the single-vehicle type, Smith (2003) [6] et al established a bi-objective scheduling optimization model based on balancing the maximum number of deviations and minimum unused slack time. Gebeyehu (2008) [7] et al applied the GIS technology to the design of Demand Responsive Transit routes. Ye (2015) [8] et al constructed an optimization model for taxi ridesharing routes. Li (2024) [9] et al proposed a real-time dynamic route planning algorithm for DRT. Notably, these single-vehicle studies overlooked the efficiency potential of mixed fleets, a research dimension that subsequent multi-fleet studies have begun to address. In terms of multi-vehicle type, Golden (1984) [10] et al first proposed the multi-vehicle route planning problem. Tarantilis (2003) [11] et al designed a metaheuristic algorithm to solve it with a fixed vehicle size. Dondo (2008) [12] et al, Barkaoui (2013) [13] et al and Goeke (2015) [14] et al proposed a hybrid local improvement algorithm, improved adaptive genetic algorithm, and hybrid heuristic algorithm respectively. Gasque (2022) [15] et al established two mixed-integer programming models for taking delivery without separation as well as taking delivery with separation and proposed an adaptive large-neighborhood search element heuristic algorithm. Although these multi-vehicle studies optimized routes, they rarely combined mixed types with detour management.

Though existing research has made significant progress in fares and scheduling models, there remain the following problems: the fixed fare is typically adopted, without considering the effect of detours. Concerning vehicle scheduling, scholars pay less attention to the variability of vehicle types. With respect to algorithms, the Adaptive Genetic Algorithm (AGA) is more widely used because of its high robustness and efficiency, while suffers from problems such as premature convergence and local optimization. Aiming at the above problems, this paper simultaneously considers the passenger detour and the mixed vehicle types and proposes a passenger detour rebate mechanism. With the goal of maximizing the profit of the Airport Reservation Bus (ARB) enterprise, then the ARB scheduling model is constructed. Finally, an Improved Adaptive Genetic Algorithm (IAGA) is designed to solve it.

## 2 Airport reservation bus scheduling model based on passenger detour compensation

### 2.1 Problem description

The problem is divided into the delivery stage and pick-up stage, described as follows: the delivery stage involves

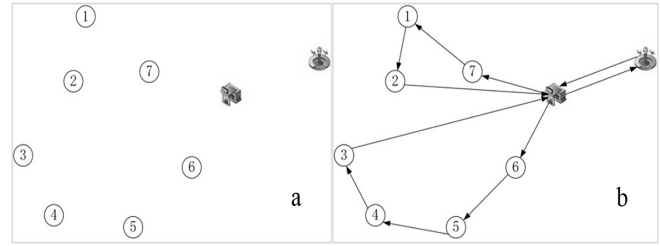


Figure 1. Passengers boarding at the airport and their routes a) Passengers; b) Routes for them  
Source: Own elaboration.

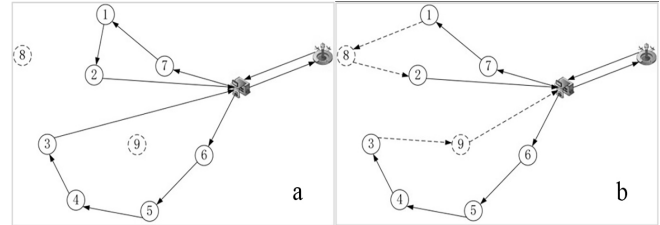


Figure 2. Add passengers alighting at the airport a) Add passengers; b) Final routes  
Source: Own elaboration.

transporting passengers boarding at the airport. In this stage, the origin is fixed at the airport. The pick-up stage is to collect passengers alighting at the airport. According to distance of detours, a fare discount is rebated to detour passengers.

The process of generating the routes of the ARB is shown in Fig. 1 (a) – 2 (b). The demands of passengers boarding at the airport and their routes are in Fig. 1 (a) - (b). Based on this, taking passengers alighting at the airport into routing consideration, the final planning is in Fig. 2 (a) - (b).

The solid area in the above figure is for passengers boarding at the airport and the dashed is for passengers alighting at the airport. The ARB delivers passengers to the destination while picking up passengers to the airport. Upon completion of the pick-up and drop-off, the bus returns to the terminal to wait for the next round of pick-ups and drop-offs.

### 2.2 Model building

#### 2.2.1 Model assumptions

- (1) The seat reservations are accepted only between the airport and the points of demand, not between points of demand;
- (2) For passengers alighting/boarding at the airport, only their arrival/departure time window at the airport is considered.
- (3) The vehicle type and fleet size are known;
- (4) Vehicle speed is constant and known.
- (5) There is only one airport within the service area.
- (6) The vehicle makes only one round trip at a given time.

#### 2.2.2 Definition of parameters

The definition of the parameters involved are in Table 1.

Table 1.

Parameter Definition.

Symbol	Definition
$J$	Airport.
$G$	Freeway entrance/exit.
$M$	The set of boarding and alighting points, $m$ is the total number of points.
$K$	The set of vehicle types, $K = \{1, 2, \dots, h\}$ , $h$ is the sequence of the vehicle type.
$K_h$	The set of the number for vehicles type $h$ , $K_h = \{1, 2, \dots, k\}$ , $k$ is sequence of the vehicle.
$Q$	The set of passengers.
$Q_a$	The set of passengers alighting at the airport.
$Q_b$	The set of passengers boarding at the airport.
$i$	The sequence of the point, $i \in M$ .
$q$	The sequence of the passenger, $q \in Q$ .
$l_{ij}$	Ideal distance traveled from point $i$ to point $j$ .
$Q_{ij}^k$	Number of passengers for vehicle $k$ from $i$ to the $j$ .
$p^k$	Fare per kilometer of vehicle $k$ in the urban area.
$g(l_{ij}^{kf})$	Floating fare for vehicle $k$ from $i$ to $j$ .
$C_p$	Value of time for passengers.
$L_{ij}^k$	Actual distance traveled by vehicle $k$ from $i$ to $j$ .
$\lambda_{lim}$	Passenger detour coefficient.
$C_{h0}$	Fixed costs of type $h$ .
$N$	The service life of the vehicle.
$C_{h1}$	Variable cost of unit distance for vehicle type $h$ .
$C_d$	Wage for driver.
$V$	Speed of vehicle.
$t_0$	Individual passenger boarding or alighting time.
$\varphi$	Penalty cost factor for late arrival of vehicles at the airport.
$Q_l^k$	Number of passengers late arrival for vehicle $k$ .
$T_{dj}^k$	Departure moment of vehicle $k$ from $j$ .
$[T_q^e, T_q^l]$	Expected arrival time window, $q \in Q_a$ . Expected departure time window, $q \in Q_b$ .
$Q_{ik}$	Number of passengers in vehicle $k$ arriving at point $i$ .
$Q_k$	Capacity of vehicle $k$ .
$T_q^w$	Waiting time of passenger $q$ .
$T_q^{max}$	Maximum tolerated waiting time for passenger $q$ .
$T_{max}$	Maximum travel time of vehicle.
$Y_{ij}^k$	1, vehicle $k$ traveling from $i$ to $j$ . 0, otherwise.
$Y_q^k$	1, passenger $q$ served by vehicle $k$ . 0, otherwise.

Source: Own elaboration.

### 2.2.3 Model assumptions

Route planning is a major task of vehicle scheduling. This paper formulates a route planning model to maximize the profit of ARB enterprises by optimizing operational efficiency. The model introduces a differential pricing mechanism that rebates passengers for detours and imposes penalty fees if their time requirements are unmet. The objective function is defined as:

$$\max P = R - C_1 - C_2 - C_3 - C_4 \quad (1)$$

Where  $P, R, C_1, C_2, C_3, C_4$  mean profit, fare revenue, fixed cost, variable cost, penalty cost for late arrival and for late departure respectively.

#### 1. Fare revenue $R$

The fare revenue  $R$  consists of the basic fare  $R_{bf}$  and the rebate  $R_r$  based on mileage pricing.

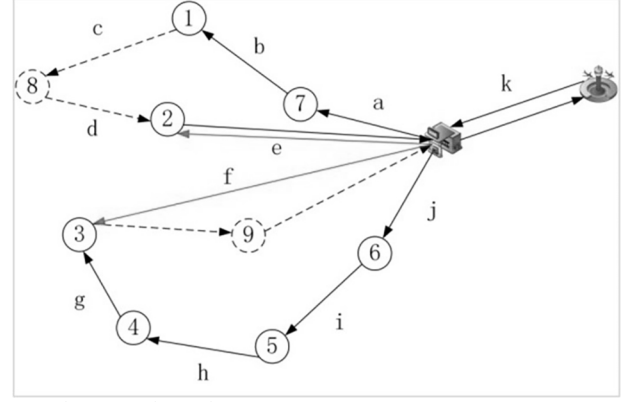


Figure 3 Shortest and actual routes.

Source: Own elaboration.

$$R = R_{bf} - R_r \quad (2)$$

The basic fare  $R_{bf}$  is a primary function proportional to the ideal distance of passengers [16-18].

$$R_{bf} = \sum_{h \in K} \sum_{k \in K_h} \sum_{i \in M} \sum_{j \in M} [p^k \cdot l_{ij} \cdot (Q_{ij}^k + Q_{ji}^k)] \quad (3)$$

The rebate  $R_r$  is related to the passenger detour distance. The formula proposed in this paper is as follows.

$$R_r = \sum_{h \in K} \sum_{k \in K_h} \sum_{i \in M} [(g(l_{ij}^{kf}) \cdot Q_{ij}^k + g(l_{ji}^{kf}) \cdot Q_{ji}^k)] \quad (4)$$

$$g(l_{ij}^{kf}) = \begin{cases} [C_v \cdot (L_{ij}^k - \lambda_{lim} \cdot l_{ij})] / V, & L_{ij}^k / l_{ij} \geq \lambda_{lim} \\ 0, & L_{ij}^k / l_{ij} < \lambda_{lim} \end{cases} \quad (5)$$

When a passenger detour is greater than or equal to  $\lambda_{lim}$ , passenger time delayed by the detour is converted into money and rebated to him. The shortest and actual distance for passengers are shown in Fig. 3.

For passenger 6, the actual distance is ideal distance, so detour does not exist. For passenger 3, whose ideal distance is  $f + k$ , the actual distance is  $g + h + i + j + k$ . If  $(g + h + i + j + k) / (f + k) > \lambda_{lim}$ , it is necessary to rebate him.

#### 2. Fixed cost $C_1$

Fixed cost  $C_1$  is related to the number of vehicles and their service life [16-18].

$$C_1 = \frac{\sum_{h \in K} \sum_{k \in K_h} C_{h0}}{365N} \quad (6)$$

#### 3. Variable cost $C_2$

Variable cost  $C_2$  includes fuel consumption and driver cost, which are related to distance [16-18].

$$C_2 = \sum_{h \in K} \sum_{k \in K_h} \sum_{i \in M} \sum_{j \in M} (C_{h1} \cdot l_{ij} \cdot Y_{ij}^k + C_d \cdot (\frac{l_{ij} \cdot Y_{ij}^k}{V} + \frac{\sum_{i \in M} \max(Q_{ij}^k, Q_{ji}^k) \cdot t_0}{60})) \quad (7)$$



#### 4. Penalty cost for late arrival at the airport $C_3$

$C_3$  is the penalty cost for vehicles arriving late at the airport. Since airport passengers are highly time sensitive, late arrival may cause passenger miss their flights and incur a great loss [16-18].

$$C_3 = \begin{cases} \sum_{q \in Q_a} \sum_{h \in K} \sum_{k \in K_h} (\varphi \cdot Y_q^k), (T_{X1} > T_q^l) \\ 0, (T_{X1} \leq T_q^l) \end{cases} \quad (8)$$

$$T_{X1} = T_{dJ}^k + \frac{\sum_{i \in M} \sum_{j \in M} l_{ij} Y_{ij}^k}{V} + \frac{\sum_{i=1}^m \max(Q_{ij}^k, Q_{ji}^k) \cdot t_0}{60} \quad (9)$$

#### 5. Penalty cost for late departure from the airport $C_4$

$C_4$  is the penalty cost for a vehicle departing the airport late. If a vehicle leaves the airport later than  $T_q^l$ , it will cause the passenger wait too long. The formula proposed is as follows.

$$C_4 = \begin{cases} 0.5 \sum_{q \in Q_a} \sum_{h \in K} \sum_{k \in K_h} C_{X2}, (0 < T_{dJ}^k - T_q^l \leq 5) \\ 0.73 \sum_{q \in Q_a} \sum_{h \in K} \sum_{k \in K_h} C_{X2}, (5 < T_{dJ}^k - T_q^l \leq 20) \\ 100 \sum_{q \in Q_a} \sum_{h \in K} \sum_{k \in K_h} C_{X2}, (T_{dJ}^k - T_q^l > 20) \end{cases} \quad (10)$$

$$C_{X2} = (T_{dJ}^k - T_q^l) \cdot Y_q^k \quad (11)$$

### 2.2.4 Constraints

#### 1. Origin and destination constraints

Vehicles entering and exiting a point of demand are the same.

$$\sum_{i \in M} Y_{ij}^k \leq 1, (j \in M, k \in K_h) \quad (12)$$

#### 2. Vehicle capacity constraints

The number of passengers in a vehicle is less than or equal to the its capacity.

$$\begin{cases} Q_{ik} \leq Q_k \\ Q_{ik} + Q_{ij}^k - Q_{ji}^k \leq Q_k, (k \in K_h, i \in M) \end{cases} \quad (13)$$

#### 3. Connection service supply constraints

Each demand is served by only one vehicle.

$$\sum_{h \in K} \sum_{k \in K_h} Y_q^k = 1, (q \in M) \quad (14)$$

#### 4. Maximum travel time of vehicle

$$\frac{\sum_{i \in M} \sum_{j \in M} l_{ij} \cdot Y_{ij}^k}{V} + \frac{\sum_{i \in M} \max(Q_{ij}^k, Q_{ji}^k) \cdot t_0}{60} \leq T_{max}, (k \in K_h) \quad (15)$$

#### 5. Passenger detour constraints

$$\lambda = \left( \frac{L_{ij}^k}{V} + \frac{\sum_{i \in M} \max(Q_{ij}^k, Q_{ji}^k) \cdot t_0}{60} \right) / \frac{l_{ij}}{V} \leq \lambda_{lim} \quad (16)$$

### 3 Improved adaptive genetic algorithm

The problem studied in this paper is the Vehicle Routing Problem with Time Window constraints, which is a well-known NP-hard problem solved by heuristic algorithms efficiently. Genetic Algorithm (GA) has the advantages of parallelism and global optimization. It continuously generates new individuals and populations in the process of reproduction, and seeks a better solution, which is applicable to the solution of complex optimization problems.

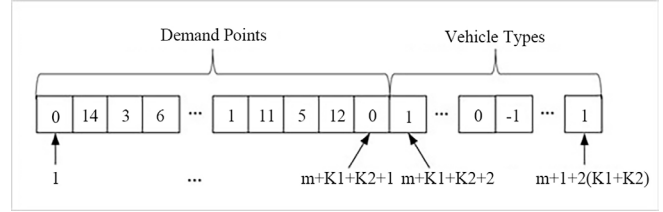


Figure 4 Chromosome coding schematic.  
Source: Own elaboration.

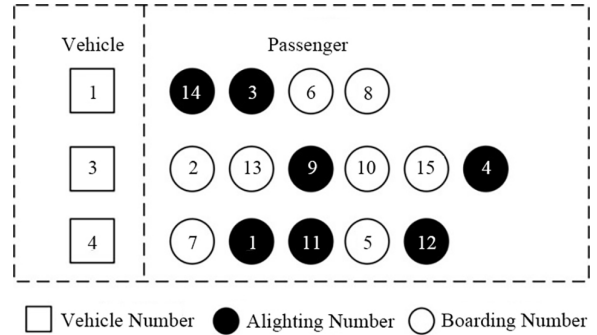


Figure 5 Chromosome coding forms.  
Source: Own elaboration.

In the traditional GA, the crossover probability  $P_c$  and mutation probability  $P_m$  are fixed values. In the process of large-scale problem, the early maturity often occurs. This paper proposes an IAGA to set  $P_c$  and  $P_m$  as dynamic values, which improves the solving efficiency while setting the minimum value of  $P_c$  and  $P_m$  to ensure the evolution speed in the early stage is high enough to avoid falling into the local optimal solution.

#### 3.1 Chromosome coding and population initialization

##### 3.1.1 Chromosome coding

Considering mixed vehicle types, it is necessary to add vehicle type auxiliary codes for chromosome coding. The chromosome is encoded into individuals of length  $m + 1 + 2(K_1 + K_2)$ . The coding scheme is shown in Fig. 4.

In this paper, there are two vehicle types. Where 1 in the vehicle types represents the type a, -1 is the vehicle type b, and 0 means the vehicle is not being used. The demand point 0 is the airport.

Taking (0,14,3,6,8,0,0,2,13,9,1,4,0,7,1,11,5,12,0,1,0,-1,-1) as an example, the chromosome coding form is shown in Fig. 5. There are 15 demand points and 4 vehicles, with two each of vehicle type a and b.

Vehicle 1 (a): Airport - Point 14 - Point 3 - Point 6 - Point 8 - Airport

Vehicle 2 (a): Non-operational

Vehicle 3 (b): Airport - Point 2 - Point 13 - Point 9 - Point 10 - Point 15 - Point 4 - Airport

Vehicle 4 (b): Airport - Point 7 - Point 1 - Point 11 - Point 5 - Point 12 - Airport

### 3.1.2 Population initialization

In this paper, a randomized generation method was chosen to generate the initial population. A passenger is randomly selected and assigned to a vehicle. If the number of passengers does not exceed the capacity, add the point into the route. Otherwise, re-select a vehicle among the rest and determine whether it is overcrowded until the passenger is assigned to a particular vehicle. Repeat until all demands are met.

## 3.2 Genetic operation

### 3.2.1 Selection operation

In this paper, the selection operation is based on Monte Carlo Method, and the selection probability of a chromosome is the ratio of its fitness value to the sum of the fitness values of all chromosome. Therefore, the larger the fitness value, the greater the probability of being selected.

### 3.2.2 Crossover operation

The Adaptive Genetic Algorithm (AGA) proposed by M. Srinivas makes the crossover probability  $P_c$  relevant to the fitness value, which can solve the problem of premature convergence effectively. However, in the early stage of AGA, the evolution speed of good individuals is slow, which reduces the operational efficiency and even leads to the local optimum.

This paper improves the crossover probability  $P_c$  of AGA, which ensures that the fitness value can flexibly change the crossover probability to improve the operational efficiency. Meanwhile, the minimum crossover probability is set to ensure that it evolves quickly in the early stage, to avoid falling into the local optimum. The improved formula are as follows.

$$P_c = \begin{cases} P_{c1} - \frac{(P_{c1} - P_{c2})(f_{up} - f_{mean})}{f_{max} - f_{mean}}, & f_{up} \geq f_{mean} \\ P_{c1}, & f_{up} < f_{mean} \end{cases} \quad (17)$$

Where

$f_{max}$ —Maximum fitness value of all chromosomes

$f_{up}$ —Larger fitness value in two chromosomes

$f_{mean}$ —Mean of all chromosome fitness values

$P_{c1}$ —Maximum crossover probability

$P_{c2}$ —Minimum crossover probability

When chromosome X and Y perform crossover operation, point chain 1 of vehicle i is randomly selected from X, and point chain 2 of vehicle j is randomly selected from Y. The type of vehicle i and j may be the same or different.

(1) The same vehicle type.

In this case, it does not need to consider vehicle type crossover and only chain crossover can be considered.

Step 1: add the points in chain 2 to chain 1 sequentially. For each point, conduct a feasibility test of the corresponding vehicle type on chain 1. If the constraints are satisfied, insert it into chain 1 and delete points duplicated with chain 1 on other chains of the X chromosome. Otherwise, remain in chain 2.

Step 2: update the chromosome X.

Step 3: set the operated vehicle in chain 2 on chromosome Y to 0, complement missing demand points and randomly select an assigned vehicle to deliver the demand points. If points cannot be assigned to them, arrange for a new vehicle. If it is not available, keep the original chromosome Y to enter the offspring.

(2) The different vehicle types.

Step 1: if vehicle i and j are type a and b respectively, draw out the points in chain 1, and sequentially place the drawn points into chain 2 until the constraint of type b is satisfied.

Step 2: conduct the aforementioned procedure for the same vehicle type according to the case where both vehicles are type a and both are type b respectively, to obtain temporary chromosome  $X_1$  and  $X_2$ .

Step 3: calculate the fitness  $f_1$  and  $f_2$  for  $X_1$  and  $X_2$ . Generate a random number  $\gamma$ , if  $\gamma \leq \frac{f_1}{f_1 + f_2}$ , remain  $X_1$  into the offspring, otherwise remain  $X_2$ . Swap the sequence of chromosomes X and Y and perform the above operation.

### 3.2.3 Mutation operation

The improved mutation probability  $P_m$  of AGA proposed by M. Srinivas plays the same role as  $P_c$ . Therefore, it is necessary to set a minimum mutation probability. The improved formula are as follows.

$$P_m = \begin{cases} P_{m1} - \frac{(P_{m1} - P_{m2})(f_{up} - f_{mean})}{f_{max} - f_{mean}}, & f_{up} \geq f_{mean} \\ P_{m1}, & f_{up} < f_{mean} \end{cases} \quad (18)$$

Where

$P_{m1}$ —Maximum mutation probability

$P_{m2}$ —Minimum mutation probability

The mutation operation is divided into two stages, point mutation and vehicle type mutation. The procedure is as follows:

Step I: select individuals in turn from the crossover operation.

Step II: determine whether the individual is mutated or not. If mutated, turn to step III. Otherwise, turn to step V.

Step III: Stage 1 - Point Mutation.

Step 1: randomly select an assigned vehicle and record its point chain.

Step 2: randomly choose a point  $x$  in the chain and remove it.

Step 3: add point  $x$  to the chain of another assigned vehicle, if the new chain satisfies the capacity constraints of the corresponding vehicle type, then the insertion is successful. Otherwise, search for the next vehicle. If fail to assign it, then determine whether a vehicle is available. If there is, assign the point to the new vehicle, otherwise turn to Step IV;

Step 4: update the chromosome.

Step IV: Stage 2 - Vehicle type mutation.

Step 5: randomly select a vehicle and record its chain and type.

Step 6: determine whether the chain satisfies the constraints of the other vehicle type. If so, turn to Step 8, otherwise, turn to the next step.

Step 7: draw out all points in the chain sequentially until the capacity constraint of the other type is satisfied. Then, assign the drawn points to other assigned vehicles for the other type. If failed, arrange a new vehicle. If there are no available vehicles, readjust the point drawn scheme. If all schemes can not satisfy the constraints, the mutation fails and remain the chromosome. Otherwise, turn to the next step.

Step 8: replace the vehicle type with the other one.

Step V: update the chromosome.

### 3.3 Solution flow

The IAGA is used for model solving, and the specific flow is shown in Fig. 6.

### 3.4 Algorithm comparison

In order to verify the advantages of the IAGA, the algorithms are compared with 20 and 30 demands

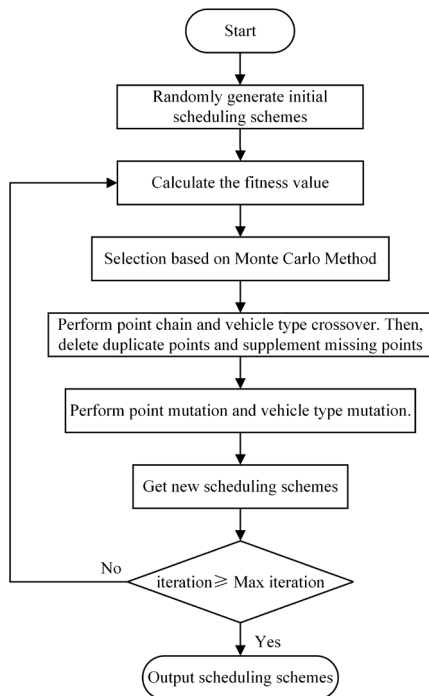


Figure 6 Schematic diagram of the IAGA.

Source: Own elaboration.

Table 2.

Algorithm comparison data.

Demand	Longitude	Latitude	Time	Demand	Longitude	Latitude	Time
1	101.27	31.05	13:45	16	101.29	31.07	14:00
2	101.3	31.02	13:50	17	101.24	31.02	14:30
3	101.21	31.06	13:45	18	101.24	31	13:55
4	101.25	31.03	13:45	19	101.2	31.04	14:15
5	101.21	31.02	13:50	20	101.27	31.03	14:25
6	101.23	31.1	14:25	21	101.28	31.04	14:30
7	101.22	31.01	14:30	22	101.25	31.02	14:15
8	101.25	31.01	13:55	23	101.27	31.04	14:05
9	101.22	31.08	13:30	24	101.29	31.09	13:50
10	101.22	31.02	14:25	25	101.23	31.04	14:00
11	101.2	31.05	13:55	26	101.3	31.03	13:55
12	101.2	31.05	14:30	27	101.28	31.05	13:45
13	101.21	31.05	14:00	28	101.28	31.02	14:10
14	101.27	31	13:25	29	101.26	31.06	14:05
15	101.3	31.09	14:25	30	101.27	31.03	14:00

Source: Own elaboration.

respectively. The fitness of the traditional GA is set as the value of the objective function and the algorithm parameters are the same as the IAGA. Taking the arrival time window at the airport as an example, the data in the table is  $T_q^l$ , and  $T_q^e$  is 15 minutes in advance, shown in Table 2. The 20 demands are the top 20 data in Table 2.

The changes in the objective function values for each group are in Fig. 7 (a), 7 (b) and the results is in Table 3, 4.

Compared with the traditional GA, the running time of the IAGA corresponding to 20 and 30 demands decreased by 12.02% and 14.08% respectively and the number of iterations has been reduced by 23.6% and 35.7%.

## 4 Case study

### 4.1 Service areas and example profiles

Take Changchun Nanguan District, an area with high density passenger flow, as the object.

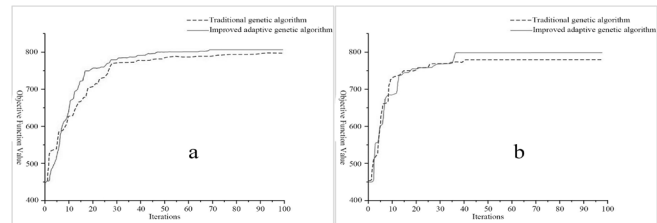


Figure 7 Different demands a) Demands = 20; b) Demands = 30.

Source: Own elaboration.

Table 3.

Comparison of the results of 20 demands.

Algorithm	Running time (s)	Iterations	objective function value
Traditional GA	43.76	89	797.66
IAGA	38.5	68	806.3
Change (%)	-12.02	-23.6	+1.08

Source: Own elaboration.

Table 4.

Comparison of the results of 30 demands.

Algorithm	Running time (s)	Iterations	objective function value
Traditional GA	49.08	42	1094.0
IAGA	42.17	27	1131.3
Change (%)	-14.08	-35.7	+3.41

Source: Own elaboration.



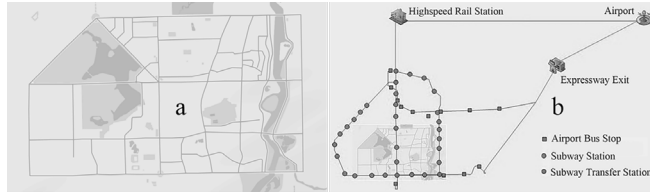


Figure 8 Road information a) Road network; b) Public transportation.  
Source: Own elaboration.



Figure 9 Reservation demand distribution.  
Source: Own elaboration.

The road network is in Fig. 8 (a), and the coverage of public transportation around the area is shown in Fig. 8 (b). The existing transportation modes from urban area to Changchun Longjia International Airport (International Air Transport Association: CGQ) are in Fig. 8 (b)

Taking arrival flights of 19:00-22:30 and departure flights of 22:30-00:30 as an example, 50 passenger demand points are randomly generated. The total number of passengers is 58, where 44 passengers board at airport and 14 passengers alight at airport. The distribution of demand points are in Fig. 9 and the demand data is shown in Table 5, in which point 51 and 52 are freeway entrance/exit and airport.

Table 5.  
Passenger travel data.

No.	Longitude	Latitude	Expected time window		Number of passengers	
			Arrival	Departure	Boarding	Alighting
1	125.316731	43.860387	-	20:15-20:20	1	0
2	125.319349	43.861980	-	20:05-20:10	1	0
3	125.324971	43.861299	-	19:35-19:40	1	0
4	125.324628	43.859814	21:00-21:15	-	0	1
5	125.320465	43.855977	-	20:20-20:25	1	0
6	125.331581	43.858541	-	20:35-20:40	1	0
7	125.334927	43.860804	-	20:40-20:45	1	0
8	125.329863	43.862197	-	20:10-20:15	1	0
9	125.333983	43.854801	-	20:05-20:10	2	0
10	125.339648	43.858576	20:50-21:05	-	0	1
11	125.328876	43.858515	-	19:55-20:00	2	0
12	125.348403	43.860031	-	20:20-20:25	1	0
13	125.341665	43.855296	-	20:35-20:40	2	0
14	125.357851	43.863526	-	19:10-19:15	1	0
15	125.359611	43.857728	-	19:55-20:00	1	0
16	125.354776	43.862816	-	20:30-20:35	1	0
17	125.359396	43.848783	-	20:05-20:10	2	0

No.	Longitude	Latitude	Expected time window		Number of passengers	
			Arrival	Departure	Boarding	Alighting
18	125.346879	43.848828	-	19:00-19:05	1	0
19	125.340528	43.85053	21:10-21:25	-	0	1
20	125.339305	43.848333	-	20:15-20:20	1	0
21	125.334412	43.849757	21:30-21:45	-	0	1
22	125.327803	43.849076	-	20:10-20:15	1	0
23	125.330335	43.845795	21:45-22:00	-	0	1
24	125.335206	43.843195	22:15-22:30	-	0	1
25	125.327775	43.855069	-	19:10-19:15	1	0
26	125.323619	43.848271	-	20:30-20:35	1	0
27	125.322503	43.843474	22:40-22:55	-	0	1
28	125.325529	43.847861	22:00-22:15	-	0	1
29	125.291347	43.845888	21:30-21:45	-	0	1
30	125.29787	43.844278	21:05-21:20	-	0	1
31	125.300273	43.841369	-	19:35-19:40	1	0
32	125.297628	43.846277	-	20:20-20:25	1	0
33	125.299694	43.848287	-	20:40-20:45	2	0
34	125.305144	43.834249	-	20:30-20:35	1	0
35	125.296861	43.834125	-	19:00-19:05	1	0
36	125.293965	43.838057	22:10-22:25	-	0	1
37	125.306467	43.845906	-	20:35-20:40	1	0
38	125.310582	43.845887	-	19:10-19:15	1	0
39	125.320104	43.846667	-	20:20-20:25	1	0
40	125.311192	43.851894	-	19:05-19:10	2	0
41	125.314478	43.837229	21:15-21:30	-	0	1
42	125.309758	43.834102	-	19:10-19:15	2	0
43	125.310594	43.838707	-	20:15-20:20	1	0
44	125.331036	43.840939	-	20:35-20:40	1	0
45	125.330659	43.846738	21:05-21:20	-	0	1
46	125.326877	43.845568	-	19:35-19:40	1	0
47	125.332513	43.837778	22:10-22:25	-	0	1
48	125.34159	43.840317	-	20:20-20:25	1	0
49	125.341247	43.835673	-	19:05-19:10	2	0
50	125.347856	43.836292	-	20:05-20:10	1	0
51	125.470987	43.903319	-	-	-	-
52	125.705079	43.998125	-	-	-	-

Source: Own elaboration.

Table 6.  
Model parameters.

Parameter	Definition	Value
$h$	1, fleet size of vehicle type a (vehicle)	10
	2, fleet size of vehicle type b (vehicle)	10
$p^k$	Fare per kilometer of vehicle k (yuan/PAX)	1.3 (daytime), $k \in K_1$
		1.6 (evening), $k \in K_1$
		1.5 (daytime), $k \in K_2$
		1.8 (evening), $k \in K_2$
$C_p$	Value of time for passengers (yuan/h)	43.78
$\lambda_{lim}$	Passenger detour coefficient	1.2
$C_{h0}$	Fixed cost of vehicle k (yuan/h)	32.5, $k \in K_1$
		40, $k \in K_2$
$C_{h1}$	Variable cost of unit distance for vehicle k (yuan/km)	1, $k \in K_1$
		1.2, $k \in K_2$
$C_d$	Wage for driver (yuan/h)	33
$V$	Speed of vehicle (km/h)	55
$t_0$	Passenger boarding or alighting time (min)	1/6
$\varphi$	Penalty cost factor for late arrival (yuan/PAX)	10000
$Q_k$	Capacity of vehicle k (PAX)	7, $k \in K_1$
		12, $k \in K_2$
$T_{max}$	Maximum driving hours per vehicle (h)	2
$NP$	Initial population	300
$F$	Maximum Iterations	300

Source: Own elaboration.

#### 4.2 Scheduling and planning analysis

The parameter calibration is shown in Table 6.

The evolutionary iteration process is shown in Fig. 10, which illustrate the relationship of the iterations and optimal value. The objective function value increases with the number of iterations and stabilizes after 210 iterations.

The routes and corresponding vehicle allocation scheme are shown in Table 7. According to Table 7, a total of six vehicles are assigned, including two 7-seat and four 12-seat vehicles. 58 passengers are all delivered to their destinations. Specific route information is illustrated in Table 8, which shows that all vehicles return CGQ within 2h.

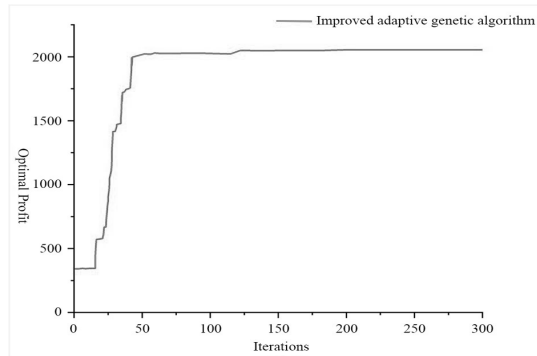


Figure 10 Iterative diagram of the evolution of the optimal solution.  
Source: Own elaboration.

Table 7.  
Solution results.

No.	Vehicle type	Route	Number of passengers (PAX)	Route length (km)	Average travel time (min)
1	b	52-51-14-18-49-42-35-38-40-25-4-10-51-52	13	104.6	47.11
2	a	52-51-3-30-31-41-46-45-19-51-52	7	96.54	44.13
3	a	52-51-11-15-29-21-51-52	5	99.4	43.66
4	b	52-51-12-1-5-20-48-43-39-32-36-28-47-24-51-52	12	106.51	46.59
5	b	52-51-8-2-9-22-23-50-17-51-52	9	100.64	49.36
6	b	52-51-16-13-7-6-26-33-37-34-44-27-51-52	12	100.22	46.78

Source: Own elaboration.

Table 8.  
Route information.

Route	Point	Boardings or alightings	Persons in vehicle	Travel distance (km)	Detour factor	Basic fare (yuan)	Rebate (yuan)	Final Fare (yuan)	Arrival time
1	52	+11	11	-	-	-	-	-	19:10
	51	-0	11	-	-	-	-	-	19:40
	14	-1	10	35.40	1.00	52.30	0.00	52.30	19:53
	18	-1	9	36.60	1.00	54.10	0.00	54.10	19:55
	49	-2	7	38.70	1.00	57.25	0.00	57.25	19:57
	42	-2	5	43.00	1.01	62.95	0.00	62.95	20:02
	35	-1	4	45.90	1.06	63.85	0.00	63.85	20:05
	38	-1	3	47.60	1.11	63.40	0.00	63.40	20:07

Route	Point	Boardings or alightings	Persons in vehicle	Travel distance (km)	Detour factor	Basic fare (yuan)	Rebate (yuan)	Final Fare (yuan)	Arrival time
2	40	-2	1	50.70	1.28	58.60	2.53	56.07	20:10
	25	-1	0	53.10	1.33	58.90	4.25	54.65	20:13
	4	+1	1	40.80	1.04	57.85	0.00	57.85	20:15
	10	+1	2	37.20	1.00	55.00	0.00	55.00	20:19
	51	-0	2	-	-	-	-	-	20:35
	52	-3	0	-	-	-	-	-	21:04
	52	+3	3	-	-	-	-	-	19:35
	51	-0	3	-	-	-	-	-	20:05
	3	-1	2	35.40	0.91	59.47	0.00	59.47	20:22
	30	+1	3	44.74	1.05	63.89	0.00	63.89	20:27
3	31	-1	2	39.96	0.94	64.15	0.00	64.15	20:27
	41	+1	3	41.98	1.01	62.46	0.00	62.46	20:30
	46	-1	2	42.69	1.09	59.47	0.00	59.47	20:30
	45	+1	3	40.90	1.05	59.47	0.00	59.47	20:31
	19	+1	4	37.50	1.00	57.39	0.00	57.39	20:35
	51	-0	4	-	-	-	-	-	20:51
	52	-4	0	-	-	-	-	-	21:20
	52	+3	3	-	-	-	-	-	19:55
	51	-0	3	-	-	-	-	-	20:25
	11	-2	1	38.20	1.00	58.30	0.00	58.30	20:41
4	15	-1	0	40.70	1.11	56.22	0.00	56.22	20:44
	29	+1	1	44.50	1.09	61.68	0.00	61.68	20:50
	21	+1	2	38.50	1.00	58.69	0.00	58.69	20:57
	51	-0	2	-	-	-	-	-	21:14
	52	-2	2	-	-	-	-	-	21:43
	52	+8	8	-	-	-	-	-	20:20
	51	-0	8	-	-	-	-	-	20:50
	12	-1	7	35.00	1.00	54.14	0.00	54.14	21:03
	1	-1	6	38.40	1.02	57.78	0.00	57.78	21:07
	5	-1	5	40.20	1.05	58.56	0.00	58.56	21:09
5	20	-1	4	43.80	1.19	56.61	0.00	56.61	21:13
	48	-1	3	45.40	1.19	58.30	0.00	58.30	21:14
	43	-1	2	48.25	1.15	63.11	0.00	63.11	21:18
	39	-1	1	48.76	1.23	60.38	0.80	59.58	21:18
	32	-1	0	51.66	1.12	68.83	0.00	68.83	21:21
	36	+1	1	43.85	1.00	65.84	0.00	65.84	21:24
	28	+1	2	40.55	1.02	60.25	0.00	60.25	21:27
	47	+1	3	38.75	0.95	61.81	0.00	61.81	21:29
	24	+1	4	37.90	1.00	57.91	0.00	57.91	21:30
	51	-0	4	-	-	-	-	-	21:47
6	52	-4	0	-	-	-	-	-	22:15
	52	+8	8	-	-	-	-	-	20:10
	51	-0	8	-	-	-	-	-	20:40
	8	-1	7	38.10	1.00	58.17	0.00	58.17	20:56
	2	-1	6	41.40	1.10	57.52	0.00	57.52	21:00
	9	-2	4	40.70	1.09	57.13	0.00	57.13	21:03
	22	-1	3	44.30	1.16	58.17	0.00	58.17	21:07
	23	+1	4	39.54	1.02	59.08	0.00	59.08	21:09
	50	-1	1	53.80	1.38	59.34	5.57	53.77	21:12
	17	-2	2	54.34	1.45	57.52	7.34	50.18	21:12
	51	-0	2	-	-	-	-	-	21:29
	52	-2	0	-	-	-	-	-	21:59
	52	+11	11	-	-	-	-	-	20:40
	51	-0	11	-	-	-	-	-	21:10
	16	-1	10	34.80	1.00	51.40	0.00	51.40	21:23
	13	-2	8	37.60	1.02	54.40	0.00	54.40	21:26
	7	-1	7	41.40	1.10	55.60	0.00	55.60	21:30
	6	-1	6	42.90	1.13	56.05	0.00	56.05	21:32
	26	-1	5	43.49	1.10	58.45	0.00	58.45	21:33
	33	-2	3	45.99	1.08	62.95	0.00	62.95	21:35
	37	-1	2	46.32	1.09	62.95	0.00	62.95	21:36
	34	-1	1	49.02	1.15	63.10	0.00	63.10	21:39
	44	-1	0	50.82	1.24	60.55	1.38	59.17	21:40
	27	+1	1	38.70	1.00	57.25	0.00	57.25	21:43
	51	-0	1	-	-	-	-	-	22:00
	52	-1	0	-	-	-	-	-	22:30

Source: Own elaboration.

The cost and revenue for each route is illustrated as Table 9. The total profit is 2033 yuan and total cost is 1363 yuan. All of the penalty cost for vehicle is 0 and there are no passengers arriving late at the airport. In addition, a majority of passenger time window are met.

Table 9.  
Rebate and cost of each route.

Route	$R$	$C_1$	$C_2$	$C_3$	$C_4$	$P$
1	753.69	40	188.46	0	5	520.23
2	426.3	32.5	154.56	0	0	239.24
3	293.19	32.5	159.11	0	0	101.58
4	722.72	40	223.84	0	0	458.88
5	501.34	40	211.46	0	0	249.88
6	698.67	40	180.56	0	14.8	463.31
Total	3395.91	225	1117.99	0	19.8	2033.12

Source: Own elaboration.

Fare rebate is given to some passengers due to detours, shown in Table 10.

Table 10.  
Rebate passenger information.

Route	Point	Distance (km)		Basic fare (yuan)	Rebate (yuan)	Final fare (yuan)
		Ideal	Actual			
1	40	39.6	50.70	58.60	2.53	56.07
	25	39.8	53.10	58.90	4.25	54.65
4	39	39.8	48.76	60.38	0.80	59.58
	17	37.6	54.33	57.52	7.34	50.18
5	50	39	53.80	59.34	5.57	53.77
	44	40.9	50.81	60.55	1.38	59.17

Source: Own elaboration.

The layout of each route is shown in Fig. 11 (a) - 13 (b).

### 4.3 Comparison of connection methods

In order to compare different connection modes, it assumes the distribution of demand remains the same. Point 44 is taken as an example to compare each connection mode, and the calculation results are in Table 11. Due to the inability to measure the walking and waiting time of passengers, The travel time of airport bus and railway are its running time.

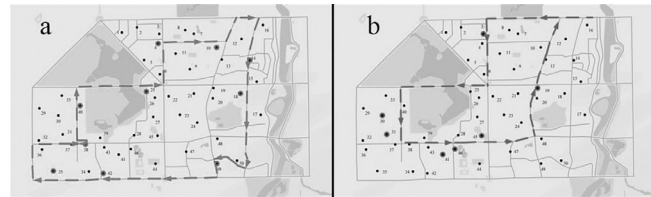


Figure 11 Vehicle routes 1-2 a) Route 1; b) Route 2.  
Source: Own elaboration.

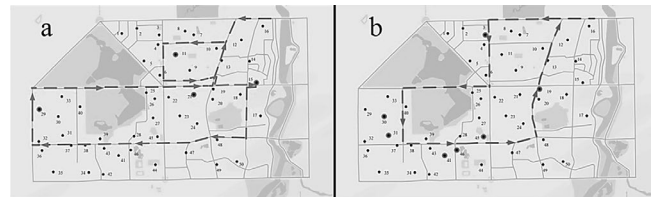


Figure 12 Vehicle routes 3-4 a) Route 3; b) Route 4.  
Source: Own elaboration.

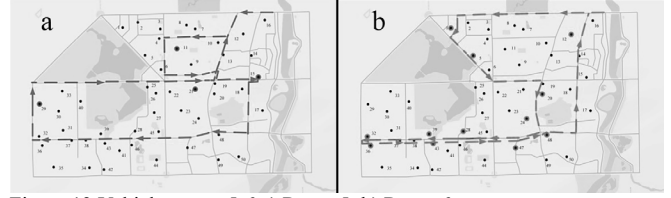


Figure 13 Vehicle routes 5-6 a) Route 5; b) Route 6.  
Source: Own elaboration.

Table 11.  
Comparison of each mode.

Indicator		Airport bus	Railway	Cab	ARB
Daytime	Travel time (min)	46	30	45	55
	Fare (yuan)	27	13	76	39
Night	Travel time (min)	-	-	45	55
	Fare (yuan)	-	-	76	48
Convenience		2	2	1	1

Note. '1': door-to-door, '2': non-door-to-door.

Source: Own elaboration.

No matter during the daytime or at night, even though ARB has a small increase in travel time compared to cab, the former is at least 39% less than the latter in terms of fare. As a consequence, ARB can attract most of the passengers. During the daytime, although the travel time for airport bus and railway is less than that of ARB, the former does not take walking time and waiting time into account, so it is highly likely that the former's is greater than that of the latter. Moreover, ARB offers door-to-door transportation compared to the other two modes, and despite the fact that its fare is relatively higher, it is still a good choice for those seeking efficiency or persons with large luggage.

## 5 Discussion

### 5.1 The ARB model balances cost and convenience.

The proposed ARB achieves a fare reduction of more than 39% compared with taxis through a bypass rebate mechanism and mixed vehicle scheduling, while the door-to-door service makes up for the shortcomings of traditional public transportation that requires walking, which verified the feasibility of "low cost + high adaptability".

### 5.2 A double breakthrough in pricing and algorithms

The pricing mechanism breaks through the limitations of traditional fixed fares and combines detour distance with time value, which solves the defect that dynamic pricing proposed by Emele [3] et al does not consider detours. Compared with traditional GA, the IAGA reduces the running time by 12%/14% and the number of iterations by 23%/35%, effectively avoiding the problem of premature convergence.

### 5.3 Limitations and future directions

The model assumes that there is no traffic congestion, but it is inevitable in practice. Future research will consider

integrating real-time traffic data to improve the model's adaptability.

As the case study with concentrated demand points, future research may partition cities into districts to set differentiated vehicle round-trip time limits based on demand distribution.

## 6 Conclusion

In order to meet the personalized travel demands and improve the quality and efficiency of airport connections, this paper proposes ARB mode, which improves convenience for passengers, avoids high fares, and provides a new choice. The main research content and innovation points of the paper are summarized as follows.

(1) This paper incorporates rebate mechanism into the model. The rebate mechanism makes it possible to accommodate benefits of both passengers and enterprise in the same objective function, which makes the model more reasonable.

(2) An IAGA is proposed. Setting the minimum crossover probability and mutation probability improves the evolutionary speed in the early stage and avoid it falling into local optimum while producing a better and faster result.

## References

- [1] Zhou, J., and Lam, W.H., A bi-level programming approach—Optimal transit fare under line capacity constraints. *Journal of advanced transportation*, 35(2), pp. 105-124, 2001. DOI: <https://doi.org/10.1002/atr.5670350204>
- [2] Borndörfer, R., Karbstein, M., and Pfetsch M.E., Models for fare planning in public transport, *Discrete Applied Mathematics*, 160(18), pp. 2591-2605, 2012. DOI: <https://doi.org/10.1016/j.dam.2012.02.027>
- [3] Emele, C.D., Oren, N., Zeng, C., Wright, S., Velaga, N., Nelson, J., Norman T.J., and Farrington, J., Agent-Driven variable pricing in flexible rural transport services, *Communications in Computer and Information Science*, 365, pp. 26-35, 2013. DOI: [https://doi.org/10.1007/978-3-642-38061-7\\_4](https://doi.org/10.1007/978-3-642-38061-7_4)
- [4] Kamel, I., Shalaby, A., and Abdulhai, B., A modelling platform for optimizing time-dependent transit fares in large-scale multimodal networks, *Transport Policy*, 92, pp. 38-54, 2020. DOI: <https://doi.org/10.1016/j.tranpol.2020.04.002>
- [5] Guo, Q., Sun, Y., Schonfeld, P., and Li, Z., Time-dependent transit fare optimization with elastic and spatially distributed demand, *Transportation Research Part A: Policy and Practice*, 148, pp. 353-378, 2021. DOI: <https://doi.org/10.1016/j.tra.2021.04.002>
- [6] Smith B.L., Demetsky M.J. and Durvasula P.K., A multiobjective optimization model for flexroute transit service design, *Journal of Public Transportation*, 6(1), pp. 81-100, 2003. DOI: <https://doi.org/10.5038/2375-0901.6.1.5>
- [7] Gebeyehu, M., and Takano, S.E., Demand responsive route design: GIS application to link downtowns with expansion areas[J]. *Journal of Public Transportation*, 11(1), pp. 43-62, 2008. DOI: <https://doi.org/10.5038/2375-0901.11.1.3>
- [8] Ye, Q., Ma, C., He, R., Xiao, Q., and Zhang, W., Multi-objective optimisation for taxi ridesharing route based on non-dominated sorting genetic algorithm, *Int. J. of Wireless and Mobile Computing*, 8(3), pp. 262-270, 2015. DOI: <https://doi.org/10.1504/IJWMC.2015.069409>
- [9] Li, H. and Kim, S., Efficient route planning for real-time demand-responsive transit, *Computers, Materials & Continua*, 79(1), pp. 473-492, 2024. DOI: <https://doi.org/10.32604/cmc.2024.048402>
- [10] Golden, B., Assad, A., Levy, L., and Gheysens, F., The fleet size and mix vehicle routing problem, *Computers & Operations Research*, 11(1), pp. 49-66, 1984. DOI: [https://doi.org/10.1016/0305-0548\(84\)90007-8](https://doi.org/10.1016/0305-0548(84)90007-8)
- [11] Tarantilis, C.D., Kiranoudis, C.T., and Vassiliadis, V.S., A list based threshold accepting metaheuristic for the heterogeneous fixed fleet vehicle routing problem, *Journal of the Operational Research Society*, 54(1), pp. 65-71, 2003. DOI: <https://doi.org/10.1057/palgrave.jors.2601443>
- [12] Dondo, R.G. and Cerdá, J., A hybrid local improvement algorithm for large-scale multi-depot vehicle routing problems with time windows, *Computers & Chemical Engineering*, 33(2), pp. 513-530, 2009. DOI: <https://doi.org/10.1016/j.compchemeng.2008.10.003>
- [13] Barkaoui, M. and Gendreau, M., An adaptive evolutionary approach for real-time vehicle routing and dispatching, *Computers & Operations Research*, 40(7), pp. 1766-1776, 2013. DOI: <https://doi.org/10.1016/j.cor.2013.01.022>
- [14] Goeke, D. and Schneider, M., Routing a mixed fleet of electric and conventional vehicles, *European Journal of Operational Research*, 245(1), pp. 81-99, 2015. DOI: <https://doi.org/10.1016/j.ejor.2015.01.049>
- [15] Gasque, D., and Munari, P., Metaheuristic, models and software for the heterogeneous fleet pickup and delivery problem with split loads, *Journal of Computational Science*, 59, 2022. DOI: <https://doi.org/10.1016/j.jocs.2021.101549>
- [16] Wang, L., Zeng, L., Ma, W., et al. Integrating passenger incentives to optimize routing for demand-responsive customized bus systems, *IEEE Access*, 9, pp. 21507-21521, 2021. DOI: <https://doi.org/10.1109/ACCESS.2021.3055855>
- [17] Han, S., Fu, H., Zhao, J., et al. Modelling and simulation of hierarchical scheduling of real-time responsive customised bus, *IET Intelligent Transport Systems*, 14(12), pp. 1615-1625, 2020. DOI: <https://doi.org/10.1049/iet-its.2020.0138>
- [18] Zhang, J., Huang, A., Jiang, R., et al. Flexible scheduling model of bus services between venues of the Beijing winter olympic games, *Journal of Advanced Transportation*, 2022(1), art. 2134806, 2022. DOI: <https://doi.org/10.1155/2022/2134806>

**J. Li**, received the BSc., MSc., and PhD in Department of Transportation Planning and Management, Jilin University, Changchun, China, in 1991, 1996, and 2003, respectively. From 2009 to 2010, she was a visiting scholar at the Department of Civil and Environmental Engineering at the University of Texas at Austin, USA. She is an associate professor at the Transportation College of Jilin University currently. Her research interests include transportation economics and urban and regional transportation planning. ORCID: 0000-0001-8783-4881

**L. Chen**, received the BSc. Eng. in 2022 from Jilin University, Jilin, China. He is now studying for MSc. in Department of Transportation Planning and Management, Jilin University. His research interests include scheduling and network planning in demand responsive transit. ORCID: 0009-0007-5251-5267

**X.W. Li**, received her BSc. and MSc. in Transportation Planning and Management from Jilin University, in 2020 and 2023, respectively. Her research interests include scheduling and network planning in flexible transit. ORCID: 0009-0001-5611-3528

**H.S. Liu**, received the BSc., MSc, and PhD in Department of Transportation Planning and Management, Jilin University, Changchun, China, in 2009, 2012, and 2015, respectively. He is currently an associate professor at the Transportation College of Jilin University. His research interests include traffic accident analysis, traffic simulation, and sustainable transportation. ORCID: 0000-0002-2635-999X

# Enhancing urban E-commerce efficiency: a fleet composition benchmark

Mauricio Peña-Acosta, Raúl Fabián Roldán-Nariño & Nicolás Rincón-García

*Departamento de Ingeniería Industrial, Pontificia Universidad Javeriana, Bogotá, Colombia. pena.mauricio@javeriana.edu.co, rroldan@javeriana.edu.co, nicolas.rincon@javeriana.edu.co*

Received: February 24<sup>th</sup>, 2025. Received in revised form: June 10<sup>th</sup>, 2025. Accepted: June 18<sup>th</sup>, 2025.

## Abstract

In Colombia's competitive e-commerce market, accurately estimating last-mile delivery fleets is essential for reducing operational costs. The absence of comprehensive models with operational constraints leads to inefficient resource use and limits sustainable practices. This study proposes a heterogeneous fleet composition model to reduce costs and integrate electric and low-consumption vehicles. The methodology includes a literature review, operational characterization of the target company, and an optimization model for a tactical planning period. A Monte Carlo simulation evaluates demand uncertainty through various scenarios. Results indicate a 9.92% cost reduction and over 200% increase in electric vehicle usage within the fleet, supporting environmental goals. The proposed model offers a decision-making benchmark for Colombian e-commerce companies, enhancing competitiveness and contributing to reduced urban pollution.

**Keywords:** last-mile; heterogeneous fleet composition; E-commerce, low-emission vehicles; Monte Carlo simulation

# Mejorando la eficiencia del comercio electrónico urbano: una referencia para la composición de flotas

## Resumen

En el competitivo mercado colombiano de comercio electrónico, estimar con precisión las flotas para la logística de última milla es clave para reducir los costos operativos. La falta de modelos integrales con restricciones operativas genera un uso ineficiente de recursos y limita prácticas sostenibles. Este estudio propone un modelo de composición de flota heterogénea orientado a disminuir costos e incorporar vehículos eléctricos y de bajo consumo. La metodología incluye una revisión bibliográfica, la caracterización operativa de la empresa objetivo y la formulación de un modelo de optimización para un periodo táctico de planificación. Mediante simulación Monte Carlo se evalúa la incertidumbre de la demanda en distintos escenarios. Los resultados muestran una reducción del 9,92 % en los costos y un aumento superior al 200 % en el uso de vehículos eléctricos, posicionando el modelo como una referencia para la toma de decisiones en empresas de comercio electrónico en Colombia, con beneficios económicos y ambientales.

**Palabras clave:** última milla; composición heterogénea de flota; comercio electrónico; vehículos de bajas emisiones; simulación Monte Carlo.

## 1 Introduction

E-commerce in Latin America has experienced increase in 2023, reaching 5.5% of total retail sales [1]. The COVID-19 pandemic accelerated this trend, introducing millions of new users to online shopping [2]. However, last-mile logistics in urban areas face challenges such as

significant growth, with a projected 25.6%

environmental regulations, traffic congestion, and insufficient infrastructure [3]. Major players like Mercado Libre, Rappi, Amazon, and Shopee are reshaping logistics to address these issues and meet regulatory demands [1,2].

**How to cite:** Peña-Acosta, M., Roldán-Nariño, R.F., and Rincón-García, N., Enhancing urban E-commerce efficiency: a fleet composition benchmark. DYNA, (92)238, pp. 19-25, July - September, 2025.

Last-mile logistics play a strategic role in operating costs and consumer perception. Despite its importance, fleet estimation is often performed empirically or using manual tools. While extensive research exists on the Vehicle Routing Problem (VRP), studies on strategic fleet composition remain limited [4].

A heterogeneous fleet composition model is proposed to optimize last-mile logistics by integrating real operational constraints. The model incorporates electric vehicles and alternative distribution methods to reduce costs and enhance efficiency within a tactical timeframe. It defines fleet requirements based on operational performance, vehicle capacity, and origin-destination matrices. Using insights from literature and service center-specific constraints, the model ensures cost savings, meets sales-driven capacity needs, and implements sustainable transport solutions.

The proposed model undergoes performance evaluation by incorporating stochastic demand behavior, defining an acceptable error margin, and estimating confidence intervals. The results are compared against existing costs, assessing potential improvements and replication feasibility in other last-mile operations to strengthen Colombia's logistics sector.

## 2 Literature review

The rapid expansion of e-commerce has transformed customer expectations regarding delivery speed, traceability, customization, and location flexibility [5]. However, the concentration of deliveries in urban areas presents significant environmental, regulatory, and logistical challenges [6]. Consequently, last-mile logistics have evolved to integrate sustainability, customer-centric strategies, and cost-efficiency [7].

Last-mile delivery, accounting for up to 50% of total supply chain costs, is critical for customer satisfaction but faces challenges such as demand uncertainty and seasonal variations [7]. Mathematical programming models have been employed to optimize demand management in this context [8,9]. Furthermore, integrating production and distribution remains a complex issue due to fluctuating demand and logistical constraints, addressed through routing optimization algorithms [10,11].

Urban delivery operations are influenced by traffic regulations, congestion, and access restrictions. Load consolidation models have been proposed to improve efficiency [12], while the impact of e-commerce on transport policies has been analyzed through consumer surveys [13].

Fleet composition further complicates last-mile logistics, as heterogeneous fleets introduce additional constraints related to cost, route length, work shifts, and environmental impact [4,14-16].

Fleet optimization methodologies encompass mathematical programming for demand-based vehicle allocation [17-20], heuristic and metaheuristic approaches for solving complex routing problems [21-26], and machine learning techniques for demand forecasting [27,28]. Stochastic variables are frequently integrated into heterogeneous fleet models to address demand uncertainty, employing dynamic programming [21], two-stage optimization frameworks [17,29], and decision tree-based fleet analysis [20].

Research on stochastic vehicle routing predominantly relies on exact methods (51%), followed by metaheuristics (32%) [30]. Multi-stage stochastic optimization has been applied using Sample Average Approximation (SAA) [31], while Monte Carlo simulations have demonstrated effectiveness in fleet cost evaluation [29]. These methodologies contribute to the ongoing development of robust and efficient fleet composition models for last-mile logistics.

## 3 Problem statement

The case study examines a Colombian e-commerce company operating twelve service centers in major cities and surrounding areas. These centers function as cross-docking platforms, dispatching parcels without storage. Parcel destinations are typically confirmed six hours before departure, requiring volume estimates for fleet planning, with tactical projections set four months in advance and strategic projections one year ahead. The vehicle fleet consists of logistics provider alliances (small vans, electric motorcycles, conventional motorcycles, and electric vans) and owned vehicles, all subject to geographic and security constraints, as detailed in Table 1.

Currently, vehicle allocation is performed manually, with monthly calculations and updates 24 hours before departure, disregarding package volume and specific destinations. This results in inefficiencies, including a 9.44% reserve fleet requirement and an additional 1.95% fleet allocation due to routing mismatches and oversized packages. In total, 11.39% of the chartered fleet is used to compensate for these inefficiencies.

Table 1.  
Types of vehicles that can be used.

Vehicle Type	Geography	Security	Autonomy	Package Size
Small Van	All	No zone restriction, can carry an assistant	Unlimited	All
Company-Branded Small Van	All	Zone restrictions due to theft risk, can carry an assistant	Unlimited	All
Auto Rickshaw	Flat	Zone restrictions, cannot carry an assistant	Limited to 60 km	Volume restricted
Motorcycles	All	No zone restriction, cannot carry an assistant	Unlimited	Volume restricted
Electric Van	All	Zone restrictions due to theft risk, can carry an assistant	Limited to 80 km	All
Crowdsourcing	All	No zone restriction, cannot carry an assistant	Limited to 40 km	Volume restricted
Delivery Cell	All	Zone restrictions, cannot carry an assistant	Limited to 5 km	Volume restricted

Source: Created by the authors

Table 2.  
Operational characterization.

	Service center	Areas to be served	Type of product	Type of vehicle	Operational period
	12 service centers	148 nodes	3 typologies	9 typologies	6 days
Characterization		Areas to be served from each service center	- Demand	- Cost per vehicle - Capacity limits - Type of contract (own / rented)	- Forecast performance evaluation

Source: Created by the authors

Given Colombia's competitive e-commerce landscape, costs is essential. A more efficient approach would enhance fleet utilization by incorporating electric and low-consumption vehicles while considering geographic and volumetric constraints. This strategy would not only reduce operational costs and fleet procurement expenses but also minimize emissions and urban traffic congestion. The research proposes a heterogeneous fleet composition model that integrates sustainable transport solutions to optimize operational efficiency. The key vehicle allocation parameters and constraints are summarized in Table 1.

#### 4 Data analysis

A structured framework for fleet composition modeling is proposed, based on a comprehensive bibliographic review. The framework characterizes operational logistics by defining a distribution network through destination nodes and clustering final customers according to geographic and cost-related factors.

Volumetric package characterization is conducted using a 12-month historical sales analysis, segmenting products into small, medium, and large categories. This segmentation aligns with vehicle load capacities, restricting large packages to high-capacity vehicles. Historical parcel data informs projected volumes per destination, facilitating the construction of an estimation matrix.

Fleet operations are characterized by evaluating loading and travel times, work shifts, delivery durations, capacity constraints, and route dispersion limits over a 12-month period. Additionally, an origin-destination tariff matrix is developed to determine vehicle operating costs, incorporating surcharges for remote deliveries. A summary of these key elements is presented in Table 2.

Finally, a sales forecast analysis compares actual versus estimated performance, assessing error margins by service center and target population. This analysis, fundamental for the stochastic evaluation of the model, will be presented in a subsequent section.

#### 5 Deterministic fleet composition model

We will first take models developed by [17,18] Next, the formulation of a proposal for a mixed integer linear programming mathematical model is detailed, taking the data in the previous chapter as the source for an evaluation period of a typical week. The percentage share of demand for each destination node is taken as fixed for the model, and a

optimizing last-mile delivery maximum limit of packages is defined for each type of vehicle. Regarding this model, volumetric capacity restrictions associated with the characteristics of the packages are defined to each area.

##### Model notation

Definition of the sets precedes the presentation of the parameters and decision variables, as shown in Tables 3 to 5. The section concludes with the mathematical model that integrates these components into a coherent and structured formulation

Table 3.  
Model sets.

Notation	Description
I	Areas to be served
K	Types of vehicle to rent
M	Types of vehicle to own
T	Operation day

Source: Created by the authors

Table 4.  
Model parameters.

Notation	Name
$D_{it}$	Demanded delivery in area I in day t
$RCAP_k$	Capacity of rented vehicle type k
$OCAP_m$	Capacity of owned vehicle type m
$CR_{kt}$	Cost of operating rented vehicle type k per day
$CO_m$	Cost of owned vehicle type m in planning period
$RE_{ik}$	1: If area i can be served with rented vehicle type k, 0: otherwise
$OE_{im}$	1: If area i can be served with owned vehicle type m, 0: otherwise

Source: Created by the authors

Table 5.  
Model variables.

Notation	Name
$RV_{kt}$	Number of rented vehicles of type k to rent in day t
$OV_m$	Number of vehicles of type m to be owned
$RVD_{kit}$	Number of rented vehicles of type k to serve zone i in day t
$OVD_{mit}$	Number of owned vehicles of type m to serve zone i in day t

Source: Created by the authors

#### 6 Objective function

The objective function minimizes the total vehicle operating cost in period intervals, there are two sets of type of vehicles i) Rented Vehicles and ii) Owned Vehicles. This implies that the number of rented vehicles may vary each day, whereas the number of owned



vehicles remains fixed throughout the entire time horizon (1).

$$\min Z = \sum_k^K \sum_t^T CR_{kt} \cdot RV_{kt} + \sum_m^M CO_m OV_m$$

Restrictions

The following is a list of the restrictions contemplated in the model:

$$\sum_i^I RVD_{kit} \leq RV_{kt} \quad \forall k \in K, t \in T \quad (2)$$

$$\sum_i^I OVD_{mit} \leq OV_m \quad \forall m \in M, t \in T \quad (3)$$

$$\sum_k^K RCAP_k \cdot RVD_{kit} + \sum_m^M OCAP_m \cdot OVD_{mit} \geq D_{it} \quad \forall i \in I, t \in T \quad (4)$$

$$\frac{D_{it}}{\sum_k^K RVD_{kit} + \sum_m^M OVD_{mit}} \leq 48 \quad \forall i \in I, t \in T \quad (5)$$

$$RCAP_k \cdot RVD_{kit} \leq RE_{ki} \cdot D_{it} \quad \forall i \in I, t \in T, \forall k \in K \quad (6)$$

$$OCAP_m \cdot OVD_{mit} \leq OE_{im} \cdot D_{it} \quad \forall i \in I, t \in T, \forall m \in M \quad (7)$$

Eq. (2) constrains that the number of rented vehicles sent to each area in each day cannot be greater than the total vehicles to rent in each day. Eq. (3) constrains that the number of owned vehicles sent to each area in each day cannot be greater than the total vehicles to own. Eq. (4) ensures that the demand of each area is satisfied according to the capacity and number of vehicles sent to that area in that day. Eq. (5) ensures that in average vehicle are not planned with more than 48 deliveries to satisfy a working day (10 min per delivery). Eq. (6) ensures that vehicles are not sent to areas that cannot be served with that type of rented vehicle, Eq. (7) ensures that vehicles are not sent to areas that cannot be served with that type of owned vehicle.

The model is implemented using the open-source optimization package Pyomo in Python. Pyomo is selected for its compatibility with mathematical notation, ease of under stochastic demand conditions.

$$Q(\varepsilon) = E \left[ \min Z = \sum_k^K \sum_t^T CR_{kt} \cdot RV_{kt} + \sum_m^M CO_m OV_m \right] \quad (8)$$

$$(\varepsilon) = \frac{1}{N} \sum_{\varepsilon=1}^N [Q(\varepsilon)] \quad (9)$$

defining constraints, and integration with data handling (Pandas), graphing (matplotlib), and stochastic modeling (pysp). It supports multiple solvers, including AMPL, CBC, CPLEX, Gurobi, and GLPK, offering flexibility in both commercial and freeware environments.

The proposed model presents certain limitations derived from its own structural assumptions. First, by assuming that the number of owned vehicles remains fixed throughout the entire planning horizon, operational flexibility is constrained in the face of demand fluctuations or unforeseen events. Although the model allows for daily variability in the number of rented vehicles, this is bounded by a maximum daily limit, which may lead to bottlenecks in areas with high demand. Additionally, the model does not account for costs associated with vehicle underutilization or penalties for unmet demand. The constraint of a maximum of 48 deliveries per day, based on an average of 10 minutes per delivery, overlooks potential variations in traffic conditions, service times, and the geographical dispersion of delivery points. Finally, while the restrictions on vehicle accessibility by type are necessary, they may limit service coverage without offering alternative mechanisms to address these areas, potentially compromising overall system efficiency in more complex real-world scenarios.

## 7 Monte Carlo simulation

After defining the deterministic model, the stochastic behavior of demand is integrated into the fleet composition model. A historical analysis of forecast accuracy over the past 15 months is conducted, evaluating normal, logistic, exponential, gamma, and beta distributions using sum of squared errors (SSE), p-value, and Akaike's Information Criterion (AIC) (Table 6). The logistic distribution is identified as the best fit due to its lowest AIC value.

Based on the forecast analysis, a set of stochastic demand parameters ( $\varepsilon$ ) is generated to estimate operating costs. Using Sample Average Approximation (SAA), the expected cost function (Eq. 8) is reformulated (Eq. 9) under a logistic distribution. The required sample size ( $N$ ) for a 95% confidence level is determined as 80 (Eq. 10), considering idle vehicle costs. Monte Carlo simulation is then applied to compute confidence intervals (Eq. 11) and estimate the expected error (Eq. 12), ensuring robust fleet composition modeling

$$N = \left( \frac{Z_{95\%} \times \sigma}{ME} \right)^2 = 80.4 \approx 80 \quad (10)$$

$$\bar{X} \mp Z_{95\%} \times \frac{\sigma}{\sqrt{N}} \quad (11)$$

$$Error = \frac{Sup. interval - Inf. interval}{2} \quad (12)$$

Table 6.  
Input analysis results.

Created by the authorsCriteria	Normal	Logistic	Exponential	Gamma	Beta
SSE	0.0726	0.0363	0.4161	0.0761	0.0739
AIC	1.3768	0.6854	3.1232	3.4249	5.3943
P-Value	0.0358	0.6876	0.0020	0.0239	0.0311

Source: Created by the authors

Table 7.

Fleet composition model scenarios.

Source: Created by the authors

	Current Scenario	Deterministic Results	Mean	Inferior Interval	Superior Interval
<b>Total cost (M COP)</b>	\$436,400	\$397,000	\$395,700	\$394,600	\$396,900
<b>Demand</b>	151.140	151.140	151.401	149.697	152.049
<b>Vehicles</b>	2.415	2.454	2.438	2.432	2.418
<b>Cost per package</b>	\$2,888	\$2,627	\$2,614	\$2,636	\$2,611
<b>Cost per vehicle</b>	\$180,717	\$161,800	\$162,335	\$162,260	\$164,155
<b>Saving vs actual Cost per Vehicle</b>	0.000%	11.690%	11.320%	11.370%	10.090%

Source: Created by the authors

## 8 Results

The company's operations were analyzed through an origin-destination matrix, defining routes by distance, geographic restrictions, and service cost. A 12-month sales analysis identified package volume profiles per destination, and historical demand share was assessed. Vehicle typologies were characterized based on key operational parameters, including load and travel time, work shifts, and volumetric constraints. A tariff matrix with surcharges for remote areas was also developed.

The deterministic fleet composition model optimized vehicle allocation, identifying cost-efficient distribution methods. Execution time was 3.4 minutes on an Intel Core i5-337U with 4GB RAM. The model prioritized vehicles with lower costs per package while considering volume constraints, leading to 9.92% operational savings, reaching up to 28.6% in specific service centers. Savings varied across locations, and compliance with demand restrictions, work shifts, and geographic distribution was validated. Fig. 1 compares the current and proposed fleet compositions.

A Monte Carlo simulation with 80 demand scenarios assessed model robustness, requiring 58.1 minutes for execution. Cost per vehicle savings of 11.69% were observed in the deterministic model, with a stochastic savings estimate of 11.32% at a 95% confidence level, even in worst-case scenarios yielding a 10.09% cost reduction. The model error was \$1,155,621 (0.29% of total costs). Table 7 presents cost and demand variations, showing reduced inefficiencies.

Electric vehicle use increased by 277%, from 20 to 86 units per week, while motorcycle-type vehicles decreased from 24 to 14 units. Low-emission motorcycles increased by 57%, reducing costs and CO<sub>2</sub> emissions. The standard deviation in fleet size was 87 weekly units, with daily variations of 3.6%. Compared to the current 11.39% inefficiency, this represents a potential 7.79% fleet reduction. Even in outlier scenarios, savings of 6.76% were achieved despite a 2.56% demand increase. Fig. 2 details the fleet composition adjustments.

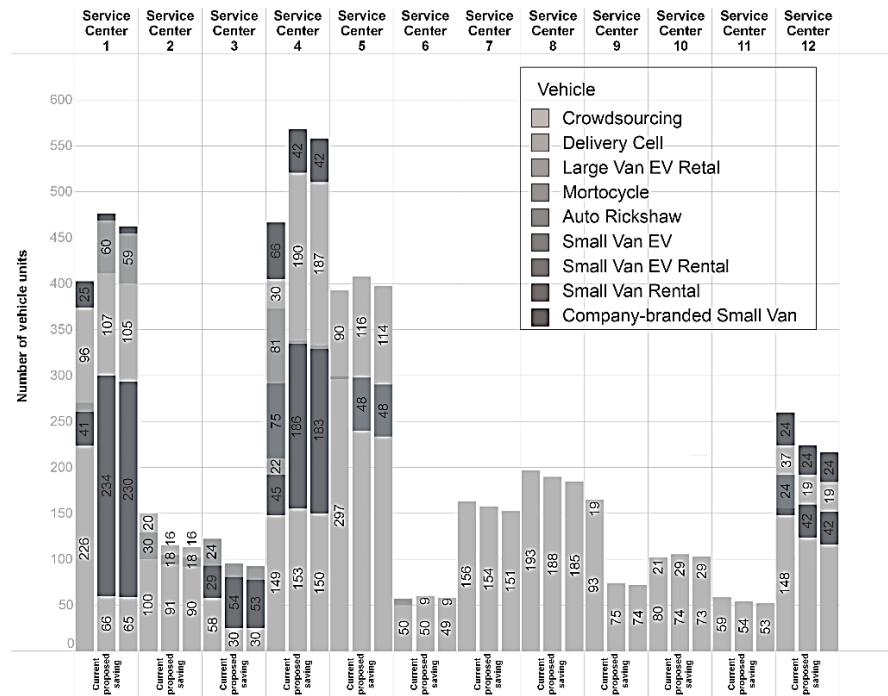


Figure 1. Linear programming model execution results.

Source: Created by the authors

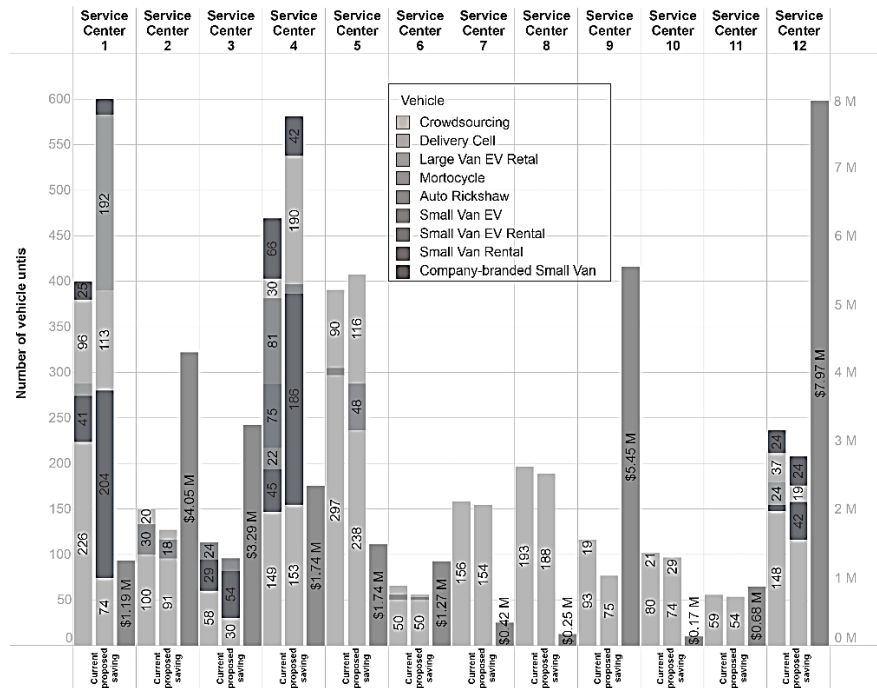


Figure 2. Results comparison.  
Source: Created by the authors

## 9 Conclusions and future research

The objective was to propose a heterogeneous fleet composition model to determine the fleet required to reduce operating costs in last-mile logistics for an e-commerce company in Colombia. This goal was achieved by incorporating key operational constraints and demonstrating an expected cost reduction of 9.92% under a deterministic model. Additionally, the integration of stochastic demand behavior led to an expected savings of 10.27% under uncertainty conditions. This result highlights the relevance of combining deterministic models with stochastic components to better reflect and predict real-world dynamics.

Practically, the model offers companies a structured approach to defining fleet size and type, facilitating informed decisions that align with both cost-efficiency and operational feasibility. The proposed methodology supports replication in similar last-mile logistics contexts and enables the creation of a tailored fleet strategy based on actual operational characteristics. For decision-makers, this provides a robust analytical tool to evaluate trade-offs, anticipate variability in demand, and justify investments in diverse vehicle types, including electric or low-emission alternatives.

Furthermore, the development of a comprehensive reference framework for heterogeneous fleet composition—based on key research trends and solution methods—provides a valuable resource for practitioners seeking to optimize logistics operations. The application of Monte Carlo simulation enhances the model's utility by offering confidence intervals for scenario-based planning, thereby

strengthening its use in real-world strategic decision-making. Future work may incorporate two-stage stochastic programming to further enhance the probabilistic robustness of the model.

## Funding

This research did not receive additional funding beyond an academic investigation within the university

## References

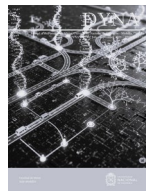
- [1] McKinsey and Company. E-commerce in Latin America: Building trust, [online], 2023 Available at: <https://www.mckinsey.com/industries/retail/our-insights/e-commerce-in-latin-america-building-trust>.
- [2] Oxford Business Group. How Covid-19 triggered a Latin American e-commerce boom. [online], 2021 Available at: <https://oxfordbusinessgroup.com/news/how-covid-19-triggered-latin-american-e-commerce-boom>.
- [3] Think with Google. The future of e-commerce in Latin America. [online], 2021 Available at: <https://www.thinkwithgoogle.com/intl/en-154/consumer-insights/consumer-trends/future-e-commerce-latin-america>.
- [4] Jabali, O., Gendreau, M., and Laporte, G.A., Continuous approximation model for the fleet composition problem. *Transportation Research Part B: Methodological*, 46(10), pp. 1591–1606, 2012. DOI: <https://doi.org/10.1016/j.trb.2012.06.004>
- [5] Janjevic, M., and Winkenbach, M., Characterizing urban last-mile distribution strategies in mature and emerging e-commerce markets. *Transportation Research Part A: Policy and Practice*, 133, pp. 164–196, 2020. DOI: <https://doi.org/10.1016/j.tra.2020.01.003>
- [6] Janjevic, M., Winkenbach, M., and Merchán, D., Integrating collection-and-delivery points in the strategic design of urban last-mile e-commerce distribution networks. *Transportation Research Part E:*

- Logistics and Transportation Review, 131, pp. 37–67, 2019. DOI: <https://doi.org/10.1016/j.tre.2019.09.001>
- [7] Peppel, M., Ringbeck, J., and Spinler, S., How will last-mile delivery be shaped in 2040? A Delphi-based scenario study. *Technological Forecasting and Social Change*, 177, art. 121493, 2021. DOI: <https://doi.org/10.1016/j.techfore.2022.121493>
- [8] Errico, F., Crainic, T.G., Malucelli, F., and Nonato, M.A., survey on planning semi-flexible transit systems: Methodological issues and a unifying framework. *Transportation Research Part C: Emerging Technologies*, 36, pp. 324–338, 2013. DOI: <https://doi.org/10.1016/j.trc.2013.08.010>
- [9] Uchoa, E., Pecin, D., Pessoa, A., Poggi, M., Vidal, T., and Subramanian, A., New benchmark instances for the capacitated vehicle routing problem. *European Journal of Operational Research*, 257(3), pp. 845–858, 2017. DOI: <https://doi.org/10.1016/j.ejor.2016.08.012>
- [10] Adulyasak, Y., Cordeau, J.F., and Jans, R., The production routing problem: a review of formulations and solution algorithms. *Computers and Operations Research*, 55, pp. 141–152, 2015. DOI: <https://doi.org/10.1016/j.cor.2014.01.011>
- [11] Li, Y., Chu, F., and Feng, C., Integrated production inventory routing planning for intelligent food logistics systems. *IEEE Transactions on Intelligent Transportation Systems*, 20(3), pp. 867–878, 2019. DOI: <https://doi.org/10.1109/TITS.2018.2839900>
- [12] Simoni, M.D., Bujanovic, P., Boyles, S.D., and Kutanoglu, E., Urban consolidation solutions for parcel delivery considering location, fleet and route choice. *Case Studies on Transport Policy*, 6(1), pp. 112–124, 2018. DOI: <https://doi.org/10.1016/j.cstp.2017.11.002>
- [13] Björger, A., Bjerkan, K.Y., and Hjelkrem, O.A., E-groceries: sustainable last mile distribution in city planning. *Research in Transportation Economics*, 87, art. 100805, 2021. DOI: <https://doi.org/10.1016/j.retrec.2019.100805>
- [14] Hoff, A., Andersson, H., Christiansen, M., Hasle, G., and Løkketangen, A., Industrial aspects and literature survey: fleet composition and routing. *Computers and Operations Research*, 37(12), pp. 2041–2061, 2010. DOI: <https://doi.org/10.1016/j.cor.2010.03.015>
- [15] Islam, M.A., and Gajpal, Y., Optimization of conventional and green vehicles composition under carbon emission cap. *Sustainability (Switzerland)*, 13(12), art. 6940, 2021. DOI: <https://doi.org/10.3390/su13126940>
- [16] Al-dal'ain, R., and Celebi, D., Planning a mixed fleet of electric and conventional vehicles for urban freight with routing and replacement considerations. *Sustainable Cities and Society*, 73, art. 103105, 2021. DOI: <https://doi.org/10.1016/j.scs.2021.103105>
- [17] Mardaneh, E., Lin, Q., and Loxton, R.A., Heuristic algorithm for optimal fleet composition with vehicle routing considerations. *Optimization Methods and Software*, 31(2), pp. 272–289, 2016. DOI: <https://doi.org/10.1080/10556788.2015.1062890>
- [18] Pinto, R., and Lagorio, A., Supporting the decision-making process in the urban freight fleet composition problem. *International Journal of Production Research*, art. 1753896, 2021. DOI: <https://doi.org/10.1080/00207543.2020.1753896>
- [19] List, G.F., Wood, B., Nozick, L.K., Turnquist, M.A., Jones, D.A., Kjeldgaard, E.A., and Lawton, C.R., Robust optimization for fleet planning under uncertainty. *Transportation Research Part E: Logistics and Transportation Review*, 39(3), pp. 209–227, 2003. DOI: [https://doi.org/10.1016/S1366-5545\(02\)00026-1](https://doi.org/10.1016/S1366-5545(02)00026-1)
- [20] Serrano-Hernandez, A., Cadarso, L., and Faulin, J.A., Strategic multistage tactical two-stage stochastic optimization model for the Airline Fleet Management Problem. *Transportation Research Procedia*, 47, pp. 473–480, 2020. DOI: <https://doi.org/10.1016/j.trpro.2020.03.152>
- [21] Loxton, R., Lin, Q., and Teo, K.L., A stochastic fleet composition problem. *Computers and Operations Research*, 39(12), pp. 3177–3184, 2012. DOI: <https://doi.org/10.1016/j.cor.2012.04.004>
- [22] Lee, Y.H., Kim, J.I., Kang, K.H., and Kim, K.H., A heuristic for vehicle fleet mix problem using tabu search and set partitioning. *Journal of the Operational Research Society*, 59(6), pp. 833–841, 2008. DOI: <https://doi.org/10.1057/palgrave.jors.2602421>
- [23] Stavropoulou, F., The consistent vehicle routing problem with heterogeneous fleet. *Computers and Operations Research*, 140, art. 105644, 2021. DOI: <https://doi.org/10.1016/j.cor.2021.105644>
- [24] Repoussis, P.P., and Tarantilis, C.D., Solving the fleet size and mix vehicle routing problem with time windows via adaptive memory programming. *Transportation Research Part C: emerging Technologies*, 18(5), pp. 695–712, 2010. DOI: <https://doi.org/10.1016/j.trc.2009.08.004>
- [25] Keskin, M., and Çatay, B., Partial recharge strategies for the electric vehicle routing problem with time windows. *Transportation Research Part C: Emerging Technologies*, 65, pp. 111–127, 2016. DOI: <https://doi.org/10.1016/j.trc.2016.01.013>
- [26] Goeke, D., and Schneider, M., Routing a mixed fleet of electric and conventional vehicles. *European Journal of Operational Research*, 245(1), pp. 81–99, 2015. DOI: <https://doi.org/10.1016/j.ejor.2015.01.049>
- [27] Jun, S., and Lee, S., Evolutionary neural network for learning of scalable heuristics for pickup and delivery problems with time windows. *Computers and Industrial Engineering*, 169, art. 108282, 2021. DOI: <https://doi.org/10.1016/j.cie.2022.108282>
- [28] Oudouar, F., Lazaar, M., and El Miloud, Z., A novel approach based on heuristics and a neural network to solve a capacitated location routing problem. *Simulation Modelling Practice and Theory*, 100, art. 102064, 2019. DOI: <https://doi.org/10.1016/j.simpat.2019.102064>
- [29] Malladi, S.S., Christensen, J.M., Ramirez, D., Larsen, A., and Pacino, D., Stochastic fleet mix optimization: Evaluating electromobility in urban logistics. *Transportation Research Part E: Logistics and Transportation Review*, 158, art. 102554, 2020. DOI: <https://doi.org/10.1016/j.tre.2021.102554>
- [30] Martínez-Bernal, J., Cuervo-Cruz, R.A., y Orjuela-Castro, J.A., Modelos logísticos estocásticos: una revisión de la literatura. *Aibi Revista de Investigación, Administración e Ingeniería*, 8(S1), pp. 269–285, 2021. DOI: <https://doi.org/10.15649/2346030x.2470>
- [31] Shapiro, A., and Philpott, A., A tutorial on stochastic programming. Manuscript, pp. 1–35, 2007. Available at: <http://stoprog.org/stoprog/SPTutorial/TutorialSP.pdf>, 2007.

**M. Peña-Acosta**, is a MSc in Industrial Engineering with specialized training in Logistics and Transportation. He has extensive experience in designing distribution models aimed at resource optimization, strengthening commercial strategies, and evaluating frameworks that ensure a meaningful impact on customer experience. He currently serves as Control Tower Supervisor – Routing at Mercado Libre, where he leads operational strategies for efficient route management and data-driven decision-making within the supply chain.  
ORCID: 0009-0002-6868-4368

**R.F. Roldán-Nariño**, is a Bsc. Eng. in Electronic Design and Automation Engineer from the Universidad de La Salle in Bogotá, Colombia. He holds a MSc. in Industrial Engineering from the Universidad Distrital Francisco José de Caldas and a PhD. in Engineering from the Mondragon University in Spain. He currently leads the operations research section in the Department of Industrial Engineering, where he oversees academic and research projects focused on the optimization and analysis of production systems. His main research interests include logistics and supply chain management, with an emphasis on operational efficiency and decision-making supported by quantitative models.  
ORCID: 0000-0001-6315-999X

**N. Rincón-García**, is a Bsc. Eng. In Industrial Engineer from the Pontificia Universidad Javeriana in Bogotá, Colombia. MSc. in Logistics and Supply Chain Management from the University of Westminster in London, UK, and a PhD. in Engineering from the University of Southampton, also in the UK. He is currently the director of the Master's Program in Intelligent Supply Chain Management at Pontificia Universidad Javeriana, where he leads academic and research initiatives aimed at transforming logistics systems through the adoption of advanced technologies and sustainable approaches.  
ORCID: 0000-0001-9214-982X



## Integration of AI, RPA and Big Data in strategic accounting management and consulting: perspectives and challenges

William Alberto Guerrero <sup>a</sup>, Stefanny Camacho-Galindo <sup>a</sup>, Laura Estefanía Guerrero-Martin <sup>a</sup>, John Carlos Arévalo <sup>a</sup> & Camilo Andrés Guerrero-Martin <sup>b,c,d</sup>

<sup>a</sup> Fundación de Educación Superior San José, Bogotá, Colombia. waguerrero@hotmail.com, setefa110992@gmail.com, guerrero.laura.9705@gmail.com, john.c.arevalo@gmail.com.

<sup>b</sup> Federal University of Pará – Campus Salinópolis - Department of Engineering (FAE), Salinópolis, PA, Brazil. camilo.guerrero@poli.ufpr.br

<sup>c</sup> Grupo de pesquisa em Energia e Mar, Universidade Federal do Pará.

<sup>d</sup> Universidade Federal do Pará, Programa de Pós-Graduação em Engenharia Mecânica. Belém, PA, Brasil

Received: February 9<sup>th</sup>, 2025. Received in revised form: May 19<sup>th</sup>, 2025. Accepted: May 28<sup>th</sup>, 2025.

### Abstract

The integration of advanced technologies such as Artificial Intelligence (AI), Robotic Process Automation (RPA) and Big Data is revolutionizing strategic accounting management and consulting. AI optimizes repetitive tasks, improves accuracy in financial data processing and facilitates fraud detection. RPA automates audits, reconciliations and reporting, reducing errors and increasing operational efficiency. Big Data, on the other hand, improves the analysis of financial trends and risk management, enabling more strategic decisions. However, the implementation of these technologies faces significant challenges: resistance to organizational change, digital skills gaps, the need for a robust technological infrastructure and regulatory compliance in data security. This study employs a mixed methodology, combining a systematic literature review, case studies in accounting firms in Colombia and Brazil (PwC, Datactil) and interviews with accounting and technology experts. The findings indicate that while the adoption of AI, RPA and Big Data improves efficiency and client confidence, their success depends on continuous training, change management strategies and sound regulatory frameworks. It is concluded that these technologies are redefining modern accounting, promoting more informed decisions and increasing the competitiveness of the financial sector

**Keywords:** efficiency; automation; predictive analytics; risk management; decision making and technology integration.

## Integración de IA, RPA y Big Data en la gestión y consultoría estratégica contable: perspectivas y desafíos

### Resumen

La integración de tecnologías avanzadas como la Inteligencia Artificial (IA), la Automatización Robótica de Procesos (RPA) y Big Data está revolucionando la gestión y consultoría contable estratégica. La IA optimiza tareas repetitivas, mejora la precisión en el procesamiento de datos financieros y facilita la detección de fraudes. La RPA automatiza auditorías, conciliaciones y generación de informes, reduciendo errores y aumentando la eficiencia operativa. Big Data, por su parte, mejora el análisis de tendencias financieras y la gestión de riesgos, permitiendo decisiones más estratégicas. No obstante, la implementación de estas tecnologías enfrenta desafíos significativos: resistencia al cambio organizacional, brechas en competencias digitales, necesidad de una infraestructura tecnológica robusta y cumplimiento normativo en seguridad de datos. Este estudio emplea una metodología mixta, combinando revisión sistemática de literatura, estudios de caso en firmas contables de Colombia y Brasil (PwC, Datactil) y entrevistas con expertos en contabilidad y tecnología. Los hallazgos indican que, si bien la adopción de IA, RPA y Big Data mejora la eficiencia y confianza del cliente, su éxito depende de capacitación continua, estrategias de gestión del cambio y marcos regulatorios sólidos. Se concluye que estas tecnologías están redefiniendo la contabilidad moderna, promoviendo decisiones más informadas y aumentando la competitividad del sector financiero.

**Palabras clave:** eficiencia; automatización; análisis predictivo; gestión de riesgos; toma de decisiones e integración tecnológica.

**How to cite:** Guerrero, W.A., Camacho-Galindo, S., Guerrero-Martin, L.E., Arévalo, J.C., and Guerrero-Martin, C.A., Integration of AI, RPA and Big Data in strategic accounting management and consulting: perspectives and challenges. DYNA, (92)238, pp. 26-34, July - September, 2025.



## 1 Introduction

Modern accounting is undergoing an unprecedented transformation driven by the integration of Artificial Intelligence (AI), Robotic Process Automation (RPA), and Big Data. These disruptive technologies are not merely automating routine tasks but are actively redefining how financial information is processed, interpreted, and used for strategic decision-making. AI has proven capable of automating repetitive processes, analyzing vast datasets, and detecting fraudulent activities in real time, which significantly enhances the analytical capacity of organizations [1]. Meanwhile, RPA has brought measurable improvements in core accounting operations, such as account reconciliation, internal auditing, and the generation of financial statements, by reducing lead times and minimizing human error [2-4]. Big Data, through predictive modeling and data mining, enables the identification of behavioral patterns in financial activity, thereby strengthening risk management systems and improving the accuracy of economic forecasts [5-7].

Despite their benefits, the implementation of these technologies presents significant challenges. Organizational resistance to change, the lack of professionals with advanced digital and cybersecurity skills, and the need for substantial investment in technological infrastructure remain key obstacles [8-10]. In addition, companies must address growing concerns regarding regulatory compliance, especially when managing large volumes of sensitive financial data under privacy and data protection standards [11-13].

This study adopts a mixed-methods approach, combining a systematic literature review, case studies of prominent firms such as PwC and Dataciti, and fieldwork involving structured surveys and interviews with accounting and technology experts. It seeks to address the following research questions:

1. How do Artificial Intelligence, Robotic Process Automation, and Big Data affect the efficiency and accuracy of accounting processes?
2. What organizational, technical, and regulatory challenges hinder the effective adoption of these technologies in accounting firms?
3. Which practical strategies can accounting professionals and firms apply to successfully implement these technologies in real-world settings?

By addressing these questions, the study aims to provide an integrated understanding of the opportunities and limitations associated with digital transformation in accounting and to offer actionable insights for its successful adoption, particularly in emerging market contexts

## 2 Theoretical framework

Modern accounting is undergoing an accelerated transformation process due to the integration of emerging technologies such as Artificial Intelligence (AI), Robotic Process Automation (RPA), and Big Data. These technologies have reshaped financial management by improving operational efficiency, increasing the accuracy of

data analysis, and enabling more strategic decision-making [1-3]. Through automation, organizations can reduce human error, detect complex patterns, and manage large volumes of financial data in real time.

AI, in particular, has played a central role in this transformation. Its capabilities include advanced fraud detection, predictive analysis, and the automation of complex reports, enhancing decision-making at multiple levels [4-6,40]. Studies demonstrate that AI can audit transactions in real time, reduce risk exposure, and increase the transparency of accounting processes [7]. However, its adoption continues to face challenges such as resistance to change, lack of skilled personnel in data analytics, and the need for investment in technological infrastructure [8, 9].

Likewise, RPA has enabled significant improvements in accounting operations. By automating routine tasks such as account reconciliation, invoice processing, and internal auditing, RPA reduces cycle times and increases consistency [10,11]. Companies like PwC and Dataciti have reported reductions of up to 60% in processing time after implementing RPA solutions [12]. Nevertheless, challenges persist in terms of system compatibility, staff retraining, and high initial costs [13].

Big Data has also become essential in accounting by allowing the integration and analysis of massive volumes of structured and unstructured data [14,15]. Its application in auditing processes helps identify anomalies and anticipate financial risks with greater accuracy [16]. Studies highlight its impact on reporting quality and predictive financial modeling [17,18,39]. Despite these advances, organizations must address infrastructure limitations, staff training, and data security compliance to fully leverage Big Data [19,20].

The combined use of AI, RPA, and Big Data creates powerful synergies. These technologies not only optimize accounting operations but also generate strategic insights that support long-term planning [21]. Research indicates that their integration enhances risk management, regulatory compliance, and the efficiency of audit processes [22]. For example, AI and RPA have reduced audit costs while increasing accuracy, while Big Data has strengthened transparency and data-driven decision-making [23].

To understand how organizations adopt these technologies, several theoretical models are relevant. One is the Technology Acceptance Model (TAM), which explains that technology is more likely to be adopted when users perceive it as useful and easy to use [24]. This is crucial in the accounting field, where professionals are more willing to use AI and RPA when they improve task execution and are compatible with existing systems.

In addition, the integration of digital technologies into accounting requires internal transformation. Lewin's Change Management Model outlines a three-stage process—unfreezing, changing, and refreezing—that helps organizations navigate transitions [25]. Kotter's eight-step model extends this by highlighting the need for leadership, communication, and employee engagement throughout the change process [26]. These theories are highly applicable when firms must overcome cultural resistance to automation or redefine professional roles in the face of intelligent systems.



The Dynamic Capabilities Theory is also highly relevant. It posits that organizations must develop the ability to integrate, build, and reconfigure internal competencies to adapt to technological change [27]. In the accounting context, this means investing in infrastructure, data governance, and talent development to align with emerging digital tools.

Equally important is Christensen's Theory of Disruptive Innovation, which explains how technologies initially considered marginal can transform entire industries [28]. This is evident in how AI and Big Data are changing traditional auditing models by enabling real-time analysis, reducing dependence on manual sampling, and improving overall reporting quality.

Empirical studies have emphasized that successful implementation depends on strategic alignment between technological resources, organizational structures, and regulatory frameworks [29]. Firms that fail to address these dimensions often experience low adoption rates or operational inefficiencies [30]. On the other hand, companies that invest in digital transformation benefit from increased productivity, reduced error rates, and greater agility in responding to market demands [31].

Finally, ongoing innovation in accounting technologies points to the importance of preparing for future developments such as blockchain, cloud-based platforms, and algorithmic governance models. These trends will likely demand even greater coordination between technology, talent, and strategy [32].

### 3 Methods

To assess the impact of the integration of Artificial Intelligence (AI), Robotic Process Automation (RPA), and Big Data on strategic accounting management and consulting, a mixed-methods approach was adopted, combining both qualitative and quantitative techniques. This approach enabled a comprehensive analysis including a systematic literature review, case studies, structured interviews, and multi-level data analysis [1].

The systematic literature review aimed to establish a strong theoretical foundation on the integration of digital technologies in accounting. To ensure relevance and quality, inclusion and exclusion criteria were established. The review prioritized articles published between 2010 and 2024 and was conducted in databases such as JSTOR, Scopus, Google Scholar, and PubMed. More than 400 initial documents were identified, and after applying filters for scientific quality, scope, and topic relevance, 120 key investigations were selected for full-text analysis [33-35]. This process allowed identifying global trends regarding the benefits, barriers, and strategic uses of AI, RPA, and Big Data in accounting contexts.

To analyze real-world experiences, case studies were conducted in two organizations recognized for their adoption of emerging technologies in financial operations: PwC Colombia and Datacil Brasil. These companies were selected due to their advanced digital infrastructure and documented implementation of AI and RPA [22,23]. Data collection involved internal documentation and interviews with accounting managers and financial technology experts.

According to internal reports, RPA implementation reduced account reconciliation time by up to 70%, while AI contributed to improving the accuracy of fraud detection algorithms [36,37]. Despite the successes, resistance to change remained a significant obstacle, reinforcing the need for institutional change management and continued staff training [10].

To deepen the understanding of expert perspectives on accounting digitalization, structured interviews were carried out with 30 out of 40 invited professionals from the financial and technology sectors. The instrument included targeted questions on perceived benefits, implementation barriers, and technological strategies. Interviews were recorded, transcribed, and analyzed using thematic coding and classification into categories such as operational efficiency, regulatory adaptation, and human resource readiness. Findings revealed that 83% of participants considered AI as a catalyst for improving accounting procedures, while 17% noted internal resistance within their organizations. Additionally, 67% highlighted cybersecurity as a critical concern in the adoption of financial technologies [38,26].

A combined analysis of qualitative and quantitative data was then performed. The quantitative component integrated descriptive statistics, logistic regression, and correlation analysis to evaluate the relationship between the adoption of digital tools and performance indicators in the firms studied. Results showed that AI led to a 50% reduction in accounting processing time, and RPA was associated with a 60% decrease in audit errors. Nonetheless, 50% of respondents cited the lack of robust digital infrastructure as a limiting factor for full-scale implementation [31,32].

The qualitative component employed content analysis and thematic classification to interpret interview responses and documentary evidence. This approach allowed understanding not only technological outcomes, but also cultural, structural, and strategic implications of technology adoption in the accounting function.

Finally, the entire process followed the PRISMA guidelines (Preferred Reporting Items for Systematic Reviews and Meta-Analyses). The search strategy included Boolean operators applied as follows:

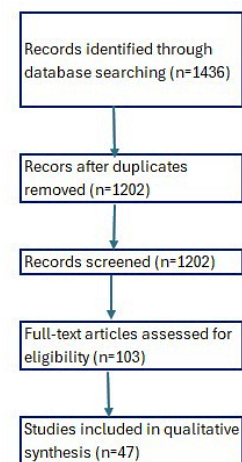


Figure 1. Prisma.  
Source: Authors



("artificial intelligence" OR "machine learning") AND ("accounting" OR "financial reporting") AND ("RPA" OR "robotic process automation") AND ("Big Data") AND ("adoption" OR "implementation")

Selection and exclusion procedures are illustrated in Fig. 1 – PRISMA diagram [33], and the results of the review were integrated with empirical data to inform the recommendations and conclusions of this study

### 3.1. Limitations of the Mixed-Methods approach

While the mixed-methods design adopted in this study provided a comprehensive perspective on the integration of AI, RPA, and Big Data in accounting, several limitations should be noted. First, the qualitative component—especially interviews—generated more in-depth data than the quantitative survey, which may have led to interpretative asymmetries [1]. To address this, thematic findings were cross-validated using literature and case data.

Second, the purposive sampling of case studies and expert participants, although strategically justified, limits the generalizability of the results to broader accounting contexts [2]. Additionally, social desirability bias may have influenced some interview responses. This was mitigated by ensuring anonymity and triangulating with internal documentation [3].

Finally, the systematic review was constrained by database indexing and potential omissions due to keyword variations [4]. Despite careful design of the Boolean search and inclusion criteria, some relevant literature may have been inadvertently excluded.

These limitations do not undermine the validity of the findings but suggest avenues for future research, including larger samples, longitudinal studies, and expanded geographic coverage to strengthen the empirical base on accounting digitalization

## 4. Results

Research on the integration of Artificial Intelligence (AI), Robotic Process Automation (RPA) and Big Data in strategic accounting management has identified significant gains in efficiency, accuracy and resource optimization within accounting firms. Through a combination of qualitative and quantitative methods, including systematic literature review, case studies, structured interviews and data analysis, key findings on the benefits, challenges and critical factors affecting the adoption of these technologies have been obtained.

The systematic literature review evidenced an exponential growth in the adoption of these technologies within the accounting sector over the last decade. More than 400 studies published between 2010 and 2024 have been identified, highlighting that AI has allowed optimizing the speed and accuracy of accounting tasks, particularly in fraud detection and predictive analysis of financial risks [1,15]. Likewise, it has been documented that automation through RPA has reduced account reconciliation times by up to 70%, minimizing errors in internal audits and increasing operational consistency [2,3]. As for the use of Big Data, it

has been shown to enable the processing of large volumes of information in real time, facilitating the identification of market trends and new business opportunities [5,6].

Case studies conducted in leading accounting firms, such as PwC and Dataciti, have demonstrated substantial improvements in operational efficiency through the implementation of these technologies. At PwC, the use of RPA for automating financial reporting and audits has reduced the time required to prepare accounting statements by 60% [22,23]. In addition, the adoption of AI has enabled more accurate detection of accounting irregularities, improving the reliability of financial reports [39]. For its part, Dataciti has focused its digital transformation on the implementation of Big Data and predictive analytics models, managing to reduce operating costs by 40% and improve the accuracy of financial analysis by 30% [36,37].

Through structured interviews with 30 accounting and technology experts, key insights on the impact of digitization on the industry were identified. Eighty-three percent of respondents noted that AI has optimized the execution of accounting tasks, reducing errors and facilitating the analysis of large volumes of data in real time. However, 17% mentioned that resistance to organizational change has been a significant barrier to the adoption of this technology [38]. Regarding automation with RPA, 50% of the interviewees highlighted that their company has used this technology mainly for account reconciliation, while 33% have implemented it in financial reporting and 16% in internal audits. In addition, 67% of the participants highlighted that the use of Big Data has improved the ability of companies to identify business opportunities and foresee financial risks; however, 50% indicated that the lack of adequate technological infrastructure is a major barrier to its adoption [27,28].

Quantitative data analysis allowed an accurate assessment of the effects of AI, RPA and Big Data implementation on accounting efficiency. Descriptive, correlational and logistic regression analysis techniques were applied, identifying that AI has reduced accounting processing times by 50%, while automation with RPA has reduced audit errors by 60%. Likewise, companies that have implemented Big Data have reported a 40% improvement in the accuracy of their financial reporting, compared to those that still rely on traditional methods [40]. In terms of operating costs, automation with RPA has led to a 30% reduction in administrative costs, which has facilitated the reallocation of resources towards strategic areas of growth and business development [31].

Despite the observed benefits, the study also identified significant challenges in the implementation of these technologies. Thirty-three percent of respondents indicated that lack of training in emerging technologies and organizational resistance to change have slowed the adoption of accounting digitization. Also, 50% of the companies analyzed reported that they do not have adequate technological infrastructure for the effective implementation of AI and Big Data, which limits their capacity for analysis and automation [12]. In terms of regulation and compliance, there are concerns related to data protection and privacy, especially in the use of Big Data for accounting decision making [11].

The results of this article confirm that the integration of AI, RPA and Big Data has significantly transformed efficiency and accuracy in strategic accounting. However, their effective adoption depends on the implementation of organizational change management strategies, continuous training and development of a robust technology infrastructure. In the following section, we will analyze these findings in the context of the existing literature and discuss strategies for overcoming implementation challenges and maximizing the positive impact of these technologies in accounting consulting

#### 4.1. Interviews

The following graphs (Figs. 1 to 10) present the results of the interviews conducted with people who manage small and medium-sized companies:

The answers to question 1. What impact has the implementation of AI had on your accounting processes? are shown in Fig. 2:

83% of respondents believe that Artificial Intelligence has greatly enhanced operational efficiency and result quality in accounting, noting improvements in speed, accuracy, and analytical capability, which support better decision-making and fewer human errors. Meanwhile, 17% point to staff resistance—driven by fear, lack of training, or reluctance to adopt new tools—as a key barrier to full implementation. Overcoming these challenges calls for change management strategies and ongoing education.

The responses to question 2, What routine tasks have you automated with RPA in your organization?, are presented in Fig. 3

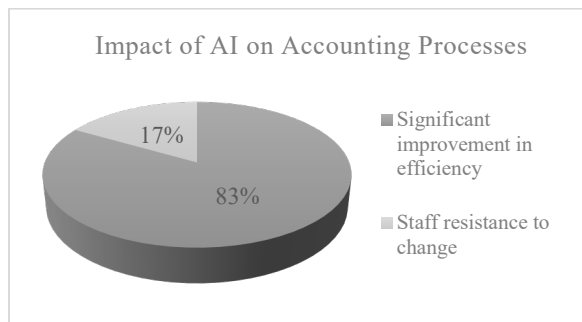


Figure 2. Survey results to question 1.  
Source: Authors

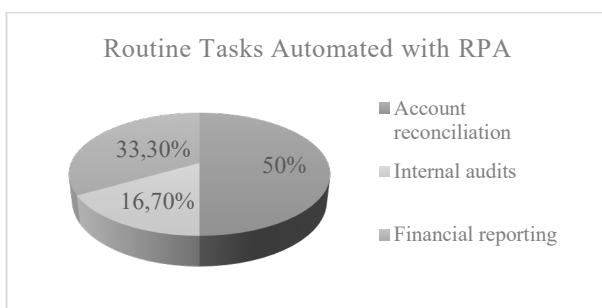


Figure 3. Survey results to question 2.  
Source: the authors

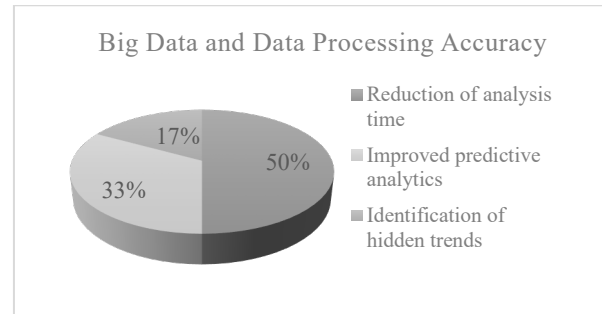


Figure 4. Survey results to question 3.  
Source: Authors

Half of the respondents reported that Account Reconciliation is the primary area where RPA has been applied, emphasizing how automation has made this key financial process faster and more accurate. Additionally, 16.7% pointed out that internal audits have also seen improvements, with RPA enhancing the speed and consistency of data review, helping the organization better meet regulatory requirements. Meanwhile, 33.3% highlighted significant gains in Bank Reporting, where automation has enabled quicker and more precise report generation, supporting strategic decisions. Overall, RPA has become a valuable tool across multiple areas, boosting efficiency, accuracy, and agility in financial operations.

Views on question 3, How has the accuracy of data processing improved with the use of Big Data? are shown in Fig. 4.

Half of the respondents believe Big Data has enhanced the accuracy of predictive analytics, boosting the organization's ability to anticipate situations and make well-informed decisions. Another 33% emphasize how automation has reduced the time needed for complex analyses, allowing for quicker and more efficient responses. The remaining 17% appreciate Big Data's role in revealing hidden trends and uncovering opportunities and risks that had gone unnoticed. Altogether, Big Data has played a key role in refining both strategic and operational decision-making.

The answers to question 4, What type of technology infrastructure do you consider essential to implement AI and RPA?, are shown in Fig. 5 below.

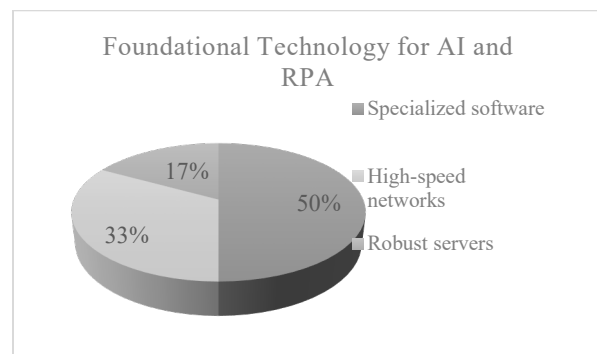


Figure 5. Survey results to question 4.  
Source: Authors

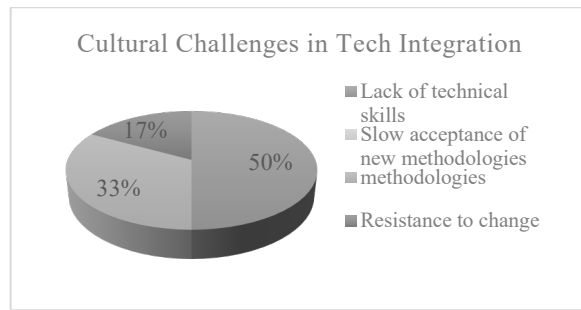


Figure 6. Survey results to question 5.  
Source: Authors

50% of respondents believe that, in order to effectively implement Artificial Intelligence (AI) and Robotic Process Automation (RPA), it is essential to have a technological infrastructure based on specialized software. On the other hand, 33% of respondents say that the key to successful implementation lies in the availability of high-speed networks, as they enable more efficient and faster processing and transmission of data, 17% believe that robust servers are necessary.

The answers to question 5, What cultural challenges have you faced in integrating these technologies? are shown graphically in Fig. 6 below.

When it comes to cultural challenges in adopting new technologies, two main issues stand out. Half of the respondents point to a lack of technical knowledge as a key obstacle, indicating that many employees are not yet equipped to work effectively with AI and RPA. Another 33% mention the slow acceptance of new technologies, reflecting a broader reluctance to embrace innovation in the workplace. Additionally, 17% specifically highlight resistance to change as a major concern. Together, these insights stress the importance of investing in employee training and change management strategies to support the smooth and successful integration of these technologies.

The reactions to question 6 ¿What specialized skills do you consider necessary to handle AI, RPA and Big Data? visually in Fig. 7.

67% of respondents view data analytics and statistics as crucial for managing AI, RPA, and Big Data. Meanwhile, 17% emphasize cybersecurity, and another 17% highlight programming skills. Overall, the results point to the need for multidisciplinary training to fully leverage these technologies.

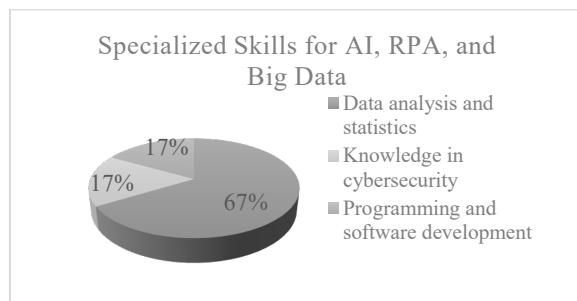


Figure 7. Survey results to question 6.  
Source: the authors

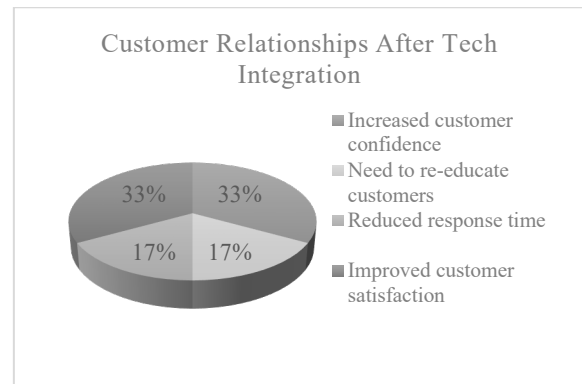


Figure 8. Survey results to question 7.  
Source: Authors

The answers to question 7, How has the integration of these technologies affected your relationship with your customers? are graphically illustrated in Fig. 8 below.

The integration of advanced technologies has greatly enhanced the customer experience. 33% of respondents note improved satisfaction through more efficient, personalized services, while another 33% highlight faster response times. Additionally, 17% mention increased customer trust due to greater accuracy and reliability, and 17% point to the need for customer re-education to adapt to new processes. Together, these factors strengthen relationships and improve service quality.

The views on question 8, What security measures have you implemented to protect the data handled by these technologies?, are illustrated in Fig. 9 below.

Data security in advanced technologies relies on strict policies and technical solutions. 50% of organizations use role-based access controls, multi-factor authentication, and password management, while the other 50% invest in advanced tools like next-generation firewalls and intrusion prevention systems. Additionally, encryption, endpoint protection, cloud-specific measures, continuous monitoring, and employee training strengthen the overall security framework.

The responses to question 9, What additional benefits have you observed with the adoption of Big Data in your accounting consultancy? are illustrated in Fig. 10 below.

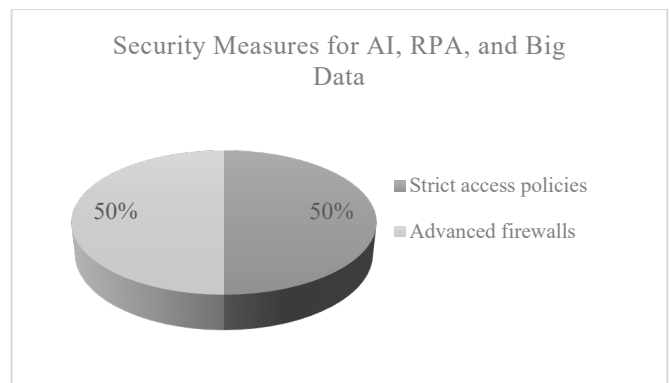


Figure 9. Survey results to question 8.  
Source: Authors

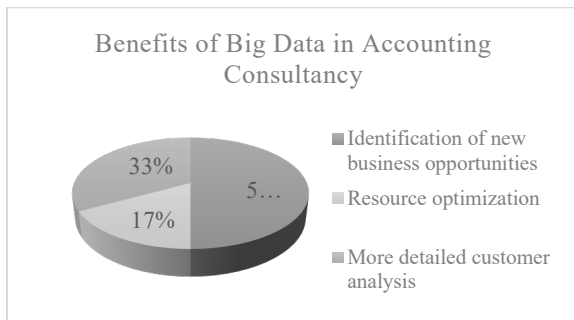


Figure 10. Survey results to question 9.  
Source: Authors

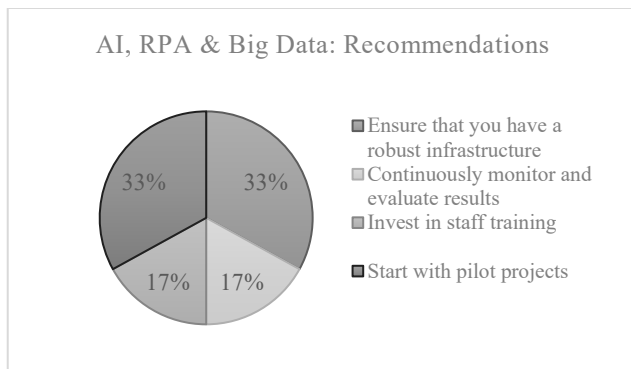


Figure 11. Survey results to question 10.  
Source: Authors

The adoption of Big Data in accounting consulting has brought several key benefits. Half of the respondents highlight its role in identifying new business opportunities by revealing hidden patterns and market trends. Another 33% point to deeper client analysis, enabling more personalized services and stronger relationships. Meanwhile, 17% emphasize resource optimization, with Big Data improving operational efficiency and cost management.

The opinions on question 10, What recommendations would you give to other organizations considering integrating AI, RPA and Big Data?, are illustrated in Fig. 11 below.

When adopting advanced technologies like AI, RPA, and Big Data, several strategies are essential. 33% of organizations begin with pilot projects to test and refine implementation. 17% focus on staff training to ensure effective tool usage, while another 17% emphasize continuous monitoring and evaluation to improve outcomes. Lastly, 33% highlight the need for a robust infrastructure to meet technological demands. These approaches support successful and beneficial integration.

## 5. Discussion

The results obtained in this research support the premise that the integration of Artificial Intelligence (AI), Robotic Process Automation (RPA) and Big Data in accounting management represents a significant transformation in operational efficiency, financial reporting accuracy and

strategic decision making. Previous studies have indicated that the digitization of accounting processes generates a substantial improvement in the speed and accuracy of administrative and analytical tasks. In line with these findings, our results evidence that accounting automation through AI and RPA has reduced financial processing times by 50%, while the use of Big Data has increased the accuracy of financial analysis by 40%.

Comparison with existing literature shows that the benefits of these technologies have been widely documented, particularly in sectors that require a high degree of accuracy and efficiency in data handling. In this context, our findings confirm that the application of AI in accounting not only optimizes routine tasks such as account reconciliation and fraud detection, but also significantly improves financial risk prediction capabilities. In addition, data collected through case studies show that companies that have adopted RPA for internal audits have reduced errors by 60%, aligning with previous research suggesting that automation minimizes inconsistencies in accounting processes.

Despite these benefits, the adoption of these technologies is not without its challenges. The literature suggests that organizational resistance to change and lack of training in emerging technologies are critical barriers to the implementation of digitization in the accounting sector. In our research, 33% of respondents indicated that the main barrier to AI and RPA adoption in their organization is a lack of expertise, while 50% indicated that inadequate technology infrastructure hinders the effective implementation of Big Data. These findings reinforce previous studies that highlight the importance of investing in training and infrastructure development to maximize the impact of these technologies on strategic accounting.

Another key issue identified in our research is the relationship between automation and workforce reconfiguration in the accounting sector. While some studies warn of potential job reductions due to automation, our results suggest that, rather than replacing accountants, these technologies allow them to focus on more value-added strategic tasks, such as financial data interpretation and business consulting. However, to capitalize on these benefits, it is critical to redesign accounting training programs to include skills in data analysis, programming and IT security.

From a regulatory perspective, challenges related to data protection and regulatory compliance were identified in the adoption of Big Data and accounting automation. Previous studies have warned that the management of large volumes of information in digital environments can generate vulnerabilities in terms of security and privacy. In this research, 50% of respondents highlighted the need to implement stricter security protocols, including the use of multi-factor authentication and advanced encryption to ensure the protection of accounting data. In addition, the results indicate that companies that have adopted international cybersecurity regulations have managed to reduce associated risks by 30% compared to those that have not implemented these regulations.

In terms of strategies for overcoming implementation barriers, three fundamental approaches were identified that have proven to be effective in integrating these technologies

in accounting firms. First, the implementation of pilot projects, which allow the benefits and challenges of AI, RPA and Big Data to be evaluated in a controlled environment prior to full deployment. Second, the adoption of continuous training programs, designed to train staff in the use of automation and data analysis tools. And third, the strengthening of the technological infrastructure, ensuring interoperability between traditional accounting systems and new digital platforms.

The results of this article highlight the importance of organizational adaptability and change management as key factors for the success of digitization in strategic accounting. The integration of AI, RPA and Big Data not only improves operational efficiency and accuracy, but also redefines the role of the accountant within organizations, giving them a more strategic and analytical approach. However, to maximize these benefits, it is critical that firms adopt a holistic approach that combines technology, human talent and appropriate regulatory standards

## 6. Conclusions

The integration of Artificial Intelligence (AI), Robotic Process Automation (RPA), and Big Data into strategic accounting represents more than a technological evolution—it marks a profound transformation in how financial information is processed, interpreted, and used for decision-making. This study reveals that these technologies contribute significantly to improving operational efficiency, reducing audit errors, enhancing fraud detection, and accelerating reporting processes. However, their successful adoption is not solely a matter of technical implementation; it depends on organizational culture, training, infrastructure, and leadership.

One of the central findings is the uneven pace of technological adoption across firms, influenced by factors such as budget constraints, resistance to change, and skills gaps. While some companies, like PwC and Datactil, show strong integration results, others remain in exploratory stages, facing challenges related to cybersecurity, interoperability, and compliance frameworks. These disparities reflect broader structural and institutional barriers that still limit the scalability of digital transformation in accounting. From a strategic perspective, the study highlights that automation and intelligent systems can elevate the role of accountants from transactional executors to analytical advisors. This shift demands a reevaluation of traditional workflows, talent profiles, and educational curricula in the accounting field.

Despite the progress identified, several knowledge gaps remain open for future research. First, there is limited empirical evidence on the long-term financial returns of automation in small and medium-sized enterprises (SMEs). Second, the ethical implications of algorithmic decision-making in audit and reporting require deeper exploration, especially in light of transparency and accountability. Third, comparative studies across countries could provide insights into how regulatory environments shape technological integration in accounting practices.

Finally, this study reaffirms the need for a

multidimensional strategy—technological, organizational, and human—that ensures not only adoption, but also effective and sustainable transformation. Future research should aim to build frameworks that guide firms in implementing AI, RPA, and Big Data ethically, efficiently, and strategically.

## 7. Recommendations

The integration of AI, RPA, and Big Data in accounting requires more than technical deployment—it demands coordinated strategies in training, organizational culture, and infrastructure. First, firms should invest in continuous training for accountants, focusing on data analytics, cybersecurity, and digital tools. Academic programs must update their curricula to include AI and automation topics to prepare future professionals [4,5].

Second, managing resistance to change is crucial. Organizations should adopt structured change management models, such as those proposed by Lewin or Kotter, to facilitate the transition [25,26]. These models involve leadership alignment, stakeholder engagement, and effective communication strategies.

Third, technological modernization is essential. Accounting systems must operate on secure, integrated platforms that support automation and real-time data processing. Investments in cloud infrastructure, ERP integration, and cybersecurity protocols are fundamental for sustainable digital adoption [19,32].

Lastly, firms should maintain dialogue with regulatory entities to align technological innovation with compliance frameworks. Participation in pilot projects and industry forums can help anticipate legal requirements and guide responsible implementation of algorithmic tools [38].

Together, these recommendations provide a roadmap for firms seeking to transform their accounting functions through intelligent technologies while addressing technical, cultural, and strategic challenges

## References

- [1] Othman, A., Artificial Intelligence in accounting: transforming financial management and decision-making 2025. DOI: <https://doi.org/10.13140/RG.2.2.25950.34882>
- [2] Yi, Z., Cao, X., Chen, Z., and Li, S., Artificial intelligence in accounting and finance: challenges and opportunities. *IEEE Access*, 11, pp 129100-129123, 2023. DOI: <https://doi.org/10.1109/ACCESS.2023.3333389>
- [3] Kokina, J., and Blanchette, S., Early evidence of digital labor in accounting: Innovation with robotic process automation. *International Journal of Accounting Information Systems*, 35, art. 100431, 2019. DOI: <https://doi.org/10.1016/j.accinf.2019.100431>
- [4] Bhardwaj, A., RPA in Accounting. 2021. DOI: <https://doi.org/10.1515/9783110676693-013>
- [5] Olagoke, M.F., The role of predictive analytics in enhancing financial decision-making and risk management. *Journal of Financial Risk Management*, 14, pp. 47–65, 2025. DOI: <https://doi.org/10.4236/jfrm.2025.141004>
- [6] Aro, O.E., Predictive analytics in financial management: enhancing decision-making and risk management. 2024. DOI: <https://doi.org/10.55248/gengpi.5.1024.2819>
- [7] Chowdhury, R.H., Al Masum, A., Farazi, M.Z.R., and Jahan, I., The impact of predictive analytics on financial risk management in businesses. *World Journal of Advanced Research and Reviews (WJARR)*, 23(3), pp. 1378-1386, 2024. DOI: <https://doi.org/10.30574/wjarr.2024.23.3.2807>

- [8] Kaur, R., Gabrijelčić, D., and Klobučar, T., Artificial intelligence for cybersecurity: Literature review and future research directions. *Information Fusion*, 97, art. 101804, 2023. DOI: <https://doi.org/10.1016/j.inffus.2023.101804>
- [9] Korol, S., and Romashko, O., Artificial Intelligence in Accounting. *Scientia Fructuosa*, 154(2), pp. 145–157, 2024. DOI: [https://doi.org/10.31617/1.2024\(154\)08](https://doi.org/10.31617/1.2024(154)08)
- [10] Schweitzer, B., Artificial intelligence (AI) ethics in accounting. *Journal of Accounting, Ethics and Public Policy*, JAEPP, 25(1), pp. 67–67, 2024. DOI: <https://doi.org/10.60154/jaepp.2024.v25n1p67>
- [11] Lehner, O.M., Ittonen, K., Silvola, H., Ström, E., and Wührleitner, A., Artificial intelligence-based decision-making in accounting and auditing: ethical challenges and normative thinking. *Accounting, Auditing & Accountability Journal*, 35(9), pp. 109–135, 2022. DOI: <https://doi.org/10.1108/AAAJ-09-2020-4934>
- [12] Schweitzer, B., Artificial intelligence (AI) ethics in accounting. *Journal of Accounting, Ethics and Public Policy*, JAEPP, 25(1), pp. 67–67, 2024. DOI: <https://doi.org/10.60154/jaepp.2024.v25n1p67>
- [13] Song, M., The role of big data in financial risk assessment. *Journal of the Association for Information Science and Technology*. 2023.
- [14] Olagoke, M.F., The role of predictive analytics in enhancing financial decision-making and risk management. *Journal of Financial Risk Management*, 14, pp. 47–65. 2025. DOI: <https://doi.org/10.4236/jfrm.2025.141004>
- [15] Fosso-Wamba, S., Queiroz, M.M., Guthrie, C., and Braganza, A., Industry experiences of artificial intelligence (AI): benefits and challenges in operations and supply chain management. *Production planning and control*, 33(16), pp. 1493–1497, 2022. DOI: <https://doi.org/10.1080/09537287.2021.1882695>
- [16] Assidi, S., Omran, M., Rana, T., and Borgi, H., The role of AI adoption in transforming the accounting profession: a diffusion of innovations theory approach. *Journal of Accounting and Organizational Change*, art. 0124, 2025. DOI: <https://doi.org/10.1108/JAOC-04-2024-0124>
- [17] Mwachikoka, C.F., Effects of artificial intelligence on financial reporting accuracy. *World Journal of Advanced Research and Reviews*, 23(3), pp. 1751–1767. 2024. DOI: <https://doi.org/10.30574/wjarr.2024.23.3.2791>
- [18] Hasan, A., Artificial intelligence (AI) in accounting and auditing: a literature review. *Open Journal of Business and Management*, 10, pp. 440–465, 2022. DOI: <https://doi.org/10.4236/ojbm.2022.101026>
- [19] Theodorakopoulos, L., Thanasis, G., and Halkiopoulou, C., Implications of big data in accounting: challenges and opportunities. *Emerging. Science Journal*, 8(3), pp. 1201–1214, 2024. DOI: <https://doi.org/10.28991/ESJ-2024-08-03-024>
- [20] Olaiya, O.P., Cynthia, A.C., Usoro, S.O., Obani, O.Q., Nwafor, K.C., and Ajayi, O.O., The impact of big data analytics on financial risk management. *International Journal of Science and Research Archive*, 12(2), pp. 821–827, 2024. DOI: <https://doi.org/10.30574/ijrsra.2024.12.2.1313>
- [21] Kureljusić, M., and Karger, E., Forecasting in financial accounting with artificial intelligence. A systematic literature review and future research agenda. *Journal of Applied Accounting Research*, 25(1), pp. 81–104, 2023. DOI: <https://doi.org/10.1108/JAAR-06-2022-0146>
- [22] Ayinla, B.S., Atadoga, A., Ike, C.U., Ndubuisi, L.N., Asuzu, O.F., and Adeleye, R.A., The role of robotic process automation (RPA) in modern accounting: Investigating how automation tools are transforming traditional accounting practices. *Engineering Science & Technology Journal*, 5(2), pp. 427–447, 2024. DOI: <https://doi.org/10.51594/estj.v5i2.804>
- [23] Rama-Maneiro, E., Vidal, J.C., and Lama, M., Deep learning for predictive business process monitoring: review and benchmark. *IEEE Transactions on Services Computing*, 16(1), pp. 739–756, 2021. DOI: <https://doi.org/10.1109/TSC.2021.3139807>
- [24] Khalifa, R., and Htay, S.N., Big data analytics and financial reporting quality: qualitative evidence from Canada. *Journal of Financial Reporting and Accounting*, 19(3), pp. 344–362, 2021. DOI: <https://doi.org/10.1108/JFRA-12-2021-0489>
- [25] Harast, S.A., and Liu, Y., Robotic Process Automation (RPA) in auditing: a commentary. 2023. DOI: <https://doi.org/10.53106/256299802022120401003>
- [26] Botkers, J., Integrating RPA with existing systems: a case study. *Automation Today*, 14(3), pp. 122–135, 2023. DOI: <https://doi.org/10.1016/j.autotoday.2023.08.004>
- [27] Teece, D.J., Pisano, G., and Shuen, A., Dynamic capabilities and strategic management. *Strategic Management Journal*, 18(7), pp. 509–533, 1997. DOI: [https://doi.org/10.1002/\(SICI\)1097-0266\(199708\)18:7<509::AID-SMJ936>3.0.CO;2-Z](https://doi.org/10.1002/(SICI)1097-0266(199708)18:7<509::AID-SMJ936>3.0.CO;2-Z)
- [28] Huerta, D., and Jensen, R., Auditing and Big Data. 2017. DOI: <https://doi.org/10.32479/ijefi.8556>
- [29] Adelakun, B.O., The impact of AI on internal auditing: transforming practices and ensuring compliance. *Finance and Accounting Research Journal*, 4(6), pp. 350–370, 2022. DOI: <https://doi.org/10.51594/farj.v4i6.1316>
- [30] Krahel, J.P., and Vasarhelyi, M.A., Continuous auditing: theory and Application. *Journal of Information Systems*, 29(2), pp. 5–21, 2015. DOI: <https://doi.org/10.2308/isis-10456>
- [31] Parker, C.A., Issa, H., Rozario, A., and Søgaard, J.S., Robotic Process Automation (RPA) implementation case studies in accounting: a beginning-to-end perspective. *Accounting Horizons*. Advance online publication, art. 8330, 2022. DOI: <https://doi.org/10.2139/ssrn.4008330>
- [32] Johansson, K., Digital transformation in accounting. 2022. DOI: <https://doi.org/10.30574/wjarr.2024.23.3.2807>
- [33] Almeida, F., et. al., Systematic review on AI and RPA integration. 2024. DOI: <https://doi.org/10.56578/jisc020304>
- [34] Bou-Reslan, F., and Jabbour, A.I. Maalouf, N., Assessing the transformative impact of AI adoption on efficiency, fraud detection, and skill dynamics in accounting practices. *Journal of Risk and Financial Management*, 17(12), art. 577, 2024. DOI: <https://doi.org/10.3390/jrfm17120577>
- [35] Antwi, B.O., Adelakun, B.O., and Eziefule, A.O., Transforming financial reporting with AI: enhancing accuracy and timeliness. *International Journal of Advanced Economics*, 6(6), pp. 205–223, 2024. DOI: <https://doi.org/10.51594/ijae.v6i6.1229>
- [36] Al-Qudah, A.A., Artificial Intelligence for sustainable finance and sustainable technology, 2022. DOI: <https://doi.org/10.33394/jk.v8i4.6137>
- [37] Napier, H., Digital transformation in accounting education, 2021. DOI: <https://doi.org/10.15680/IJIRSET.2025.1401014>
- [38] Khashman, A., Credit risk evaluation using neural Networks: Emotional vs. Conventional models. *Applied Soft Computing*, 11(8), pp. 5477–5486, 2011. DOI: <https://doi.org/10.1016/j.asoc.2011.05.011>
- [39] Huang, A.H., and You, H., Artificial Intelligence in financial decision making. *SSRN*, 2022. DOI: <https://doi.org/10.2139/ssrn.4235511>
- [40] Huerta, C., Big Data in public accounting: opportunities and challenges. *Accounting Perspectives*, 18(3), pp. 72–85, 2017. DOI: <https://doi.org/10.1016/j.acper.2017.08.002>

**W.A. Guerrero**, is a BSc in Economist, Business Administrator, and Accountant, with a Sp. in Finance and a MSc. in Education, he currently works as a technical and accounting instructor at the Servicio Nacional de Aprendizaje (SENA), and as a research professor at the Fundación de Educación Superior San José (UsanJose).  
ORCID: 0000-0002-8826-5307

**L.E. Guerrero-Martín**, is a BSc. Eng. in Environmental Engineer from the Universidad Distrital Francisco José de Caldas, Colombia. She currently works as a research professor at the Fundación de Educación Superior San José (UsanJose), where she applies her extensive experience in integrated management systems and environmental impact assessment.  
ORCID: 0000-0002-8563-6977

**S. Camacho-Galindo**, is a Lawyer, with Sp in Administrative Law. Currently serving as Financial Vice-Rector of the Fundación de Educación Superior San José (UsanJose).  
ORCID:0009-0007-2552-8978

**J.C. Arévalo**, He holds a Bsc. Eng. in Telecommunications Engineering from the Universidad Abierta y a Distancia (UNAD,) and a Diploma in Radio Links. He has experience working for contracting companies for Ecopetrol. He currently works as a professor and researcher at the Fundación de Educación Superior San José (UsanJose).  
ORCID: 0000-0002-8195-5196

**C.A. Guerrero-Martín**, He holds a BSc. Eng. in Petroleum Engineering from the UIS, and Industrial Engineering from the UsanJose, MSc. in Polymer Science and Technology (UFRJ) and a PhD in Energy Planning (UFRJ). He is a professor at the Federal University of Pará.  
ORCID: 0000-0002-5979-8542



# Implementation of Google App script for automatic generation of pre-registration form

Jorge Lira-Camargo, José Antonio Ogoši-Auqui & Francisca Sonia Vera-Tito

*Facultad de Ingeniería de Sistemas, Universidad Nacional Federico Villareal, Perú. jlira@unfv.edu.pe, jogosi@unfv.edu.pe, fvera@unfv.edu.pe*

Received: November 26<sup>th</sup>, 2024. Received in revised form: June 6<sup>th</sup>, 2025. Accepted: June 20<sup>th</sup>, 2025.

## Abstract

The present study aims to implement Google App Script to optimize the automatic generation of the pre-registration form at FIIS-UNFV. The methodology used is based on applied descriptive research, focused on improving the registration process through automated tools. The results highlight an improvement in the control of quotas, avoiding excesses in courses, as well as the elimination of waiting times for students when completing the process online. Student satisfaction resulting from these changes is 50%, reflecting a positive impact, although there are still strategies to improve to increase satisfaction to 100%.

**Keywords:** automation; enrollment; time; App Script.

# Implementación de Google app script para la generación automática de la ficha de pre-matrícula

## Resumen

El presente estudio tiene como objetivo implementar Google App Script para optimizar la generación automática de la ficha de pre-matrícula en la FIIS-UNFV. La metodología empleada se basa en una investigación descriptiva aplicada, enfocada en mejorar el proceso de matrícula mediante herramientas automatizadas. Los resultados destacan una mejora en el control de cupos, evitando excedentes en los cursos, así como la eliminación de tiempos de espera para los estudiantes al realizar el proceso en línea. La satisfacción estudiantil resultante de estos cambios se sitúa en un 50%, reflejando un impacto positivo, aunque aún existe estrategias para mejorar para incrementar la satisfacción al 100%.

**Palabras-clave:** automatización; matrícula; tiempo; App Script.

## 1 Introduction

In recent years, the automation of administrative processes in education has experienced significant growth, driven by the development of new technologies that facilitate the optimisation of routine tasks. In particular, the automatic generation of enrolment forms and quota management have emerged as key solutions to improve efficiency and student satisfaction in higher education institutions [1]. These solutions not only reduce the time needed to complete enrolment processes, but also eliminate problems such as long queues and human error, providing a smoother experience for students [2].

The use of tools such as Google App Script has enabled educational institutions to automate various functions, significantly improving administrative efficiency (Miller and Zhang, 2020). This approach has not only been applied in the context of enrolment, but also in areas such as inventory management and management information systems [3]. On the other hand, the implementation of automated systems not only streamline processes, but also improves the user experience, which is crucial for maintaining high levels of student satisfaction [4]. Integrating technologies such as Google App Script into educational administration not only streamlines enrolment processes, but also facilitates the customisation of systems to the specific needs of each

**How to cite:** Lira-Camargo, J., Ogoši-Auqui J.A., and Vera-Tito, F.S., Implementation of Google App script for automatic generation of pre-registration form. DYNA, (92)238, pp. 35-38, July - September, 2025.







Figure 1. Phases of implementation

Source: Own

institution [5]. This approach has been widely adopted in several institutions, which have reported significant improvements in operational efficiency and accuracy of automatically generated data [6]. By enabling the automation of routine tasks, institutions can focus their resources on more strategic aspects, such as academic development and technological innovation [1].

On the other hand, recent studies have shown that automated enrolment systems not only benefit educational institutions in terms of operational efficiency, but also offer advantages in data management and strategic decision-making based on real-time information [7]. Optimising these processes also allows administrators to adapt platforms to the changing needs of users, ensuring greater flexibility and customisation [8].

This paper focuses on the implementation of Google App Script as a tool for the automatic generation of the pre-enrolment form at the Faculty of Industrial and Systems Engineering (FIIS) of the Federico Villarreal National University (UNFV). The research aims to explore how this technology can optimise the enrolment process, improve quota control, eliminate queues for counselling and increase student satisfaction.

## 2 Method

Three phases are developed for the implementation of Google App Script for the automatic generation of the FIIS-UNFV pre-enrolment form. See Fig. 1.

**Spatial scope:** The present project is focused on the Faculty of Industrial Engineering and Systems at the Universidad Nacional Federico Villarreal.

**Temporal scope:** This project has a timeframe of 2024.

**Universe:** Students from the first to the fifth year of Professional School and Systems Engineering.

**Sample:** 141 students from the first to the fifth year of Professional School and Systems Engineering.

**Instrument:** Pre-enrolment form, quota visualisation tool and questionnaire.

**Technique:** Data analysis, surveys.

## 3 Results

### 3.1 Control of course quotas through automatic generation of the Enrolment Form

A Script has been implemented that allows the automation of the quota control in real time, avoiding the over-allocation of enrolled students in the courses, see Fig. 2. An event has been created that allows to control every minute the availability of courses, for example, the course "100375-INGLES I -A-M-I" is available in the Pre-Enrolment form when the number of enrolled students is less or equal to the available limit (25), the Google Apps Script event controls the maximum limit, hiding the available course so that the following students cannot be enrolled.

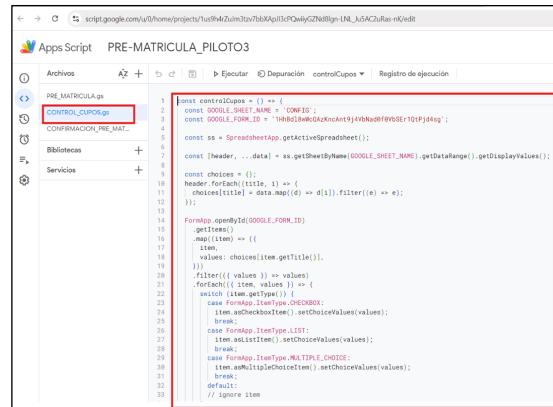


Table 2.

TO-BE

To register the registration form using the following form	The counsellor gives attention to the student and reviews the student's file	Submits approval and/or comments on observations to be raised.	SUM OCRAC's technical office registers the Cards that were approved by the advisor in its system.
10 and 15 MIN	5 MIN	1 MIN	3 MIN

Source: Own

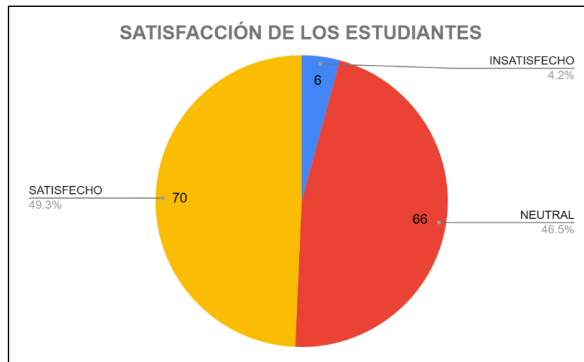


Figure 4 - Level of satisfaction

Source: Own

Upon registration of the Pre-Enrolment form the status changes to "Pending Review", the next step is the review by the counsellor. The online enrolment flow eliminates the waiting time to be seen by the counsellor.

### 3.3 Student satisfaction

Students have expressed greater satisfaction with the tool's contribution to eliminating the queue and controlling quotas. To evaluate the level of satisfaction we will use the graded table or scales, for this we will evaluate the questions How easy was it to use the automatic generation tool of the Enrolment Form? and How satisfied are you with the accuracy of the information generated in the Enrolment Form? In the following Fig. 4, you can see the results obtained from the student surveys.

On the result, 50% were satisfied with the use of the Google App Script tool, 46% indicated that they have a neutral opinion, that it can be improved with training and coaching and 4% indicated that they had problems when generating their Pre-Enrolment Form. In addition, evaluating other questions, it is mentioned that the ease of generating the Pre-Enrolment Form is 73.6% and 95% consider that the use of the tool reduces the time of the enrolment process.

## 4 Discussions

### 4.1 Control of course quotas through automatic generation of the Enrolment Form

Preliminary results show that the implementation of a Google App Script to automate quota control has been effective, allowing real-time updating of course availability and eliminating over-allocation of students (Fig. 2). This

approach is consistent with previous studies highlighting the benefits of automation in educational administration. For example, Miller and Zhang (2020) demonstrated that the integration of Google App Script significantly improves the accuracy and speed of administrative processes, reducing human error and increasing system efficiency.

The ability of the script to automatically hide courses once the quota limit is reached improves management and avoids conflicts that could arise from over-enrolment. This mirrors the findings of Lee and Kim (2022), who found that automating enrolment systems improves resource allocation and reduces the workload of administrative staff. When comparing these results with other implementations, such as the one presented by Ordoñez Valencia et al. (2022), it is evident that automation not only avoids course overload, but also optimises the Pre-Enrolment process, contributing to a smoother experience for students.

However, as Firmansyah and Sari (2021) suggest, one of the challenges of automated systems is the dependence on technology and internet connectivity. During implementation, the need to ensure a stable technological infrastructure was identified to avoid possible delays in updating quotas.

### 4.2 Elimination of queues through automatic generation of the Enrolment Card

The second key result is the elimination of physical queues during pre-enrolment, which has allowed students to complete the entire process online, saving time and avoiding crowds (Table 1). This finding is consistent with previous research showing that the digitisation of administrative processes significantly reduces waiting times and the need for face-to-face procedures. Calampa Tantachuco (2021) observed similar results in the implementation of a web platform for enrolment, showing that the use of technological tools facilitates organisation and access to administrative services.

Time saving is one of the main benefits, and this result is aligned with the findings of Fandiño Rangel and Álvarez Peniche (2021), who reported an improvement in operational efficiency through digitalisation. Students no longer have to wait for long periods of time to be served by counsellors, which contributes to higher overall satisfaction. In addition, the elimination of physical queues has positive implications for logistics and space management within educational institutions, which Gualoto Garcés (2021) also identified as a key benefit in his study on optimising enrolment processes.

### 4.3 Improving student satisfaction through automation

Preliminary results indicate that students have responded positively to the new automated enrolment system. In a satisfaction survey, 57.4% of students rated the tool as "easy" or "very easy" to use, reflecting a high level of acceptance. These results are in line with studies showing how the implementation of intuitive and efficient technologies improves the user experience. According to Baxter et al. (2020), simplicity and accessibility of technological tools are key factors in achieving high user satisfaction.

Furthermore, 73.6% of students completed their pre-enrolment in less than 10 minutes, highlighting the speed of the new process compared to the manual system. This finding is consistent with the research of Martinez and Garcia (2023), who found that automated systems significantly reduce enrolment times, improving the efficiency of administrative procedures.

Finally, 50% of the surveyed students are satisfied. This reinforces the idea that automation not only optimises processes, but also improves users' perception of service quality, as suggested by Johnson and Williams (2021).

## 5 Conclusions

- The implementation of Google App Script to improve the quota control of the courses through the automatic generation of the enrolment form, verifies every minute that it does not exceed the maximum limit of enrolled students, in case of parallel registrations due to student attendance in a certain time, it can be limited to a value lower than the limit to ensure that the maximum quota will not be exceeded.
- By implementing Google App Script to eliminate queues through the automatic generation of the enrolment form, the entire process is completed online, the system time for a student is approximately 24 minutes, while the manual process was 33 minutes, without considering the waiting time generated when the enrolment date is more crowded. For the busiest day for the review of their enrolment forms, the waiting time is reduced with the greatest amount of resource allocation (counsellors),
- The results of the pilot implementation show that 50% are satisfied with the generation of the automatic enrolment form; this indicator can be improved by training students.
- The pilot implementation of Google App Script optimised the automatic generation of the pre-enrolment form at the FIIS-UNFV, eliminating queues and controlling quotas in order to avoid reprocessing.

## 6 Recommendations

- Use an institutional Google account because it has better functionality than conventional mail.
- Propose an elective course in basic programming with the javascript language for all engineering majors.
- Propose an elective course on automation with the App Script tool to support process improvement in public and private companies.

## References

- [1] Ordoñez-Valencia, M.L., Argadoña-Moreira, J.G., Espinoza Rivero, Z.H., y Cedeño Wheatley, K.J., Sistema de Registro de Estudiantes Para el Proceso de Matriculación Para el Instituto Superior Técnico y Tecnológico de Esmeraldas. Dominio de las Ciencias, 8(2), pp. 1209–1220, 2022. DOI: <https://doi.org/10.23857/dc.v8i2.2701>
- [2] Nweke, P.O., The role of digital administrative system in transforming organizational culture in higher institution. DOI: <https://doi.org/10.1007/s10639-020-10339-2>
- [3] Firmansyah F.H. y Sari, I.P., Mejora de la función Google Classroom para que sea más cómodo de usar con Google App Script, en Séptima Conferencia Internacional sobre Ingeniería Eléctrica, Electrónica e Informática (ICEEIE). Malang, Indonesia, 2021, pp. 1–6. DOI: <https://doi.org/10.1109/ICEEIE52663.2021.9616783>
- [4] Suazo-Galdames, I.C., and Chaple-Gil, A.M., Impact of intelligent systems and AI automation on operational efficiency and user satisfaction in higher education. Ingénierie des Systèmes d'Information, 30(4), art. 300421, 2025, DOI: <https://doi.org/10.18280/isi.300421>
- [5] Petrović, N., Roblek, V., Radenković, M., and Nejković, V., Approach to rapid development of data-driven applications for smart cities using AppSheet and Apps Script, en AIIT International Conference on Applied Internet and Information Technologies, 2020, pp. 77–81.
- [6] Gualoto-Garcés, D.P., Optimización de los procesos de matriculación y revisión vehicular para la unidad técnica municipal de transporte terrestre, tránsito y seguridad vial del GADM del cantón Chambo, 2021.
- [7] Martinez, L., and Garcia, M., Assessing the efficiency of automated enrollment systems in higher education, Computers & Education, 172, art. 104348, 2023.
- [8] Fandiño-Angel, L., y Álvarez-Peniche, P., Desarrollo de una aplicación para gestión de la información de tecnología biomédica de la empresa Health and Life IPS. Repositorio Institucional de la Escuela Colombiana de Ingeniería Julio Garavito, 2021.

**J.L. Camargo**, PhD in Systems Engineering. With 17 years of professional experience in public and private entities as an analyst, specialist, and consultant.

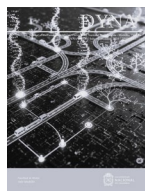
ORCID: 0000-0003-2364-5226

**J.A. Ogosi-Auqui**, is a BSc. Eng. in Systems Engineer by profession and a MSc. in Information Technology Management, he has experience in management and leadership in innovation and engineering fields. He has experience in IT project management, process management, university teaching and information systems development, IT project management with a PMI approach, people management, and business process management (BPM). His skills include analytical, technical, managerial, and interpersonal skills.

ORCID: 0000-0002-4708-610X

**F.S. Vera-Tito**, is a BSc. Eng. Systems Engineer, with a MSc. in Business Administration, with doctoral studies in Systems Engineering, leadership with an eminently humanistic, dynamic, scientific and technological training. I participate individually, collectively or forming multidisciplinary teams and with a systemic point of view with experience in General Management in Educational Management and Quality, personnel management, Administrative work, carrying out program designs for training teaching and administrative staff, experience in working with adolescents, young people, and families with different problems, conducting workshops with leadership studies and the ability to function and communicate in different cultural and denominational contexts. Experience and solid knowledge in the IT and Administrative fields.

ORCID: 0000-0002-7258-2391



# A framework for environmental performance evaluation in resource-constrained air navigation services: a Cuban case study

Yohana Depestre-Wray <sup>a</sup>, Rosa Mayelin Guerra-Bretaña <sup>b</sup>, Oridayma Tarano-Artigas <sup>b</sup> & Fridel Julio Ramos-Azcuy <sup>b, c</sup>

<sup>a</sup> Empresa Cubana de Navegación Aérea, La Habana, Cuba. yohanadepestre@gmail.com

<sup>b</sup> Universidad de La Habana, La Habana, Cuba. mayelin@biomat.uh.cu, oridayma@gmail.com

<sup>c</sup> Pontificia Universidad Católica del Ecuador, Sede Manabí, Portoviejo, Ecuador. fjrmosa@pucesm.edu.ec

Received: January 21<sup>st</sup>, 2025. Received in revised form: June 11<sup>th</sup>, 2025. Accepted: July 7<sup>th</sup>, 2025.

## Abstract

The aeronautical sector confronts unprecedented challenges to mitigate its environmental impact amid accelerated climate change and stringent regulations. This study's objective was to design and apply a methodology for evaluating environmental performance at the Cuban Air Navigation Company through a mixed-methods case study. Based on ISO 14001 and 14031 standards, the methodology's design integrated systematic literature review and documentary analysis and was validated using inductive-deductive and systemic approaches. The results, based on three premises and six key indicators, revealed high compliance in environmental objectives (92.3%) and waste management (102%). However, the evaluation also highlighted key areas for improvement, such as electromobility strategies (70% compliance) and the environmental training plan (83.6% compliance). The resulting framework not only enables monitoring environmental practices to ensure regulatory compliance but also serves as a strategic tool for advancing sustainability and driving continuous management improvement.

**Keywords:** climate change; environmental performance; methodology; environmental management; sustainability; environmental training.

## Evaluación del desempeño ambiental en navegación aérea con recursos limitados: estudio de caso en Cuba

### Resumen

El sector aeronáutico enfrenta desafíos inéditos para mitigar su impacto ambiental ante un cambio climático acelerado y regulaciones más estrictas. Este estudio diseñó y aplicó una metodología para evaluar el desempeño ambiental en la Empresa Cubana de Navegación Aérea mediante un estudio de caso mixto. La metodología, basada en las normas ISO 14001 y 14031, integró la revisión sistemática de literatura y el análisis documental, y fue validada mediante métodos inductivo-deductivos y sistémicos. Los resultados, a partir de tres premisas y seis indicadores clave, mostraron alto cumplimiento en objetivos ambientales (92,3%) y gestión de residuos (102%), pero también revelaron áreas de mejora como la electromovilidad (70%) y la formación ambiental (83,6%). El marco resultante facilita el monitoreo de prácticas ambientales, el cumplimiento normativo y sirve como herramienta estratégica para promover la sostenibilidad y la mejora continua de la gestión.

**Palabras clave:** cambio climático; desempeño ambiental; metodología; gestión ambiental; sostenibilidad; formación ambiental.

## 1 Introduction

In recent decades, the relationship between human activities and changes in the natural environment has become critically important. One of the most extensively studied phenomena is climate change, which involves significant and

long-term variations in global and regional climate patterns, primarily driven by human activities such as the burning of fossil fuels, deforestation, and industrialization [1]. These activities contribute to the increase in greenhouse gas concentrations, such as carbon dioxide (CO<sub>2</sub>) and methane, in the atmosphere, thus driving global warming [2].

**How to cite:** Depestre-Wray, Y., Guerra-Bretaña, R.M., Tarano-Artigas, O., and Ramos-Azcuy, F.J., A framework for environmental performance evaluation in resource-constrained air navigation services: a Cuban case study. DYNA, (92)238, pp. 39-46, July - September, 2025.



The aeronautical sector is responsible for approximately 2% to 3% of global CO<sub>2</sub> emissions due to the large quantities of fossil fuels consumed during flight operations. These operations significantly impact the environment through air pollution and other contributions to climate change [3,4]. In addition to CO<sub>2</sub> emissions, the sector also contributes to climate change through other environmental impacts such as noise pollution and the consumption of resources, including fuel and water, required to maintain operations [5, 6]. These factors underscore the urgent need to explore strategies for mitigating the environmental footprint of the sector.

### **1.1 Environmental management in the aeronautical sector**

The International Organization for Standardization (ISO), through consensus among its member countries, establishes systems and methodological tools to address the environmental impacts of organizational management. The ISO 14000 family of standards, developed by the ISO/TC 207 Technical Committee on environmental management, provides a set of international benchmarks to guide organizations in minimizing their environmental impacts [7]. Within this series, the ISO 14050:2020 standard defines environmental management as "the coordinated set of activities within an organization related to its environmental aspects" [8] (p. 3).

Grounded in the principles of sustainable development, environmental management seeks to balance industrial growth with environmental preservation [9]. In the aviation industry, this balance is pursued through policies, procedures, and practices designed to mitigate the environmental effects of operations [10]. To this end, frameworks like the Cuban standard NC-ISO 14001:2015, Environmental Management Systems—Requirements with Guidance for Use, equip organizations with a formal system to control environmental impacts, continuously improve performance, and demonstrate a commitment to sustainability. The standard aims to ensure regulatory compliance and address risks and opportunities by promoting interrelated actions, such as setting clear objectives and implementing integrated processes [1].

Identifying and quantifying the environmental impacts of an organization's activities is therefore essential for strategic decision-making. It allows for setting clear objectives, implementing preventive or corrective measures, and seizing opportunities to enhance environmental performance [11]. The NC-ISO 14001:2015 standard defines an environmental impact as any change to the environment, whether adverse or beneficial, resulting wholly or partially from an organization's environmental aspects [1]. An environmental aspect, in turn, is defined as any element of an organization's activities, products, or services that interacts or can interact with the environment.

Consequently, implementing an Environmental Management System in air service companies requires specific methods to evaluate environmental performance. This process entails measuring and analyzing operational impacts on the environment, local communities, and the economy. Furthermore, it involves designing sustainable

strategies and fostering a culture of continuous improvement in environmental management [12].

### **1.2 Context, framework, and rationale for environmental performance evaluation**

The Cuban context presents unique challenges that heighten the importance of this study. The national aeronautical sector operates under significant economic constraints that limit access to cutting-edge, fuel-efficient technologies and international capital for green infrastructure projects [13]. Furthermore, as an island nation, Cuba is particularly vulnerable to the impacts of climate change, such as rising sea levels and an increase in the frequency of extreme weather events, which directly affect airport operations and safety. These factors create a pressing need for innovative, low-cost, and highly adaptable environmental management methodologies that can be effectively implemented within the existing resource framework, making the Cuban case a relevant model for other developing nations facing similar circumstances.

In line with national policies to reduce the environmental impacts of aviation, the Instituto de Aeronáutica Civil de Cuba (IACC) is responsible for developing aeronautical standards and regulations. These are based on the international requirements of the International Civil Aviation Organization (ICAO), which promotes global cooperation in the sector [14]. Consequently, Cuban companies in the aeronautical sector are mandated to implement practices to conserve resources, improve and rehabilitate environmental conditions, and monitor impacts and risks. These control actions must involve both workers and managers and be conducted in accordance with relevant budgets, ensuring compliance with all national and international regulations [15-18].

The Empresa Cubana de Navegación Aérea (ECNA), the focus of this research, provides air navigation services within the Havana Flight Information Region (FIR), operating through a Central Level with seven directorates and eleven Base Business Units [19]. The company has implemented an Environmental Management System (EMS) based on NC-ISO 14001:2015, certified by national and international bodies. This system aligns its operations with ICAO policies and follows a process-based approach for predictable results [20,21]. For this research, the specific unit of study selected from ECNA's eleven Base Business Units was the Air Traffic Control Center (Centro de Control de Tránsito Aéreo - CCTA).

The selected unit, CCTA, is located in proximity to several potential sources of environmental interaction, including an electrical substation, a warehouse facility, and the hangars of the Cuban Aviation Company. The nearest residential area is a populated settlement approximately 2 km from the site, featuring well-developed infrastructure such as drainage and aqueduct systems and multi-story buildings. Although a portion of the CCTA workforce resides in this settlement, no environmental conflicts related to the unit's operations had been formally reported at the time of the study. This physical and social context is relevant for identifying baseline environmental conditions and potential

community-related environmental aspects.

While an EMS provides a foundation, its effectiveness hinges on a robust process for environmental performance evaluation (EPE). The ISO 14031:2021 standard defines EPE as an internal process employing indicators to measure and promote continuous improvement, structured around the Plan-Do-Check-Act (PDCA) cycle. In the Plan stage, key indicators are selected, which fall into two main categories: Environmental Condition Indicators and Environmental Performance Indicators. The first category, Environmental Condition Indicators (ECIs), provides information on the environmental context affected by the organization. The second category, Environmental Performance Indicators, is further subdivided into two types: Management Performance Indicators (MPIs) and Operational Performance Indicators (OPIs). MPIs focus on management commitment and socio-economic benefits, while OPIs analyze the efficiency of organizational operations [22].

Following the cycle, the Do stage involves the systematic collection and analysis of reliable, high-quality data, which are transformed into actionable information to support environmental objectives (EO) and facilitate communication with stakeholders. During the Check and Act phases, results are compared against established objectives using statistical tools to identify progress or deficiencies. These findings are then communicated to senior management to support strategic decision-making and drive continuous improvements [22]. To ensure its utility and promote accountability, ISO 14031:2021 also stipulates that all EPE information must be relevant, comprehensive, transparent, consistent, and accurate.

The execution of such a detailed process requires a structured methodology. Fernández Sotelo [23] describes a methodology as a sequence of methods, procedures, and techniques that integrate actions, resources, and tools to achieve defined objectives. Furthermore, de Armas Ramírez et al. [24] emphasize that an effective methodology must be built upon clear premises and include specific objectives, stages, and implementation recommendations to ensure its applicability.

Considering the above, and despite its certified EMS, ECNA's management identified a critical gap. There was a recognized need to set more specific environmental goals to prevent pollution, eliminate hazards, and reduce risks. Concurrently, it was observed that there was insufficient information to identify strategic opportunities, track trends in environmental performance, and establish clear objectives against which performance could be measured. This lack of a systematic process for understanding its environmental impact was identified as the core research problem. Consequently, the objective of this research was to design and apply a methodology for evaluating environmental performance within ECNA, enabling the organization to address these gaps and achieve its sustainability goals.

## 2 Method

### 2.1 Research design and approach

This study employed a mixed-method research design, combining qualitative analysis with practical application. The qualitative phase involved systematic literature and documentary reviews to establish a theoretical foundation.

The practical phase consisted of the pilot-testing of the resulting methodology within a specific organizational context. This integrated approach allowed for a comprehensive examination of the intervention's effectiveness. The research was structured as a single-case study of the Air Traffic Control Center, a Base Business Unit within the Empresa Cubana de Navegación Aérea.

### 2.2 Study participants and collaborators

The design and validation of the methodology were conducted in collaboration with an expert panel. This panel consisted of three researchers specializing in environmental management, with affiliations to ECNA, the University of Havana, and the Pontifical Catholic University of Ecuador, ensuring a blend of internal and external academic perspectives.

The pilot implementation of the methodology was carried out at the CCTA. The study population comprised all 166 employees of the unit. Their participation was defined as follows: direct participation involved key personnel, such as managers and department heads, who actively engaged in providing data and feedback during the evaluation process. Indirect participation included the remainder of the workforce, whose departmental activities, resource consumption data, and waste generation figures were essential for the overall environmental performance analysis. All organizational data were anonymized and handled with strict confidentiality to protect the privacy of the company and its employees.

### 2.3 Methodology development and application

The development of the methodology began with a systematic review of scientific and technical literature to establish a theoretical foundation. This review utilized databases such as Scopus, Web of Science, and Google Scholar, with key search terms including "environmental management," "environmental performance," "service companies," and "aviation."

Simultaneously, a comprehensive documentary analysis was conducted on the following key standards, regulations, and internal procedures relevant to the aeronautical sector:

- NC-ISO 9001:2015 Quality Management Systems - Requirements.
- NC-ISO 14001:2015 Environmental management systems - Requirements with guidance for use.
- ISO 14031:2021 Environmental management - Environmental performance evaluation - Guidelines.
- Aeronautical Regulation No. 16. Environmental Protection - Part 1. Environmental Management [15].
- Procedure P.01-15. Environmental Aspects. Internal procedure to identify, evaluate, and control environmental aspects at CCTA [25].

To facilitate a comprehensive diagnostic of ECNA's environmental performance, a checklist was developed, grounded in the elements provided by standards NC-ISO 14001:2015 and ISO 14031:2021. This tool comprised 29 criteria, whose relevance was validated through unanimous approval by ECNA's senior management, ensuring alignment



with the organization's operational and strategic needs.

Using this diagnostic checklist in conjunction with other documentary analysis techniques, including systematic comparison, critical analysis, and comparison matrices, a gap analysis was performed. This involved comparing the principles and requirements from the literature and official documentation against ECNA's existing practices to identify key deficiencies and areas for improvement.

Based on the results of the gap analysis, relevant environmental performance indicators were selected and subsequently adapted to the specific processes and activities of ECNA. This step ensured that all proposed indicators were directly applicable to the organization's operational context.

The proposed methodology and its adapted indicators then underwent a rigorous validation by an expert panel. This validation was conducted through a structured consensus workshop where each indicator was systematically assessed against SMART criteria (Specific, Measurable, Achievable, Relevant, and Time-bound). Indicators were collectively discussed, revised, and formally adopted upon reaching expert consensus on their practical applicability, robustness, and strategic alignment with ECNA's goals.

Following the validation, the application phase of the study was conducted. Data corresponding to the selected environmental performance indicators (energy consumption, emissions, waste generation) were collected from existing operational records within CCTA. The collected data were then processed and analyzed using descriptive statistical techniques. Furthermore, comparative analyses were performed to identify areas with the greatest potential for improvement and those with outstanding performance, providing the quantitative basis for the evaluation. All data processing and analysis were conducted using Microsoft Excel.

### 3 Results

#### 3.1 Framework of the proposed methodology

The methodology was developed based on three fundamental premises:

1. The ECNA operates within an environmentally sensitive sector, necessitating robust environmental management to address the challenges posed by climate change.
2. The methodology aims to ensure compliance with both national and international regulations related to sustainability and environmental management.
3. The organization's success is contingent upon its ability to adapt operations to climate and environmental challenges, aiming to reduce negative impacts while enhancing operational efficiency.

Based on these premises, the objective of the methodology was to establish a structured framework for systematically evaluating ECNA's environmental performance and providing reliable data to support strategic decision-making. The resulting framework, depicted in Figure 1, is structured around the PDCA cycle and is designed to transform a series of key inputs into tangible outputs through four distinct stages.

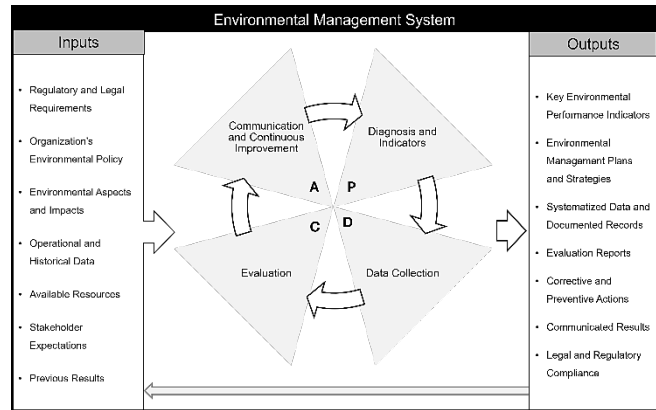


Figure 1. Framework of the Methodology for EPE based on the PDCA Cycle  
Source: Own elaboration.

The proposed methodology requires a set of essential inputs to ensure its alignment with the principles of an ISO 14001-based Environmental Management System and its effective implementation within the organization. These inputs are:

- The mandatory reference framework established by local, national, and international regulations applicable to the aeronautical sector.
- The organization's environmental policy, serving as a strategic guide that reflects senior management's commitment to improving environmental performance and preventing pollution.
- A thorough identification and prioritization of environmental aspects and impacts related to the organization's activities, products, and services (e.g., emissions, waste generation, and the consumption of natural resources).
- Operational and historical data, including records of energy consumption, emissions, water use, and waste generation, which form the basis for analysis and planning.
- All available resources for implementation and monitoring, including equipment, measurement systems, trained personnel, and financial assets (allocated budgets).
- The expectations and concerns of relevant stakeholders, such as communities, regulators, and customers, which are taken into account to influence strategic decision-making.
- The findings from previous audits, initial assessments, or past evaluations, which are integrated within the operational framework of the PDCA cycle to ensure a systematic approach to continuous improvement.

The methodology systematically processes the inputs through the four stages shown in Figure 1, which correspond to the PDCA cycle. Table 1 provides a detailed summary of the key actions performed within each of these stages, from the initial diagnosis and planning to the final communication and implementation of improvements.



Table 1.  
Summary of Methodology Stages, Actions, and PDCA Cycle Mapping

PDCA Phase	Methodology Stage	Key Corresponding Actions
Plan	Diagnosis and Indicators	<ul style="list-style-type: none"> <li>Identify and prioritize significant environmental aspects.</li> <li>Select and design SMART performance indicators (MPIs, OPIs).</li> <li>Align indicators with strategic objectives and regulations.</li> </ul>
		<ul style="list-style-type: none"> <li>Develop standardized protocols for data gathering.</li> </ul>
Do	Data Collection	<ul style="list-style-type: none"> <li>Collect reliable, verifiable, and traceable data for each indicator.</li> <li>Organize information in a centralized database.</li> </ul>
		<ul style="list-style-type: none"> <li>Analyze data and compare performance against established targets.</li> </ul>
Check	Evaluation	<ul style="list-style-type: none"> <li>Identify deviations, non-conformities, and opportunities for improvement.</li> <li>Generate structured reports for senior management.</li> </ul>
		<ul style="list-style-type: none"> <li>Formulate and implement corrective and preventive action plans.</li> </ul>
Act	Communication and Continuous Improvement	<ul style="list-style-type: none"> <li>Communicate performance results to all relevant stakeholders.</li> <li>Periodically review and adjust indicators and processes.</li> </ul>

Source: Own elaboration.

Applying the methodology yields a series of concrete outputs that enhance the organization's environmental performance and reinforce its alignment with the EMS objectives. The principal outputs are:

- A tailored set of environmental performance indicators to monitor critical areas such as emissions reduction, resource efficiency, and waste minimization.
- The creation of environmental management plans and strategies, which are supported by the indicators and include targeted programs to mitigate significant impacts, optimize processes, and meet established goals.
- Systematized data and documented records, encompassing monitoring results, measurements, and findings from internal and external audits, which provide verifiable evidence of the organization's environmental performance.
- Periodic evaluation reports that detail compliance with indicators and objectives, identify areas for improvement or non-conformities, and propose corresponding corrective and preventive actions.
- The promotion of a continuous improvement cycle, reflected in updates to procedures, processes, or technology, ensuring the ongoing optimization of environmental performance.
- The effective communication of performance results to all relevant stakeholders, fostering transparency and reinforcing confidence in the organization's environmental commitment.
- Periodic updates to the environmental policy based on achieved results, consolidating long-term sustainability and ensuring lasting environmental, social, and economic benefits.

Table 2.  
Design and measurement criteria for MPI

Indicator	Method of measurement	Reference point	Score breakdown
MPI 1	$CEO = \frac{TEO (actual)}{TEO (plan)} * 100$	$A = CEO \geq 90\% = 1$	$A + B = 2$ $A + B = 1$
	$CEA = \frac{TC}{TP} * 100$	$B = CEA \geq 90\% = 1$	$A + B = 0$
MPI 2	$CETP = \frac{ETA (real)}{ETA (plan)} * 100$	$CETP \geq 95\%$	$CETP \geq 95\%$ $CETP < 95\%$
	Score from worker environmental perception survey	$E. P \geq 4$	$E. P \geq 4$ $E. P < 4$
MPI 3	Complaints received	$C = 0$	$C = 0$ $C \neq 0$
			1 0

Note. The formulas use the following abbreviations: TEO = Tasks contributing to compliance with EO; TC = Tasks Completed; TP = Tasks Planned; ETA = Environmental Training Actions.

Source: Own elaboration.

### 3.2 Design of performance indicators

To assess environmental performance in accordance with the integrity principle outlined in ISO 14031:2021 (ISO, 2021), three management performance indicators (MPI) and three operational performance indicators (OPI) were defined. The design and measurement criteria for the MPI are detailed in Table 2, while the criteria for the OPI are presented in Table 3. The design and measurement of environmental condition indicators were entrusted to external specialized entities, which conducted evaluations under service contracts for agreed-upon environmental categories.

Designed Management Performance Indicators:

- MPI 1: Compliance with Environmental Objectives and Actions (CEO and CEA).
  - Objective: Determine the extent to which ECNA achieves its environmental improvement goals.
  - Information Sources: Environmental strategic plan, monitoring reports, environmental committee meeting minutes, internal compliance audits.
- MPI 2: Compliance with the Environmental Training Plan (CETP).
  - Objective: Assess how well the organization promotes environmental awareness among its employees.
  - Information Sources: Training records, attendance logs, post-training satisfaction surveys, environmental competency evaluations, training session minutes.
- MPI 3: Stakeholder Satisfaction Level.
  - Objective: Evaluate whether ECNA's environmental management meets the expectations of its stakeholders.
  - Information Sources: Stakeholder surveys and interviews, complaint and suggestion records.

Designed Operational Performance Indicators:

- OPI 1: Compliance with the Route Realignment Plan (CRRP).
  - Objective: Assess progress in redesigning airspace to

achieve more direct and efficient routes, optimizing flight times and fuel consumption.

- Information Sources: Flight plans, airspace redesign reports, route time and fuel consumption statistics, air traffic monitoring software reports.

## 2. OPI 2: Compliance with the Emissions Reduction Program (CERP).

- Objective: Measure the degree to which ECNA meets its commitments to adopt more efficient technologies.
- Information Sources: Flight emission records, electric technology migration project (ETMP), energy efficiency audits.

## 3. OPI 3: Compliance with the Recyclable Waste Delivery Plan (CRWDP)

- Objective: To verify how the organization ensures the fulfillment of commitments made for the sustainable management of its waste.
- Sources of Information: Records of recyclable waste delivery and reception, agreements with recycling companies, waste management audits, environmental compliance reports.

Through the integration of these indicators, ECNA ensures a structured and evidence-based approach to monitoring and improving environmental performance, while aligning its strategic objectives and regulatory requirements.

### 3.3 Performance evaluation results

The application of the designed indicators yielded the results summarized in Figure 2, which compares the achieved performance against the established targets for each key indicator.

Table 3  
Design and measurement criteria for OPI

Indicator	Method of measurement	Reference point	Score breakdown
OPI 1	$\text{CRRP} = \frac{R(\text{actual})}{R(\text{plan})} * 100$	CRRP = 100 %	CRRP = 100 % CRRP < 100 % 0
OPI 2	$\text{ETMP} = \frac{TA(\text{real})}{TA(\text{plan})} * 100$ $\text{RCE} = \frac{ER(\text{real})}{ER(\text{plan})} * 100$	A: ETMP ≥ 85 % = 1 B: RCE ≥ 100 % = 1	A + B = 2 A + B = 1 A + B = 0 2 1 0
OPI 3	$\text{CRWDP} = \frac{DQ(\text{real})}{PR(\text{plan})} * 100$	CRWDP ≥ 100 %	CRWDP ≥ 100 % CRWDP < 100 % 1 0

*Note.* The formulas use the following abbreviations: R = Realignment of routes; TA = Total actions; ER = Climate equipment replaced; DQ = Delivered quantities; PR = Potential material to be recycled. The score for OPI 2 is a composite of two components: component A (Compliance with the technological migration program) and component B (Replacement of climate equipment with ecological refrigerant).

Source: Own elaboration.

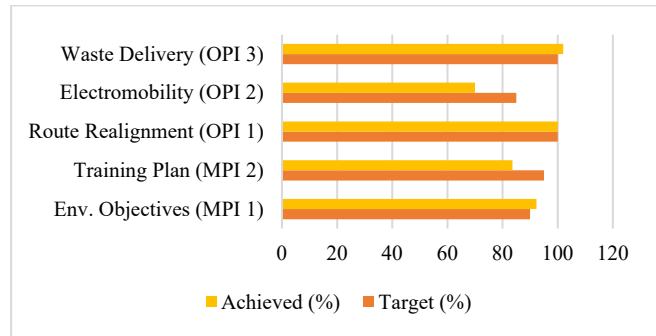


Figure 2. Target vs. achieved compliance for key performance indicators  
Source: Own elaboration.

The evaluation shows full compliance (100%) was achieved in the Route Realignment Plan (OPI 1). The target for Recyclable Waste Delivery (OPI 3) was exceeded, reaching 102%, while the overall Environmental Objectives (MPI 1) achieved a 92.3% compliance. In contrast, the performance for the electromobility component of the Emissions Reduction Program (OPI 2) was 70%, and the Environmental Training Plan (MPI 2) reached an 83.6% completion rate.

## 4 Discussion

### 4.1 Interpretation of key findings

The evaluation of ECNA's environmental performance reveals a profile of strong compliance in established operational and administrative areas, contrasted with significant challenges in technology-intensive domains. Full compliance in the Route Realignment Plan (OPI 1) and high achievement in Environmental Objectives (MPI 1) suggest that the organization excels at optimizing existing processes and administrative controls. However, the most telling findings are the nuanced results. The overachievement in Waste Delivery (OPI 3 at 102%), for instance, was not a simple success in disposal, but rather an indicator of a successful, underlying digitalization strategy that reduced paper consumption. This highlights a key strength of the methodology: its ability to uncover causal relationships between seemingly unrelated initiatives.

Conversely, the shortfalls in the Environmental Training Plan (MPI 2 at 83.6%) and the electromobility strategy (OPI 2 at 70%) point to systemic issues. The link between inadequate training completion and lower employee satisfaction ratings on environmental education programs suggests that investment in human capital is a critical prerequisite for performance. The primary challenge, however, remains the implementation of capital-intensive technologies like electromobility, where progress is clearly hindered by the broader economic and logistical constraints faced by the organization.

### 4.2 Contribution and novelty of the methodological framework

The primary contribution of this research is the development of a valid and effective tool for EPE within an Environmental Management System. The methodology's

practical applicability was demonstrated by its successful adaptation to the specific operational characteristics of an air navigation service provider. The findings confirm that its implementation enables the systematic identification of significant environmental aspects and the formulation of targeted improvement actions, thereby aligning with the core requirements of the ISO 14031 standard.

When contextualized within existing international frameworks, the specific contribution of this methodology becomes evident. While the ICAO (2019) provides extensive environmental guidance, its tools are often structured for large-scale airport operators with significant resource availability. The framework developed in this study distinguishes itself by being specifically tailored for an entity operating under resource constraints. Its novelty derives not from proposing new theoretical constructs, but from the systematic integration of established ISO standards with national regulations and specific operational realities. This results in a pragmatic and adaptable framework, offering a valuable alternative to more prescriptive, universal models.

### 4.3 Implications for practice and replicability

The model's potential for replicability in other developing nations is a significant implication of this study. The operational challenges identified at ECNA—such as limited capital for green technologies and heightened vulnerability to climate impacts—are prevalent in many countries, particularly in small island developing states. Consequently, the proposed methodology, with its emphasis on leveraging internal data and expertise within the recognized ISO structure, offers a robust and transferable framework. Other organizations can adopt the core PDCA architecture while customizing the performance indicators to align with their specific environmental priorities, such as water stewardship in arid regions or biodiversity conservation near sensitive ecosystems.

From a management perspective, the results underscore that achieving environmental goals requires a dual focus: optimizing internal processes and securing strategic resources for technological upgrades. The mechanisms for communicating results, defined via a formal procedure involving periodic reports and feedback meetings, proved effective in refining strategies and ensuring stakeholder alignment.

### 4.4 Limitations and future research

Despite the successful application, this study has limitations. The evaluation relied primarily on existing historical data, which in some areas was incomplete, and the single-case study design limits the generalizability of the specific quantitative results. Based on these findings, it is recommended that the organization accelerate the implementation of advanced technological strategies and develop a more comprehensive training plan to address the identified shortfalls.

Future research should therefore focus on applying this methodology in other air navigation service providers to further validate its adaptability. Additionally, developing

cost-effective, in-house methods for monitoring key Environmental Condition Indicators could enhance the autonomy and comprehensiveness of the evaluation.

## 5 Conclusions

This research successfully designed and applied a tailored methodology for environmental performance evaluation at ECNA. The study confirms that a systematic, evidence-based approach structured around the PDCA cycle is highly effective for identifying critical performance areas, even under significant resource constraints. The resulting framework not only provides a valid tool for ECNA's continuous improvement but also offers a replicable model for other organizations facing similar environmental and economic challenges, contributing a practical and relevant tool to the field of sustainable aviation management.

The key outcomes that substantiate this contribution are:

- The designed framework proved to be an effective and replicable tool for monitoring and improving environmental practices within a resource-constrained aeronautical entity.
- The evaluation successfully identified areas of strong performance, such as route realignment, while pinpointing critical weaknesses in the environmental training plan and the electromobility strategy.
- A new risk related to regulatory non-compliance due to deficiencies in worker environmental training was uncovered, alongside a strategic opportunity to quantify emissions reductions from route optimization.

These findings carry significant policy implications for the Cuban aviation sector. The validated methodology provides the Cuban Institute of Civil Aeronautics (IACC) with a proven model that can be promoted as a best practice for other national aeronautical entities. It demonstrates that robust, data-driven environmental oversight is achievable and can serve as a foundation for developing and refining future national environmental standards, ensuring that Cuba's aviation industry aligns with international sustainability goals and national climate policies.

Based on the results and challenges identified, the following strategic recommendations are proposed for ECNA and similar organizations:

1. Immediately enhance environmental training programs to address the identified performance gap and mitigate the associated risk of non-compliance.
2. Urgently review pending measures in the emissions reduction program, assessing the feasibility of alternative or phased approaches to the electromobility strategy given the existing constraints.
3. Secure the necessary inputs to formally quantify and report the aircraft emissions reduction index resulting from the use of optimized RNAV routes.
4. For future cycles, reinforce the methodology's effectiveness by integrating participatory workshops for stakeholder engagement and utilizing digital dashboards for real-time performance monitoring.
5. Initiate medium- and long-term impact studies to quantitatively evaluate how these environmental actions contribute to broader frameworks, such as the UN's Sustainable Development Goals.

In essence, by systematically integrating established standards with operational realities, the methodology provides a pragmatic pathway for similar organizations to transition from reactive compliance to proactive environmental stewardship.

## References

- [1] Oficina Nacional de Normalización, Sistemas de Gestión Ambiental - Requisitos con orientación para su uso (NC-ISO 14001:2015), La Habana, Cuba, 2015.
- [2] Intergovernmental Panel on Climate Change, Climate Change 2023: Synthesis Report [Online], 2023, [date of reference September 15<sup>th</sup>, 2024]. Available at: <https://www.ipcc.ch/report/ar6/syr/>
- [3] Intergovernmental Panel on Climate Change, Climate change 2021: the physical science basis. Working group I contribution to the sixth assessment report of the intergovernmental panel on climate change [Online], 2021, [date of reference December 5<sup>th</sup>, 2024]. Available at: [https://www.ipcc.ch/report/ar6/wg1/downloads/report/IPCC\\_AR6\\_WGI\\_Full\\_Report.pdf](https://www.ipcc.ch/report/ar6/wg1/downloads/report/IPCC_AR6_WGI_Full_Report.pdf)
- [4] International Energy Agency, Net zero roadmap: a global pathway to keep the 1.5 °C goal in reach Analysis [Online], 2023, [date of reference December 5<sup>th</sup>, 2024]. Available at: [https://iea.blob.core.windows.net/assets/8ad619b9-17aa-473d-8a2f-4b90846f5c19/NetZeroRoadmap\\_AGlobalPathwaytoKeepthe1.5CGoalinReach-2023Update.pdf](https://iea.blob.core.windows.net/assets/8ad619b9-17aa-473d-8a2f-4b90846f5c19/NetZeroRoadmap_AGlobalPathwaytoKeepthe1.5CGoalinReach-2023Update.pdf)
- [5] Díaz-Olariaga, O., Aeropuerto verde, concepto y marco general de desarrollo, Hábitat Sustentable, 13(2), pp. 10-21, 2023. DOI: <https://doi.org/10.22320/07190700.2023.13.02.01>
- [6] Razavi-Termeh, S.V., Sadeghi-Niaraki, A., Yao, X.A., Naqvi, R.A., and Choi, S.M., Assessment of noise pollution-prone areas using an explainable geospatial artificial intelligence approach, Journal of Environmental Management, 370, art. 122361, 2024. DOI: <https://doi.org/10.1016/j.jenvman.2024.122361>
- [7] International Organization for Standardization, ISO 14000 family - Environmental management [Online], 2024, [date of reference January 15<sup>th</sup>, 2025]. Available at: <https://www.iso.org/standards/popular/iso-14000-family>
- [8] International Organization for Standardization, Environmental management Vocabulary (ISO 14050:2020) [Online], 2020, [date of reference October 30<sup>th</sup>, 2024]. Available at: <https://www.iso.org/obp/ui/#iso:std:iso:14050:ed-4:v1:en>
- [9] García-Parra, M., de la Barrera, F., Plazas-Leguizamón, N., Colmenares-Cruz, A., Cancimance, A., and Soler-Fonseca, D., Los Objetivos de Desarrollo Sostenible en América: Panorama, LA GRANJA. Revista de Ciencias de la Vida, 36(2), pp. 45-59, 2022. DOI: <https://doi.org/10.17163/lgr.n36.2022.04>
- [10] International Civil Aviation Organization, Management of environmental impacts around airports [Online], 2019, [date of reference February 14<sup>th</sup>, 2025]. Available at: [https://www.icao.int/Meetings/A40/Documents/WP/wp\\_104\\_en.pdf](https://www.icao.int/Meetings/A40/Documents/WP/wp_104_en.pdf)
- [11] Massolo, L., Introducción a las herramientas de gestión ambiental [Online], 2015, [date of reference September 15<sup>th</sup>, 2024]. Available at: [http://sedici.unlp.edu.ar/bitstream/handle/10915/46750/Documento\\_completo.pdf?sequence=3&download=1](http://sedici.unlp.edu.ar/bitstream/handle/10915/46750/Documento_completo.pdf?sequence=3&download=1)
- [12] Ferreira, D., Baltazar, M.E., and Santos, L., Developing a comprehensive framework for assessing airports' environmental sustainability, Sustainability (Switzerland), 16(15), art. 6651, 2024. DOI: <https://doi.org/10.3390/su16156651>
- [13] Economic Commission for Latin America and the Caribbean (ECLAC), Economic Survey of Latin America and the Caribbean, 2024. Executive summary [Online], Santiago, 2025, [date of reference December 10<sup>th</sup>, 2024]. Available at: <https://repositorio.cepal.org/server/api/core/bitstreams/08599480-95c7-4311-b4fa-3c5eac7d310/content>
- [14] International Civil Aviation Organization, About ICAO [Online], 2024, [date of reference March 5<sup>th</sup>, 2025]. Available at: <https://www.icao.int/about-icao/Pages/default.aspx>
- [15] Instituto de Aeronáutica Civil de Cuba, Regulación Aeronáutica No.16 Protección al Medio Ambiente - Parte I. Gestión Ambiental [Online], 2022, [date of reference August 29<sup>th</sup>, 2024]. Available at: <https://www.iacc.gob.cu/wp-content/uploads/2022/05/RAC16-ParteI.pdf>
- [16] Rangel-Mendoza, R., Mitigación y adaptación al cambio climático en Cuba. Acciones de la Tarea Vida. Revista Panameña de Ciencias Sociales, 7, pp. 100-109, 2023. Available at: <https://dialnet.unirioja.es/servlet/articulo?codigo=9454386>
- [17] Chen, Y., Yang, S., and Yu, J., A quantitative research on climate resilience in coastal airports from the perspective of adaptation, Environmental Systems Research, 13(1), art. 29, 2024. DOI: <https://doi.org/10.1186/s40068-024-00362-7>
- [18] Estrada-Gamboa, W., Martínez-Castellanos, M.A., and Negrin-Domínguez, Y., Medidas adoptadas por Cuba para el enfrentamiento al cambio climático, en: Ambimed2022 [Online], 2022, [date of reference November 22<sup>nd</sup>, 2024]. Available at: <https://ambimed.sld.cu/index.php/ambimed22/2022/paper/viewPaper/41>
- [19] Empresa Cubana de Navegación Aérea, Gestión Empresarial (M.01-01), La Habana, Cuba, 2022.
- [20] Oficina Nacional de Normalización, Sistemas de gestión de la calidad Fundamentos y vocabulario (NC-ISO 9000:2015), La Habana, Cuba, 2015.
- [21] International Civil Aviation Organization, Report of the executive committee on agenda Item 17 [Online], 2022, [date of reference October 30<sup>th</sup>, 2024]. Available at: [https://www.icao.int/Meetings/a41/Documents/WP/wp\\_658\\_en.pdf](https://www.icao.int/Meetings/a41/Documents/WP/wp_658_en.pdf)
- [22] International Organization for Standardization, Environmental management - Environmental performance evaluation - Guidelines (ISO 14031), Geneva, Switzerland, 2021.
- [23] Fernández-Sotelo, A., Obtención de una metodología, como resultado científico, en investigaciones sobre dirección, Saber, Ciencia y Libertad, 6(1), pp. 119-126, 2011. DOI: <https://doi.org/10.18041/2382-3240/saber.2011v6n1.1766>
- [24] de Armas-Ramírez, N., Marimón-Carranza, J.A., Guelmes-Valdés, E.L., Rodríguez-del Castillo, M.A., Rodríguez-Palacios, A. and Lorences-González, J., Caracterización de los resultados científicos como aportes de la investigación educativa, Centro de Ciencias e Investigaciones Pedagógicas, 2012.
- [25] Empresa Cubana de Navegación Aérea, Aspectos Ambientales (P.01-15), La Habana, Cuba, 2022.

**Y. Depestre-Wray**, received the MSc. in Quality and Environmental Management. She is currently an Environmental Management Specialist at the Cuban Air Navigation Company (ECNA), Havana, Cuba, where her work focuses on the implementation and auditing of environmental management systems based on ISO standards.  
ORCID: 0009-0001-6443-1673

**R.M. Guerra-Breñaña**, received the BSc. in Physics from Saint Petersburg University, Russia, and the PhD. in Chemical Sciences from the National Center for Scientific Research (CNIC) in Cuba. She is a Titular Professor and Senior Researcher at the University of Havana, where she presides over the Chair of Quality, Metrology, and Standardization and coordinates the Master's programs in Quality and Environmental Management. Her research focuses on quality management systems and innovation in educational and health services.  
ORCID: 0000-0002-0561-6678

**O. Tarano-Artigas**, received the MSc. in Chemical Sciences from the University of Havana, Cuba. She is a researcher in the Department of Polymeric Biomaterials at the University of Havana's Center for Biomaterials. Her research is focused on the development and characterization of polymer composites for biomedical applications and integrated management systems.  
ORCID: 0000-0001-8879-7664

**F.J. Ramos-Azcuy**, received the MSc. in Quality and Environmental Management from the University of Havana, Cuba, and the PhD. in Educational Sciences. He is a professor and researcher at the Pontifical Catholic University of Ecuador - Manabí Campus and an affiliated researcher with the University of Havana. His research is centered on quality management and impact evaluation methodologies in higher education, with a particular focus on designing instruments for assessing the effectiveness of postgraduate training programs, including those in quality and environmental management.  
ORCID: 0000-0001-5945-446X



# Classification of pothole distress severity in asphalt pavements using YOLOv8

Átila Marconcine de Souza, Vinicius Fier Cestari & Heliana Barbosa Fontenele

*Departamento de Construção Civil, Universidade Estadual de Londrina, Londrina, Brasil. atila.marconcine@uel.br, vinicius.fier.cestari@uel.br, heliana@uel.br*

Received: May 9<sup>th</sup>, 2025. Received in revised form: June 27<sup>th</sup>, 2025. Accepted: July 7<sup>th</sup>, 2025.

## Abstract

Potholes are a type of distress that occurs in pavement surfaces. According to the method adopted for distress surveys, potholes are classified into three levels of severity: low, medium, and high. The severity assessment is traditionally performed through slow and labor-intensive manual procedures. To automate this process, this study employed the YOLOv8s and YOLOv8m models to detect pothole distress and classify its severity. During the training phase, YOLOv8m achieved the best evaluation metrics, while YOLOv8s outperformed in the testing phase, particularly in recognizing high-severity potholes. However, both models failed to effectively detect low and medium severity levels, indicating the need for improvements before field application. One possible explanation for this limitation is the lack of depth information in the input images, a factor that will be addressed in future research.

**Keywords:** deep learning; machine learning; computer vision; object detection.

# Clasificación de la severidad del deterioro tipo bache en pavimentos asfálticos utilizando YOLOv8

## Resumen

Los baches son un tipo de deterioro que ocurre en las superficies de los pavimentos. De acuerdo con el método adoptado para el levantamiento de deterioros, los baches se clasifican en tres niveles de severidad: baja, media y alta. La determinación del nivel de severidad se realiza mediante procedimientos manuales que son lentos y extenuantes. Con el objetivo de automatizar este proceso, este estudio utilizó los modelos YOLOv8s y YOLOv8m para detectar el deterioro tipo bache y clasificar su severidad. En la etapa de entrenamiento, el modelo YOLOv8m obtuvo las mejores métricas, mientras que en la etapa de prueba el YOLOv8s mostró el mejor desempeño, destacándose en el reconocimiento de baches con severidad alta. No obstante, ambos modelos fueron incapaces de reconocer con precisión los niveles de severidad baja y media, lo que indica la necesidad de mejoras para su aplicación en campo. Una posible explicación de esta limitación es la ausencia de información de profundidad en las imágenes utilizadas, cuestión que será abordada en estudios futuros.

**Palabras clave:** aprendizaje profundo; aprendizaje automático; visión por computadora; detección de objetos.

## 1. Introduction

The quality of roadways is essential to daily life, directly influencing user safety and comfort, as well as impacting vehicle and roadway maintenance costs. Asphalt pavements, due to their cost-effectiveness and ability to withstand heavy loads, are widely used but are susceptible to the emergence of distresses that can significantly compromise their functionality.

Thus, pavement performance must be monitored, and maintenance (both preventive and corrective) should occur at the appropriate time [1]. For this purpose, the implementation of a Pavement Management System (PMS) is required. The PMS is responsible for managing the existing road infrastructure, ensuring optimal traffic conditions. The core component of the PMS is pavement evaluation. Through this process, it is possible to identify the current condition of the pavement, the existing distresses, their severity level, and their location.

**How to cite:** de Souza, A.M., Cestari, V.F., and Fontenele, H.B., Classification of pothole distress severity in asphalt pavements using YOLOv8. DYNA, (92)238, pp. 47-56, July - September, 2025.



Among the various types of distresses, potholes are particularly notable, as they represent the most common and impactful form of pavement deterioration, severely compromising serviceability, according to [2]. Potholes are cavities of varying sizes that can appear in any part of the pavement surface [3]. This type of distress can be caused by traffic loads and weather conditions (particularly in areas with interconnected cracking), construction failures, or disintegration due to mix design deficiencies [4]. Potholes are categorized into three severity levels (low, medium, and high), with each level defined based on area and depth [3].

Determining the severity level of distresses is fundamental for identifying which roads require Maintenance and Rehabilitation (M&R). Several methodologies exist for distress severity classification, such as ASTM D6433-24 [5], the Distress Identification Manual (DIM) [6], and the Brazilian Distress Identification Manual (Manual de Identificação de Defeitos - MID) [3]. Although each procedure presents distinct methods, they share a common characteristic: all require manual, in-field evaluation conducted by engineers and/or technicians. Due to the reliance on human labor, these evaluations are not only time-consuming and tiring but also prone to errors and subjectivity.

In the past decade, [7] observed a significant increase in studies employing smartphones in conjunction with Machine Learning (ML) techniques, thus providing a more automated methodology for processing field-acquired data. There are numerous ML and Deep Learning (DL) algorithms. Among the models capable of recognizing objects in images, the You Only Look Once (YOLO) architecture stands out. The first version of YOLO was developed by [8], and currently, the object detector has over ten versions, with YOLOv8 [9], YOLOv9 [10], YOLOv10 [11], YOLOv11 [12] and YOLOv12 [13] being the most recent. YOLO architectures are applied across various domains, such as medicine [14, 15] and agriculture [16,17]. In engineering, YOLO is used for the automatic detection of pavement distresses, being capable of identifying potholes [18-20], cracks [21-23], and multiple distresses simultaneously [24-26].

However, the aforementioned studies only explore the models' capability to detect distresses, without addressing severity classification. In the literature, the automatic classification of pavement distress severity levels remains underexplored, with few published works. Among the studies that address this topic using YOLO architectures, [27-29] can be mentioned. [27] used different versions of YOLOv5 to detect block cracks at two severity levels (low and high) using images obtained from an evaluation vehicle. The best results were achieved with YOLOv5m, which attained a precision of 72.3%, recall of 78.2%, and mAP of 76.7%. [28] employed three object detectors (YOLOv5, YOLOv8, and CenterNet) for the detection of five types of cracks (longitudinal, transverse, fatigue, diagonal, and block) and their respective three severity levels. YOLOv8 achieved the best results, with a precision of 52%, recall of 58.4%, and

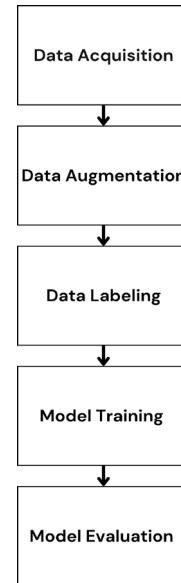


Figure 1. Methodology Steps  
Source: The Authors.

mAP of 60%. However, despite addressing severity, the criteria used to define it were not specified. In [29], the authors trained three public datasets using YOLOv4 for the recognition of multiple distresses and their severity levels. The distresses studied included cracks (fatigue, longitudinal, transverse, and edge), patching, and potholes. The reported precision, recall, and mAP were 90%, 90%, and 87.44%, respectively. Nonetheless, the authors noted that no depth-related information on the potholes was available, and severity classification was based solely on image texture (i.e., darker textures were assumed to represent higher severity and vice versa).

Given the above, the present study aims to evaluate, in an automated manner, the severity classification of potholes in urban asphalt pavements. To this end, two versions of the YOLOv8 object detector (YOLOv8s and YOLOv8m) were used, trained on a proprietary dataset in which the severity levels were determined through field measurements. The YOLOv8 architecture was selected due to the optimized accuracy-speed tradeoff, making it suitable for real time object detection in diverse applications [9]. Furthermore, YOLO effectiveness in pavement distress and severity detection has been demonstrated in recent literature [27-29].

## 2. Methodology

This section presents and discusses all the procedures carried out throughout the study. It is divided into six stages (Fig. 1), namely: Data Acquisition, Data Augmentation, Data Labeling, Model Training, and Model Evaluation.

### 2.1 Data acquisition

The first stage consisted of image collection, during which an initial dataset of pothole images from urban roads was compiled. These images were captured using a Galaxy M52 smartphone equipped with a 64-megapixel camera.



Table 1.  
Severity classification.

Severity	Depth (cm)	Area (m <sup>2</sup> )
Low	< 2.5	< 0.28
Medium	< 2.5	> 0.28
Medium	2.5 a 5.0	< 0.28
Medium	> 5.0	< 0.10
High	2.5 a 5.0	> 0.28
High	>5,0	> 0.10

Source: The Authors.

In addition to photographing the distresses, field measurements were also conducted to determine their severity levels. For this purpose, MID [3] was employed. According to [3], potholes must be measured based on their depth (in centimeters) and surface area (in square meters). The area is determined using a circumscribed rectangle, with one side aligned parallel to the road axis.

Table 1 presents the severity classification criteria according to the MID. A total of 20 images were collected for each severity level (high, medium, and low), totaling 60 images. Of these, 36 were used for model training, 12 for validation, and 12 for testing. Additionally, the dataset developed by [30] was used, which includes 12 potholes images — 10 of high severity and 2 of medium severity.

## 2.2 Data augmentation

Due to the limited number of collected images, data augmentation techniques were applied. This technique is commonly used to increase the size and diversity of training sets by applying transformations to the original images [31]. Various transformations can be employed; in this study, zoom, shear, rotate, 90° rotation, and flip were used. The Python library Augmentor was used to implement data augmentation, via the PyCharm Integrated Development Environment (IDE). Figure 2 displays the code used, with each line representing an applied operation.

A total of 60 images underwent augmentation, including 48 original images and 12 from [30]. As a result, 2,618 images were generated — 2,225 for training (85%) and 393 for validation (15%). Table 2 shows the distribution of images per severity level in the final dataset.

## 2.3 Data labeling

After augmentation, the images were annotated. This process involved manually drawing bounding boxes around the objects of interest in the dataset. In this study, the target objects were potholes on pavements and their associated severity levels. All 2,618 images were manually labeled using the LabelStudio platform, as shown in Fig. 3.

## 2.4 Model training

The model selected for training was YOLOv8, a version released in 2023 by Ultralytics (also responsible for YOLOv5 and more recently YOLOv11). YOLOv8 offers state-of-the-art performance in terms of accuracy and speed compared to previous YOLO versions [9].

Its architecture is divided into Backbone, Neck, and Head, as illustrated in Fig. 4. Although structurally similar to YOLOv5, key differences, according to [32], include:

- Use of a modified CSPDarknet53 convolutional neural network in the Backbone;
- Replacement of the CSPLayer (used in YOLOv5) with the C2f module;
- Incorporation of a Spatial Pyramid Pooling Fast (SPPF) layer, which accelerates computation by pooling features into a fixed size map;
- Each convolution is followed by batch normalization and a SiLU activation;
- The Head is decoupled to process classification and regression tasks independently.

Table 2.  
Dataset Split.

Severity	Training	Validation
Low	396	132
Medium	569	129
High	1260	132
Total	2225	393

Source: The Authors.

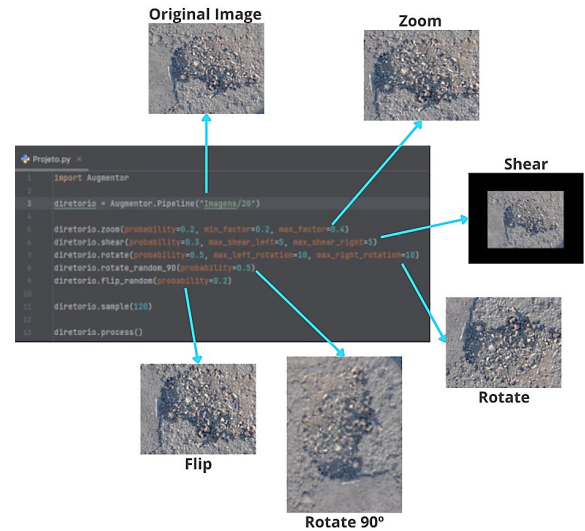


Figure 2. Code and Operations.  
Source: The Authors.

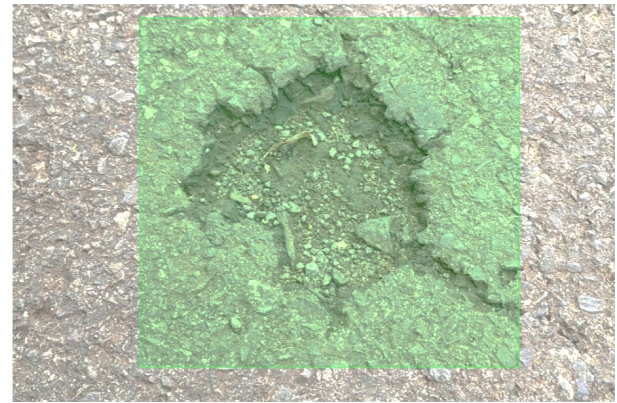


Figure 3. Labeling via LabelStudio  
Source: The Authors.



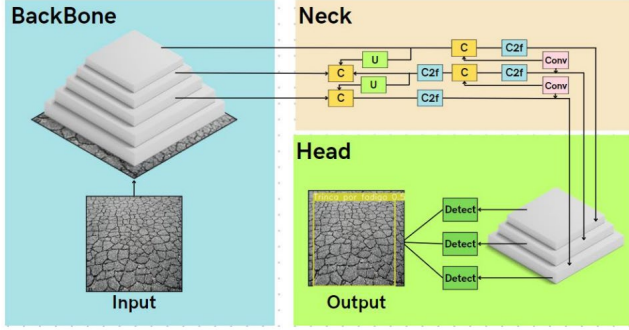


Figure 4. YOLOv8 architecture.  
Source: [24].

YOLOv8 is available in five versions: YOLOv8n (nano), which is lightweight and fast but less accurate; YOLOv8s (small); YOLOv8m (medium); YOLOv8l (large); and YOLOv8x (extra-large), which is slower and heavier but delivers higher accuracy. In this study, the YOLOv8s and YOLOv8m versions were used.

Model training was conducted locally using the Anaconda development environment and the PyTorch library. YOLOv8s was trained on a notebook with an NVIDIA GeForce GTX 1660 Ti GPU, Intel Core i7 9th generation processor, and 16 GB of RAM, while YOLOv8m was trained on a notebook with an NVIDIA GeForce RTX 4050 GPU, Intel Core i7 13th generation processor, and 32 GB of RAM.

## 2.5 Model evaluation

To assess the model's performance, standard machine learning evaluation metrics were employed, including Confusion Matrix, Precision, Recall, Average Precision (AP), and mean Average Precision (mAP).

The Confusion Matrix (Fig. 5) is a 2x2 matrix in which the main diagonal represents correct predictions, and the secondary diagonal represents errors. The main diagonal includes True Positive (TP) and True Negative (TN) values. A TP occurs when the model correctly detects a pothole; a TN occurs when the model correctly identifies the absence of potholes. The secondary diagonal includes False Positive (FP) and False Negative (FN) values. An FP indicates the model predicted a pothole when there was none, while an FN indicates the model failed to detect an existing pothole.

Precision (eq. 1) uses TP and FP values to measure the model's ability to correctly identify and localize objects. Recall (eq. 2) uses TP and FN values to determine how many of the actual objects were correctly detected.

Using Precision and Recall, the precision-recall curve is generated. The area under this curve represents the AP (eq. 3), which quantifies the model's performance for a specific class. For performance across all classes, mAP (eq. 4) is used.

According to [24], YOLOv8 outputs two mAP values at the end of training: mAP@50 and mAP@50-95. The first measures performance at a 50% confidence threshold, while the latter evaluates performance across multiple thresholds ranging from 50% to 95%.

In addition to these metrics, the model was also evaluated through testing using 12 unseen images (4 per severity level) to assess practical performance in real-world conditions.

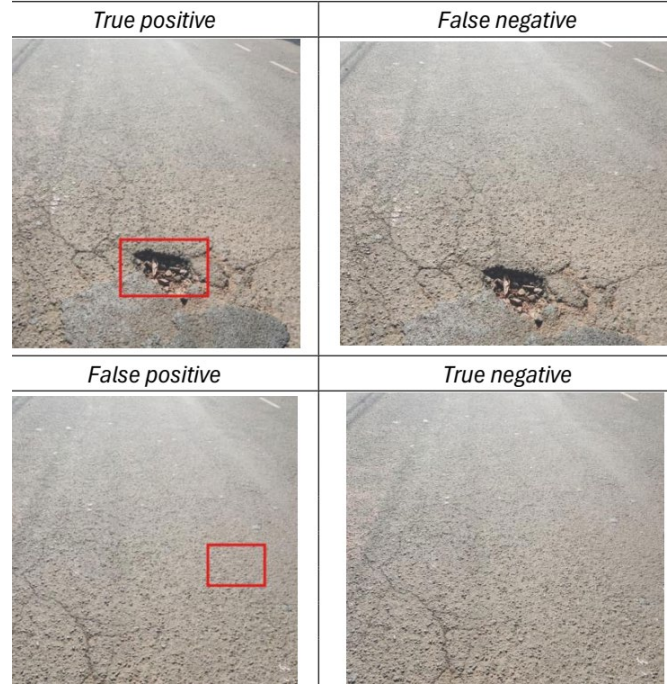


Figure 5. Confusion Matrix  
Source: The Authors.

## 3. Results and discussions

### 3.1 Training results

This section presents the results of the training and testing processes for YOLOv8s and YOLOv8m. The training for YOLOv8s was configured for 200 epochs, with the best results obtained at epoch 163.

$$Precision = \frac{TP}{TP + FP} \quad (1)$$

$$Recall = \frac{TP}{TP + FN} \quad (2)$$

$$AP = \int_0^1 Precision(recall) drecall \quad (3)$$

$$mAP = \frac{1}{Number\ of\ classes} \times \sum_{i=1}^{Number\ of\ classes} AP_i \quad (4)$$

Fig. 6 shows the precision-recall curve, which relates the precision and recall metrics and is used to calculate the AP for each class and the overall mAP. The curve indicates that the model achieved a satisfactory mAP@50 of approximately 50%. High and medium severity levels yielded above-average AP values — 59.60% and 77.60%, respectively — while the low severity class underperformed, achieving only 9% AP.

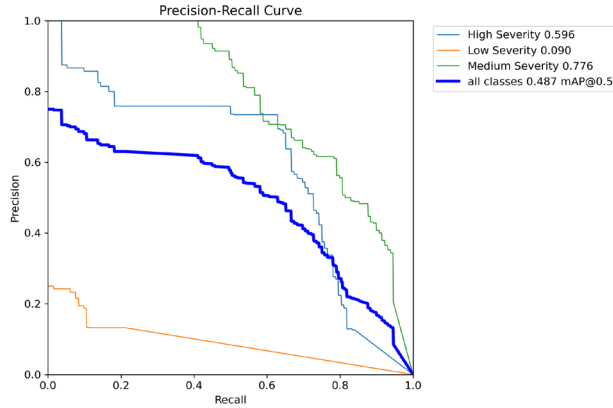


Figure 6. YOLOv8s Precision-Recall Curve  
Source: The Authors

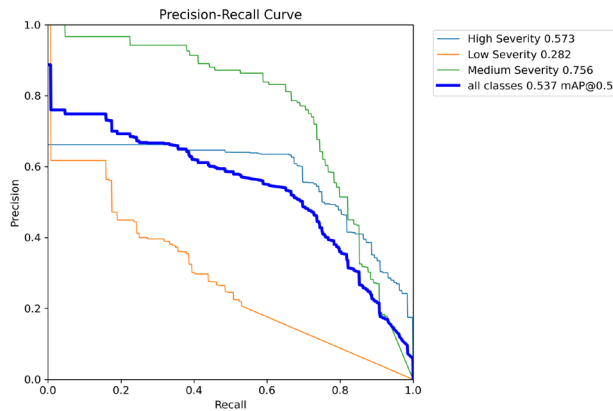


Figure 7. YOLOv8m Precision-Recall Curve  
Source: The Authors.

For YOLOv8m, the precision-recall curve in Fig. 7 shows that the low severity class achieved better performance than with YOLOv8s, reaching 28.10% AP at epoch 125 — a 19.10% improvement. This also positively impacted the mAP@50 across all classes, which increased from 48.70% with YOLOv8s to 53.70% with YOLOv8m.

Table 3 presents the evaluation metrics for the best-performing epochs of the YOLOv8s and YOLOv8m models. It shows that the low severity class had the worst performance in YOLOv8s, with a precision of 23.80% and a recall of just 1.52%. However, significant improvement was observed in YOLOv8m, where the low severity class had the highest precision (61.30%). Additionally, recall improved for all three severity levels, reaching 76.6% for high severity.

Despite these improvements, YOLOv8m showed a decrease in precision and mAP@50 for the medium and high severity levels. Nevertheless, this decline did not affect the overall model performance. In conclusion, YOLOv8m outperformed YOLOv8s, achieving 56.90% precision, 56.20% recall, 53.70% mAP@50, and 32.40% mAP@50–95.

To potentially achieve better training evaluation metrics, more advanced versions such as YOLOv8x and YOLOv8xl could be considered. These models include more parameters and tend to produce better results. However, their training time is significantly longer and requires greater computational power.

Table 3.

Evaluation Metrics for the Training Phase

Model	C	Evaluation Metrics (%)			
		Precision	Recall	mAP50	mAP50-95
YOLOv8s	LS	23.80	1.52	9.03	3.83
	MS	70.40	60.50	77.60	50.8
	HS	68.80	64.40	59.60	35.10
	All	54.30	42.10	48.70	29.90
YOLOv8m	LS	61.30	15.90	28.0	12.10
	MS	60.20	76.00	75.60	51.3
	HS	49.30	76.60	57.30	33.90
	All	56.90	56.20	53.70	32.40

Legend: C: Class; LS: Low Severity; MS: Medium Severity; HS: High Severity.

Source: The Authors.

Table 4.

Confusion Matrix and Evaluation Metrics for the Test Phase

Model	C	NI	Predicted				EM (%)	
			LS	MS	HS	NC	P	R
YOLOv8s	LS	4	0	0	2	2	0.00	0.00
	MS	4	0	0	2	2	0.00	0.00
	HS	4	0	1	3	0	42.86	75.00
	All	12	0	1	7	4	14.29	25.00
YOLOv8m	LS	4	0	1	1	2	0.00	0.00
	MS	4	1	0	3	0	0.00	0.00
	HS	4	1	2	3	0	42.86	50.00
	All	12	2	3	7	2	14.29	16.67

Legend: C: Class; NI: Number of Images; LS: Low Severity; MS: Medium Severity; HS: High Severity; NC: Not Classified; P: Precision; R: Recall; EM: Evaluation Metrics.

Source: The Authors

### 3.2 Test results

As previously mentioned, 12 images from the dataset — 4 for each severity level — were reserved for testing and excluded from the training process. These 12 images were evaluated by both trained models using a 30% confidence threshold. Table 4 presents the confusion matrices with the testing results for both models.

Table 4 shows that during testing, both models yielded unsatisfactory results for the low and medium severity levels, failing to correctly detect any of the four images in each class, thus resulting in precision and recall values of 0%. In contrast, the high severity class showed better performance, 42.86% precision and 75.00% recall for YOLOv8s, and 42.86% precision and 50.00% recall for YOLOv8m. These stronger results for the high severity class can be attributed to its greater representation in the dataset.

Tables 5, 6, and 7 provide a more detailed view of how the models classified the images. Table 5 shows the test results for the high severity class. It explains the drop in recall from 75% with YOLOv8s to 50% with YOLOv8m. This drop was due to the bounding box overlap in YOLOv8m (see IDs 1 and 2 in Table 5): while YOLOv8s correctly detected a single high-severity pothole, YOLOv8m assigned multiple severity levels to the same distress. Thus, YOLOv8s performed better for high severity in testing, correctly identifying 3 out of 4 images.

Tables 6 and 7 show the results for medium and low severity classes. As previously stated, no true positives were recorded in these classes, which justifies the precision and

recall values of 0%. These test results suggest that the models are not yet viable for recognizing medium and low severity potholes.

One plausible explanation for these inadequate results is the absence of depth information in the images. As previously discussed, severity classification for potholes is based on both area and depth. However, all images used in training and testing were 2D, which means YOLO only extracted features in two dimensions, disregarding depth — a third-dimensional parameter. This hypothesis is supported by cases such as potholes in IDs 2 and 4 in Table 6 and ID 3 in Table 7. These potholes have large surface areas but shallow depths. In the field, they were classified as medium or low severity, but the model interpreted them as high severity due to their large visible area.

There are several alternatives to address this issue. As previously mentioned, [29] used texture-related information to estimate pothole depth. They converted RGB images to grayscale and applied image enhancement techniques, including Histogram Equalization, Average Filtering, Median Filtering, and Gaussian Filtering.

Another solution was proposed by [33], who first trained RetinaNet for pothole detection without considering severity levels, achieving 99.0% precision and recall. Then, they




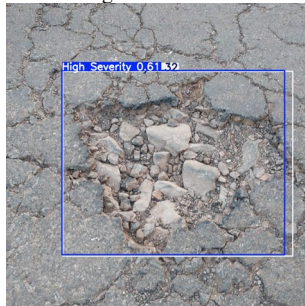
applied the photogrammetric process of Structure from Motion (SfM) to derive 3D geometric data from 2D images. This process produced a point cloud, which was used in a Python script to estimate pothole depth and, consequently, classify its severity. Their methodology first applies DL for defect detection, followed by severity estimation based on 3D analysis.

In addition to these approaches, sensors and lasers (e.g., LiDAR) can provide precise 3D data. However, such devices are typically expensive. [34] mention more affordable options such as Microsoft Kinect, Structure Sensor, and Intel RealSense.


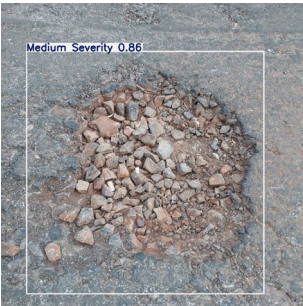


Other computer vision techniques like 3D object detection, monocular 3D object detection, and monocular depth estimation may also prove useful for future research. However, the literature has not reported the use of these techniques for pothole detection.

Finally, it is worth noting that the YOLO architecture has undergone further development beyond YOLOv8, with significant improvements in versions YOLOv9 [10], YOLOv10 [11], YOLOv11 [12], and YOLOv12 [13]. Future research is encouraged to explore these newer architectures.

Table 5.  
Testing Stage for High Severity


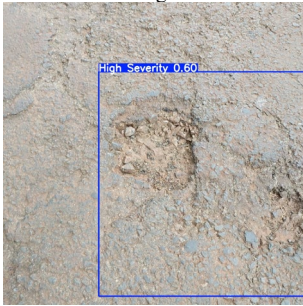


ID	Manual Field Measurements (cm)			Severity (in-situ)	Severity (YOLOv8s)	Severity (YOLOv8m)
	Length	Width	Depth			
1	36.60	33.50	6.40	High	High	Low and High
						
2	47.80	38.70	5.20	High	High	High and Medium
						
3	56.30	51.10	5.30	High	Medium	Medium







4	43.70	23.90	5.90	High		
					High	High
						

Source: The Authors.



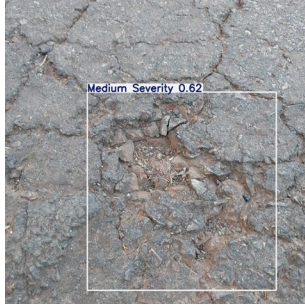

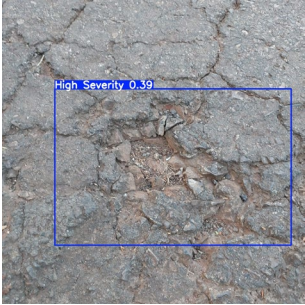
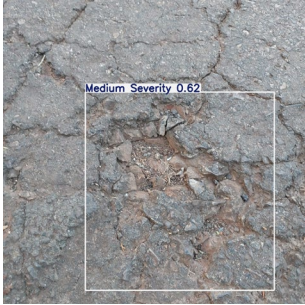
Table 6.  
Testing Stage for Medium Severity

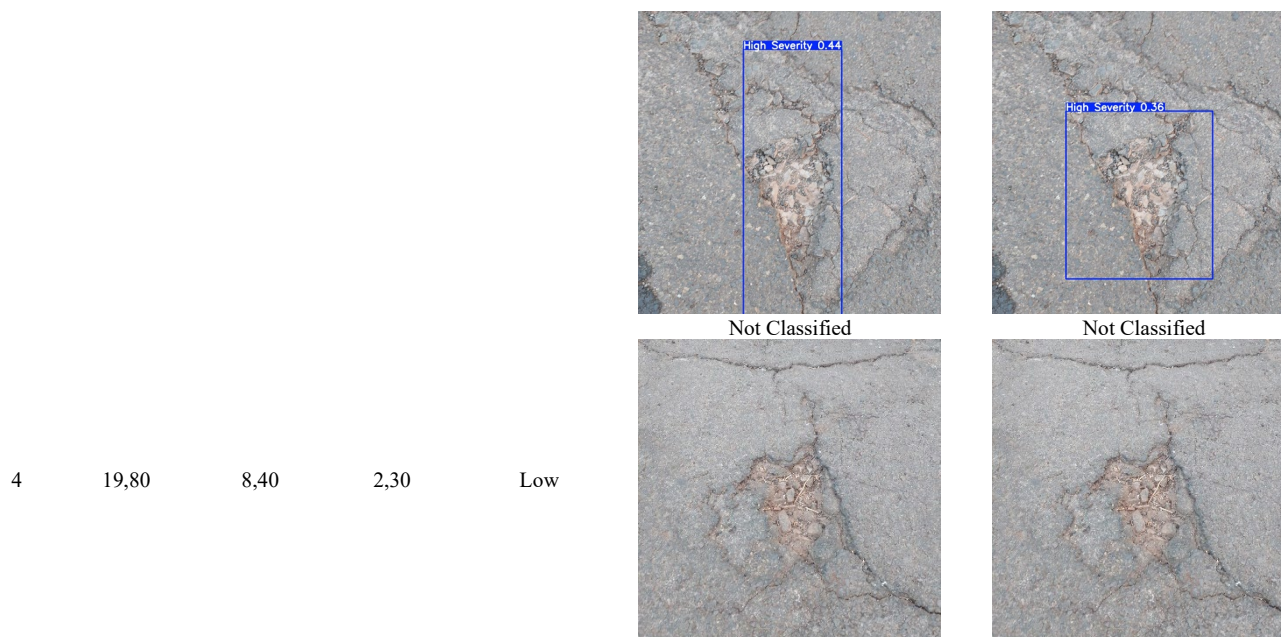
ID	Manual Field Measurements (cm)			Severity (in-situ)	Severity (YOLOv8s)	Severity (YOLOv8m)
	Length	Width	Depth			
1	21.50	19.40	2.80	Medium	Not Classified	High
						
2	31.30	18.90	3.10	Medium	High	High
						
3	31.80	24.30	2.90	Medium	Not Classified	Low

4	29.70	19.90	3.10	Medium		
					High	High
						
					High Severity 0.51	High Severity 0.71

Source: The Authors.

Table 7.  
Testing Stage for Low Severity

ID	Manual Field Measurements (cm)			Severity (in-situ)	Severity (YOLOv8s)		Severity (YOLOv8m)	
	Length	Width	Depth		Not Classified		Not Classified	
1	7.90	7.30	2.20	Low				
					High	Medium	High	High
2	11.50	6.40	2.30	Low				
3	19.90	14.40	2.50	Low	High	High		



Source: The Authors.

Other object detectors outside the YOLO family may also be viable, such as R-CNN [35] and RetinaNet [36]. Furthermore, the use of deep learning architectures with segmentation blocks and monocular depth estimation blocks, as used in [37], can also provide better results in the accurate recognition of potholes and their severity levels.

#### 4. Conclusion

In this study, two versions of the YOLOv8 architecture (YOLOv8s and YOLOv8m) were trained to recognize the severity level of pothole distresses in asphalt pavements. Based on the training results, the version with a larger number of parameters — YOLOv8m — achieved better evaluation metrics. However, during the testing phase, YOLOv8s showed superior performance, particularly in detecting high-severity potholes. For medium and low severity levels, both models proved ineffective, failing to correctly identify these classes — a shortcoming that may be attributed to the lack of depth-related data in the input images. It can be concluded that the trained models require significant improvements before being viable for practical applications.

Future studies will explore the possibility of developing a system capable of detecting potholes and determining their severity while incorporating depth information. In addition, new pothole images will be added to the database, thus improving the generalization capacity of YOLO models and their applicability in real-world.

#### Acknowledgements

The authors would like to thank the Brazilian Coordination for the Improvement of Higher Education Personnel (CAPES) for the scholarship granted, as well as the Transportation Engineering Laboratory of the Center for

Technology and Urbanism (LET-CTU) and the State University of Londrina (UEL) for the infrastructure provided.

#### References

- [1] Zanchetta, F., Sistema de Gerência de Pavimentos Urbanos: avaliação de campo, modelo de desempenho e análise econômica, PhD dissertation, Departamento de Transportes, Universidade de São Paulo, São Carlos, 2017.
- [2] Singh, P., Wijethunga, R., Sadhu, A., and Samarabandu, J., Expert evaluation system for pothole defect detection. *Expert Systems with Applications*, 277, art. 127280, 2025. DOI: <https://doi.org/10.1016/j.eswa.2025.127280>
- [3] Domingues, F.A.A., MID: manual de identificação de defeitos de revestimentos asfálticos de pavimentos. São Paulo: Camargo Campos, 1993.
- [4] Bernucci, L.B., Motta, L.M.G., Ceratti, J.A.P., and Soares, J.B., Pavimentação asfáltica: formação básica para engenheiros, 2a ed. Rio de Janeiro: petrobras: ABEDA, 2022.
- [5] ASTM, D6433., Standard practice for roads and parking lots pavement condition index surveys, ASTM International, 2024.
- [6] Miller, J.S., and Bellinger, W.Y., Distress identification manual for the long-term pavement performance program, 2014.
- [7] Souza, V.M.A., Giusti, R., and Batista, A.J.L., Asfalt: a low-cost system to evaluate pavement conditions in real-time using smartphones and machine learning. *Pervasive and Mobile Computing*, 51, pp. 121–137, 2018. DOI: <https://doi.org/10.1016/j.pmcj.2018.10.008>
- [8] Redmon, J., Divvala, S., Girshick, R., and Farhadi, A., You only look once: unified, real-time object detection, *Proc. IEEE Comput. Soc. Conf. Comput. Vis. Pattern Recognit.*, pp. 779–788, 2016. DOI: <https://doi.org/10.1109/CVPR.2016.91>.
- [9] Ultralytics, Ultralytics YOLOv8. [online]. 2025 [consultation, May 09<sup>th</sup> of 2025]. Available at: <https://docs.ultralytics.com/models/yolov8/>
- [10] Wang, C.Y., Yeh, I.H. and M.-Liao, H.Y., YOLOv9: learning what you want to learn using programmable gradient information [online]. 2025 [consultation May 09<sup>th</sup> of 2025]. Available at: <https://arxiv.org/abs/2402.13616>
- [11] Wang, A., et., al., YOLOv10: real-time end-to-end object detection. *advances in neural information processing systems*, 37 (NeurIPS), pp. 1–28, 2024. DOI: <https://doi.org/10.48550/arXiv.2405.14458>
- [12] Ultralytics, Ultralytics YOLOv11. [online]. 2025 [consultation May 09<sup>th</sup> of 2025]. Available at: <https://docs.ultralytics.com/models/yolo11/>
- [13] Tian, Y., Ye, Q., and Doermann D., YOLOv12: attention-centric real-time object detectors, [online]. 2025 [consultation May 09<sup>th</sup> of 2025]. Available at: <https://arxiv.org/abs/2502.12524>



- [14] Sobek, J., et., al., MedYOLO: a medical image object detection framework. *Journal of Imaging Informatics in medicine*, pp. 3208–3216, 2024. DOI: <https://doi.org/10.1007/s10278-024-01138-2>
- [15] Liu, Y., et., al., SOCR-YOLO: small objects detection algorithm in medical images. *International Journal of Imaging Systems and Technology*, 34(4), 2024. DOI: <https://doi.org/10.1002/ima.23130>
- [16] Ajayi, O.G., Ashi, J., and Guda, B., Performance evaluation of YOLO v5 model for automatic crop and weed classification on UAV images. *Smart Agricultural Technology*, 5(3), art. 100231, 2023. DOI: <https://doi.org/10.1016/j.atech.2023.100231>
- [17] Lippi, M., Bonucci, N., Carpio, R.F., Contarini, M., Speranza, S., and Gasparri, A.A., YOLO-based pest detection system for precision agriculture. In 2021 29th Mediterranean Conference on Control and Automation, MED 2021, Bari, Puglia, Italy, pp. 342–347, 2021. DOI: <https://doi.org/10.1109/MED51440.2021.9480344>
- [18] Omar, M., and Kumar, P., PD-ITS: pothole detection using YOLO variants for intelligent transport system. *SN Computer Science*, 5(5), 2024. DOI: <https://doi.org/10.1007/s42979-024-02887-1>
- [19] Bučko, B., Lieskovská, E., Záborská, K., and Záborský, M. computer vision-based pothole detection under challenging conditions. *Sensors*, 22(22), pp. 1–18, 2022. DOI: <https://doi.org/10.3390/s22228878>
- [20] Park, S.S., Tran, V.T., and Lee, D.E., Application of various yolo models for computer vision-based real-time pothole detection. *Applied Sciences*, 11(23), art. 1229, 2021. DOI: <https://doi.org/10.3390/app11231229>
- [21] Wang, S., et., al., Measurement of asphalt pavement crack length using YOLO V5-BiFPN. *Journal of Infrastructure Systems*, 30(2), pp. 1–10, 2024. DOI: <https://doi.org/10.1061/jitse4.iseng-2389>
- [22] Chen, D.R., and Chiu, W.M., Deep-learning-based road crack detection frameworks for dashcam-captured images under different illumination conditions. *Soft Computing*, 27(19), pp. 14337–14360, 2023. DOI: <https://doi.org/10.1007/s00500-023-08738-0>
- [23] Yao, H., Liu, Y., Li, X., You, Z., Feng, Y., and Lu, W., A detection method for pavement cracks combining object detection and attention mechanism. *IEEE Transactions on Intelligent Transportation Systems*, 23(11), pp. 22179–22189, 2022. DOI: <https://doi.org/10.1109/TITS.2022.3177210>
- [24] Souza, A.M., Oliveira, C.E., Decker, P.H.B., Amorim, G.E.R., Correa, A.L.S.C., and Fontenele, H.B., Defect detection using YOLOv8 for determining the condition of asphalt pavements. *ALCONPAT*, 15(1), pp. 79–91, 2025. DOI: <https://doi.org/10.21041/ra.v15i1.781>
- [25] Yao, H., Fan, Y., Wei, X., Liu, Y., Cao, D., and You, Z. Research and optimization of YOLO-based method for automatic pavement defect detection. *Electronic Research Archive*, 32(3), pp. 1708–1730, 2024. DOI: <https://doi.org/10.3934/ERA.2024078>
- [26] Du, Y., Pan, N., Xu, Z., Deng, F., Shen, Y., and Kang, H., Pavement distress detection and classification based on YOLO network. *International Journal of Pavement Engineering*, 22(13), pp. 1659–1672, 2021. DOI: <https://doi.org/10.1080/10298436.2020.1714047>
- [27] Valipour, P.S., Golroo, A., Kheirati, A., Fahmani, M., and Amani, M.J., Automatic pavement distress severity detection using deep learning. *Road Materials and Pavement Design*, 25(8), pp. 1830–1846, 2023. DOI: <https://doi.org/10.1080/14680629.2023.2276422>
- [28] Ganeshan, D., Sharif, M.S., and Apeagyei, A., road deterioration detection: a machine learning-based system for automated pavement crack identification and analysis. In 2023 International Conference on Innovation and Intelligence for Informatics, Computing, and Technologies, 3ICT 2023, 2023, pp. 188–194. DOI: <https://doi.org/10.1109/3ICT60104.2023.10391802>
- [29] Peraka, N.S.P., Biligiri, K.P., and Kalidindi, S.N., Development of a multi-distress detection system for asphalt pavements: transfer learning-based approach. *Transportation Research Record*, 2675(10), pp. 538–553, 2021. DOI: <https://doi.org/10.1177/03611981211012001>
- [30] Ferrari, E.C., Garcia, C., Júnior, C.A.P.D.S., and Fontenele, H.B., Classificação do defeito buraco a partir de modelos 3D, in 37o ANPET - Congresso de Pesquisa e Ensino em Transportes, Santos, São Paulo, Brasil, [online], pp. 1–12, 2023. Available at: <https://proceedings.science/anpet-2023/trabalhos/classificacao-do-defeito-buraco-a-partir-de-modelos-3d?lang=pt-br>
- [31] Buslaev, A., Iglovikov, V.I., Khvedchenya, E., Parinov, A., Druzhinin, M., and Kalinin, A.A., Albumentations: fast and flexible image augmentations. *Information*, 11(2), pp. 1–20, 2020. DOI: <https://doi.org/10.3390/info11020125>
- [32] Terven, J., Córdova-Esparza, D.M., and Romero-González, J.A.A., Comprehensive review of YOLO architectures in computer vision: from YOLOv1 to YOLOv8 and YOLO-NAS. *Machine Learning and Knowledge Extraction*, 5(4), pp. 1680–1716, 2023. DOI: <https://doi.org/10.3390/make5040083>
- [33] Ranyal, E., Sadhu, A., and Jain, K., Automated pothole condition assessment in pavement using photogrammetry-assisted convolutional neural network. *International Journal of Pavement Engineering*, 24(1), art. 83401, 2023. DOI: <https://doi.org/10.1080/10298436.2023.2183401>
- [34] Ranyal, E., Sadhu, A., and Jain, K., Automated pothole condition assessment in pavement using photogrammetry-assisted convolutional neural network. *International Journal of Pavement Engineering*, 24(1), 83401, 2023. DOI: <https://doi.org/10.1080/10298436.2023.2183401>
- [35] Ren, S., He, K., Girshick, R., and Sun, J., Faster R-CNN: towards real-time object detection with region proposal Networks. In *Advances in Neural Information Processing Systems 28 (NIPS 2015)*, pp. 91–99, 2015. DOI: <https://doi.org/10.1109/TPAMI.2016.2577031>
- [36] Lin, T.Y., Goyal, P., Girshick, R., He, K., and Dollar, P., Focal loss for dense object detection. In *IEEE International Conference on Computer Vision (ICCV 2017)*, pp. 2980–2988, 2017. DOI: <https://doi.org/10.1109/ICCV.2017.324>
- [37] Dong, J., et., al., CBAM-Optimized automatic segmentation and reconstruction system for monocular images with asphalt pavement potholes. *IEEE Transactions on Intelligent Transportation Systems*, 25(8), pp. 10313–10330, 2024. DOI: <https://doi.org/10.1109/TITS.2024.3353257>

**Á.M. de Souza**, received his BSc. Eng. in Civil Engineering from the State University of the Tocantins Region of Maranhão (UEMASUL) in 2023, where he participated in research, innovation, and outreach projects in the areas of pavements and geotechnics. He is currently pursuing a MSc. in Civil Engineering at the State University of Londrina (UEL) and is a scholarship holder from the Brazilian Coordination for the Improvement of Higher Education Personnel (CAPES). His research interests include artificial intelligence, with a focus on the application of deep learning and computer vision for the automatic detection of pavement distresses.  
ORCID: 0000-0002-4328-5558

**V.F. Cestari**, received his BSc. Eng. in Civil Engineering from the State University of Londrina (UEL) in 2025. He currently works in the field of hydraulics at ENGITEQ, focusing on the development of water supply, sewage, and fire prevention projects.  
ORCID: 0009-0006-8127-3802

**H.B. Fontenele**, received her BSc. Eng. in Civil Engineering from the University of the Amazon (UNAMA) in Belém in 1997, and obtained her Ph.D. in Sciences in the field of Transportation Infrastructure from the University of São Paulo (USP) at the São Carlos School of Engineering (EESC) in 2012. Since 2010, she has been a professor at the State University of Londrina (UEL). She is the author of two books, more than 50 scientific papers, and holds one registered software. Her research interests include Pavement Management Systems, the use of artificial intelligence focused on pavement management, pavement performance, and road environmental performance.  
ORCID: 0000-0003-2046-0568





# Agent-based models for integrated water resource management: quantifying land use changes by integrating economic and social incentives. Case study: Vista Hermosa (Meta)

Nicol Chicacausa <sup>a</sup>, Martín Otalora-Low <sup>b</sup>, Natalia Carrillo-Acosta <sup>b</sup>, María Cristina Arenas-Bautista <sup>b</sup>  
& Antonio Preziosi-Ribero <sup>a</sup>

<sup>a</sup> Facultad de Ingeniería Civil, Universidad Santo Tomás, Bogotá, Colombia. nicolachicacausa25@gmail.com, apreziosir@udistrital.edu.co

<sup>b</sup> Facultad de Estudios Ambientales y Rurales, Pontificia Universidad Javeriana, Bogotá, Colombia. m\_otalora@javeriana.edu.co, natalia-carrillo@javeriana.edu.co, maria.arenasb@javeriana.edu.co

Received: January 31<sup>st</sup>, 2025. Received in revised form: July 2<sup>nd</sup>, 2025. Accepted: July 14<sup>th</sup>, 2025.

## Abstract

Water management is essential in the face of growing global demand for domestic consumption, food production, and energy generation. This study applies the Integrated Water Resources Management (IWRM) approach to the Güejar River basin in Colombia, a complex system with productive activities such as agriculture, livestock farming, and oil extraction. An agent-based model developed in NetLogo was used to analyze land use changes under a climate scenario characterized by reduced precipitation and increased temperature. The analysis integrated hydrological data from the GR2M model, a high-resolution land cover map, and a causal diagram representing decision-making processes related to water use and land occupation. The study area covered 2,372 km<sup>2</sup>. Results show that shrublands and secondary forests are the most vulnerable, with losses of approximately 25% and 15%, respectively. In contrast, grazing areas increased by 35%, and small-scale producers declined by 40%, displaced by larger actors. These findings underscore escalating socio-environmental risks.

**Keywords:** Güejar River; land use changes; causal diagram; AGENT-based modeling.

# Modelo basado en agentes para la gestión integral del recurso hídrico: cuantificación de los cambios en el uso del suelo mediante la integración de incentivos económicos y sociales. Estudio de caso: Vista Hermosa (Meta)

## Resumen

La gestión del agua es fundamental ante la creciente demanda global para consumo, producción alimentaria y energética. Este estudio aplica el enfoque de Gestión Integral de Recursos Hídricos (GIRH) en la cuenca del río Güejar (Colombia), un sistema complejo con actividades productivas como agricultura, ganadería y explotación petrolera. Se utilizó un modelo basado en agentes en NetLogo para analizar cambios en el uso del suelo frente a un escenario climático con menor precipitación y mayor temperatura. Se integraron datos hidrológicos del modelo GR2M, un mapa de coberturas de alta resolución y un diagrama causal sobre decisiones de uso del agua y del suelo. El análisis de 2.372 km<sup>2</sup> mostró que arbustos y bosques secundarios son los más vulnerables, con pérdidas del 25% y 15%, respectivamente. En contraste, las áreas ganaderas aumentan un 35%, y los pequeños productores disminuyen un 40%, desplazados por actores de mayor escala.

**Palabras clave:** Río Güejar; cambios uso del suelo; diagramas causales; modelación basada en agentes.

**How to cite:** Chicacausa, N., Otalora-Low, M., Carrillo-Acosta, N., Arenas-Bautista, M.C., and Preziosi-Ribero A., Agent-Based models for integrated water resource management: quantifying land use changes by integrating economic and social incentives. Case study: Vista Hermosa (Meta). DYNA, (92)238, pp. 57-65, July - September, 2025.

Universidad Nacional de Colombia.  
Revista DYNA, (92)238, pp. 57-65, July - September, 2025, ISSN 0012-7353  
DOI: https://doi.org/10.15446/dyna.v92n238.118608



## 1 Introduction

Water, an indispensable element for sustaining life and fostering human development, is confronted with substantial challenges in the contemporary context. These challenges are directly related to population growth, industrial expansion, and the intensification of agricultural activities. These factors have increased water demand to levels that exceed the natural renewal capacity of water systems in many regions [1]. Over the past two decades, water consumption has increased by 0.8% annually, a rate that has consistently exceeded the estimated population growth rate of 1% [2]. Furthermore, climate change is altering hydrological cycles, and land use transformations are degrading ecosystems essential for water regulation [3].

Despite its abundant water resources, including more than 2,132 major rivers, an average annual precipitation of 2,600 mm, and a total available annual water supply (TAWS) of 900,000 Mm<sup>3</sup>, Colombia is confronted with challenges related to its water resources. The uneven distribution of rainfall throughout the year gives rise to agricultural, economic, and social dynamics that give rise to dissatisfaction with water access, affecting communities. In the Orinoquia region, the average annual precipitation is 2,740 mm/year, with a TAWS of 267,000 m<sup>3</sup>, representing 32% of the country's water reserves [4]. Conversely, the region exhibits a 35% land transformation rate due to deforestation and the conversion of forests into monocrop such as rice and corn, which has reduced the soil's capacity to retain water. According to González (2022), over 30% of the forests in the Serranía de la Macarena (Meta) have been converted into agricultural areas, impacting both surface water availability and biodiversity, which sustains local communities. The repercussions of the armed conflict, which for years promoted the establishment of illicit crops and hindered the sustainable management of resources, continue to be a challenge. Subsequent to the ratification of peace accords in 2016, initiatives promoting the transition to legal crops such as cacao and coffee have been implemented with the objective of mitigating environmental degradation and providing economic alternatives to local communities. Nevertheless, these initiatives continue to confront obstacles, including constrained access to legitimate markets and enduring disputes concerning land utilization.

From an integrated perspective, contemporary water management must acknowledge that water constitutes not only a natural resource but also an economic and social asset with profound ramifications for public health, food security, and economic growth. In this context, Integrated Water Resources Management (IWRM) has emerged as a key strategy to address these issues. This approach aspires to achieve a balance between economic development, social welfare, and environmental protection. In Colombia, Law 896 of 2017 signifies a landmark in this endeavor, as it establishes regulations for the efficient use of water and promotes sustainable practices. However, the implementation of this legislation has been uneven, as over 60% of municipalities lack the institutional capacity to meet the established standards, creating a significant gap between policies and their application. Furthermore, the interaction between traditional water users, such as rural and indigenous communities, and new economic actors, such as large agricultural companies, has led

to an escalation in social conflicts.

A notable challenge pertains to the limited integration of social and physical factors within water management models. Historically, hydrological models operated under the assumption that water demands remained constant, failing to account for the adaptive capacity of users. This methodological shortcoming has hindered a comprehensive understanding of water systems and the efficacy of public policies [5]. However, recent advancements have introduced innovative tools such as Agent-Based Modeling (ABM). This methodology facilitates the simulation of interactions between human decisions and environmental dynamics. For instance, in simulated scenarios, agents representing farmers, water users, and managers have been employed to identify more effective policies for the sustainable management of water resources. These tools have also facilitated the design of long-term strategies that integrate social and economic realities [6].

The present study aims to quantify changes in land use under different economic and social incentives, analyzing its potential as a tool for implementing IWRM at the regional and local levels. The integration of simulation models, such as Agent-Based Modeling (ABM), is a central tenet of this study. The objective is to identify more effective policies to promote water sustainability, balancing the needs of the agricultural, livestock, industrial, and domestic sectors. This approach will not only deepen the understanding of the interactions between human decisions and environmental dynamics but also contribute to the design of adaptive strategies that acknowledge the social, economic, and ecological realities of Colombian regions.

## 2 Methodology

### 2.1 Study area

The municipality of Vista Hermosa, located in the southern department of Meta, is a region of strategic importance both economically and ecologically (Fig. 1). It borders the departments of Caquetá and Guaviare, and its location in a transition zone between the Andes, Orinoquia, and Amazon regions endows it with exceptional biodiversity and a wide variety of ecosystems [7,19]. In terms of natural resources, the area is rich in mining, agriculture, forestal, and water, and its biodiversity includes a remarkable variety of flora and fauna as well as natural landscapes [7].

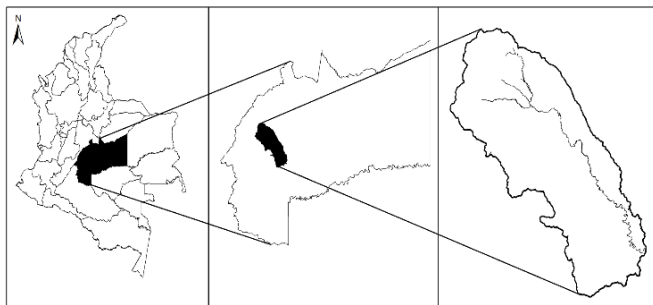


Figure 1. Study area map: the Güejar river basin, Meta, Colombia  
Source: Authored

Vista Hermosa's water resources are primarily linked to the Güejar River basin, one of the country's most important river systems. The basin is crucial for the local ecosystem, feeding a system of wetlands and swamps in its alluvial zone, creating an ecologically valuable habitat. The region is also part of the Macarena Special Management Area (AMEM), a protected area due to its ecological importance, although it is undergoing rapid changes due to recent socioeconomic dynamics, such as the expansion of cattle ranching, affecting both governance and environmental conservation [7].

The tropical climate of the region is characterized by an annual rainfall of more than 2,000 mm, divided into two rainy seasons: the first from March to June and the second from October to December. The remaining months are dry, which affects the hydrological dynamics of the basin. The Güejar River has an average annual flow of 2,361 m<sup>3</sup>/s, with marked seasonal variability, reaching maximum flows ( $Q_5$ ) of 4,298 m<sup>3</sup>/s and minimum flows ( $Q_{95}$ ) of 1,578 m<sup>3</sup>/s. The average annual temperature in Vista Hermosa remains above 24°C, and elevations range from 50 m to 3,700 meters above sea level, supporting diverse microclimates and ecosystems.

## 2.2 Materials and methods

### 2.2.1. Data sources

The digital elevation model (DEM) was derived from SRTM with a height correction of the HydroSHED system [8], with a 30 m resolution, covering the coordinates 3° 05' 13.6" N and 73° 49' 46.9" W. This DEM has an average vertical error of 6.2 m (at a 90% confidence level) and a geolocation error of 9 m for South America. Physical parameters, such as elevation and slopes, were extracted from this DEM. The closing point of the basin was located at the Piñalito station (cod 32077070), and the drainage networks provided by the Instituto Geográfico Agustín Codazzi (IGAC) were used to delineate and characterize the basin.

The study area was delineated using ArcGIS software version 10.0. With the basin delineated, land cover types were identified qualitatively using the Corine Land Cover methodology, which was obtained from the open IDEAM repository. The most recent map with information is from 2018, and comes with information on six different detail levels. For the case of the study area, the first three levels of detail were used, and the total number of land covers was estimated to be 20.

Meteorological and hydrological data in Colombia are freely accessible through the Institute of Hydrology, Meteorology, and Environmental Studies (IDEAM). For this study, daily rainfall data from stations covering the entire Güejar basin were used. A missing data analysis was conducted, ensuring that only stations with less than 10% missing data were included. Additionally, 39 variables, categorized as Ordinary Climate, Main Climate, Limnigraphic, Limnometric, and Pluviometric, were considered for the analysis based on the basin area. Precipitation within the basin was estimated using the Thiessen method [9,10], while Evapotranspiration (ET<sub>o</sub>) was calculated using the Hargreaves-Samani method [11,12].

The calibration period for the model was set between

1991 and 2010, while the validation data came from 2010 to 2020. Missing values for the calibration period were filled in using linear regression methods. With the calibrated data, it was possible to estimate the minimum and maximum flows for the basin over 5, 10, and 20-year periods, and to conduct a preliminary analysis of potential flood areas using the Rainfall-Runoff-Inundation (RRI) model.

### 2.2.2. Hydrological model GR2M

The GR2M model is a simple basin conceptual hydrologic model developed by CEMAGREF (Center for Agricultural Research and Environmental Engineering of France). It is one of the most widely used models in the world for estimating runoff in river basins, especially in situations where data availability is limited. This model is based on a reservoir approach, where multiple reservoirs simulate the hydrological processes occurring in a basin (Fig. 2). The GR model consists of four key components, or reservoirs, that simulate the transformation of precipitation into streamflow:

- **Precipitation and Evapotranspiration:** These are the main inputs, with precipitation determining water storage and evapotranspiration controlling water loss from the system.
- **Production Reservoir:** Simulates the conversion of precipitation into water available for runoff, releasing accumulated water to the stream.
- **Interception Reservoir:** This reservoir handles small variations in runoff from intense rainfall by storing water before it reaches the drainage system.
- **Drainage reservoir:** Manages excess water from precipitation and releases it into the main stream of the watershed.

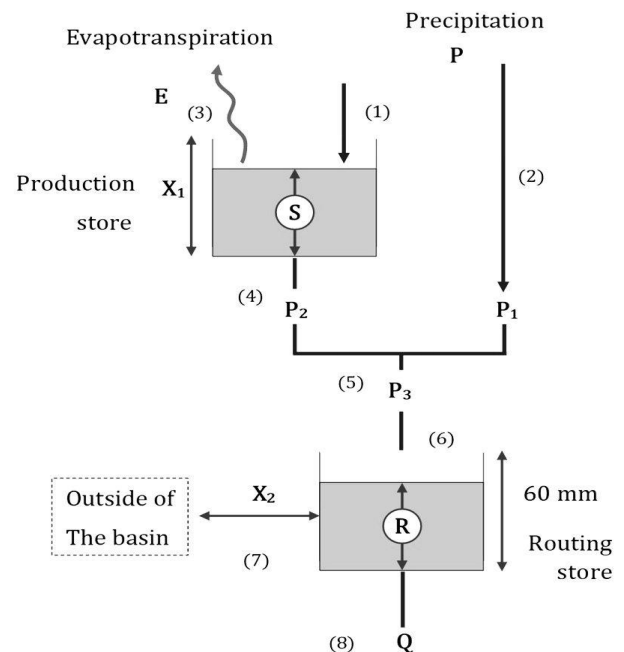


Figure 2. Structure GR2J Hydrological Model  
Source: Dittthakit et al., 2021. [13]

The GR model assumes that the hydrologic behavior of a watershed can be represented by the response of the system to precipitation and evapotranspiration, considering that runoff depends on the storage capacity of the reservoirs. In simple terms, the model uses a reservoir approach with a limited number of parameters to describe the dynamics of the basin. One of the main advantages of this model is its simplicity and low data requirements, making it suitable for basins with limited data. However, the predictive ability of the model is directly influenced by the quality of the input data, such as the accuracy of precipitation and evapotranspiration. In addition, the GR2M model is monthly, i.e. it estimates outputs (flows) based on a monthly time frame, which simplifies the analysis of large amounts of data over the long term.

The GR2M model requires calibration of its parameters, which are typically adjusted using optimization techniques such as least squares or evolutionary algorithms to improve the match between observed and simulated flows. The main parameters that require calibration include: the storage capacity of reservoirs, coefficients for converting precipitation to runoff, and coefficients for the drainage and evapotranspiration processes. For the validation of the hydrological model, the Nash-Sutcliffe Efficiency (NSE) (Eq. 1) was used as a goodness-of-fit metric. The NSE assesses the predictive performance of hydrological models by comparing observed and simulated flows, serving as an objective function to evaluate the accuracy of model simulations [14,15]. Observed flow data from the study area were employed to validate the model by directly comparing them with the flows simulated during the analysis period.

$$NSE = 1 - \frac{\sum_{i=1}^n (O_i - S_i)^2}{\sum_{i=1}^n (O_i - \bar{O})^2} \quad (1)$$

Where: NSE represents the efficiency in fractional terms,  $O_i$  represents the observations,  $S_i$  represents the simulation, and  $\bar{O}$  represents the average of the observations.

### 2.2.3. Causal diagram

A causal diagram is a theoretical structure that illustrates the cause-and-effect relationships between variables [16]. It demonstrates how changes in one variable can directly influence others, visually highlighting the many factors that contribute to a particular observed outcome [17]. To enhance clarity and organization, the design of the diagram seeks to minimize overlapping arrows, ensuring a more precise representation of the drivers and dynamics behind land-use transformation.

The data processing for the designated study area was conducted using Vensim software, a program that facilitated the creation of a causal diagram that represents the causal relations in the region [17]. The development of the diagram was informed by three primary inputs: ecosystems, activities, and economic incentives. These elements were connected by arrows of varying thickness to indicate the strength of the relationship, color to denote the primary input, and direction to represent whether the relationship was positive or

negative. A meticulous examination of the feedback loops within the diagram was undertaken to identify reinforcing and balancing interactions that affect the system.

### 2.2.3. Agent-Based Model

The Agent-Based Model (ABM) was developed in Netlogo Software [18]. This ABM has the previously described hydrological model and causal diagram as inputs, seeking to represent the decision-making of different actors within the basin, considering their main economic activity and available area [19].

At setup, we established the random seed at 10 (it could go from -9007199254740992 to 9007199254740992), to guarantee replicable randomness. Also, at setup, the user can select from three scenarios to see changes in the basins productive landscape: Reforestation, where there are active economic incentives to reforest the riparian forest; Protection, where the extirpation of small local farmers is lessened; Neutral, where there is no protection nor restoration.

When the user selects the scenario, a map of the catchment is drawn where each patch is assigned a land cover based on the Corine Land Cover Level 3 methodology with a pixel size of 30 meters. As the patches acquire their land cover, agents are also placed at random (based on the seed), are given a “scale” (small-scale family farmer or big expansionist producer), and acquire the corresponding productive activity (i.e. if they land on open grass, they have cattle as productive activity). With the positions set, the simulation begins according to the selected scenario, however, all scenarios run for 120 ticks which represent ten years (each tick being one month).

If the neutral scenario was selected, every big expansionist would search for the nearest non-occupied patch and transform it into its productive activity. If this agent finds a forest patch it will destroy it, changing its color and name. If, in its search for a patch, encounters a small-scale farmer, it can “eliminate” it and take the land. Both of these actions account for real processes that occur within the basin.

However, if the protection scenario was activated, an additional factor is added to the expansionists where they have to give the small-scale farmers a chance to stay. This action is called by randomness dictated by the same seed and by distance where closeness makes it more likely for small-scale farmers to disappear.

Likewise, if the restoration scenario is active, the riparian forest begins a healing process that is restrained by density factor, where each patch of riparian forest counts how many more of them are within a 2-patch radius, and if there are not enough (“enough” was subjectively stated as less than 35% and it can be changed within the code) then the closest grass patch has a chance of becoming a forest patch.

## 3 Results

### 3.1 Hydrological model GR2M

The calibration of the hydrological model yielded a Nash-Sutcliffe Efficiency (NSE) coefficient of 0.52, indicating a

moderate correlation between the simulated and observed flows of the Guéjar River at the closure station. As shown in the figure, the model effectively captures the seasonal variability of the flow during the period analyzed, showing a general agreement between simulated and observed values. However, it struggles to accurately represent extreme events, particularly during peak flow conditions, where significant discrepancies are evident. This suggests that further parameter adjustments could improve the model's ability to reproduce extreme hydrological events, which is essential for flood risk management and water resource planning in the basin [19].

The application of this calibrated model provided the median flow rate of 137.30 m<sup>3</sup>/s, a critical result that not only serves as a baseline, but also allows the definition of a variability range (Fig. 3). This range of variability was then incorporated into the agent-based model to increase the robustness of the overall framework. By introducing this variability, the agent-based model can better simulate the dynamic interactions within the system, providing a more comprehensive understanding of the hydrological processes at play. In turn, this integration allows the analysis of both typical and extreme scenarios, providing valuable insights for more effective management of water resources and preparation for potential flood risks. Although the hydrological model has limitations in reproducing extreme events, its performance in capturing seasonal trends and its response to precipitation variability make it a suitable tool for this analysis, particularly in understanding average monthly patterns and assessing the impact of climate variability on the system.

Despite these limitations, the results can be considered satisfactory for the purposes of this study, which focuses on the analysis of average monthly patterns of climatic and hydrological variables. The response of the model to precipitation variability is physically consistent, indicating that its conceptual framework is appropriate for representing the hydrological behavior of the basin at a monthly scale. This reinforces its usefulness as a tool for assessing the impact of climate variability and supporting decision-making in water resource management in the region [19].

### 3.2 Causal diagram

The causal diagram of Vista Hermosa (Fig. 4), highlights the complex interplay between changes in land use, economic activities, and environmental degradation. Agricultural practices (Fig. 4.-3), including coffee, rice, corn, and

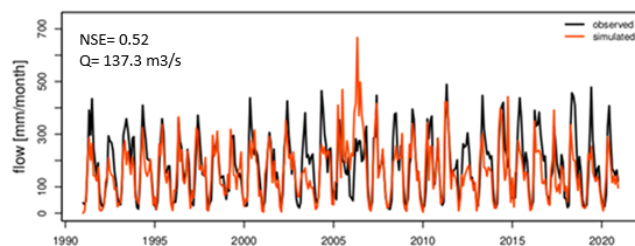


Figure 3. Hydrological model calibration  
Source: Authored

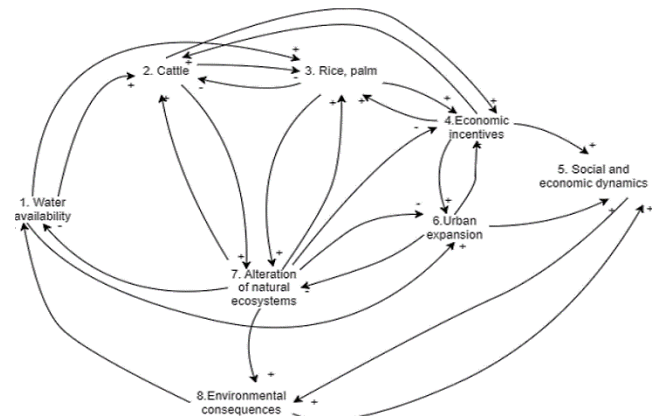


Figure 4. Causal Diagram of Vista Hermosa  
Source: Authored

sugarcane farming, in conjunction with pasture grazing, have been identified as significant contributors to deforestation. These activities have been identified as key contributors to the transformation of dense forests into pastures and fragmented vegetation, resulting in a reduction of biodiversity and ecosystem alterations. Furthermore, the tourism, commercial and manufacturing sectors, in their indirect role, contribute to the exacerbation of these land-use changes by increasing demand for land and natural resources. While Tourism offers the potential for sustainable development, its benefits can be undermined in the absence of adequate regulations to prevent habitat destruction.

The environmental consequences (Fig. 4.-8) of these activities are profound, with deforestation resulting in the proliferation of secondary vegetation and fragmented forests that exhibit a diminished capacity to support biodiversity and regulate water cycles. Critical ecosystems, such as gallery forests, are particularly vulnerable to land conversion and urban expansion, which threatens their ecological functions and climate-regulating capacities. To elucidate these relationships, a causal diagram was constructed using the Vensim software [19]. This diagram represents the intricate interplay among ecosystems, activities, and economic incentives within the Vista Hermosa region. The direction of the arrows in the diagram is indicative of the strength, nature (positive or negative), and key drivers of these relationships. This analysis revealed feedback loops that highlight how human activities and natural processes reinforce one another, worsening environmental degradation if left unchecked.

Social and economic dynamics (Fig. 4.-5) play a pivotal role in the observed changes in land use in Vista Hermosa. Communities, particularly resettled families and small-scale farmers, frequently prioritize short-term economic survival due to constrained access to alternative livelihoods and deficient infrastructure. These conditions give rise to unsustainable practices, including deforestation and overgrazing, which in turn further degrade the integrity of the ecosystems. Socio-economic inequalities influence community participation in conservation initiatives, often marginalizing those who depend most on natural resources. The implementation of targeted programs, complemented by economic incentives that promote sustainable practices, is



imperative for ensuring long-term environmental sustainability and enhancing community well-being.

Although stronger conservation laws provide an essential framework for sustainable land management, they alone are insufficient to address the complex and interconnected challenges of environmental degradation. While stricter penalties for illegal deforestation and well-enforced zoning policies to ecosystems, such as gallery forest, are crucial steps, they must be complemented by strategies that go beyond regulatory measures.

Economic incentives (Fig. 4-4), such as subsidies for sustainable farming practices or financial rewards for ecosystem services, play a pivotal role in aligning individual and community actions with conservation goals. However, incentives alone may falter without effective organization and collaboration among users. Capacity-building programs that empower local communities with the knowledge and resources to implement sustainable practices are key. Additionally, promoting alternative livelihoods can reduce the reliance on environmentally damaging activities, creating a more resilient socio-economic foundation.

The synergy between legal frameworks, economic incentives, and grassroots organization is essential. By fostering networks of cooperation among users, enabling shared governance, and ensuring equitable distribution of benefits, communities in regions like Vista Hermosa can collectively work toward preserving natural ecosystems while achieving sustainable development. This multifaceted approach tackles both the underlying causes and the visible effects of environmental degradation, laying a solid foundation for sustainable long-term solutions.

### 3.3 Agent-based model

Social and economic incentives are clearly observed in a protection scenario where the local population has a higher prevalence compared to scenarios without incentives. This is illustrated in Fig. 5, which shows the evolution of the relative population in the community of Vista Hermosa, Meta, over time under different scenarios of social and economic incentives. The X-axis represents the simulation time steps (1 tick = 1 month), while the Y-axis shows the relative population of residents. Several series of data are compared: the population with no incentives, the population with standard protection, the population with an additional 20% increase in incentives, and the total impact of social and economic incentives on the community.

Fig. 5-A indicate that in the absence of incentives, the local population experiences a rapid decline over time (from 280 to 260 in 37.5 ticks), suggesting migration or displacement due to adverse socio-economic conditions. In contrast, the implementation of conservation strategies slows down the rate of population loss, suggesting improved community stability with support measures. In particular, a 20% increase in social incentives results in even greater demographic stability, mitigating the out-migration of local residents. These findings are particularly relevant in Vista Hermosa, a region with a history of armed conflict and an economy largely based on agriculture and livestock, where population retention is critical for sustainable development.

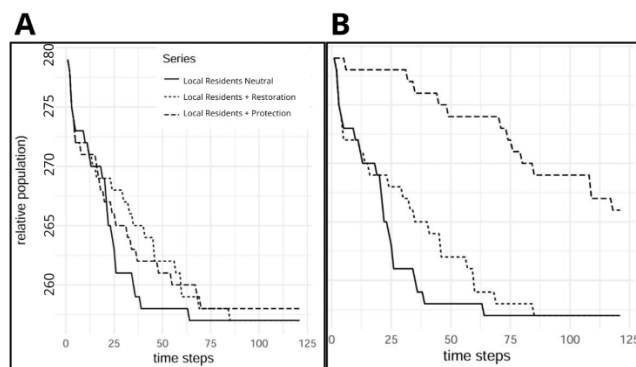


Figure 5. Comparison of the evolution of the relative population of local producers under different incentive scenarios. A- Social incentive scenario. B- Economic incentive scenario.

Source: Authored

In this context, the results of the model shown in Fig. 5-B reinforce these conclusions. The evolution of the relative population of local producers under different restoration conditions-no restoration, 5% restoration, and 9% restoration-shows how different strategies can affect population dynamics. The most favorable scenario appears to be the 9% restoration, where the population stabilizes around 253 individuals despite some decline. This scenario mirrors findings from the broader study, where social incentives and restoration efforts contribute to demographic stability and can help mitigate displacement, further supporting the idea that well-designed conservation and incentive strategies are critical to promoting socioeconomic stability, reducing vulnerability, and fostering resilient communities in regions like Vista Hermosa.

Fig. 6-A shows a direct relationship between the implementation of restoration strategies and the evolution of vegetation cover in Vista Hermosa, Meta. The observed trend shows a steady increase in grasslands in the absence of incentives, suggesting a continued expansion of the agricultural frontier, possibly at the expense of natural ecosystems. In contrast, the 5% and 9% restoration scenarios show a smaller reduction in natural forests and shrubs, demonstrating that economic incentives for conservation have a positive impact on the region's environmental resilience.

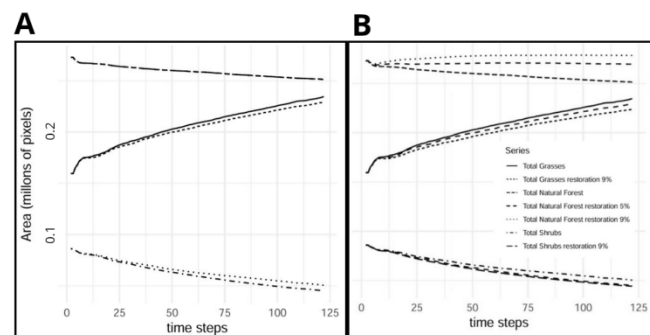


Figure 6. Analysis of the Coverage Areas by Time Steps. A- Social incentive scenario. B- Economic incentive scenario.

Source: Authored

Fig. 6-B shows that the 9% restoration scenario has a significant effect of economic incentives to mitigate the loss of natural habitat. These incentives, combined with restoration efforts, reduce the expansion of grasslands and help maintain a more balanced ecosystem. The expansion of grasslands without incentives highlights the pressure that agricultural activities place on the landscape, particularly in a region where livestock and agriculture have historically been dominant. This suggests that without intervention mechanisms, ecosystem degradation could continue, affecting biodiversity and essential ecosystem services such as water regulation and erosion control. Therefore, integrating economic incentives into restoration strategies not only promotes environmental sustainability, but also contributes to the long-term resilience of the region by ensuring a more sustainable coexistence between agriculture, livestock and natural ecosystems.

On the other hand, the changes in rice and oil palm area under three protection scenarios: no incentives, 5% protection and 20% protection (Fig. 7). For both crops, there is a significant reduction in area in the first 10 months. For rice, the no-incentive scenario shows the largest reduction, while the 5% protection scenario is the most advantageous in mitigating this loss. For oil palm, the most favorable scenario is the 20% protection scenario, which minimizes the reduction in area.

The geographic representation of changes in the study area (Vista Hermosa, Meta) under different protection scenarios (Fig. 8) allows the identification of specific areas where these changes are most pronounced.

In addition, Fig. 9 illustrates the geographic transformation of the region under 5% and 9% restoration scenarios, highlighting the positive impact of economic incentives and conservation policies in promoting restoration and sustainability. These maps provide a more detailed understanding of where the most significant changes are occurring, highlighting regions where forest protection and restoration efforts - supported by economic incentives - are leading to improved environmental outcomes. The geographical concentration of these changes highlights the targeted nature of the interventions and helps to identify areas that may require further attention to maximize the benefits of conservation strategies.

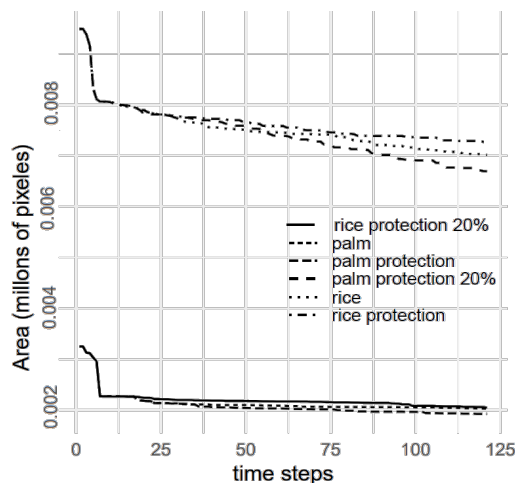


Figure 7. Changes in rice and oil palm area under three protection scenarios. Source: Authored

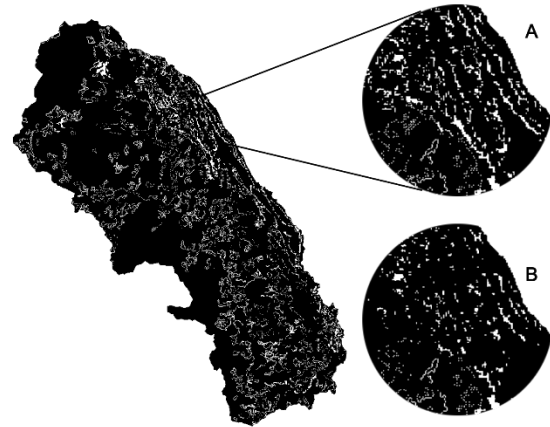


Figure 8. Geographic transformation of riparian forest where no incentives are active. A- initial moment of the model (tick 1), B- consolidated at the end of the simulation (120 ticks), if no modification (local protection or restoration) is activated. The white color represents the riparian forest in the neutral scenario. Source: Authored

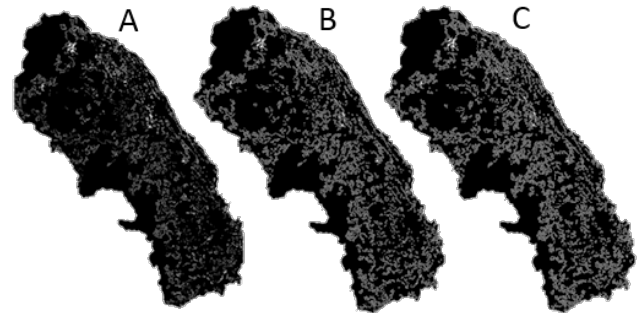


Figure 9. Geographic change under restoration scenarios. A. Scenario without incentives or restoration. B- Final scenario with 5% restoration, and C- Final scenario with 9% restoration. Source: Authored

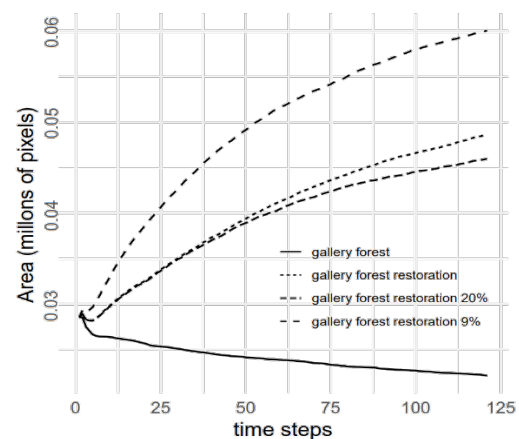


Figure 10. Gallery Forest restoration with economic incentives. Source: Authored

In the restoration scenario, the primary goal is to restore the gallery forest, as it is located closest to the water source. Fig. 10 shows four (4) scenarios faced by this forest: (i) no



restoration or economic incentive, (ii) 5% restoration, (iii) 9% restoration, and (iv) a restoration scenario where rice and oil palm crops are adapted to retain 20% more water. The results show a significant difference, highlighting that if no incentives or restoration efforts are applied, the gallery forest tends to disappear. In contrast, under scenarios with incentives and restoration efforts—regardless of the percentage applied—the forest area not only avoids disappearance but increases significantly. The most favorable outcome is observed under the 9% restoration scenario, where the forest area expands to 0.06 million pixels.

#### 4 Discussion

Based on the results obtained, it is possible to identify significant patterns in the response of vegetation cover and the socio-economic dynamics of the region with respect to the integration of economic and social incentives. These findings highlight the interconnectedness of human and environmental systems and emphasize the importance of well-designed incentives in promoting sustainability.

Social incentives proved to be effective in mitigating local population decline, particularly in the conservation scenarios. As shown in Fig. 3, the relative population of locals in a neutral scenario declines rapidly, reaching critical levels in less than 40 months. However, conservation scenarios with a 5% increase in incentives significantly prolong the retention of the local population, underscoring the importance of social policies to support local producers. This not only ensures the permanence of local communities, but also creates conditions for improved natural resource management and stronger social ties, which are essential for long-term sustainability.

The analysis of vegetation cover further supports the effectiveness of these measures. Fig. 4 shows that protection scenarios have a positive impact on land use, with grassland areas increasing and natural forests and shrubs declining at a slower rate compared to scenarios without incentives. This shows that social incentives not only benefit communities, but also promote more sustainable land use practices that contribute to the conservation of biodiversity and the maintenance of ecological functions. However, the consistent increase in grassland area across all scenarios raises concerns about potential over-expansion, which could lead to soil degradation and biodiversity loss. This highlights the need for complementary strategies to regulate land use change and balance grassland expansion with forest and shrub conservation.

Economic incentives, especially in restoration scenarios, also have a significant positive impact on the conservation and restoration of critical ecosystems, such as gallery forests. These forests, which are essential for hydrological regulation and biodiversity, are at risk of disappearing in scenarios without incentives. As shown in Figs. 7 through 10, restoration scenarios—especially those with a 9% increase—achieve substantial recovery, with areas reaching up to 0.06 million pixels. This highlights the potential of targeted economic incentives to protect ecosystems critical to environmental health and water regulation. At the same time, restoration scenarios show that natural forest and shrub cover

declines less drastically compared to neutral conditions, suggesting that economic incentives can influence local actors to adopt more sustainable practices. However, the expansion of grasslands in all scenarios highlights the importance of balancing incentives to avoid unintended consequences that could compromise ecosystem integrity.

The dynamics of rice and palm provide further insight into the effectiveness of these incentives. Both crops show an initial decline in area in the first 10 months under all scenarios. However, protection incentives, especially those that include a 5% increase and water use restrictions that require crops to use 20% more water, mitigate this trend. For rice, the 5% protection scenario proves to be the most favorable, demonstrating the need to tailor incentives to the specific dynamics of each crop to maximize effectiveness and minimize negative impacts on the local economy.

When considering the relative population of local producers, restoration scenarios with a 9% increase in incentives prove to be the most beneficial, maintaining the population at a relatively stable level of 253 individuals. This highlights the importance of combining social and economic incentives to ensure the sustainability of both human and environmental systems. Social incentives help stabilize local populations and reduce pressure on ecosystems, while economic incentives drive the restoration and conservation of critical areas such as gallery forests. Together, these measures create a positive feedback loop that promotes resilience and long-term sustainability.

The integration of well-designed social and economic incentives is proving essential to achieving sustainability in the region. Social incentives stabilize local populations, promote community resilience, and reduce pressure on ecosystems. At the same time, economic incentives promote the restoration and conservation of vital ecosystems. Their success depends on careful design and implementation to ensure that they meet the specific needs of the region while minimizing unintended consequences. Taken together, these approaches are a powerful tool for promoting sustainable development and preserving the delicate balance between human and environmental systems.

#### 5 Conclusions

The integration of social and economic incentives in environmental management demonstrates significant potential to promote sustainability by addressing both human and ecological challenges. Social incentives, focused on protecting local communities, effectively mitigate the decline of local populations, as seen in protection scenarios where their permanence is extended. This not only supports the socio-economic fabric of the region but also contributes to more sustainable resource management by reducing pressure on ecosystems. Furthermore, economic incentives aimed at restoration, particularly those targeting critical ecosystems like gallery forests, show substantial benefits for biodiversity and hydrological regulation. Restoration scenarios, especially with higher levels of investment, lead to significant recovery of forested areas, highlighting the effectiveness of targeted interventions in preserving key ecological functions.

The findings also underscore the need for a balanced approach to incentive design, as unintended consequences, such as the overexpansion of grasslands, may arise. Tailoring economic measures to the specific needs of crops, such as rice and palm, and integrating restrictions on resource use, ensures greater effectiveness while mitigating adverse effects on the local economy. The combination of social and economic incentives proves crucial for achieving long-term sustainability, as these measures work synergistically to stabilize local populations, foster sustainable land-use practices, and conserve vital ecosystems. This study demonstrates that a strategic, context-sensitive application of incentives can serve as a powerful tool for addressing the complex interplay between human and environmental systems, paving the way for resilient and sustainable development.

## References

- [1] FAO. Afrontar la escasez de agua: un marco de acción para la agricultura y la seguridad alimentaria. Organización de las Naciones Unidas para la Alimentación y la Agricultura-FAO. [en línea] 2013. Available at: <https://www.fao.org/4/i3015s/i3015s.pdf>
- [2] Sordo-Ward, A., Granados, A., Iglesias, A., Garrote, L., and Bejarano, M.D., Adaptation effort and performance of water management strategies to face climate change impacts in six representative basins of Southern Europe. *Water (Switzerland)*, 11(5), art. 51078, 2019. DOI: <https://doi.org/10.3390/w11051078>
- [3] Vieira, F., and Ramos, H.M., Optimization of operational planning for wind/hydro hybrid water supply systems. *Renewable Energy*, 34(3), pp. 928–936, 2009. DOI: <https://doi.org/10.1016/j.renene.2008.05.031>
- [4] Instituto de Hidrología, Meteorología y Estudios Ambientales - Ideam. Estudio Nacional del Agua 2022. Ideam. 2023.
- [5] Loaiza-Usuga, J.C. y Valentijn, N., Desarrollo de modelos hidrológicos y modelación de procesos superficiales. Caso de estudio para vertientes de alta montaña. *Gestión y Ambiente*. 14, pp. 23-31, 2011.
- [6] Albertini, C., Mazzoleni, M., Totaro, V., Iacobellis, V., and Baldassarre, G., Di. Socio-Hydrological Modelling: the influence of reservoir management and societal responses on flood impacts. *Water*, 12(5), art. 1384, 2020. DOI: <https://doi.org/10.3390/W12051384>
- [7] Murcia-García, U.G., Guerrero-Rojas M.B., y Vanegas, D., SINCHI. El territorio ordenado es nuestra oportunidad aportes ambientales para actualizar el esquema de ordenamiento territorial. Municipio de Vista Hermosa, Meta. Guía con resultados del proyecto Desarrollo Local Sostenible y Gobernanza Para la Paz, 2019.
- [8] Lehner, B., Verdin, K., and Jarvis, A., New global hydrography derived from spaceborne elevation data. *Eos*, 89(10), pp. 93–94, 2008. DOI: <https://doi.org/10.1029/2008EO100001>
- [9] Ruelland, D., Guinot, V., Levassasseur, F., and Cappelaere, B., Modelling the long-term impact of climate change on rainfall-runoff processes over a large Sudano-Sahelian catchment. *IAHS-AISH Publication*. 333, pp. 59-68, 2009.
- [10] Wagner, P.D., Fiener, P., Wilken, F., Kumar, S., and Schneider, K., Comparison and evaluation of spatial interpolation schemes for daily rainfall in data scarce regions. *Journal of Hydrology*, pp. 464–465, and pp. 388–400, 2012. DOI: <https://doi.org/10.1016/j.jhydrol.2012.07.026>
- [11] Hargreaves, G.H., and Allen, R.G., History and evaluation of Hargreaves evapotranspiration equation. *Journal of Irrigation and Drainage Engineering*, 129, pp. 53-63, 2003. DOI: [https://doi.org/10.1061/\(ASCE\)0733-9437\(2003\)129:1\(53\)](https://doi.org/10.1061/(ASCE)0733-9437(2003)129:1(53))
- [12] Hargreaves, G.H., and Samani, Z.A., Estimating potential evapotranspiration. *Journal of Irrigation and Drainage Engineering*, 108, pp. 223-230, 1982.
- [13] Dittthakit, P., Pinthong, S., Salaeh, N., Binnui, F., Khwanchum, L., and Pham, Q.B., Using machine learning methods for supporting GR2M model in runoff estimation in an ungauged basin. *Scientific Reports*, 11(1), art. 99164-5, 2021. DOI: <https://doi.org/10.1038/s41598-021-99164-5>
- [14] Dakhlou, H., Ruelland, D., Trambay, Y., and Bargaoui, Z., Evaluating the robustness of conceptual rainfall-runoff models under climate variability in northern Tunisia. *Journal of Hydrology*, 550, pp. 201–217, 2017. DOI: <https://doi.org/10.1016/j.jhydrol.2017.04.032>
- [15] Jeong, H., and Adamowski, J., A system dynamics-based socio-hydrological model for agricultural wastewater reuse at the watershed scale. *Agricultural Water Management*, 171, pp. 89–107, 2016. DOI: <https://doi.org/10.1016/j.agwat.2016.03.019>
- [16] Shahar, E., and Shahar, Causal diagrams and the cross-sectional study. *Clinical Epidemiology*, 57, art. 42843, 2013. DOI: <https://doi.org/10.2147/CLEP.S42843>
- [17] Bouchet, L., Thoms, M.C., and Parsons, M., Using causal loop diagrams to conceptualize groundwater as a social-ecological system. *Frontiers in Environmental Science*, 10, art. 36206, 2022. DOI: <https://doi.org/10.3389/fenvs.2022.836206>
- [18] Tissue, S., Wilensky, U., and Tissue, S., NetLogo: design and implementation of a multi-agent modeling environment, 2004.
- [19] Chicacausa N., Otalora-Low M., Carrillo N., Arenas-Bautista M.C, y Preziosi-Ribero A., Exploración de cambios en la sabana: integración de sistemas agroecológicos con modelos multiagentes. Congreso Latinoamericano de Hidráulica, Medellín, Colombia. 2024.

**N. Chicacausa**, received her BSc. Eng. in Civil Engineering in 2025 from Universidad Santo Tomas, Bogota, Colombia. Her work has focused on hydrological modeling coupled with agent models through her participation in the project Agroecological and Hydrological Systems: an approach to coupled models for IWRM based on agents, developed and funded by the Pontificia Universidad Javeriana in the framework of the VRI04-2022 call. ORCID: 0000-0002-4351-1260

**M. Otálora-Löw**, received his BSc. in Ecology in 2022 and MSc. in Conservation and Biodiversity Use in 2023, both from the Pontificia Universidad Javeriana, Bogotá, Colombia. He has worked in land use and water distribution simulations employing Agent-Based Modelling as his main tool. ORCID: 0000-0002-5176-6837

**N. Carrillo-Acosta**, received her BSc. in Ecology in 2023 from the Pontificia Universidad Javeriana, Bogotá, Colombia. She has worked in land use and causal diagram for analysis of water distribution simulations using agent-based modeling. ORCID: 0000-0003-0633-7336

**M.C. Arenas-Bautista**, received the BSc. Eng. in Agricultural Engineering in 2010, the MSc. in Agricultural Engineering in 2011, and the PhD in Civil Engineering in 2020, all of them from the Universidad Nacional de Colombia. Bogotá, Colombia. She is currently assistant professor at the School of Environmental and Rural Studies, Pontificia Universidad Javeriana. Her research interests include: simulation, modeling and forecasting in hydrology; time series analysis; water management and coupled hydrological models with social aspects. ORCID: 0000-0003-1578-5157

**A. Preziosi-Ribero**, received the BSc. Eng. in Civil Engineering in 2010, from the Universidad Nacional de Colombia, the MSc. in Environmental planning and assessment in 2011 from the Politecnico di Torino, and the PhD in Civil Engineering in 2021 from the Universidad Nacional de Colombia. Bogotá, Colombia. He is currently assistant professor at the School of Civil Engineering at Santo Tomas University. His research interests include: Hydrodynamics, Numerical modeling and Statistical Methods. ORCID: 0000-0002-0202-8870



# The adoption of cutting software in small furniture manufacturers: a survey in Brazil

Nádyá Zanin Muzulon<sup>a\*</sup>, Pedro Rochavetz de Lara Andrade<sup>a</sup>, Rafael Henrique Palma Lima<sup>a</sup>, Juliana Verga Shirabayashi<sup>b</sup> & Gislaine Camila Lapasini Leal<sup>c</sup>

<sup>a</sup> Department of Production Engineering, Federal University of Technology - Paraná, Ponta Grossa, Brazil. \* nadyamuzulon@gmail.com, pedroandrade@utfpr.edu.br, rafaelhlma@utfpr.edu.br

<sup>b</sup> Department of Production Engineering, Federal University of Paraná, Jandaia do Sul, Brazil. juliana.verga@ufpr.br

<sup>c</sup> Department of Production Engineering, State University of Maringá, Maringá, Brazil. gclleal@uem.br

Received: March 18<sup>th</sup>, 2025. Received in revised form: July 7<sup>th</sup>, 2025. Accepted: July 15<sup>th</sup>, 2025.

## Abstract

The scientific literature often addresses the Cutting Stock Problem in the furniture industry from the perspective of mathematical modeling and optimization. However, there has been little research exploring how companies—particularly small ones—adopt software tools that implement these methods. This study investigates the adoption of cutting optimization software in the Brazilian furniture sector, focusing on small and medium-sized enterprises (SMEs). A structured survey was conducted with 73 furniture manufacturers across different company sizes. The questionnaire covered company characteristics, production processes, and software usage. Descriptive statistical analysis and ANOVA tests were applied to examine the data. Additionally, a market analysis was conducted to identify and characterize the main software tools currently in use. The findings reveal that adoption rates are significantly higher among medium and large companies, and the most common features of the software tools used in the sector were identified.

**Keywords:** cutting stock problem; furniture industry; software; small and medium-sized enterprises (SMEs)

# Adopción de software de corte en pequeños fabricantes de muebles: una encuesta en Brasil

## Resumen

El problema del corte de stock en la industria del mueble se aborda frecuentemente en la literatura científica desde la perspectiva del modelado matemático y la optimización. Sin embargo, existe poca investigación sobre cómo las empresas adoptan las herramientas de software que implementan estos métodos de solución. Este trabajo explora este tema y ofrece información sobre la adopción de software de optimización en la industria del mueble, con especial atención a las pequeñas empresas. El objetivo de este trabajo es identificar las características y necesidades de las empresas del mueble en Brasil con respecto al uso de software de optimización de corte. Se realizó una encuesta a 73 empresas, lo que permitió identificar el software utilizado, así como su propósito y características. Los resultados indican que la adopción de herramientas de software por parte de las grandes y medianas empresas es mucho mayor en comparación con las pequeñas empresas. Los datos recopilados también revelaron las características más comunes de los softwares utilizados por los fabricantes de muebles.

**palabras clave:** problema del corte de stock; industria del mueble; software; pequeñas y medianas empresas (PYME)

## 1 Introduction

Over the last five years, the Brazilian furniture sector has undergone an evolution in production, foreign trade, and distribution channels, with a growth trend expected to

continue in the years to come [1]. In Brazil, most furniture manufacturers are micro and small enterprises (MSEs), which suffer from weak strategic planning and lower technological capabilities when compared to larger competitors. The country has 46 furniture manufacturing

**How to cite:** Muzulon, N.Z., Andrade, P.R.deL., Lima, R.H.P., Shirabayashi, J.V., and Leal, G.C.L., The adoption of cutting software in small furniture manufacturers: a survey in Brazil. DYNA, (92)238, pp. 66-75, July - September, 2025.



clusters spread across 11 states, with a greater concentration in the Southern and Southeastern regions. Production and consumption vary from residential, institutional, and office furniture, to armchairs and mattresses [2]. Micro and small furniture companies are found throughout the country, with a large portion of firms characterized as woodworking shops that produce customized items according to customer requests [3].

The production process in the furniture sector begins with cutting boards, wood, or its derivatives into smaller items needed to manufacture the final product. After the items have been cut, they may undergo a process of thickness adjustment by bonding additional layers, in order to match the specifications of the product design. Subsequently, the parts are glued and then milled, which provides the finishing touch. After these operations, the items are grouped, drilled, and assembled. In general, how the cutting patterns are planned and executed to obtain these smaller items is a significant challenge and differs from company to company. The cutting pattern generation and Cutting Stock Problems are complex mathematical optimization problems that require computational assistance to obtain reasonable solutions within practical time windows [4].

Although there is a vast offering of software tools for the furniture industry, adopting new technologies in these organizations is still a significant challenge, especially for self-employed carpenters and MSEs. [5] argue that the lower rate of software adoption by smaller companies occurs due to the traditional culture, lack of training and limited understanding of the benefits these software tools might bring to the firm's operations. The lack of optimization software causes these companies to continue making decisions based on empiricism.

Authors such as [6] point out that SMEs face significant barriers, including limited financial resources, a shortage of specialized labor, and insufficient technological capabilities. These challenges are often compounded by improvised problem-solving approaches. Moreover, the production technology used by most furniture manufacturers remains outdated, leading to the inefficient use of solid wood panels. This waste not only increases production costs but also generates the need for more effective waste management strategies [1,7].

According to [8], pressure from customers has a positive effect on the adoption of technologies in SMEs, rever as external support from the government and partners, support from senior management, and technical knowledge of employees, which reduces resistance to change. The author also found that lower acquisition costs have a positive influence on the adoption of new technologies.

Several papers discuss the Cutting Stock Problem in the furniture industry, including [9-14,15]. However, the existing literature has a strong focus on mathematical modeling and solution methods, thus lacking a practical view of the problem from the standpoint of the development of software tools and adoption by SMEs.

The contribution of this study is to address this gap by surveying Brazilian furniture manufacturers to map their characteristics and needs regarding cutting stock software and to identify the most commonly used software tools and

their features. The survey covered a sample of 73 companies of various sizes, including micro, small, medium, and large organizations.

## 2 Theoretical foundation

Cutting problems belong to a category of NP-hard optimization and challenges where the goal is to extract a set of items from a limited number of larger objects, aiming to either minimize resource usage or maximize the total value of the resulting items. The layout of these items—known as cutting patterns—must ensure that no overlaps occur and typically must also account for geometric constraints related to the technical limitations of the cutting equipment [16-17].

Furniture such as tables, chairs, kitchen cabinets, shelves, wardrobes, among others, are the result of cutting problems [18]. Thus, a solution to the cutting problem, according to [19], can be called a cutting plan, which indicates how many times each provided cutting pattern will be used to meet the demand for all items. A cutting plan is generated according to the dimensions of all available objects and considers the demand for each item.

The one-dimensional cutting problem occurs when only one direction is essential to the cutting process, such as when bars and coils must be cut into smaller pieces.

Two-dimensional cuts have two relevant cutting directions, width and length, like larger regular boards, for producing smaller items.

Three-dimensional cuts involve greater complexity and geometric difficulty, such as those encountered in container loading. In these cases, there are three essential dimensions to be evaluated: length, width, and height, to pack different items [20].

The cutting problem can also involve irregular shapes, as in the case of cutting fabrics in garment factories, circular shapes, or vary in  $n$  dimensions.

Among the various dimensions mentioned, when the cutting problem is modeled for the furniture segment, it is common for it to be two-dimensional, as most of the raw materials available for this industry are rectangular wooden plates or sheets that vary in two dimensions.

Cutting Stock Problems are distinguished by the dimensions of their objects and items. There are also other important distinctions; some formulations consider the management of usable leftovers [19-20], which are cut objects that can be reused in future production. Another aspect in approaching the Cutting Stock Problem is its integration with other problems, such as the Lot Sizing Problem [21], which addresses the determination of optimal lot sizes, minimizing production costs, including setup and inventory costs, among others [22].

It is also essential to note that there are at least three characteristics that differentiate items and objects from each other:

- **Format:** Two figures can have the same format but vary in size and/or orientation.
- **Size:** Two figures can be the same size but vary in shape and/or orientation.
- **Orientation:** Two figures may have the same orientation but vary in shape and/or size.

In the works by [23-25], variations in shapes are used for the same segment.

Concerning the variety of items and objects, according to [3], these can be: identical (with the same shape, orientation, and size); weakly heterogeneous (with the same orientation, varying slightly in size); or strongly heterogeneous (with the same orientation, varying greatly in size)

The Cutting Stock Problem applied to the furniture segment has some relevant characteristics used as constraints when generating cutting patterns. It is common for cuts made in the cutting patterns to be guillotined, that is, made from one end to the other. This is due to the restriction of the cutting machine, which is mostly a disconnecting machine [16].

A cutting pattern, however, can be non-guillotined or nesting, meaning it cannot be cut by methods that go from one end to the other, requiring another type of equipment, different than a sectioning machine or saw.

The guillotined cutting pattern can also be divided into stages, determined by the number of times the object must be rotated by 90° to allow the guillotine cuts to be performed.

The one-stage cutting pattern is when longitudinal parallel guillotine cuts are produced. The two-stage pattern occurs when these already-cut strips are positioned one by one and new parallel transverse cuts are generated on them. If after the two stages there is no need for additional cutting, this pattern is called exact; otherwise, it is not exact and is called a three-stage pattern, up to  $n$  stages [17, 23].

A guillotined pattern can also be constrained, when there is a limit to the number of items to be cut from a given larger object, or unrestricted, when there is no such limitation.

Another strategy adopted by many industries is to allow items to be rotated ninety degrees when allocating cutting patterns. However, this is only allowed when the raw material to be cut is smooth, without textures, designs, or veins that could compromise the aesthetics of the cut items and, consequently, of the assembled product.

When the object is smooth and White, the item to be cut can be rotated 90° in the cutting pattern. With rotation, the resulting items have the same aesthetic characteristics. When the object has texture, the item is not allowed to be rotated in the cutting pattern. If the rotation happens, the resulting items will have different characteristics, which can compromise the product's aesthetics.

### 3 Research method

This research uses a survey methodology, which involves collecting data from companies through a structured questionnaire and performing descriptive and statistical analyses of the responses to generate quantitative insights about the target population—in this case, furniture manufacturers [26].

The study was conducted in six stages, with steps 1 through 5 based on the survey process described by [27]:

1. **Context selection:** It was established that any Brazilian company within the furniture segment would be able to answer the survey questionnaire. The questionnaire was not limited to MSEs to allow for comparison of their reality with that of medium and large companies.

2. **Elaboration of the questionnaire:** The elaborated questionnaire contained 20 questions, including multiple-choice, checkbox and open-ended (discursive). The questions' dimensions included the respondents' characteristics, company characteristics (location, size, products), raw material and process characteristics, software usability, and satisfaction with the current cutting process. The survey design followed the guidelines proposed by [26].
3. **Survey validation:** The pilot test was conducted with the collaboration of 3 volunteers, owners of furniture companies, were able to assess whether the questions were clear, understandable and consistent. After testing, some updates were necessary before proceeding with data collection.
4. **Data collection:** The method used for data collection involved contacting companies through emails and social networks, as provided by unions in the segment. The purpose of the work was shared and the link to answer the questionnaire was provided, both were available on Google Forms for 45 days. The sampling process adopted was non-probabilistic for convenience, as defined by [28], being a sample extracted from a source conveniently accessible to the researcher. According to [29], this type of sampling prioritizes practical generalization, that is, ensuring that the knowledge obtained is representative of the population from which the sample was taken, in order to allow inferences from an accessible group. However, it is important to acknowledge that convenience sampling can introduce bias, as the sample may not fully represent the broader population, potentially limiting the generalizability of the findings.
5. **Analysis of the results:** To support interpretation, descriptive statistical techniques were applied using Excel® and Minitab® software. When appropriate, the ANOVA test was performed to identify statistically significant differences in quantitative variables among companies of different sizes.
6. **Software analysis:** In addition to the survey, a market analysis was conducted to identify available cutting optimization software. Tools mentioned by respondents and others found through online searches were analyzed. Only publicly available software (i.e., easily found on the internet) were considered. Information sources included manuals, websites, technical documents, and interviews with vendors.

### 4 Results and discussions

The results and discussions are divided into two sections: Section 4.1 presents the survey results, and Section 4.2 highlights the analysis of software tools.

#### 4.1 Survey results

The questionnaire was distributed to approximately 150 companies in the segment, resulting in responses from 73 companies across 12 Brazilian states, as illustrated in Fig. 1.

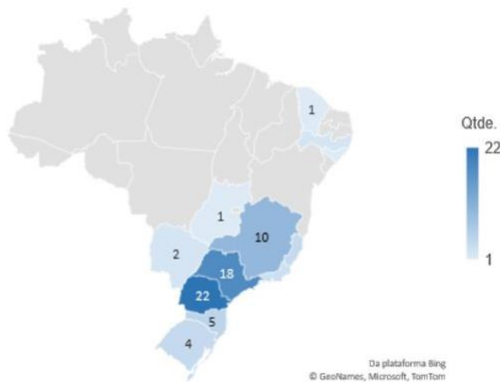


Figure 1. Geographic distribution of participating companies.  
Source: The authors.

Fig. 1 indicates a greater concentration of participating companies in the South and Southeast of the country. Although these regions have the most significant furniture centers, this result may be a research bias, in which the sample was random and, conveniently, carried out in the north of Paraná.

Regarding the size, product line, and positions held by the respondents, Fig. 2 shows the profile of these companies.

According to the classification of company sizes, used by [30], among the companies that participated in the survey, 57% are micro-companies; 21% medium-sized; 17% small-sized and 5% large-sized. Concerning location, 48% are in the Southeast and 31% in the South of the country.

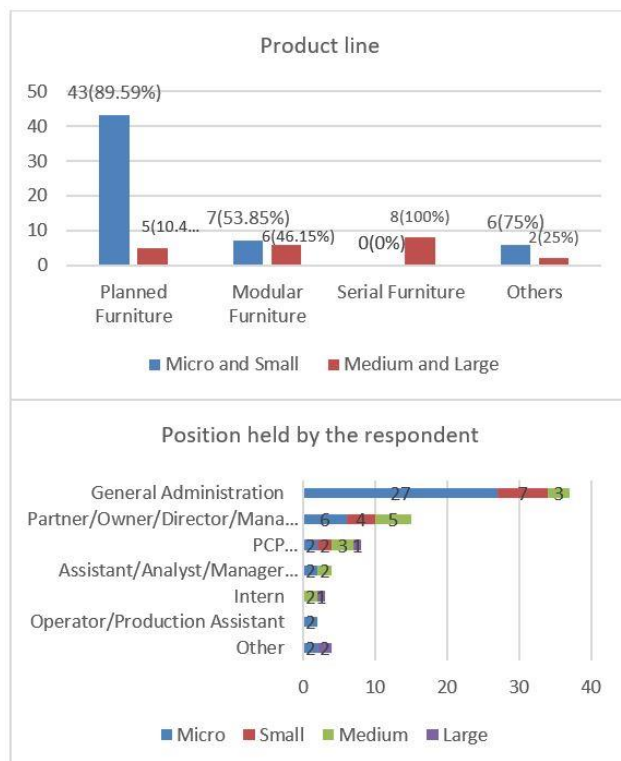


Figure 2. Profile of the companies  
Source: The authors.

Regarding the product line and characteristics of the production line represented in Fig. 2, 62% of the companies are focused on planned furniture and 17% on modular furniture, which reflects production of micro and small companies. Among those who answered series production, 62.5% are medium and 37.5% are large companies. Manufacturers of decorative, rustic, children's furniture, office furniture, and gaming furniture also participated in the research.

To plan cuts and achieve good results, it is essential that the person responsible for the activity has the necessary knowledge to execute it effectively. Thus, those responsible for this step in these companies were evaluated and represented in Fig. 3.

The highlight in Fig. 3 represents the difference between those responsible for cutting planning in micro and small companies when compared to medium and large companies. In medium and large companies, Planning and Production Control (PCP) sectors and programmers predominate in the execution of this function.

With regard to micro and small companies, there is a wide variation between the positions responsible for this activity, where the owners, carpenters or operators often plan the cut, representing 46.3% of them. This shows how specific sectors for programming, planning, and production control can still be scarce in smaller companies.

For the descriptive analysis of the data, the size of each company was also related to the characteristics of the objects and items used, the percentage of losses, and the quality of the cutting processes. Fig. 4 illustrates the variation in raw materials according to the company's size.

Fig. 4 shows a higher frequency of weakly heterogeneous objects. Micro and small companies exhibit greater variability among themselves in terms of the type of raw material, as there is no standard for this issue among companies of this size.

The raw materials used in medium and large companies are also similar to each other, predominantly weakly heterogeneous objects.

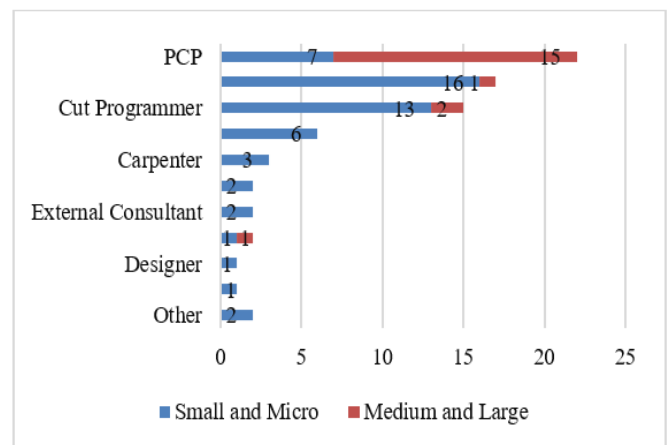


Figure 3. People responsible for cutting planning  
Source: The authors.

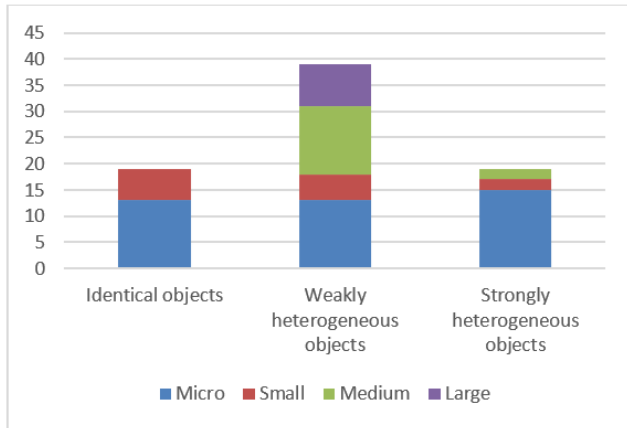


Figure 4. Variation of raw material  
Source: The authors.

Fig. 5 lists the variety of demand for items, categorized by company size.

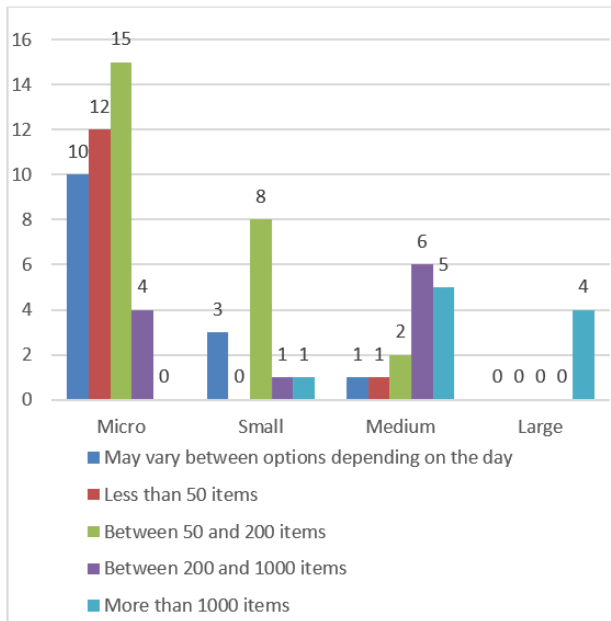


Figure 5. Demand for items  
Source: The authors.

The demand for items shown in Fig. 5 refers to the daily quantity of individual parts that need to be produced to make up the final products. According to the figure, smaller companies have different behaviors, with a large variation in the number of items. Approximately 30% of the microenterprises have demands of less than 50 items, while small companies predominantly have demands between 50 and 200 items, and may reach a demand greater than 1000 units.

Evaluating the demand of medium-sized companies, it is noted that they share the size of the demand with smaller companies but with less variability and predominating demands of 200 to 1000 items and greater than 1000.

Thus, there are indications that the growth in demand for

items is accompanied by an increase in the size of companies. That is, the larger the company, the greater the daily demand for items to be cut. This is confirmed by examining the demand for items from large companies, which consistently exceeds 1000 units.

This demand is not limited to the number of types of items required, but also to the quantity of units of each type. In microenterprises, this demand tends to be lower, both in variety and volume, while in larger companies, the quantity of items generated daily is significantly higher. This is because, as the company grows, the complexity of production increases, requiring a greater variety of parts to meet the diversification of final products. This increase in the diversity of items makes the problem of cutting inventory more challenging, as there are more possible cutting patterns to be considered, directly impacting the efficiency of material use. As a result, larger companies invest more in specialized software to optimize this process, reducing waste and improving the quality of production planning.

To evaluate whether the percentage of material loss differs according to the company size, a one-way ANOVA was performed using Minitab. The analysis compared loss percentages reported by companies categorized as micro, small, medium, and large. The results indicated no statistically significant difference among the groups ( $p = 0.699$ ), suggesting that company size does not have a measurable impact on the percentage of material loss in the sample analyzed.

Although the one-way ANOVA indicated no statistically significant differences in loss percentage among company sizes ( $p = 0.699$ ), the boxplot revealed notable distribution patterns across the groups (Fig. 6). Micro and small companies demonstrated higher variability in material loss, with several outliers observed in the micro category, suggesting inconsistency in production processes or less efficient cutting operations. In contrast, medium-sized companies showed the lowest median loss and a more compact distribution, indicating greater process stability. Large companies also demonstrated a relatively low median loss, though with broader variability. These visual trends suggest that, despite the lack of statistical significance, company size may still influence cutting efficiency and material waste in practical terms.

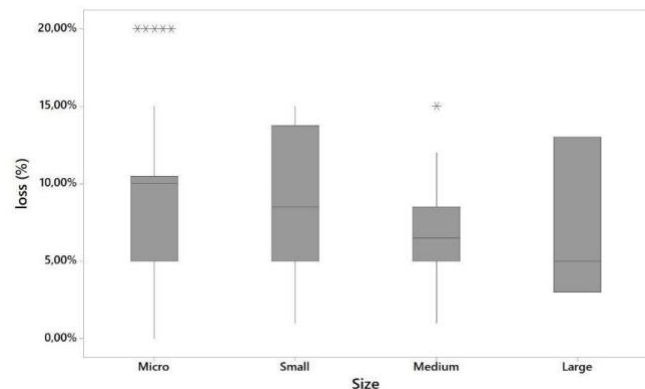


Figure 6. Percentage of losses  
Source: The authors.



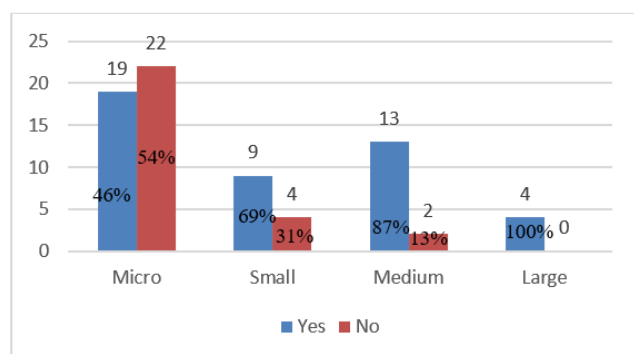


Figure 7. Use of software tools  
Source: The authors.

The use of software tools in the planning and execution of the cutting plan was also evaluated in the applied questionnaire (Fig. 7).

In Fig. 7, it is possible to observe that approximately 46% of micro companies, 69% of small companies, 87% of medium companies, and one 100% of large companies use software, which represents 62% of the total. Thus, a propensity to increase software adoption is noticeable as company size increases, and the number of "No" responses regarding software usage decreases accordingly.

A comparison between the boxplot of material loss and the chart on the use of software tools reveals a potential relationship between cutting software adoption and process efficiency across company sizes. As illustrated, microenterprises exhibit both the lowest adoption rate of software tools (46%) and the highest variability in material loss, with several outliers, suggesting inconsistent or inefficient cutting practices. In contrast, medium and large companies, which report higher adoption rates (87% and 100%, respectively), show lower median losses and more compact distributions in the boxplot, indicating greater process control and reduced waste.

These trends suggest that the use of cutting optimization software may be associated with lower material losses and greater operational consistency. Although causality cannot be confirmed from this observational data, the pattern whereby microenterprises exhibit both lower levels of software adoption and higher, more variable material losses highlights the potential role of technology in improving production efficiency.

Regarding the difficulties faced by companies, Table 1 shows that most problems stem from a lack of qualified labor or a person responsible for implementing the cuts, as well as high material loss and delay in cutting planning. Such problems may be directly related to the lack of a software tool or the presence of a tool that is difficult to use, which is often the case in smaller companies.

Cutting planning carried out without an adequate software tool or empirically, which is the case of smaller companies, results in high losses (as shown in Fig. 9) and excessive times for generating cutting plans, becoming susceptible to errors and combinations of standards that are not great. When the lack of tools is combined with the absence of a qualified employee, the likelihood of mistakes can be even greater.

Table 1.  
Difficulties faced by companies in the furniture segment

Difficulty	Micro and Small Companies (%)	Medium and Large Companies (%)
Lack of skilled labor	31.5%	26.3%
Demanded items not cut in stipulated time	27.8%	26.3%
High material loss	22.2%	26.3%
Cut planning is carried out empirically without prior planning	18.5%	21%
It takes time to plan cutting plans	14.8%	5.3%
Tool or Software difficult to use	9.2%	10.5%
There is no one responsible for cutting planning	7.4%	5.3%

Source: The authors.

The software used by the participating companies is shown in Fig. 8.

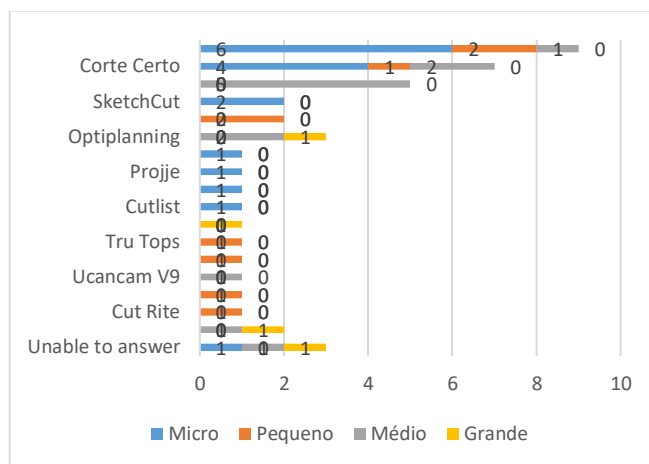


Figure 8. Software tools  
Source: The authors

Among the Information Systems used by the 45 companies, there is a wide variety, which reflects the availability of software on the market. The software tools Promob Cut Pro, Corte Certo, and Ardis Cutting Optimizer appeared more often among the responses, but large companies did not report their use.

Among the responses, Enterprise Resource Planning (ERP) and Corel Draw were cited, but such tools, although used by some companies, do not generate cutting plans independently. Thus, they were not considered in the graphical analyses. Such responses indicate that micro and small companies lack adequate knowledge on this subject. The Audaxis software was also mentioned by one of the companies that manufactures sofas, but it is used in the fabric-cutting process and not in wood and derivatives.

To better analyze the behavior of losses by company size and software usage, a boxplot was generated, as shown in Fig. 9.

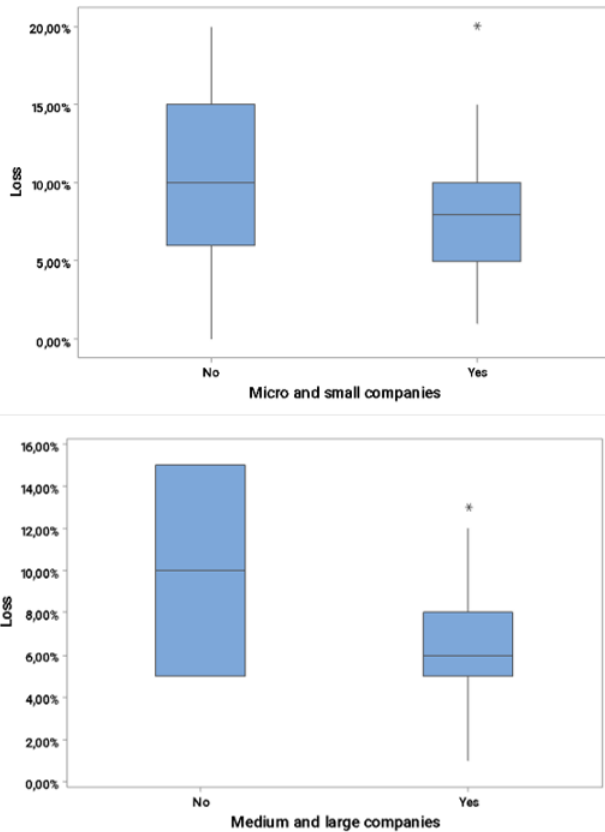


Figure 9. Losses and use of software according to the size of the company  
Source: The authors.

The graphs in Fig. 9 indicate that micro and small companies that do not use software demonstrate variability and a greater amplitude in the percentage of losses. They also present losses greater than 10%. Regarding companies that use software, 50% of micro and small companies have losses lower than 8%, while 50% of medium and large companies have losses lower than 6%.

It is not possible to draw conclusions about the losses of medium and large companies that do not use software tools due to the small sample size; although, it is possible to infer that their losses also increase significantly.

#### 4.2 Analysis of software tools

In order to analyze some software tools available on the market and used by companies participating in the survey, a selection was made based on their responses, and an exploratory search was conducted for commercial Cutting Stock Problem software usable to the furniture sector.

The characteristics of these software were analyzed and listed based on information contained in manuals, websites, and online interviews carried out with suppliers.

Table 2 presents a summary and analysis of these software tools, based on the characteristics of the cutting problem and software requirements. The information was obtained from manuals and observations resulting from using these tools.

The software tools are available in several formats: web-based, downloadable, or as smartphone applications. Some

also offer diagrams of the automatically generated section planes, while others require manual construction. Additionally, there are cases where the automatically generated section planes can be manually adjusted.

Some of these software tools offer free versions, which may have limitations in functionality, paid versions, or personalized services tailored to customer needs. Cortecloud, Dinabox, and CutList tools can be used as plugins in Sketchup. Likewise, Ottimo Perfect Cut, Cut Rite, Optiplanning (Biesse), and Titanium are available as Promob plugins.

However, the table presented in Annex 1 provides attributes that can guide companies in the furniture segment seeking to acquire software tools.

Information was collected from 19 different software tools that create cutting plans for the furniture segment. This table lists commercial software that can help different companies, especially small ones, to choose and adhere to information technology for a daily process that can be repeated countless times and is normally performed manually.

#### 5 Final considerations

This study offers a practical perspective on the cutting problem in the furniture sector from the viewpoint of companies that need to adopt software solutions to address their issues. This process is important for understanding what the difficulties and real needs of this segment are and how companies' behavior may vary according to their size.

In this context, the survey enabled the identification of key difficulties faced by furniture manufacturers, including lack of skilled labor, high material waste, and delays in planning, which align with the barriers discussed in the literature. The findings reinforce that outdated production technologies and empirical planning practices remain prevalent among small manufacturers, leading to increased waste and reduced operational performance.

The study supports the understanding that software usage is associated with lower material losses and greater consistency in operations. Even though the ANOVA did not find statistically significant differences, the visual trends observed suggest that company size—and by extension, software adoption—can influence cutting efficiency in practical terms.

Moreover, this work contributes by providing a mapping of commonly used software tools in the sector and by making this information accessible to micro and small companies, which often lack structured processes and guidance in selecting appropriate technologies. The list of software tools identified, along with their features, offers practical value for decision-making regarding digital investments and the adoption of cutting optimization systems.

The process of selecting a software tool for a company in the furniture sector is complex in itself, primarily due to the vast diversity of tools available on the market. The different applications, characteristics, costs, and acquisition processes make this task difficult and, in most cases, time-consuming. When these difficulties are added to the lack of investment, insufficient employee knowledge, and personal resistance, the

process of acquiring a tool becomes even more challenging.

Thus, guiding these businesses to choose a tool that boosts their results becomes essential, once the difficulties these companies have in obtaining it, permeate from the self-assessment of their needs to the lack of guidance on where to find such tools, as well as a lack of direction for these processes.

Thus, the findings of this research can inform policymakers, business associations, and technology providers on how to better support digital transformation initiatives within small and medium-sized enterprises (SMEs), particularly in traditional sectors like furniture manufacturing.

However, this study is limited by the geographic scope of its sample, which focused predominantly on companies located in the Southern and Southeastern regions of Brazil. These areas are historically more industrialized and technologically developed, which may not fully represent the national reality. Future research could expand to include furniture manufacturers from other regions and explore how regional disparities impact technology adoption and production efficiency.

As future work, we suggest the development of support tools to help small manufacturers assess their technological needs and identify suitable software solutions, considering the diversity of available tools and the multiple criteria involved in this decision. Further studies may also investigate the critical success factors and barriers to software implementation, as well as the impact of digital tools on productivity and competitiveness in SMEs.

## Declaration of interest statement

The authors declare that they have no conflicting interests in this publication.

## References

- [1] Tang, M., Liu, Y., Ding, F., and Wang, Z., Solution to solid wood board cutting stock problem. *Applied Sciences*, 11(17), art. 7790, 2021. DOI: <https://doi.org/10.3390/app11177790>
- [2] Brainer, M.S.D.C.P., Furniture sector: Brazil and BNB's area of activity Analysis of general aspects. *ETENE Sectoral Notebook*, Banco do Nordeste, 6(169), 2021. [date of reference July 08<sup>th</sup> of 2025]. Available at: <https://www.bnb.gov.br/s482-dspace/handle/123456789/827>
- [3] Galinari, R., Teixeira Junior, J.R., and Morgado, R.R., The competitiveness of the Brazilian furniture industry: current situation and perspectives. *Estudo técnico*, Brasil, BNDES, 2013 [date of reference July 08<sup>th</sup> of 2025]. Available at: <http://www.bndes.gov.br/bibliotecadigital>
- [4] Wascher, G., Haußner, H., and Schumann, H., An improved typology of cutting and packing problems. *European Journal of Operational Research*, 183(3), pp. 1109–1130, 2007. DOI: <https://doi.org/10.1016/j.ejor.2005.12.047>
- [5] Prates, G.A., and Ospina, M.T., Tecnologia da informação em pequenas empresas: fatores de êxito, restrições e benefícios. *Revista de administração contemporânea*, 8, pp. 9-26, 2004. DOI: <https://doi.org/10.1590/S1415-65552004000200002>
- [6] Lopez-Nicolas, C., Soto-Acosta, P., Analyzing ICT adoption and use effects on knowledge creation: an empirical investigation in SMEs. *International journal of information management*, 30(6), pp. 521–528, 2010. DOI: <https://doi.org/10.1016/j.ijinfomgt.2010.03.004>
- [7] Kim, S.H., Jang, S.Y., and Yang, K.H., Analysis of the determinants of software-as-a-service adoption in small businesses: risks, benefits, and organizational and environmental factors. *Journal of Small Business Management*, 55(2), pp. 303–325, 2017. [date of reference July 08<sup>th</sup> of 2025]. Available at: <https://www.tandfonline.com/doi/full/10.1111/jsbm.12304>
- [8] Zamani, S.Z., Small and Medium Enterprises (SMEs) facing an evolving technological era: a systematic literature review on the adoption of technologies in SMEs, *European Journal of Innovation Management*, 25(6), pp. 735–757, 2022. [date of reference July 08<sup>th</sup> of 2025]. Available at: <https://www.emerald.com/insight/content/doi/10.1108/ejim-07-2021-0360/full/html>
- [9] Faggioli, E., and Bentivoglio, C.A., Heuristic and exact methods for the cutting sequencing problem. *European Journal of Operational Research*, 110(3), pp. 564–575, 1998. DOI: [https://doi.org/10.1016/S0377-2217\(97\)00268-3](https://doi.org/10.1016/S0377-2217(97)00268-3)
- [10] Lee, H.F., and Sewell, E.C., The strip-packing problem for a boat manufacturing firm. *IIE Transactions*, 31(7), pp. 639–651, 1999. [date of reference July 08<sup>th</sup> of 2025]. Available at: <https://link.springer.com/article/10.1023/A:1007691017460>
- [11] Yue, Q., and Gao, L., Genetic annealing algorithm for cutting stock problem in furniture industry. In *2009 IEEE 10<sup>th</sup> International Conference on Computer-Aided Industrial Design & Conceptual Design*, pp. 87–91, 2019 [date of reference July 08<sup>th</sup> of 2025]. Available at: <https://ieeexplore.ieee.org/abstract/document/5374979>
- [12] Pradenas, L., Garcés, J., Parada, V., and Ferland, J., Genotype–phenotype heuristic approaches for a cutting stock problem with circular patterns. *Engineering Applications of Artificial Intelligence*, 26(10), pp. 2349–2355, 2013. DOI: <https://doi.org/10.1016/j.engappai.2013.08.003>
- [13] Oliveira, O., Gamboa, D., and Fernandes, P., An information system for the furniture industry to optimize the cutting process and the waste generated. *Procedia Computer Science*, 100, 711–716, 2016. DOI: <https://doi.org/10.1016/j.procs.2016.09.215>
- [14] Vanzela, M., Melega, G.M., Rangel, S., and de Araujo, S.A., The integrated lot sizing and cutting stock problem with saw cycle constraints applied to furniture production. *Computers and Operations Research*, 79, pp. 148–160, 2017. DOI: <https://doi.org/10.1016/j.cor.2016.10.015>
- [15] Lima, J.R., and Carvalho, M.A.M., Descent search approaches applied to the minimization of open stacks. *Computers and Industrial Engineering*, 112, pp. 175–186, 2017. DOI: <https://doi.org/10.1016/j.cie.2017.08.016>
- [16] Martin, M., Morabito, R., and Munari, P., Two-stage and one-group two-dimensional guillotine cutting problems with defects: a CP-based algorithm and ILP formulations. *International Journal of Production Research*, 60(6), pp. 1854–1873, 2022. DOI: <https://doi.org/10.1080/00207543.2021.1876270>
- [17] Pitombeira-Neto, A.R., and Prata, B.D.A.A., Matheuristic algorithm for the one-dimensional cutting stock and scheduling problem with heterogeneous orders. *Top*, 28(1), pp. 178–192, 2020. DOI: <https://doi.org/10.1007/s11750-019-00531-3>
- [18] Morabito, R., and Arenales, M., Optimizing the cutting of stock plates in a furniture company. *International Journal of Production Research*, 38(12), pp. 2725–2742, 2000. DOI: <https://doi.org/10.1080/002075400411457>
- [19] Cherri, A.C., Arenales, M.N., Yanasse, H.H., Poldi, K.C., and Vianna, A.C.G., The one-dimensional cutting stock problem with usable leftovers A survey. *European Journal of Operational Research*, 236(2), pp. 395–402, 2014. DOI: <https://doi.org/10.1016/j.ejor.2013.11.026>
- [20] Nascimento, D.N., Cherri, A.C., Oliveira, J.F., and Oliveira, B.B., The two-dimensional cutting stock problem with usable leftovers and uncertainty in demand. *Computers and Industrial Engineering*, 186, art. 109705, 2023. DOI: <https://doi.org/10.1016/j.cie.2023.109705>
- [21] Andrade, P.R.L., de Araujo, S.A., Cherri, A.C., and Lemos, F.K., The integrated lot sizing and cutting stock problem in an automotive spring factory. *Applied Mathematical Modelling*, 91, art. 1023–1036, 2021. DOI: <https://doi.org/10.1016/j.apm.2020.10.033>
- [22] Glomb, L., Liers, F., and Rösel, F.A., Rolling-horizon approach for multi-period optimization. *European Journal of Operational Research*, 300(1), pp. 189–206, 2022. DOI: <https://doi.org/10.1016/j.ejor.2021.07.043>
- [23] Sumey, J.S., and Klinkhachorn, P., Enhancement of ALPS packing yield using a polygon cutting model. In: *Proceedings of Thirtieth Southeastern Symposium on System Theory*, IEEE, 1998, pp. 472–475.

- [date of reference July 08<sup>th</sup> of 2025]. Available at: <https://ieeexplore.ieee.org/abstract/document/660118>
- [24] Pradenas, L., Garcés, J., Parada, V., and Ferland, J., Genotype–phenotype heuristic approaches for a cutting stock problem with circular patterns. *Engineering Applications of Artificial Intelligence*, 26(10), pp. 2349–2355, 2013. DOI: <https://doi.org/10.1016/j.engappai.2013.08.003>
- [25] Konukcu, A.C., and Zhang, J., Effects of full-size panel width on cutting yield of wood-based composites as upholstery furniture frame stocks. *Bioresources*, 14(2), pp. 4181–4193, 2019. [date of reference July 08<sup>th</sup> of 2025]. Available at: [https://bioresources.cnr.ncsu.edu/wp-content/uploads/2019/04/BioRes\\_14\\_2\\_4181\\_Konukcu\\_Zhang\\_Effect\\_s\\_Fullsize\\_Panel\\_Width\\_Yield\\_Furniture\\_Frames\\_15098.pdf](https://bioresources.cnr.ncsu.edu/wp-content/uploads/2019/04/BioRes_14_2_4181_Konukcu_Zhang_Effect_s_Fullsize_Panel_Width_Yield_Furniture_Frames_15098.pdf)
- [26] Kitchenham, B.A., and Pfleeger, S.L., Personal opinion surveys. In: *Guide to advanced empirical software engineering*, London: Springer London, 2008, pp. 63–92. [date of reference July 08<sup>th</sup> of 2025]. Available at: [https://link.springer.com/chapter/10.1007/978-1-84800-044-5\\_3](https://link.springer.com/chapter/10.1007/978-1-84800-044-5_3)
- [27] Forza, C., Survey research in operations management: a process-based perspective. *International Journal of Operations and Production Management*, 22(2), pp. 152–194, 2002. [date of reference July 08<sup>th</sup> of 2025]. Available at: <https://www.emerald.com/insight/content/doi/10.1108/01443570210414310/full/html>
- [28] Andrade, C., The Inconvenient truth about convenience and purposive samples. *Indian J Psychol Med.* 43(1), pp. 86–88, 2021. [date of reference July 08<sup>th</sup> of 2025]. Available at: <https://pubmed.ncbi.nlm.nih.gov/34349313/>
- [29] Etikan, I., Musa, S.A., and Alkassim, R.S., Comparison of convenience sampling and purposive sampling. *American Journal of Theoretical and Applied Statistics*. 5(1), pp. 1–4, 2016. [date of reference July 08<sup>th</sup> of 2025]. Available at: <https://www.sciencepublishinggroup.com/article/10.11648/j.ajtas.20160501.11>
- [30] SEBRAE (Org.), Anuário do trabalho na micro e pequena empresa – 2013, 6<sup>a</sup> ed., São Paulo, DIEESE, 2013 [date of reference July 08<sup>th</sup> of 2025]. Available at: [https://www.sebrae.com.br/Sebrae/Portal%20Sebrae/Anexos/Anuario%20do%20Trabalho%20Na%20Micro%20e%20Pequena%20Empresa\\_2013.pdf](https://www.sebrae.com.br/Sebrae/Portal%20Sebrae/Anexos/Anuario%20do%20Trabalho%20Na%20Micro%20e%20Pequena%20Empresa_2013.pdf)

**N.Z. Muzulon**, graduated and MSc. in Production Engineering from the State University of Maringá (UEM) and PhD student in Production Engineering at the Federal University of Technology - Paraná (UTFPR). Develops research in the areas of Operational Research and in the development of workforce skills in the digital age.  
ORCID: 0000-0003-2882-5402

**P.R. de L. Andrade**, graduated and MSc. in Production Engineering from the Federal University of Paraná (UFPR). PhD in Production Engineering from the São Paulo State University Júlio de Mesquita Filho (UNESP), Bauri campus. He is currently a professor of Production Engineering at the Federal University of Technology - Paraná (UTFPR), Londrina campus. He is a researcher at the Data Mining and Optimization Research Group (GPOMD), working in the optimization research line.  
ORCID: 0000-0001-8142-4195

**R.H.P. Lima**, graduated the BSc. in Computer Science from the State University of Londrina (UEL) in 2004, he obtained his PhD. in Production Engineering from the São Carlos School of Engineering (EESC) / University of São Paulo (USP) in 2012. He is currently an adjunct professor in the Department of Production Engineering at the Federal University of Technology - Paraná (UTFPR Campus Londrina). He works as a teacher and researcher in the areas of Logistics and Supply Chain Management, Operations Management, Computational Intelligence and Quality Management.  
ORCID: 0000-0002-9098-3025

**J.V. Shirabayashi**, graduated the BSc. in Mathematics from the Universidade Estadual Paulista (2005), a MSc. in Electrical Engineering from the Universidade Estadual de Campinas (2009) and a PhD in Electrical Engineering (2014) from the same university. She completed her Post-Doctorate (2022 to 2023) at the Universidade Estadual de Maringá under the supervision of Prof. Dr. Linnyer Beatrys Ruiz Aylon. She is currently an

Adjunct Professor - level D at the Universidade Federal do Paraná, Advanced Campus in Jandaia do Sul. He has experience in the area of Operational Research.  
ORCID: 0000-0003-2453-0017

**G.C.L. Leal**, PhD in Electrical Engineering and Industrial Informatics from the Federal University of Technology - Paraná. Graduated in Production Engineering - Software from the State University of Maringá (2007) and in Data Processing from the University Center of Maringá (2004), with a Msc. in Computer Science from the State University of Maringá (2010). She is an associate professor at the Department of Production Engineering (DEP) and a permanent professor at the Graduate Programs in Production Engineering (PGP) and Computer Science (PCC) at UEM. She develops research in the areas of: Support for Decision Making in Production Systems and Occupational Health and Safety, Software Startups, Quality Improvement and Productivity in Software Development and Process Improvement.  
ORCID: 0000-0001-8599-0776

**Annex 1 –  
Software tools for Cutting Stock Problem in the furniture segment**

FEATURES / TOOL	Promob Cut Pro	Right cut	Ardis Opti- mizer	Sketchcut	Dinabox	Optiplanning (Biesse)	Project	Corteccloud	Simula*	Gplan	Ucancam V9	Titanium	Great Perfect Cut	Cut rite	Cut-Planning	Gmad	Maxcut	Cutlist	Cut micro
<b>Number of citations in the survey</b>	9	7	5	2	2	3	1	1	1	1	1	1	2	1	0	0	0	1	0
Data transmission to machine		✓	✓		✓	✓				✓			✓	✓	✓				
Manual item and plate data entry	✓	✓		✓	✓	✓	✓	✓	✓		✓		✓	✓	✓		✓	✓	✓
It has a library of registered items and plates					✓			✓											
Imports item and plate data	✓	✓	✓	✓		✓		✓	✓	✓	✓		✓	✓	✓		✓	✓	
Limit on the amount of input data		✓																	
Considers cutting blade thickness			✓	✓	✓			✓	✓				✓	✓			✓	✓	
Consider edge tapes	✓	✓	✓	✓	✓			✓						✓	✓		✓	✓	✓
Considers holes	✓				✓			✓									✓		
Considers fibers and grooves in the material	✓	✓	✓	✓	✓			✓	✓		✓		✓	✓	✓		✓	✓	✓
You can choose whether the item can rotate					✓				✓					✓					
Provides number of stages		✓			✓				✓									✓	
Provides number of cuts					✓				✓									✓	
Provides item priority	✓				✓									✓					
Provides costs					✓			✓	✓					✓			✓		
Provides cutting time														✓					
Provides solutions chart	✓	✓	✓	✓	✓	✓	✓		✓		✓		✓	✓	✓		✓	✓	✓
Allows manual edits to solution charts	✓	✓		✓		✓			✓		✓			✓	✓				✓
Has use of leftovers	✓	✓		✓	✓	✓			✓		✓			✓	✓				
Provides guillotine cutting	✓	✓		✓	✓			✓	✓				✓	✓	✓		✓	✓	✓
Provides nesting cut	✓				✓			✓			✓				✓				
Allows printing of results	✓			✓	✓			✓	✓				✓	✓	✓		✓	✓	✓
Provides labels	✓	✓	✓		✓	✓		✓	✓				✓		✓		✓		
Allows integration with other software	✓				✓	✓			✓	✓		✓	✓	✓					
Free Acquisition				✓	✓			✓			✓		✓				✓	✓	✓
Paid Acquisition	✓	✓	✓	✓	✓			✓	*	✓			✓	✓	✓		✓	✓	
Available online					✓			✓										✓	
Available as software	✓	✓	✓	✓					✓	✓	✓		✓	✓	✓		✓		✓
Available as an app				✓				✓							✓				
Personalized service								✓	✓	✓									

Note: \*Not currently marketed

Source: The authors.



# Cost analysis of climate change and prevention measures in the Chancay-Lambayeque Valley, Perú

Alex Segundino Armas-Blancas <sup>a, b</sup>, Silvia del Pilar Iglesias-León <sup>a</sup>, Eric Rendón-Schneir <sup>a</sup>, Guillermo Vilchez-Ochoa <sup>b</sup>, Javier Herrera-Espinoza <sup>b</sup>, Leidy Milady Ramos-Alarcón <sup>c</sup>, Jorge Luis Capuñay-Sosa <sup>a</sup>, Hellen Felicia Blancas-Amaya <sup>d</sup> & Rubén Armando Daga-López <sup>b</sup>

<sup>a</sup> Facultad de Ingeniería Geológica, Minera, Metalúrgica, Geográfica Civil y Ambiental- Minas, Universidad Nacional Mayor de San Marcos, Lima, Perú. aarmasb@unmsm.edu.pe, siglesiasl@unmsm.edu.pe, erendons@unmsm.edu.pe, jcapunays@unmsm.edu.pe

<sup>b</sup> Escuela Profesional de Ingeniería Ambiental, Universidad Nacional Tecnológica de Lima Sur, Lima, Perú. aarmasb@unmsm.edu.pe, gvilchez@untels.edu.pe, jherrerae@untels.edu.pe, rdaga@untels.edu.pe

<sup>c</sup> Universidad Nacional San Luis Gonzaga, Ica, Perú. leidy.ramos@unica.edu.pe

<sup>d</sup> Facultad de Ciencias, Universidad Nacional de Educación, Lima, Perú. hblancas@une.edu.pe

Received: February 6<sup>th</sup>, 2025. Received in revised form: July 8<sup>th</sup>, 2025. Accepted: July 16<sup>th</sup>, 2025.

## Abstract

This study analyzes the economic costs associated with climate change and the implementation of preventive measures in the Chancay-Lambayeque Valley, Peru. Through a cost-benefit analysis, the study quantifies the impact of extreme flood events on agriculture and hydraulic infrastructure, considering scenarios with and without mitigation measures. The results show that adopting structural and non-structural strategies significantly reduces economic losses and enhances the resilience of the region's water and productive systems. The findings emphasize that strengthening investments in resilient infrastructure and adaptation strategies is crucial for the economic and environmental sustainability of the watershed.

**Keywords:** climate change; economic costs; cost-benefit analysis; extreme flooding; mitigation measures.

# Análisis de costos de cambio climático y medidas de prevención en el valle de Chancay-Lambayeque, Perú

## Resumen

El estudio analiza los costos económicos asociados al cambio climático y la implementación de medidas preventivas en el Valle de Chancay-Lambayeque, Perú. A través de un análisis costo-beneficio, se cuantifica el impacto de eventos de inundaciones extremas sobre la agricultura y la infraestructura hidráulica, considerando escenarios con y sin medidas de mitigación. Los resultados evidencian que la adopción de estrategias estructurales y no estructurales reduce significativamente las pérdidas económicas y mejora la resiliencia del sistema hídrico y productivo de la región. Se concluye que fortalecer la inversión en infraestructura resiliente y estrategias de adaptación es clave para la sostenibilidad económica y ambiental de la cuenca.

**Palabras clave:** cambio climático; costos económicos; análisis costo-beneficio; inundaciones extremas; medidas de mitigación.

## 1 Introduction

Human interventions have decreased the frequency of minor floods, but extraordinary floods have increased. The inclusion of historical data is crucial to improve accuracy in

estimating future flows and risks. Extreme floods are on the rise due to climate change and the increased vulnerability of urban areas [12].

Peru is one of the 10 megadiverse countries in the world; it has the second-largest Amazonian Forest after Brazil, the

**How to cite:** Armas-Blancas, A.S., Iglesias-León, S.del P., Rendón-Schneir, E., Vilchez-Ochoa G., Herrera-Espinoza J., Ramos-Alarcón L.M., Capuñay-Sosa J.L., Blancas-Amaya H.F., and Daga-López R.A., Cost analysis of climate change and prevention measures in the Chancay-Lambayeque Valley, Perú. DYNA, (92)238, pp. 76-81, July - September, 2025.





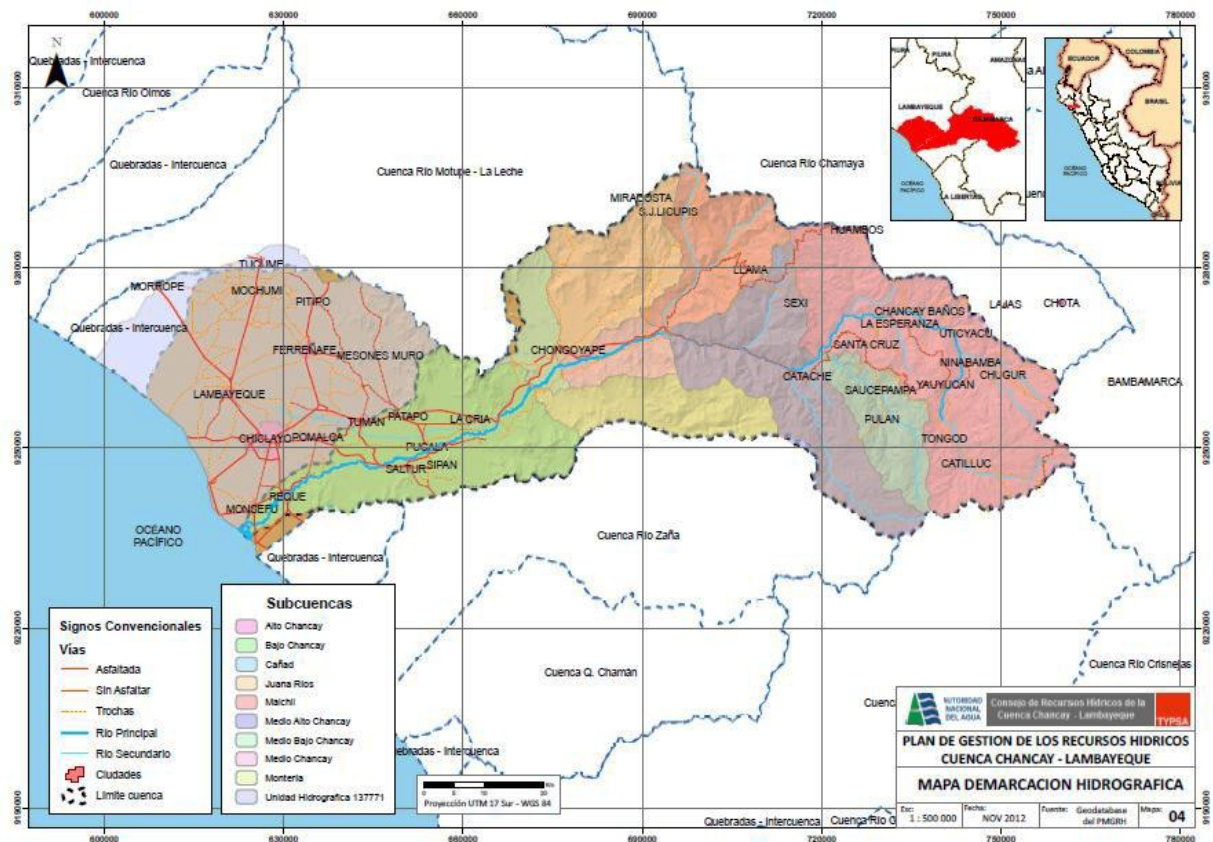


Figure 1. Location of the Chancay-Lambayeque basin.  
Source: ANA, 2015.

largest tropical mountain range, 71% of tropical glaciers, 84 of the 104 life zones identified on the planet, and 27 of the 32 climates in the world. This diversity is seriously threatened by climate change and explains much of the country's high vulnerability [8]. In addition, 21.77% of the population lives in poverty, while 4.07% experiences extreme poverty [5], increasing their vulnerability to the effects of climate change due to their dependence on agriculture.

The Chancay-Lambayeque Valley is undergoing a process of socioeconomic development with a clear upward trend, as new public and private investments are improving the productive, urban, and social services infrastructure, allowing production to grow and improving the quality of social services, which has been accompanied by a process of sustainable economic development. Fig. 1, shows the location of the Chancay-Lambayeque watershed [1].

Globally, climate change has intensified the frequency and magnitude of extreme hydrometeorological events, particularly affecting vulnerable agricultural regions [6]. In Peru, recurrent floods impact food security and water infrastructure, generating high socioeconomic costs [7]. In the Chancay-Lambayeque Valley, millions of dollars in losses have been recorded due to events such as El Niño [10]. However, there is little empirical evidence on the economic effectiveness of long-term mitigation strategies. This study employs a cost-benefit analysis to assess the effectiveness and impact of adaptation measures in this context.

## 2 Methodology

The study employs a cost-benefit analysis model to assess the economic feasibility of various climate change mitigation interventions. The methodology includes:

- Evaluation of direct and indirect costs of extreme weather events in the Chancay-Lambayeque Valley.
- Estimate of avoided costs through the implementation of preventive measures such as infrastructure reinforcement, reforestation, and land use management.
- Comparison of scenarios with and without a project, with 10, 100, and 500-year return periods.
- Incorporation of measures of the Integral Plan for flood control and disaster risk reduction in the Chancay-Lambayeque River basin [10].
- Adaptation of the avoided cost approach based on previous studies in the Chincha Valley [2] and Ghana [3].

This methodology allows quantifying the economic impact of climate change and determining the benefits of adaptation strategies. A cost-benefit analysis was performed using hydrometeorological data from the National Water Authority [1] and [10]. Return periods of 10, 100, and 500 years were determined using hydrological modeling based on historical series [2]. Avoided costs were estimated by comparing scenarios with and without adaptation measures, considering damage to crops, infrastructure, and agricultural production, following the methodology of Azumah [6].



## 2.1 Cost-benefit analysis

Risk reduction refers to the implementation of physical investments aimed at transforming economic assets and/or the environment in vulnerable areas, to prevent or reduce the negative impact of disasters associated with climate change. Examples of risk reduction include strengthening and adapting infrastructure, integrating risk into initial investments, building resilient infrastructure, improving housing, and other measures aimed at strengthening the response and adaptive capacity of communities.

In public administration, loss sharing refers to a joint and several agreements among the participants to distribute any losses incurred if one or more of the participants is unable to meet their obligations.

## 2.2 Benefits or costs avoided

The avoided cost approach was implemented using two types of approaches. The first method was to use information on the potential loss of assets that would result in the loss of environmental services provided by natural resources to estimate the costs that society would face. In this case, the researcher would estimate the potential damage to assets if the resources were not restored or conserved. Determining whether society or resource owners have invested funds to protect resource features is a second approach. In this way, expenditures to prevent the loss of ecosystem services provide an estimate of the value of those services [9].

The investment project measures aim to protect irrigated agricultural areas or land, hydraulic infrastructure (intakes and canals), protective infrastructure (levees and river defenses), public facilities (roads, bridges, electrical networks, drinking water supply infrastructure, irrigation infrastructure, etc.) from possible flooding of the Chancay Lambayeque River.

These measures help prevent or mitigate both direct and indirect damages resulting from a discharge with a return period of up to 500 years. Consequently, the avoided costs or damages represent the benefits attributed to the project when compared to the scenario without its implementation.

## 3 Results and discussion

### 3.1 Avoided costs

The summary of damages or avoided costs for the Chancay-Lambayeque Valley is presented at private prices in the "without" and "with" project situations, the difference or net benefit of which will be used for the economic evaluation of each project.

Tables 1, 2, and 3 show a summary of damages in the Chancay Lambayeque Valley in terms of sectors and types of damages for the without-project scenario. These damages will be caused by the extraordinary floods of the Chancay Lambayeque River, according to the return time and flood level.

Table 1.

Summary of Damages to Affected Sectors in the Chancay-Lambayeque Valley without Project for TR 10 years (Expressed in thousands of soles at private prices as of August 2024).

Sector	Description	Soles
Agriculture	Production Lost Flood	41985.43
	Erosion of Agricultural Areas	3862.64
	Unrealized production	41985.43
	Crop replenishment	47306.23
	Unrealized production (Hydraulic Inf.)	29758.10
Hydraulic Infrastructure	Intakes	273.25
	Channels	18413.61
	Riverine defenses	4263.14
	Wells	22949.99
	TOTAL	162,778.23

Source: The authors.

Table 2.

Summary of Damages to Affected Sectors in the Chancay-Lambayeque Valley without Project for TR 100years (Expressed in thousands of soles at private prices as of August 2024).

Sector	Description	Soles
Agriculture	Production Lost Flood	68533.60
	Erosion of Agricultural Areas	6297.78
	Unrealized production	68533.60
	Crop replenishment	76993.95
	Unrealized production (Hydraulic Inf.)	58131.73
Hydraulic Infrastructure	Intakes	2744.11
	Channels	65906.44
	Riverine defenses	8778.81
	Wells	77558.85
	TOTAL	345,132.71

Source: The authors.

Table 3.

Summary of Damages to Affected Sectors in the Chancay-Lambayeque Valley without Project for TR 500years (Expressed in thousands of soles at private prices as of August 2024).

Sector	Description	Soles
Agriculture	Production Lost Flood	82343.92
	Erosion of Agricultural Areas	7599.32
	Unrealized production	82343.92
	Crop replenishment	92977.05
	Unrealized production (Hydraulic Inf.)	70690.90
Hydraulic Infrastructure	Intakes	13725.71
	Channels	177789.26
	Riverine defenses	26632.97
	Wells	237663.58
	TOTAL	210797.81

Source: The authors.

Tables 4, 5, and 6 show a summary of damages in the Chancay-Lambayeque valley by sector and type of damage for the situation with the Project, which will be affected by the extraordinary floods of the Chancay- Lambayeque River, according to the return period and flood level. The amount of damages or avoided costs at private prices during the 10-year, 100-year, and 500-year return periods.

Table 4.

Summary of Damages to Affected Sectors in the Chancay-Lambayeque Valley with 10-Year TR Project (Expressed in thousands of soles at private prices as of August 2024).

Sector	Description	Soles
Agriculture	Production Lost Flood	909.08
	Erosion of Agricultural Areas	1889.34
	Unrealized production	909.08
	Crop replenishment	0.00
	Unrealized production (Hydraulic Inf.)	47.66
Hydraulic Infrastructure	Intakes	0.00
	Channels	0.00
	Riverine defenses	852.64
	Wells	852.64
	TOTAL	5460.43

Source: The authors.

Table 5.

Summary of Damages to Affected Sectors in the Chancay-Lambayeque Valley with Project for TR 100 years (Expressed in thousands of soles at private prices as of August 2024)

Sector	Description	Soles
Agriculture	Production Lost Flood	1483.90
	Erosion of Agricultural Areas	3148.88
	Unrealized production	1483.90
	Crop replenishment	0.00
	Unrealized production (Hydraulic Inf.)	165.22
Hydraulic Infrastructure	Intakes	0.00
	Channels	13207.71
	Riverine defenses	1755.83
	Wells	14963.53
	TOTAL	36208.96

Source: The authors.

Table 6.

Summary of Damages to Affected Sectors in the Chancay-Lambayeque Valley with Project for TR 500 years (Expressed in thousands of soles at private prices as of August 2024)

Sector	Description	Soles
Agriculture	Production Lost Flood	1781.78
	Erosion of Agricultural Areas	3778.67
	Unrealized production	1781.78
	Crop replenishment	0.00
	Unrealized production (Hydraulic Inf.)	445.35
Hydraulic Infrastructure	Intakes	0.00
	Channels	35558.11
	Riverine defenses	9095.12
	Wells	44717.98
	TOTAL	97158.79

Source: The authors.

The comparison between scenarios with and without prevention measures shows that the avoided costs are substantial in all the sectors analyzed. In particular, it was identified that:

- Losses in the agricultural sector can be reduced by up to 96.64% for a 10-year payback period.
- Water infrastructure shows a damage reduction of up to 89.50% over a 100-year return period.

- In a 500-year return period, damage mitigation reaches 53.90%, demonstrating the effectiveness of the structural measures implemented.

The implementation of adaptation measures reduced economic losses by 96.64% for 10-year return events and by 53.90% for 500-year extreme events. These results are consistent with studies in Chincha [2], where damage reduction reached 64%. However, in the case of Chancay-Lambayeque, mitigation effectiveness decreases with larger magnitude events, suggesting the need to strengthen resilient infrastructure and financial mechanisms for climate insurance. Comparison with previous studies in the Chincha Valley [2] and Ghana [3] demonstrates the effectiveness of cost-benefit analysis in planning climate adaptation investments.

### 3.2 Comparison with previous studies

The results obtained are consistent with previous research. In the Chincha Valley, flood prevention measures were able to reduce economic damages by up to 64%, demonstrating the economic viability of mitigation strategies [2]. Similarly, in Ghana, the adoption of sustainable agricultural practices significantly reduced climate impacts [3].

These findings are consistent with the study by Haer et al. [4], where cost-benefit analysis was used to identify economically efficient adaptation strategies. In this sense, the application of similar approaches in the Chancay-Lambayeque Valley could optimize investment in water infrastructure and strengthen agricultural resilience in the face of extreme climate events.

### 3.3 Green infrastructure and its role in climate mitigation

Beyond traditional structural measures, green infrastructure is emerging as a key strategy for risk reduction in urban areas. However, its implementation still faces limitations due to the lack of detailed cost and effectiveness studies. Evaluating its hydrological performance under different climate scenarios would allow optimizing resources and fostering more resilient solutions to mitigate flood impacts [11].

### 3.4 Implications for risk management and climate adaptation

The results of this study support the importance of integrating cost-benefit analysis into investment planning for climate adaptation. In particular, in the case of the Chancay-Lambayeque Valley, there is a need to strengthen water infrastructure and promote sustainable agricultural strategies to reduce the vulnerability of the productive sector.

In addition, the combination of traditional infrastructure with innovative approaches, such as green infrastructure, could provide more sustainable and cost-effective solutions for climate change mitigation. Therefore, future research should focus on evaluating their effectiveness in different climate scenarios, facilitating their incorporation into territorial planning and public risk management policies.).

#### 4 Conclusions

This study confirms that climate change mitigation strategies generate substantial economic benefits in the Chancay-Lambayeque Valley. The reduction of damages to water infrastructure and agricultural production highlights the relevance of investments in adaptation measures. To strengthen the resilience of the system, it is recommended to evaluate emerging technologies such as green infrastructure and to model higher resolution climate change scenarios. In addition, it is necessary to develop financial mechanisms to facilitate the implementation of these strategies at the regional level.

Future studies should refine climate models by incorporating localized data and improving hydrological accuracy. Long-term economic assessments of climate change impacts on water resources, agriculture, and infrastructure are necessary. The integration of geospatial AI and remote sensing can enhance monitoring and prediction. Research should explore cost-effective adaptation strategies, evaluate policies, and engage stakeholders for effective decision-making. Additionally, socioeconomic vulnerability studies and comparative analyses with similar basins can provide insights into sustainable water resource management and climate adaptation.

#### References

- [1] Autoridad Nacional del Agua, Plan de Gestión de los Recursos Hídricos de la cuenca Chancay-Lambayeque. Lima, Perú: Autoridad Nacional del Agua, 2015.
- [2] Armas, A.S., Valencia, Z., Rendón, E., y Vilchez G., "Beneficio económico de las medidas de prevención para inundaciones en el valle de chincha, mitigación y sustentabilidad," Zenodo, Art. 8866, 2021. DOI: <https://doi.org/10.5281/zenodo.5108866>.
- [3] Azumah, S.B., Adzawla, W., Osman, A., y Anani, P.Y., "Cost-benefit analysis of on-farm climate change adaptation strategies in Ghana," Ghana Journal of Geography, 12(1), pp. 29-46, Art. 2, 2020. DOI: <https://doi.org/10.4314/gjg.v12i1.2>.
- [4] Haer, T., Botzen, W.J.W., van-Rooten, V., Connor, H., Zavala-Hidalgo J., Eilander D.M., and Ward P.J., Coastal and river flood risk analyses for guiding economically optimal flood adaptation policies: a country-scale study for Mexico, Philosophical Transactions of the Royal Society A, 376(2121), art. 20170329, 2018. DOI: <https://doi.org/10.1098/rsta.2017.0329>
- [5] Instituto Nacional de Estadística e Informática, Encuesta Nacional de Hogares, INEI, [en línea] 2025. Disponible en: <https://m.inei.gob.pe/prensa/noticias/pobreza-monetaria-afecto-al-217-de-la-poblacion-del-pais-durante-el-ano-2017-10711/>.
- [6] Parry, M.L., Canziani, O.F., Palutikof, J.P., van-der-Linden, P.J., y Hanson, C.E., IPCC, Resumen para responsables de políticas, en Cambio Climático 2007: Impactos y Vulnerabilidad. Cambridge University Press, Cambridge, Reino Unido, 2007.
- [7] Loyola, R., y Orihuela, C., El costo económico del cambio climático en la agricultura peruana: el caso de la región Piura y Lambayeque. Consorcio de Investigación Económica y Social-CIES, [en línea]. 2011. Disponible en: [www.cies.org.pe](http://www.cies.org.pe).
- [8] Ministerio del Ambiente, El Perú y el Cambio climático. Segunda comunicación nacional del Perú a la convención marco de las naciones unidas sobre cambio climático 2010. MINAM, Lima, Perú, 2010.
- [9] Osorio-Múnera, J.D., Valoración económica de costos ambientales: marco conceptual y métodos de estimación, Semestre Económico, 7(13), pp. 160-192, 2004. Disponible en: <https://revistas.udem.edu.co/index.php/economico/article/view/1141>.
- [10] Proyecto especial Olmos Tinajones, elaboración del plan integral para el control de inundaciones y movimientos de masa de la cuenca del río Chancay-Lambayeque. Gobierno Regional de Lambayeque, 2020.
- [11] Reu-Junqueira, J., Serrao-Neumann S., and White, I., Developing and testing a cost-effectiveness analysis to prioritize green infrastructure alternatives for climate change adaptation, Water and Environment Journal, 37(2), pp. 242-255, art. 12832, 2022. DOI: <https://doi.org/10.1111/wej.12832>.
- [12] Zhong, Y., Ballesteros-Cánovas, J.A., Favillier, A., Corona, C., Zenhäusern, G., Muñoz-Torrero-Manchado, A., Guillet, S., Giacona, F., Eckert, N., Qie, J., Tscherrig, G., and Stoffel, M., Historical flood reconstruction in a torrential alpine catchment and its implication for flood hazard assessments. Journal of Hydrology, 629, art. 130547, 2024. DOI: <https://doi.org/10.1016/j.jhydrol.2023.130547>.

**Armas-Blancas, A.S.**, received the BSc. Eng. in Agricultural Engineering in 1990, from the National Agrarian University La Molina, Lima, Peru. MSc. in Management of Renewable Natural Resources and Environment in 1997, from the University of Los Andes, Mérida, Venezuela, and PhD. candidate in Environmental Sciences at the National University of San Marcos, Lima, Peru, since 2023. He has experience as a specialist in safety, occupational health, and environmental management in hydraulic infrastructure, sanitation, roads, and electrical transmission projects. He currently serves as the Environment and Safety Manager at JANO INGENIEROS SAC and is an associate professor at the National University of San Marcos in the Professional School of Environmental Engineering, as well as a professor at the National Technological University of Lima South.  
ORCID: 0000-0003-0168-3467

**Iglesias-León, S. del P.**, is a BSc. Eng. in Geographic Engineer from the National University of San Marcos (UNMSM), MSc. in Environmental Management and Assessment from Oxford Brookes University in England, and a PhD. from the Atlantic International University. She was Director of the Postgraduate Unit of the Faculty of Geological, Mining, Metallurgical, Civil and Environmental Geography Engineering - UNMSM (2013-2016) and Dean of said faculty (2016-2020). She currently works as an Advisor to the General Office of Cooperation and International Relations (OGCRI-UNMSM) and is CO of the Consulting Firm Environmental Specialists S.A.C.  
ORCID: 0000-0003-4616-8178

**Rendón-Schneir, E.**, is a Bsc. in economist with 30 years of professional experience, MSc. in Planning and Agrarian Policy in the Post-graduate Course in Agrarian Development (CPDA) in Rio de Janeiro - Brazil. He holds a PhD in Economics specializing in natural resource management from UNAM in Mexico and has worked for more than 10 years as an expert in water resource management, agrarian planning and projects, and environmental and risk management in the Ministry of Agriculture of Peru. Currently, he works as a senior lecturer at the Universidad Nacional Mayor de San Marcos, where he has been Director of the Professional School of Environmental Engineering and has a post-doctorate at KU Leuven in Belgium in Bioeconomy and a post-doctorate in Social Geography from the University of Caen in France. He has been a visiting professor at the University of Pittsburgh - United States, Gent in Belgium, Rennes in France, and at the University of Nitra in Slovakia.  
ORCID: 0000-0002-9413-2308

**Vilchez-Ochoa, G.**, is a Bsc. Eng. in Agricultural Engineer, professor at the National Technological University of Lima Sur, Sp.in Environment and Sustainable Development, develops work in Water Resources and Environmental Impact Studies. Currently a teacher and researcher.  
ORCID: 0000-0002-3792-0092

**Herrera-Espinoza, J.**, MSc. Eng. in Administration and Agricultural Engineering from the National Agrarian University La Molina is CEO of the company Ozonch; general manager of Jano Ingenieros SAC, regular professor at the UNTELS University of the courses: Treatment of Drinking and Residual Water, and Environmental Conflicts and Social Responsibility; at the Autonomous University of Peru of Hydraulic Engineering, and Installations and Energy Efficiency; leader in Research in technology for water treatment. He has held management positions in public and private companies. He has a diploma in Investment Systems; and Management Systems.

ORCID: 0000-0002-2571-1699

**Ramos-Alarcón, L.M.**, is a Biologist by profession from the National University of San Luis Gonzaga. She is a Sp. in biodiversity and environmental issues. She currently works as a professor at the National University of San Luis Gonzaga in Ica.

ORCID: 0000-0002-7568-0421

**Capuñay-Sosa J.L.**, is a BSc. Eng. in Geological Engineer, with a MSc. in Geological Engineering from the University of Durham, Great Britain, with doctoral studies in Environment and Sustainable Development; university professor at UNMSM in Geology and Environment topics.

ORCID code: 0000-0002-5944-7662

**Blancas-Amaya H.F.**, with a professional degree in Biological Sciences from the Universidad Nacional Mayor de San Marcos, MSc. in Entomology and Environmental Management, and a PhD in Environment and Sustainable Development. I am a teacher and researcher at the Faculty of Sciences, National University of Education EGV.

ORCID: 0000-0002-2274-0937

**Daga-López, R.A.**, is a BSc. Eng. in Geographic Engineer from the Universidad Nacional Mayor de San Marcos and MSc. in Geoinformation Sciences and Earth Observation. He currently works as a professor in the Environmental Engineering program at the Universidad Nacional Tecnológica de Lima Sur (UNTELS). His experience and specialization are oriented towards the use of geomatics and remote sensing tools for environmental management, climate change, and land use planning.

ORCID: 0000-0002-3105-1594



# Analysis of the infrastructure works on accessibility using graph theory: case study “la Línea” tunnel

David Fernando López-Patiño & Juan Pablo Londoño-Linares

Facultad de Ingeniería, Universidad de La Salle, Bogotá, Colombia. davidflopez06@unisalle.edu.co, julondono@lasalle.edu.co

Received: April 8<sup>th</sup>, 2025. Received in revised form: July 4<sup>th</sup>, 2025. Accepted: July 18<sup>th</sup>, 2025.

## Abstract

The importance of roads in the Colombian economy is undeniable, as they condition the transport of goods, this is why a method is proposed to quantify the impact of new projects, creating an additional tool for the decision makers. In this case was analyzed the impact of “la Línea” tunnel on the departments of Quindío and Tolima, calculating accessibility indexes in two states, before and after the construction of the tunnel, this analysis was complemented with the calculation of indirect costs based on operational and costs per user time. The analysis showed that the construction of the tunnel represented an improvement of the accessibility on Quindío by 5,13% and null on Tolima due to the project’s unidirectional nature, nevertheless it was obtained \$932.913.194 COP ( $\approx$ USD 229.141 for 2024) in daily savings.

**Keywords:** road network; graph theory; road user cost.

# Análisis del impacto de obras de infraestructura sobre accesibilidad mediante teoría de grafos: estudio de caso túnel de la Línea

## Resumen

Es innegable la importancia de las vías en la economía colombiana, condicionando el transporte de mercancías, es por esto que se plantea una metodología para cuantificar el impacto que ejercen proyectos nuevos sobre la accesibilidad regional, creando así una herramienta adicional para los tomadores de decisiones. Para este caso se analizó el impacto de la obra del Túnel de la Línea sobre los departamentos de Quindío y Tolima, calculando índices de accesibilidad en dos estados, antes y después de su construcción; este análisis se complementó con el cálculo de costos indirectos en función de los derivados por operación y por tiempo de usuarios. El análisis mostró que la construcción del túnel representó una mejora de la accesibilidad en Quindío del 5,13% y nula en el Tolima debido a que el proyecto tiene una sola dirección de tráfico, sin embargo, se obtuvieron \$932.913.194 COP ( $\approx$ USD 229.141 para 2024) de ahorro diario.

**Palabras clave:** red vial; teoría de grafos; costo de usuario.

## 1. Introduction

According to data of Consejo Privado de Competitividad [1], 79% of the country’s cargo was transported using the road network, highlighting the importance of the terrestrial road network in Colombia.

Ospina [2] states that “[the primary road network] is basic to the country’s integration and competitiveness (due to it joins the production areas with the consumption ones) because of this, the road infrastructure determines significantly regional markets, letting the transportation of

goods and merchandise or the movement of passengers, Binswanger et al. [3] points out three important factors regarding the influence of the roads in the economic development:

1. The development of the road infrastructure has a significant impact on the opportunities of commercialization and the costs of transaction.
2. Markets provide higher incomes for producers and reduce the price risks.
3. Better profit margins for the producers implies a better credit access, which gives greater facilities for

**How to cite:** López-Patiño, D.F., and Londoño-Linares, J.P., Analysis of the infrastructure works on accessibility using graph theory: case study “la Línea” tunnel. DYNA, (92)238, pp. 82-92, July - September, 2025.



investment for banks and financial institutions.

This impact that begins at the economic transcends to other territorial dimensions Chica [4] concludes that “a better access to roads generates positive externalities, pointing in the way of being an approximation of the state presence and governance” also point out that “the interventions in tertiary roads have positives effects in the diminution of the intensity of armed conflict” which represents a positive effect in a dimension apparently unrelated as the armed conflict, this is why the knowledge and the management of road projects are crucial for the economic and social development of a territory.

From the arguments of Binswanger et al. [3], is built a methodology to measure the impact of infrastructure projects on regional accessibility and express it as an economic value easily comparable, looking for facilitate the decision-maker's tasks during the management of projects.

### 1.1 Study case

As an example of the proposed methodological application, it was analyzed “La Línea” tunnel, a very important project in Colombia with a cost of 1 billion Colombian pesos (≈USD 245 million for 2024) and inaugurated in 2020, “La Línea” tunnel has 8.65 km long and crosses the central mountain range joining the municipalities of Cajamarca (Tolima department) and Calarcá (Quindío department), according to Pardo [5] for BBC,

*The ambition for the project was to open a commercial gate to Asia for a country of an enormous export potential, it would prevent part of the accidents that daily occurs caused by going up to the mountain's peak and it would save time, a lot of time, to the Colombians who travel by land to the west part of the country [5 para. 5]*

This implies a reduction in travel time and a higher ease for transportation of cargo between the port of Buenaventura and the capital, Bogotá. It is necessary to clarify that the tunnel is a unidirectional road, with two lanes, through the tunnel circulate the vehicles in the direction Calarcá-Cajamarca. In the opposite direction (Cajamarca-Calarcá.) the vehicles travel through the old road, also with two lanes.

In economic terms and according with INVIAS [6] data, “La Línea” tunnel generates an annual saving estimated of \$ 250.000 million COP (≈USD 61,4 million), equal to \$ 684.931.507 COP per day (\$955.928.877 COP for 2024 ≈USD 234.794), while Universidad Nacional [7], publishes a number of \$ 150.639 million COP per year (≈USD 37 million), equal to \$ 373.542.465 COP per day (\$ 521.336.844 COP for 2024 ≈USD 128.050)

For the research it was observed the economic impact of the project on the departments of Quindío and Tolima, these are the affected direct zones by the project and where the corridor is located.

### 1.2 Graph theory

The applied methodology is part of the graph theory, understanding a graph in function of the stated by Wilson [8]

as a set of nodes (also called vertices) and arcs, thus the graph theory results in the study of the interaction between nodes, and how they form networks, for this purpose two basic terms are defined:

1. According to Garrido the connectivity, that “determines the grade of reciprocal communication between vertices, and it is the grade of integration or interconnection that a network has for its internal functioning” [9. p. 85], thus it can be understood as the node's capacity to form links with another node.
2. The accessibility, which “allows to analyze the network's spatial organization, this causes that the nodes form a hierarchy in function of the facility of access from each one of them to the rest of the nodes in the graph” [9. p. 85]. This represents the measure of the facility to reach a specific node from another one inside the same network.

The distinction of these two concepts results crucial because it allows the calculation of indexes that will represent different network's characteristics, the connectivity indexes are in function of the number of links (roads) and nodes from a network, thus its nature is more general, on the other hand the accessibility indexes are in function not only of the number of links but also of the position of the nodes, thus it can be obtained general measures for the entire network and also specific measures for each node.

In this context, it has been developed researches that involves graph theory in the measuring of the vulnerability of road networks for example Haldar et al. [10], who applies graph theory methods (shimbel index and connectivity indexes) in a tool for urban planning, mapping urban accessibility values and of movement from a city point to its center, reaching a map that zones the peri-urban area in scales of accessibility and connectivity in function of the movement and travel time, highlighting critical areas for intervention.

In Colombia the research of Córdoba [11] stands out, he build a comparison between two states of the road network of the municipalities Leiva, Policarpa, Los Andes, Barbacoas, Roberto Payan, Olaya Herrera y Tumaco in the department Nariño, and compares the efficiency using graph theory, the first state in the original conditions pre-intervention and the second state with the improvement of the road surface, finding that the interventions enhanced the accessibility in *veredal* zones between 36 and 38%, showing the relevance of impact measurements for improvement and construction and highlighting the importance of tertiary roads in territorial development especially in rural areas.

Another research of impact measurement is made by E. García & Escobar, [12], including this time economic variables, calculating a global accessibility index for the Armenia's valorization-funded plan for infrastructure, that includes the construction and rehabilitation of urban roads, calculating a percentage of improvement in travel times and analyzing the beneficiary population. These researches despite their different contexts and scopes, all have in



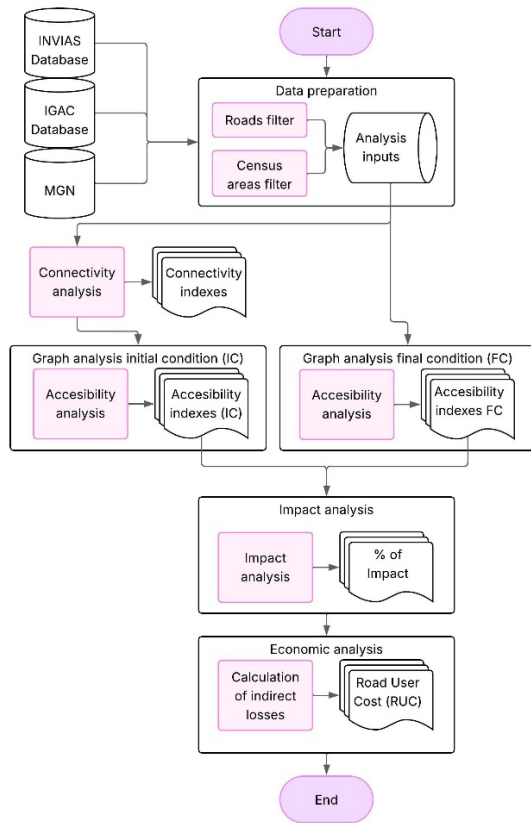


Figure 1. Methodological structure  
Source: Own elaboration

common the recognition of the importance of road accessibility in economic indexes and territorial productive efficiency and the use of graph theory as a diagnostic tool for accessibility, searching in a long term its application in territorial management.

## 2. Materials and methods

The proposed methodology is structured in three basic processes and it is summarized in the Fig. 1.

1. Graph analysis of the initial conditions (before the construction of the “La Línea” tunnel)
2. Graph analysis of the final conditions (after the construction of “La Línea” tunnel)
3. Impact analysis and calculation of the generated savings.

### 2.1 Graph analysis

#### 2.1.1 Census area filter

Due to the graph analysis uses vertices or unique points as an input, rather than polygons, is required to transform the urban areas polygons into unique points, for this the concept of *census area* is applied, defined by DANE as “the area delimited by the census perimeter of the municipal seats and populated centers” [13. p. 21] transformed into vertices finding their geometric center.

Because of the need to obtain a coherent network (a network with fully connected nodes) and due to the smallest census areas use, unidentified or ambiguously categorized roads, a census areas filter was implemented based on the population, because of this were only considered municipalities categorized as fifth category and above, according to the categorization of the Law 1551 of 2012 [14], this means municipalities with populations exceeding 10.000 inhabitants

#### 2.2 Road network filter

As noted, graphs are composed by nodes and arcs, the nodes in this case are equal to census areas, and the arcs to the road corridors, due to the presence in the National Geostatical Framework (Marco Geoestadístico Nacional) (MGN) [15] of ambiguous roads classifications, with unclear characteristics and where cannot be guaranteed that these accesses are suitable for populated centers connectivity, the roads; the same as the census areas; are filtered too, considering only those categorized as first, second or third order, according to the Resolution 1530 of 2017 [16].

Finally, a planar graph (non-intersecting arcs) is obtained, which also is coherent (a network with fully connected nodes) as illustrated in the Fig. 2, for the study area.

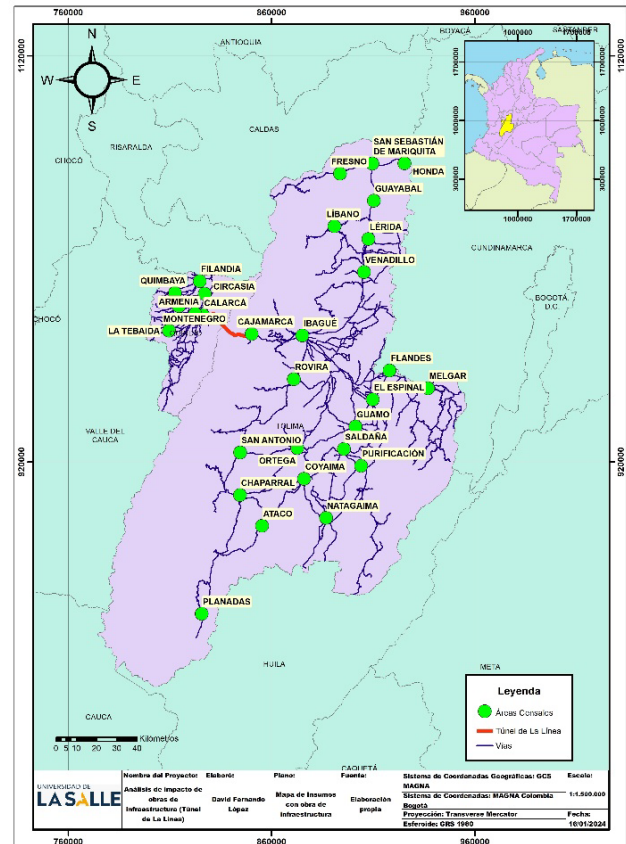


Figure 2. Road network of analysis  
Source: Own elaboration

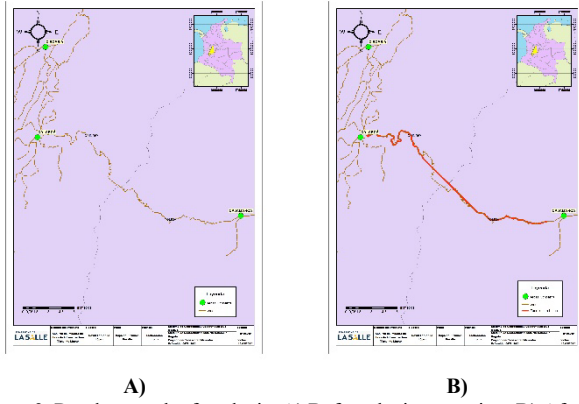


Figure 3. Road network of analysis: A) Before the intervention; B) After the intervention

Source: Own elaboration

Additionally, in Fig. 3 is presented the detail of the road network at the initial and final conditions, pre and post incorporation of the “La Línea” tunnel.

### 2.3 Connectivity and cohesion metrics

As mentioned, connectivity metrics are general network measures that depend on the total number of nodes and arcs, and its calculation helps to establish the graph's general conditions, however, the analysis post intervention of connectivity metrics is not relevant, because the only change between initial and final conditions is a single link.

It is important to say that connectivity metrics were calculated taking 619 nodes, including intersections of the roads and census areas, it is necessary to include in this case the intersections because they are an indicator of the network complexity. The connectivity metrics are presented below.

#### 2.3.1 Kansky connectivity index ( $\beta$ )

This connectivity index was introduced by Kansky [17] and represents the relation between the number of arcs ( $a$ ) and the number of nodes ( $n$ ). “Transportation networks with complicated structure will have high value of  $\beta$ , whereas networks with a simple structure will have low values” [17. p. 102]. It is defined by eq. (1).

$$\beta = \frac{a}{n} \quad (1)$$

“For planar graphs, however, the scale is from 0 to an upper limit of 3.0.” [17. p. 102].

#### 2.3.2 Gamma index ( $\gamma_{max}$ (%))

The gamma index was developed by Garrison & Marble [18] and it is defined as “a ratio between the edges and vertices of a given transportation network” [19. p. 104]. The eq. (2) shows the value of gamma index for planar graphs:

$$\gamma_{max} \% = \frac{a}{3 * (n - 2)} * 100 \quad (2)$$

#### 2.3.3 Cyclomatic number ( $\mu$ )

The cyclomatic number was first introduced by Berge [20], and represent the number of circuits that exists in a graph. Insaurralde & Cardozo defined a circuit as “each one of the multiple ways that exist to travel from a node to itself, without passing the same arc twice” [21. p. 8]. For coherent networks, the expression of the cyclomatic number is shown in the eq. (3).

$$\mu = a - (n - 1) \quad (3)$$

#### 2.3.4 Complexity or Alpha index ( $\alpha$ )

The complexity or Alpha index expressed in the eq. (6) was developed by Garrison & Marble [18] and can be defined as

*We may interpret this formula as a ratio between the observed number of circuits and the maximum number of circuits (...) For completely interconnected networks the  $\alpha$  index will be equal to one (the upper limit). For networks with a decreasing number of edges, the  $\alpha$  index will approach zero (the lower limit) [17. p. 100].*

$$\alpha = \frac{\mu}{2(n - 5)} * 100 \quad (4)$$

### 2.4 Accessibility and centrality metrics

For accessibility measures only were taken into account 30 nodes, the number of census areas, due to they represent the possible origins and destinations of the vehicles traveling through the departmental roads, from this an accessibility matrix is generated that contains the traveling distances from and to each one of the network's nodes.

#### 2.4.1 Associated König Number (KON)

It was proposed by König [22] and represent the distance needed to travel from a node till the furthest node, through the shortest path, it is extracted from the accessibility matrix, being the maximum value of each row, higher values indicate less accessible nodes.

#### 2.4.2 Shimbel number (Shim) and dispersion index (G index)

Both indexes were proposed by Shimbel [23], and they are obtained from the accessibility matrix. To find the accessibility index also known as Shimbel number, the distances of each row in the accessibility matrix are summarized, obtaining a different value for each one of the

network's nodes, a higher value indicates a less accessible node, and vice versa. The Maximum Shimbel number (Shim max) represents the most inaccessible node of the entire network, while the Minimum Shimbel number (Shim min) the most accessible.

The G index or dispersion index is obtained summarizing all the shimbel from the matrix, higher values indicate a less accessible network.

*We can characterize the measure of dispersion as an index expressing an over-all property of the network whereas the index of accessibility is a measure indicating the spatial relation between a given element of the structure and the remainder of the network [17. p. 116]*

#### 2.4.3 Average Accessibility Index (IAM)

The Average Accessibility Index (IAM) is calculated using the eq. (5), according to Muñoz et al.

*It determines an average value of the network's accessibility from the ratio between the G index and the total number of existing nodes. This network's mean can be used to compare different graphs, or for analyses inside a single graph, each node's accessibility (Shimbel number) respect to the mean (G index); those indexes above the mean are the less accessible [24. p. 78].*

$$IAM = \frac{G}{n} \quad (5)$$

#### 2.4.4 Mean centrality (C)

The mean centrality is the ratio between each node's Shimbel number and the total number of nodes minus one, this value represents each element's topological position, a higher value indicates a less central node and a lower value indicates a central node. Its expression is shown in the eq. (6)

$$C = \frac{Shim_i}{n-1} \quad (6)$$

#### 2.4.5 Impact analysis

Once obtained the results for the two network's states, a comparison was conducted using eight accessibility indexes, as mentioned the analysis of the connectivity metrics was made only for the initial conditions. The calculated accessibility indexes were G index, Average Accessibility Index (IAM), Maximum Shimbel number (Shim max), Minimum Shimbel number (Shim min), Maximum Associated König Number (KON max), Minimum Associated König Number (KON min), Average path length, Maximum Mean centrality (Cmax), Minimum Mean centrality (Cmin)

Table 1.

Inputs for the savings calculation

Input	Unit	Source
Average wage	\$COP/h/user	Decree 1572 of 2024 [27]
Climb+ Descent	m*km	Calculated from ALOS PALSAR L1.5., 2015 [28]
Horizontal Curvature	Degrees*km	Calculated from Road Information System [29]
Average speed	km/h	Law 1239 of 2008 [30] and INVIAS [6]
Average Daily Traffic (TPD)	veh/day	Historical traffic Series (TPD) [31]
Operating cost	\$COP/km/veh	Vehicle operating costs [32]

Source: Own elaboration

The impact is calculated using the eq. (7) and represents the relative percentage change:

% of impact

$$= \frac{Index_{Initial\ condition} - Index_{Final\ condition}}{Index_{Initial\ condition}} * 100 \quad (7)$$

### 2.5 Economic analysis

The final step is the saving calculation generated by the tunnel construction, based on the methodology developed by Dos Santos et al. [25, 26], who initially describes indirect losses, but in this investigation, it had a conceptual difference from the original. This calculation is made for the initial condition, using only the old road (OR) and the final condition, using in one direction the old road (OR) and in the opposite direction the road with the tunnel (RWT), for this calculation are used the eq (8) and the eq (9)

$$RUC = VOC + VOT \quad (8)$$

$$\Delta RUC = RUC_{IC} - RUC_{FC} \quad (9)$$

VOC= Vehicle operating cost

VOT= Value of time

RUC= Road User Cost

$\Delta RUC$ = Saving due to the incorporation of the project

Initially, for the calculation of the RUC, the inputs related in the Table 1 are required.

Finally, the calculation is performed factor by factor applying certain modifications to the formulas presented by Dos Santos et al. [25, 26], due to it can be reach more exactitude using the real number of vehicles from the TPD reported by INVIAS [31] instead of using a proportion for each type of vehicle.

#### 2.5.1 VOC-vehicle operating cost

For the calculation of the Vehicle operating cost, is used the eq. (10). The value of the Distance is obtained from the accessibility analysis.

$$VOC = Distance * \sum (Operating\ cost_i * TPD_i) \quad (10)$$

To appropriately determine the road operating cost, are calculated the curvature factors of the road. INVIAS [32] establishes a classification of the road alignment using the value of Climb+Descent and the Horizontal Curvature.

The value of Climb+ Descent is calculated using the eq (11) while the value of Horizontal Curvature is calculated using the eq (12).

$$Climb + Descent = \frac{\sum |z_{i+1} - z_i|}{L_T} \quad (11)$$

$$Horizontal\ Curvature = \frac{\sum \theta_i}{L_T} \quad (12)$$

$z$ = Elevation for every segment

$L_t$ = Total length of the road

$\theta_i$ = Angle between two segments of the road

These two factors are calculated for the old road and for the road with the tunnel. For the old road, the elevation information is extracted from the Alaska Satellite Facility Service, for the road with the tunnel are considered the INVIAS et al., 2021 [33] requirements for tunnel slopes, specifically for tunnels with a length superior to 3.000 m with a maximum slope of 3%.

Using these values, the road alignment can be classified in one of the next types: 1) Flat and straight, 2) Undulating and straight, 3) Gently curved and undulating, 4) Mountainous, 5) Curved and slightly undulating and 6) Steep. The terrain for the old road was classified as Steep, and for the road with the tunnel as Mountainous.

To obtain the Vehicle Operating Cost, the information related to the vehicle operating costs on paved roads (\$/km) for hdm IV (December 2016) [32] was used as an input, this information is based on market prices but does not correspond to the date of analysis, so it is needed to perform an inflation adjustment, using the eq. ((13), where the IPC values were obtained from Ministerio del Trabajo [34]:

$$\begin{aligned} Cost_{Final} = Cost_{initial} * (1 + IPC_{initial\ year}) \\ * (1 + IPC_{initial\ year+1}) \\ * ... (1 + IPC_{Final\ year}) \end{aligned} \quad (13)$$

The result for 2024 prices, good pavement and a mountainous and steep road alignment are presented in the Table 2

Table 2.  
Vehicle operating costs (2024 prices)

Type of vehicle	Type of road alignment	
	Mountainous	Steep
Cars	\$ 1.957,98	\$ 1.984,30
Buses	\$ 3.994,94	\$ 4.526,38
Trucks	\$ 5.951,27	\$ 6.999,36

Source: Own elaboration

## 2.5.2 VOT-Value of time

The users' time value is calculated using the eq. (14) the average wage per hour was \$ 5.416,00 corresponding to the minimum salary per hour for the 2024.

$$\begin{aligned} VOT = Distance * \sum (Average\ wage_i \\ * Average\ number\ of\ users_i \\ * Average\ speed_i * TPD_i) \end{aligned} \quad (14)$$

The average number of users per vehicle for cars corresponds to the average use capacity of the most common car models, for the busses the data is based on the data from the vehicle operating costs [32], while for trucks it is assumed that the only user is the driver.

At this point is necessary to establish that exists an increase in the average speed of the vehicles, which may travel faster in the final conditions because there are two lanes in the old road and two lanes in the road with the tunnel, INVIAS 2020 [6] establish an increase in the speed from 18 km/h to 60 km/h for cars, and using a proportionality based on the Law 1239 of 2008 [30], from 12 km/h to 40 km/h for trucks.

## 3. Results

### 3.1 Connectivity metrics

Initially, connectivity metrics are calculated as presented in the Table 3, to assess the general graph conditions in the initial conditions and metrics related to its complexity, the analysis was performed using a graph with 619 nodes (census areas and intersections) and 650 arcs (road links)

The obtained value of  $\beta$  was 1,05, which means that the number of nodes and arcs are similar, characteristic of a low complexity network.

For the  $\gamma_{max}$  (%) the result was of 35,12% which is equivalent to 32 circuits correspondent to the  $\mu$  index, significantly lower than the ideal of 100%, that can be reach with the inclusion of 1201 additional arcs, which would give an ideal index of road network linkage

Table 3.  
Connectivity metrics

Index	Result
$\beta$	1,05
$\gamma_{max}$ (%)	35,12%
$\mu$	32
$\alpha$	2,61%

Source: Own elaboration

Table 4.

Accessibility metrics and percentage of impact

Accessibility Index	Pre-Intervention	Post-Intervention	Difference	% of impact
G Index	122980353	121416953	1563401	1,27%
IAM	4099345	4047232	52113	1,27%
Shim min (Ibagué)	2780196	2780196	0	0,00%
Shim max (Planadas)	6828342	6828342	0	0,00%
KON min (Espinal)	171447	171447	0	0,00%
KON max (Fresno)	335293	335293	0	0,00%
Cmin (Ibagué)	95869	95869	0	0,00%
Cmax (Planadas)	235460	235460	0	0,00%

Source: Own elaboration

Additionally, the value of  $\alpha$  was 2.61%, a relatively low value, which means that the road network in Tolima and Quindío is highly dependent on specific critical links, characteristic of a fragile network. Notably the Cajamarca-Calarcá Road, stands out as a vital connection, this emphasizes the strategic importance of “La Línea” tunnel, as it is the only direct access between these two departments.

### 3.2 Accessibility metrics

In the Table 4 are presented the accessibility metrics for the network analysis, which includes the maximum and minimum Shimbél and König numbers and C index, with the comparison between the two scenarios with and without the project, as well as the difference and the percentage of impact obtained for each calculation.

The project improved the IAM, this indicates that with the tunnel is easier to access from any network's point to another one in an average of 1,27%, this value corresponds to the change of distance travel, approximately 9.7 km, between the 23 Tolima's nodes and the 7 Quindío's nodes,

The G Index improved as well, indicating that it is easier to travel to the remotest parts of the network or at least to the Quindío region, due to the direction of the tunnel.

For the maximum and minimum values of the Shimbél number there were no change, this occurs because of the unidirectional operation of the tunnel, the old road Cajamarca-Calarcá direction (East-West), has no distance change, and the points that represents maximum (Ibagué) and minimum (Planadas) accessibility are part of Tolima (East side), region that obtained no benefit in the distance factor because of the tunnel.

The same situation happens to the Mean centrality (C), as the minimum and maximum values correspond to the same census areas.

The König number did not changed, due to the longest route (San Sebastián de Mariquita- Planadas) is made from north to south, not from east to west, because of this the tunnel has no relevance in this indicator.

The results for the Shimbél number were spatialized using the Inverse Distance Weighted (IDW) interpolation method, which assigns greater weight to areas closer to each point, IDW

is used pre and post the intervention, the results are shown in the Fig. 4 and Fig. 5, respectively.

The most inaccessible node of the road network is Planadas, Tolima, point that obtained the higher Shimbél number, in the same way the municipality Fresno, also in Tolima, obtained the highest König number, which indicates that is a low accessible node, for the network analysis.

On the other hand, the best indexes were obtained for the municipalities of Ibagué in the case of the Shimbél number, and Espinal for the König number.

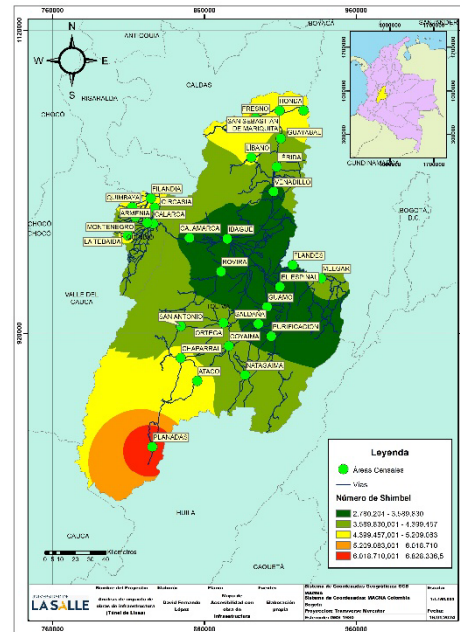


Figure 4. Accessibility map before construction of the tunnel  
Source: Own elaboration

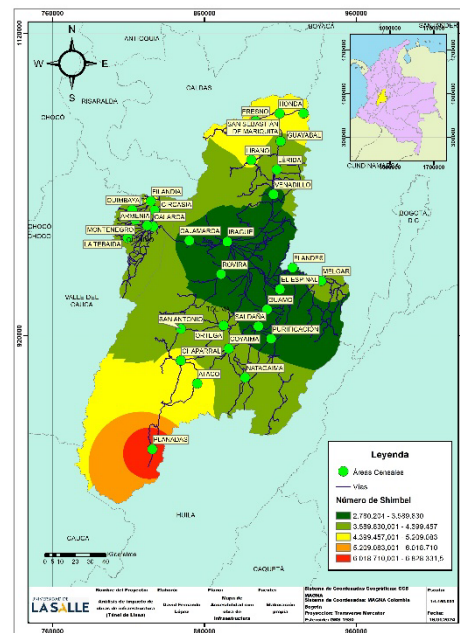


Figure 5. Accessibility map after construction of the tunnel  
Source: Own elaboration

Table 5.  
Percentage of impact for the Shimbél number for each node

Departament	Municipality	Census area	% of impact
Quindío	Calarcá	Calarcá	5,66%
Quindío	Armenia	Armenia	5,47%
Quindío	Montenegro	Montenegro	5,16%
Quindío	Circasia	Circasia	5,09%
Quindío	La Tebaida	La Tebaida	4,98%
Quindío	Quimbaya	Quimbaya	4,88%
Quindío	Filandia	Filandia	4,63%
Tolima	Ibagué	Ibagué	0,00%
Tolima	Espinal	El espinal	0,00%
Tolima	Guamo	Guamo	0,00%
Tolima	Rovira	Rovira	0,00%
Tolima	Saldaña	Saldaña	0,00%
Tolima	Flandes	Flandes	0,00%
Tolima	Cajamarca	Cajamarca	0,00%
Tolima	Venadillo	Venadillo	0,00%
Tolima	Purificación	Purificación	0,00%
Tolima	Coyaima	Coyaima	0,00%
Tolima	Lérida	Lérida	0,00%
Tolima	Ortega	Ortega	0,00%
Tolima	Melgar	Melgar	0,00%
Tolima	Natagaima	Natagaima	0,00%
Tolima	San Antonio	San Antonio	0,00%
Tolima	Armero	Guayabal	0,00%
Tolima	Líbano	Líbano	0,00%
Tolima	Chaparral	Chaparral	0,00%
Tolima	San Sebastián de Mariquita	San Sebastián de Mariquita	0,00%
Tolima	Ataco	Ataco	0,00%
Tolima	Honda	Honda	0,00%
Tolima	Fresno	Fresno	0,00%
Tolima	Planadas	Planadas	0,00%

Source: Own elaboration

The Table 5 presents the changes for the accessibility expressed in percentages for each census area.

Comparing the graphs in the initial and final states, the results clearly demonstrate the greater influence of the project on the department of Quindío, where can be noticed an average accessibility improvement of 5,13% compare with a null improvement in the department of Tolima, caused by the unidirectionality of the tunnel, this characteristic of the project reduces notably the impact on the east side of the network.

Also due to the longest routes are from north to south without crossing the tunnel, this also reduces the importance in Tolima. Despite this, in Quindío (West Side) accessibility improves for all the census areas, with all of them showing an improvement, higher in the closest zones to the project.

The Table 6 presents results of the analysis for the direct route from Calarcá to Cajamarca.

Table 6.  
Results Calarcá-Cajamarca route

Parameter	Result
Old Route (OR) distance (m)	43.730
Road With Tunnel (RWT) distance (m)	34.019
Difference (m)	9.711
% of impact	22,21%

Source: Own elaboration

Table 7.  
Inputs by type of vehicle for initial conditions (2024 prices)

Type of vehicle	Average speed (km/h)	Average number of users (users /veh)	TPD (veh/day)	Operating cost (\$COP/km/veh)
Car	18	3	3.252	\$ 1.984
Bus	18	28	2.140	\$ 4.526
Truck	12	1	2.326	\$ 6.999

Source: Own elaboration

Table 8.  
Inputs by type of vehicle for final conditions (2024 prices)

Type of vehicle	Average speed (km/h)	Average number of users (users /veh)	TPD (veh/day)		Operating cost (\$COP/km/veh)	
			OR	RWT	OR	RWT
Car	60	3	1.606	1.646	\$ 1.984	\$ 1.958
Bus	60	28	1.041	1.099	\$ 4.526	\$ 3.995
Truck	40	1	1.121	1.205	\$ 6.999	\$ 5.951

Source: Own elaboration

The analysis confirms a reduction of 22,21% in the travel distance in the direction Calarcá-Cajamarca (West-East), but the distance keeps being the same in the opposite direction.

### 3.3 Economic analysis

As mentioned, the terrain for the old road was classified as Steep, and for the road with the tunnel as Mountainous. Based on this, the inputs by type of vehicle are presented in the Table 7 for the initial conditions and in the Table 8 for the final conditions considering the old road (OR) for the East-West direction and the road with tunnel (RWT) for the West-East direction.

#### 3.3.1 VOC-vehicle operating cost

The Table 9 presents the results for the Vehicle Operating Cost expressed in function of the distance which is variable to every route.

Largest vehicles require more operating costs, making the truck sector the most benefited from the project because the savings for this item, the daily savings were of \$124.881.937/day ( $\approx$ USD 30.673) equivalent to an improvement of 17,54% for the operation costs. Cars and busses also show significant reductions in operating costs of 11,76% and 16,09% respectively.

Table 9.  
VOC-vehicle operating cost (2024 prices)

Type of vehicle	Total VOC Initial Conditions (\$COP/day)	Total VOC Final Conditions (\$COP/day)	Difference (\$COP/day)	% of impact
Car	\$ 282.197.186	\$ 249.003.887	\$ 33.193.299	11,76%
Bus	\$ 423.525.285	\$ 355.369.933	\$ 68.155.352	16,09%
Truck	\$ 711.875.634	\$ 586.993.697	\$ 124.881.937	17,54%
<b>TOTAL</b>	<b>\$ 1.417.598.104</b>	<b>\$ 1.191.367.517</b>	<b>\$ 226.230.587</b>	<b>15,96%</b>

Source: Own elaboration



Table 10.  
VOT-Value of time (2024 prices)

Type of vehicle	Total VOT Initial Conditions (\$COP /day)	Total VOT Final Conditions (\$COP /day)	Difference (\$COP /day)	% of impact
Car	\$ 128.372.523	\$ 34.183.005	\$ 94.189.518	73,37%
Bus	\$ 788.301.288	\$ 209.525.023	\$ 578.776.265	73,42%
Truck	\$ 45.903.241	\$ 12.186.417	\$ 33.716.824	73,45%
<b>TOTAL</b>	<b>\$ 962.577.053</b>	<b>\$ 255.894.446</b>	<b>\$ 706.682.607</b>	<b>73,42%</b>

Source: Own elaboration

Table 11.  
RUC-Road User Costs (2024 prices)

Type of vehicle	RUC Initial conditions (\$COP /día)	RUC Final Conditions (\$COP /día)	Difference (\$COP /día)	% of impact
Car	\$ 410.569.709	\$ 283.186.892	\$ 127.382.816	31,03%
Bus	\$ 1.211.826.574	\$ 564.894.957	\$ 646.931.617	53,38%
Truck	\$ 757.778.875	\$ 599.180.114	\$ 158.598.761	20,93%
<b>TOTAL</b>	<b>\$ 2.380.175.157</b>	<b>\$ 1.447.261.963</b>	<b>\$ 932.913.194</b>	<b>39,20%</b>

Source: Own elaboration

### 3.3.2 VOT-Value of time

The results for the value of time are presented in the Table 10.

Because of the higher number of users from busses this sector is the most benefited, but in proportion all sector presents significant reduction in the Value of time, an improvement higher to 73% equivalent to \$706.682.607 (≈USD 173.574) in total.

### 3.3.3 Road User Costs (RUC)

The final RUC for the initial and final conditions is present in the Table 11:

The results show an economic impact of 39.20% for the vehicles in general equivalent to a daily saving of \$932.913.194 (≈USD 229.141), after the intervention.

The proportion of the saving by item is shown in the Fig. 6.

The majority of savings (75,75%) were obtained from the time of the users, while 24,25% corresponds to the saving due to the value of the operation costs.

The Fig. 7 shows the savings by each type of vehicle.

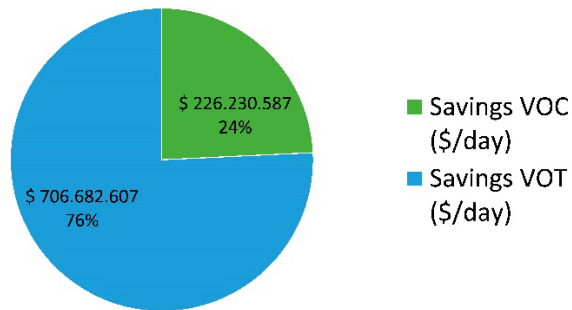


Figure 6. Saving by item  
Source: Own elaboration

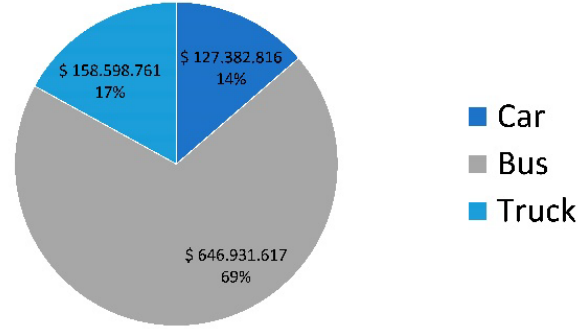


Figure 7. Saving by each type of vehicle  
Source: Own elaboration

The bus sector is the most benefited, with a 69,35% of all the savings, followed by a 17,00% for trucks and last 13,65% for cars.

## 4. Discussion

The analysis highlights a particularity, due to the country's geography, the network has a low redundancy in corridors connecting the west with the east, as a result the majority of efforts are focused in projects that facilitated this crossing, which is not large in euclidean distance, but represents great challenges caused by the mountainous terrain, this has conditioned historically the Colombia's economic and productive development.

The impact analysis resulted in a clear diagnosis which can be compared with multiples states and projects, being the economic analysis a key point, allowing to measure the influence of the infrastructure projects, the resulting data in \$/day is an ideal number to quantifying benefits. On the other hand, the impact analysis revealed that the relevance of the project diminishes with the distance from the implementation location, Calarcá and Armenia the nearest census areas from the project get a higher impact in comparison with census areas as Filandia, Quimbaya and La Tebaida.

Due to the unidirectional characteristic of the project, in terms of graph analysis, Tolima received no impact by the "La Línea" tunnel project, accessibility indexes did not change at all. In comparison the department of Quindío received an average improvement of 5.13%, this value is obtained from the sum of the travel distance improvements from each node of Quindío to any census area of the network, it is clear then that projects like a second tunnel in the opposite direction would be a key factor to improve the accessibility to Tolima and to the East part of the country.

Regardless the null impact on the Tolima's accessibility the economic analysis revealed substantial benefits of road investments that applies for the entire users of the road, reaching \$ 932.913.194 COP/day (≈USD 229.141 for 2024) of saving with the construction of "La Línea" tunnel, this represents a justification for the execution of the project and highlight its importance.

The changes in the slope of the road alignment have a significant economic impact especially on the truck sector,

which could represent significant reductions in the cost of goods transport and a possible reduction in overall prices, but the largest savings were found in the value of time, mainly due to the great reduction in time travel and the improvement in average speed representing an improvement higher to 73%.

## 5. Conclusion

“La Línea” tunnel caused no improvement in the accessibility of Tolima but was relevant to Quindío’s accessibility, this result is a reason to say that the project is relevant and represents an economic benefit for the entire region, the daily savings were \$ 932.913.194 COP/day ( $\approx$ USD 229.141 for 2024), causing significant savings in operational costs particularly because of the slope changes and largest savings in the time of the users increasing average speed and reducing time travel.

The calculated daily savings follow the same order of magnitude as calculated by INVIAS [6] of \$ 684.931.507 COP per day (\$955.928.877 COP for 2024  $\approx$ USD 234.794) and by Universidad Nacional [7] of \$ 373.542.465 COP per day (\$ 521.336.844 COP for 2024  $\approx$ USD 128.050), closer to the report of INVIAS [6] than the Universidad Nacional [7] calculation.

The methodology combined GIS with graph theory techniques, and resulted adequate and very useful, because it quantified the possible saving to the users of the regional roads, which is easily comparable with other sources and quantify the relevance of the project in the region.

Additionally, the methodology is systematic and follows a logical sequence of sub-processes, which is applicable to multiple scales and allows the comparison of projects and investment for road infrastructure projects.

## References

- [1] Consejo Privado de Competitividad, Informe Nacional de Competitividad, 1<sup>ra</sup> ed. Punto Aparte, Bogotá, Colombia, 2024, pp. 96–127.
- [2] Ospina, G., El papel de las vías secundarias y los caminos vecinales en el desarrollo de Colombia, *Revista de Ingeniería*, 47, pp. 20-27, 2016. DOI: <https://doi.org/10.16924/riua.v0i44.911>
- [3] Binswanger, H.P., Khandker, S.R., and Rosenzweig, M.R., How infrastructure and financial institutions affect agricultural output and investment in India, *Journal of Development Economics*, 41, pp. 337-366, 1993. DOI: [https://doi.org/10.1016/0304-3878\(93\)90062-R](https://doi.org/10.1016/0304-3878(93)90062-R)
- [4] Chica, A., Vías terciarias y conflicto armado en Colombia 2002-2019, MSc. Thesis, Facultad de Ciencias Económicas, Universidad Nacional de Colombia, Bogotá, 2023.
- [5] Pardo, D., Túnel de la Línea: por qué Colombia se demoró 100 años en construir su obra más importante (y qué beneficios traerá su inauguración). BBC Mundo, 2020. [Online], [Accessed, March 19<sup>th</sup> of 2025]. Available at: <https://www.bbc.com/mundo/noticias-america-latina-54021367>.
- [6] INVIAS, Resuelve los principales interrogantes sobre el túnel de La Línea, túnel de los colombianos [online]. ¿Qué es el túnel de La Línea?. Instituto Nacional de Vías, 2020 [Accessed, September 5<sup>th</sup> 2025]. Available at: <https://www.invias.gov.co/especiales/cruce-cordillera-central/faqs.php>
- [7] Universidad Nacional, Túnel de La Línea beneficiará a medio país, [Online]. Universidad Nacional, 2020. [Accessed, March 21<sup>th</sup> of 2025]. Available at: <https://agenciadenoticias.unal.edu.co/detalle/tunel-de-la-linea-beneficiara-a-medio-pais>
- [8] Wilson, R., Introduction to Graph Theory, 4<sup>th</sup> ed. Longman Group Ltd, Essex, 1972, pp. 8–21.
- [9] Garrido, J., La organización espacial de la red de carreteras en Aragón. aplicación metodológica de la teoría de grafos, *Geographicalia Universidad de Zaragoza*, 32, pp. 83–101, 1995. DOI: [https://doi.org/10.26754/ojs\\_geoph/geoph.1995321724](https://doi.org/10.26754/ojs_geoph/geoph.1995321724)
- [10] Haldar, S., Mandal, S., Bhattacharya, S., and Paul, S., Assessing and mapping spatial accessibility of peri-urban and rural neighborhood of Durgapur Municipal Corporation. India: a tool for transport planning, *Case Studies on Transport Policy*, 12, art. 100990, 2023. DOI: <https://doi.org/10.1016/j.cstp.2023.100990>
- [11] Córdoba, D., Análisis de la accesibilidad a partir de la topología de la red vial y la intervención de las vías terciarias en los municipios de Leiva, Policarpa, Los Andes, Barbacoas, Roberto Payan, Olaya Herrera y Tumaco del departamento de Nariño. MSc. Tesis, Facultad de Ingeniería Civil, Escuela Colombiana de Ingeniería Julio Garavito, Bogotá, 2019.
- [12] García, E., and Escobar, D., Evaluación del impacto de proyectos viales construidos por valorización en términos de accesibilidad territorial urbana. Caso de estudio: Armenia (Colombia), *Espacios*, 38, pp. 22–39, 2016.
- [13] Catálogo de objetos Marco Geoestadístico Nacional, 1<sup>ra</sup> ed., Departamento Administrativo Nacional de Estadística (DANE). [Online], Bogotá, Colombia, 2019. [Accessed: September 9<sup>th</sup>, 2020] Available at: <https://geoportal.dane.gov.co/geovisores/territorio/mgn-marco-geoestadistico-nacional/>
- [14] Law 1551, Congreso de la República de Colombia, Bogotá, 2012.
- [15] Guía de descarga y visualización Marco Geoestadístico Nacional, 1<sup>st</sup> ed., Departamento Administrativo Nacional de Estadística (DANE). [Online] Bogotá, Colombia, 2019. [Accessed: January 4<sup>th</sup>, 2021]. Available at: <https://geoportal.dane.gov.co/geovisores/territorio/mgn-marco-geoestadistico-nacional/>
- [16] Resolución 1530, Ministerio de Transporte de la República de Colombia, Bogotá, 2017.
- [17] Karsky, K., Measures of network structure, *FLUX Cahiers Scientifiques Internationaux Réseaux et Territoires*, pp. 89–121, 1989. DOI: <https://doi.org/10.3406/flux.1989.913>
- [18] Garrison, W.L., and Marble, D.F., Factor-analytic study of the connectivity of a transportation network, *Papers of the Regional Science Association*, 12(1), pp. 231–238, 1964. DOI: <https://doi.org/10.1007/BF01941256>
- [19] Karsky, K., Structure of transportation networks: relationships between network geometry and regional characteristics. PhD. dissertation, Department of geography, University of Chicago, Chicago, USA, 1963.
- [20] Berge, C., The Theory of Graphs, New York, Dover Publications, [Online], 1962. [Accessed: February 11<sup>th</sup>, 2021]. Available at: <https://books.google.com.co/books?id=h5BjnaoKyOwC>
- [21] Insaurralde, J.A., and Cardozo, O.D., Análisis de la red vial de la provincia de Corrientes por medio de la Teoría de Grafos, *Geográfica Digital*, 7(13), pp. 1-15, 2010. DOI: <https://doi.org/10.30972/geo.7132376>
- [22] König, D., Theorie der endlichen und unendlichen graphen: kombinatorische topologie der streckenkomplexe, *Monatsh. f. Mathematik und Physik*, 46, pp. A17–A18, 1936. DOI: <https://doi.org/10.1007/BF01792729>
- [23] Shimbel, A., Structural parameters of communication networks, *The Bulletin of Mathematical Biophysics*, 15(4), pp. 501–507, 1953. DOI: <https://doi.org/10.1007/BF02476438>
- [24] Muñoz, J., Garzón, A., and Vanegas, L., Análisis espacial de la red vial de los municipios de la Provincia del Tequendama en Cundinamarca Colombia, *Revista Universitaria Ruta*, 21(2), pp. 60–91, 2019. DOI: <https://doi.org/10.15443/RUTA20231253>
- [25] Dos Santos, B.M.B., De Picado-Santos, L.G., and Cavaleiro, V.M.P., Refinement of a simplified road-user cost model. *Proceedings of the Institution of Civil Engineers: Transport*, 167(6), pp. 364–376, 2014. DOI: <https://doi.org/10.1680/tran.12.00057>
- [26] Dos Santos, B.M.B., De Picado-Santos, L.G., and Cavaleiro, V.M.P., Simplified model of road-user costs for portuguese highways.

- Transportation Research Record, 2225, pp. 3–10, 2011. DOI: <https://doi.org/10.3141/2225-01>
- [27] Decree 1572. Presidencia de la República de Colombia, 2024.
- [28] Alos-Palsar L1.5. [Online]. Alaska Satellite Facility. 2015 DOI: <https://doi.org/10.5067/NXY378J3DFZQ>
- [29] INVIAS. Sistema de Información Vial, Bogotá, Colombia: Instituto Nacional de Vías, 2023. [Online]. Available at: <https://www.invias.gov.co/index.php/sistema-de-informacion-vial>
- [30] Law 1239, Congreso de la República de Colombia, Bogotá, 2008.
- [31] INVIAS. Serie histórica de tránsito (TPD) [Online]. 2022, Instituto Nacional de Vías, Bogotá, Colombia, 2022. Available at: <https://www.invias.gov.co/index.php/archivo-y-documentos/documentos-tecnicos/volumenes-de-transito/15791-serie-historica-de-transito-tpd-2022>
- [32] INVIAS. Costos de operación vehicular, [Online]. Instituto Nacional de Vías, Bogotá, Colombia, 2016. Available at: <https://www.invias.gov.co/index.php/archivo-y-documentos/documentos-tecnicos/6608-costos-de-operacion-vehicular>
- [33] Manual para el diseño, construcción, operación y mantenimiento de túneles de carretera para Colombia 2021, 2<sup>da</sup> ed., INVIAS, Sociedad Colombiana de Ingenieros, y Asociación Colombiana de Túneles y Obras Subterráneas, Bogotá, Colombia, 2021.
- [34] Calculadora de Inflación. [Online]. 2024. Ministerio del Trabajo. Available at: <https://filco.mintrabajo.gov.co/calculadora-inflacion/>

**D.F. López-Patiño**, received the BSc. Eng in Civil Engineering in 2021, MSc. in Territorial Planning and Management in 2024, both from the University of La Salle, Colombia. He has worked in geotechnical engineering and public space projects, and as an investigator in the methodological application and development of risk management for road corridors in cooperation with the University of La Salle and the INVIAS. His research interest includes risk management, topological analysis, graph theory, landslide hazard and urban planning.  
ORCID: 0009-0001-2545-1348

**J.P. Londoño-Linares**, is a BSc. Eng in Civil Engineer with MSc. and Dr. and 20 years of professional experience. He earned his undergraduate and MSc. from the Universidad Nacional de Colombia, and his PhD. from the Polytechnic University of Catalonia (UPC) in Barcelona, Spain. As part of the Risk Assessment Group at the International Center for Numerical Methods in Engineering (CIMNE) and the UNESCO Chair on Sustainability at UPC, he developed models for analyzing susceptibility, hazard, and disaster risk—particularly landslides—as well as methodologies for probabilistic risk analysis. These models have been validated through various projects led by Universidad Nacional of Colombia. He has recently directed several projects focusing on infrastructure analysis and adaptation to climate change.  
ORCID: 0000-0002-0830-2981



# Microstructure influence on crack propagation behavior of nodular cast iron

Carla Tatiana Mota Anflor, José David Hurtado-Agualimpia, Adrián Alberto Betancur-Arroyave, Sergio Henrique da Silva Carneiro & Jhon Nero Vaz Goulart

*Group of Experimental and Computational Mechanics, University of Brasilia, Campus Gama, Brazil*  
anflor@unb.br, jodaha@hotmail.com, aabetanc@gmail.com, shscarneiro@gmail.com, jvazgoulart@gmail.com

Received: November 25<sup>th</sup>, 2024. Received in revised form: May 19<sup>th</sup>, 2025. Accepted: July 25<sup>th</sup>, 2025.

## Abstract

This paper offers a comprehensive analysis of the crack propagation behavior of a specific type of Nodular Cast Iron (NCI) and its correlation with microstructural morphology. To estimate  $da/dN$  vs  $K$  curves, crack propagation tests were conducted utilizing Compact Test Specimens (CTS). Additionally, Scanning Electron Microscopy Analysis was employed to characterize the microstructure morphology on the surfaces of the fractured specimens, with specific attention to the size and distribution of graphite nodules within the ferritic matrix. The findings of the study suggest that the position from which the CTS is extracted is contingent upon the graphite distribution, which could have a noteworthy impact on the crack propagation behavior of the investigated NCI alloy.

**Keywords:** nodular cast iron; fracture mechanics; scanning electron microscopy; micrographic analysis

# Influencia de la microestructura en el comportamiento de propagación de grietas en fundición nodular

## Resumen

Este artículo ofrece un análisis exhaustivo del comportamiento de propagación de grietas de un tipo específico de fundición nodular (NCI) y su correlación con la morfología microestructural. Para estimar las curvas  $da/dN$  vs  $K$ , se realizaron pruebas de propagación de grietas utilizando muestras de prueba compactas (CTS). Además, se empleó análisis de microscopía electrónica de barrido para caracterizar la morfología de la microestructura en las superficies de las muestras fracturadas, con atención específica al tamaño y la distribución de los nódulos de grafito dentro de la matriz ferrítica. Los hallazgos del estudio sugieren que la posición desde la cual se extrae el CTS depende de la distribución del grafito, lo que podría tener un impacto notable en el comportamiento de propagación de grietas de la aleación NCI investigada.

**Palabras claves:** fundición nodular; mecanismos de fractura; microscopia electrónica de barrido; análisis micrográfico.

## 1. Introduction

Nodular Cast Iron (NCI) finds widespread usage in various engineering applications owing to its favorable combination of mechanical properties, including good fatigue strength, high machinability, and ductility. The chemical composition, particularly the presence of nickel, copper, and molybdenum, endows this material with desirable mechanical properties suited for diverse industrial applications. Initially introduced in

1948, NCI is characterized as a ternary Fe-C-Si alloy with proportions typically ranging from 3.5% to 3.9% for carbon and 1.8% to 2.8% for silicon [1]. Some authors also refer to NCI as Ductile Cast Iron (DCI) due to its ductile behavior [2-5], or alternatively as Spheroidal Graphite Cast Iron (SGI) [6-9] due to the manner in which the graphite nucleates. The main microstructural feature of NCI is the formation of spheroidal graphite, commonly referred to as nodules, which directly influences the physical properties of the material. NCI is

**How to cite:** Anflor, C.T.M., Hurtado-Agualimpia, J.D., Betancur-Arroyave, A.A., Carneiro, S.H.de S., and Goulart J.N.V., Microstructure influence on crack propagation behavior of nodular cast iron. DYNA, (92)238, pp. 93-102, July - September, 2025.



typically characterized by a high strength-to-weight ratio, excellent fatigue strength, high machinability, and distinctive ductile behavior, making it widely utilized in the manufacturing of various mechanical components such as manifolds, crankshafts, wheels, and gears [2,10]. These attractive characteristics are attributed to several parameters that significantly affect the mechanical properties, including the influence of manganese and copper. These elements stabilize pearlite, facilitate graphite formation, enhance strength, and improve the material's ability to withstand cyclic loads [8]. A wealth of studies has delved into the behavior of NCI, encompassing diverse topics such as: the dispersion of NCI's mechanical properties and their implications [11], analyses of matrix phase composition in fracture mechanics [12,13], the impact of graphite morphology on mechanical properties [8], micromechanical failures under impact, static, and fatigue stress [14], as well as investigations into fracture under dynamic loading [8], among other notable studies. According to [15], NCI can exhibit various structures including ferritic, pearlitic, austenitic, or intermediate structures, which depend on the chemical composition of the matrix and the applied heat treatment. NCI typically features spheroidal graphite embedded in a ferritic-pearlitic, pearlitic, or ferritic matrix, with each matrix phase composition impacting the material's behavior differently [12,16]. In addition to the significance of the cast iron matrix phase, certain characteristics of graphite nodules are equally important and extensively studied. Parameters such as the size, roundness, shape, and distribution of graphite nodules can significantly influence the performance of NCI, particularly under dynamic loading conditions [17-19]. A thorough understanding of the mechanisms involved in the spheroidization of graphite has been the subject of study for many researchers [20-22]. According to these studies, graphite nodule flotation is caused by excessive growth of certain nodules, which absorb carbon directly from the liquid. Due to their lower density, graphite nodules tend to float to the surface, a phenomenon that is more pronounced in thick sections or under slow cooling rates, resulting in inferior mechanical properties. Various articles have reported graphite flotation through metallographic analysis ([6] and [23,24]). In the field of fracture mechanics for nodular irons, previous studies were conducted under the assumption that graphite nodules had a negligible effect on the fracture mechanism. Many works in fracture mechanics were carried out on nodular cast iron, where graphite nodules were considered to have an almost negligible effect on the fracture mechanism [25-27], as the material was viewed as porous due to the low resistance of graphite. However, recent research has focused on analyzing the influence of these graphite nodules [28]. Studies have investigated failure micromechanisms in nodular cast iron under various loading conditions, including cyclic loading generating fatigue and the crack propagation process [29]. According to [30], the resistance of nodular cast iron to propagation and fatigue cracking is strongly influenced by the matrix, graphite morphological particles, and load conditions.

The same authors show in their work the influence of factors such as the stress ratio ( $R$ ), the detachment of the graphite nodules, the cleavage of the ferritic shield. Other authors such as [31], highlight the importance of graphite

nodules and the microstructure depending on the NCI matrix. For example, considering a tensile stress condition, the possible influence on the graphite nodules will depend on the type of matrix it is part of, if the matrix is completely ferritic there will be little influence of the nucleation processes and secondary crack growth inside the nodules. The microstructure influence on fatigue crack propagation NCI with different volume fractions of ferrite and pearlite for a set of samples have been also considered [32] following the ASTM E647 standard with load ratio  $R$  equals to 0.1, 0.5 and 0.75. NCI fatigue crack propagation resistance is strongly affected by the graphite nodulization and by the phase distribution (taking an important role for higher  $R$  or  $\Delta K$ ) within the microstructures. The fatigue crack propagation micromechanics in a ferritic NCI was done by means of scanning electron microscope (SEM) and digital microscope (DM) observations by [33] to observe the graphite influence over ferritic matrix during the fracture process, and he found that for low values of  $\Delta K$  and  $R$  the material did not behave in relation to homogeneous material and suggested that for high values of  $\Delta K$  or  $R$  a representative plastic zone could be generated.

According to the authors the fatigue crack propagation inside the graphite nodules was affected by the presence of a mechanical property gradient inside the graphite nodules. The mechanical gradient presented with the graphite perhaps resulted from the nodule solidification and growth mechanisms. It is also important to mention that in this work some considerations regarding the parameter  $K$  were underlined based on the experimental results. The fatigue crack propagation resistance for a ferritic NCI with degenerate nodules and compared the material behavior obtained to commercial ferritic NCIs were investigated by [34,35]. For this case the Paris's model was used [35]. In that work, the morphology and the reasons that can degenerate the graphite nodules were listed, such as, the presence of carbides, chunky graphite due to excess of rare earth additions, exploded graphite resulting from the excess of rare earth presence, compacted graphite due to low residual magnesium and/or rare earth, Graphite flotation, which potential causes can be high carbon equivalent, excess of pouring temperature, slow cooling rate in thicker sections or an insufficient inoculation, among others. Based on the analysis performed, the authors concluded that the presence of degenerated graphite influenced the crack propagation micromechanics but didn't affect the mechanical properties with respect to the resistance.

The main goal of this work is to give continuity of a comprehensive numerical and experimental characterization of nodular cast iron performed on the same batch of samples previously studied in [36,37] and [11]. In this sense the efforts turn to determine the material behavior when submitted to fatigue crack growth. The present batch of NCI presents in its morphology nearly spherical inclusions of graphite embedded in a homogeneous ferritic matrix. Depending on the graphite distribution as well as their morphology, the crack growth rate can be influenced significantly and additional tests (micrographic analyses and scanning electron microscopy equipped with energy-dispersive X-ray (SEM-EDX) analysis) are used in the

fractured specimens to support the discussions. This paper is organized as follows. Section 2 introduces the methodology employed for manufacturing of the fracture specimens, the procedure for performing the fracture tests, the Scanning Electron Microscopy analysis and the micrographic analysis. The experimental results obtained from fracture tests and the evaluations of the microstructures aspect are presented in section 3. Finally, the conclusions are presented and discussed in section 4.

## 2. Materials and methods

### 2.1 Specimens

Specimens were fabricated from a  $50 \times 50 \times 300$  mm nodular cast iron block without undergoing heat treatment. Fig.1(a) illustrates the orientations of each type of specimen, while Fig.1 (b) depicts the dimensions according to ASTM E647 standards. Although the microstructure of NCI lacks patterns akin to those found in laminated metals, certain specimens were extracted in alternative orientations to assess fracture toughness concerning graphite nodule distribution. As noted by [21], during the cooling process, graphite, being less dense, tends to migrate towards the upper surface. Consequently, there arose a necessity to analyze the influence of crack propagation in volume elements exhibiting variations in nodular density. Moreover, it is essential to highlight that production in cast condition is influenced by the cooling rate within the mold and the wall thicknesses of the cast part. Hence, the tests will be conducted with consideration given to the position of each sample within the NCI block.

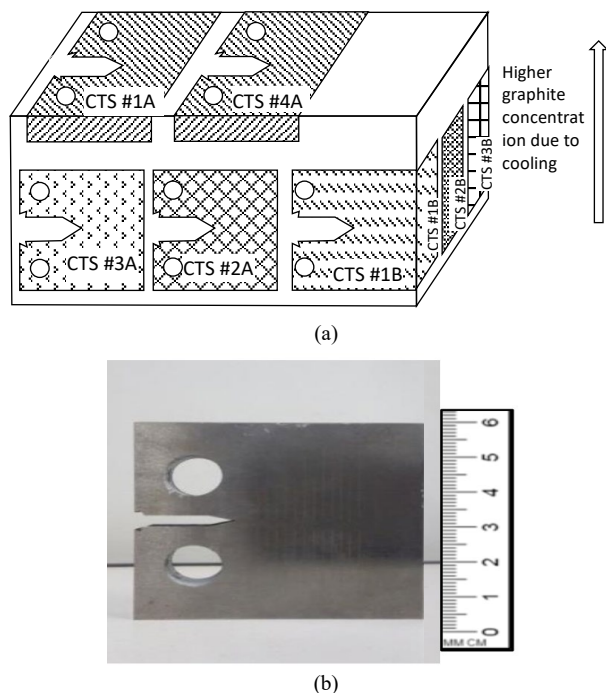


Figure 1. Details of the specimens: (a) block removal location (b) Specimen geometry.

Source: Own elaboration

### 2.2 Tensile

Due to the foundry process, nodular cast irons exhibit a wide range of mechanical properties. Various factors influence the mechanical properties of NCI, including cooling rate, chemical composition, graphite morphology, and their distribution, among others. For conducting the tests, the INSTRON 8801 universal testing machine was utilized. To furnish additional insights into the NCI under investigation, stress-strain relationships were determined through tensile testing.

### 2.3 Fatigue crack growth rate testing

For the fracture test, an MTS 810 machine was utilized, where seven CTS (ASTM) specimens with a thickness of 12mm were tested. The load ratio was set to  $R = P_{min}/P_{max} = 0.1$ , maintaining a constant load amplitude, and a sinusoidal loading waveform was applied with a frequency of 30 Hz throughout the test. The  $da/dN$  curve data were acquired and recorded for each specimen. To monitor crack growth, an MTS model 632.02 strain gauge was positioned at the opening of the specimen. Following the pre-crack propagation of the CTS, fatigue crack propagation tests were conducted to obtain the  $K_C$  and  $K_{th}$  values of the  $da/dN$  versus  $\Delta K$  curve for the NCI. Therefore,  $K_{IC}$  values from the literature for NCI were employed. The tests adhered to ASTM E647 standard recommendations for crack growth with controlled K. The test procedures included constant load amplitude tests with increasing K and decreasing K tests, aiming to obtain stages I, II, and III for the NCI.

#### 2.3.1. Test with constant load amplitude and increasing K

To conduct this test, ASTM E647 standard recommends maintaining a rising K to obtain a suitable crack growth rate for measuring the Paris curve parameters. The crack growth rate should exceed  $10^{-5}$  mm/cycle, as lower rates may pose challenges regarding fatigue pre-crack considerations. It is advised to maintain a constant load amplitude ( $\Delta P$ ) and fixed stress ratio (R) and frequency ( $\omega$ ) throughout the test. Therefore, for three (CTS #1A, CTS #2A, CTS #3A, and CTS #4A, CTS #1B) of the four CTSs used for the crack propagation tests with increasing K, the same values of  $\Delta P = 7.94$  kN were applied for each parameter, with an initial  $\Delta K$  of approximately  $12 \text{ MPa}\sqrt{\text{m}}$ . CTS #2A was the only case where a smaller load ( $\Delta P = 6.55$  kN) was utilized.

#### 2.3.2. Decreasing K test

During this type of test, the loading amplitude decreases until reaching a negative gradient of K. The aim of such tests is to determine the value of  $\Delta K_{th}$ . To achieve this, it is necessary to define a  $K_{max}$ , from which point  $\Delta K$  is decreased until a value is reached where crack growth becomes negligible. For the calculation of  $\Delta K_{th}$ , a linear regression of the logarithm of  $da/dN$  versus the logarithm of  $\Delta K$  is applied using at least five equally spaced points on the curve between  $10^{-6}$  and  $10^{-7}$  mm/cycle. The parameters for the decreasing K tests used for the three CTSs tested are  $\omega$  (Hz) = 30 Hz,  $R = 0.1$  and  $\Delta K_{max} = 15$ .



## 2.4 Scanning Electron Microscopy (SEM) and chemical composition

For the morphology analysis, a microscopy procedure was conducted on the samples resulting from the mechanical fracture test. The equipment used was a JEOL JSM 6610 Scanning Electron Microscope with a 30 kV acceleration voltage, 3nm resolution, and up to 300k X magnification capability with an EDS X-ray microanalysis system. The samples were analyzed under vacuum without prior chemical treatment, and the images were captured at 400X magnification in both the ductile fracture zone and the brittle fracture zone for two specimens previously selected. As the ductile/brittle transition zone was not precisely defined during the fracture tests, the images of each CTS were taken at stages II and III of the respective  $da/dN$  versus  $\Delta K$  curves.

## 2.5 Micrographic analysis

A micrographic analysis was conducted to characterize the morphology and distribution of graphite nodules on the samples, utilizing an optical microscope with 40X magnification equipped with a 5-megapixel camera. The aspect ratio, roundness, and nodularity were measured and classified according to ISO 16112:2006 standard values of roundness. This procedure was performed on both the brittle and ductile fracture regions of each specimen. Additionally, another investigation was undertaken to determine the existence of a transition in the morphology and distribution of graphite nodules due to the cooling process. The transition zone between brittle and ductile fracture was identified through visual inspection aided by microscopic analysis.

## 3. Experimental results

### 3.1 Tensile tests

Tensile tests were conducted, and the stress versus strain curve is depicted in Fig. 2. Mechanical properties, including yield stress( $\sigma_{0.2}$ ), ultimate stress, Young's modulus(E), and Poisson's ratio ( $\nu$ ), were obtained from the experimental curve and are reported in Table 1. These values represent the average of four tests. They were compared with values reported in the literature (Warda, 1990; Burditt, 1992) as referenced by [38].

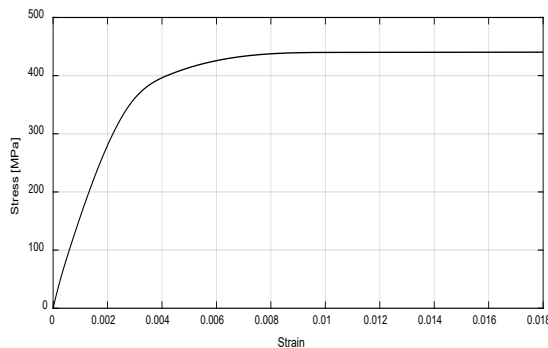


Figure 2. Stress-strain behavior of NCI determined from a tensile test. Source: Own elaboration

Table 1.

Experimental results from the tensile test.

Tensile test		
Yield stress $\sigma_{0.2}$ [MPa]	Ultimate tensile stress $\sigma_u$ [MPa]	Young's modulus E [GPa]
325	437	171

Source: Own elaboration

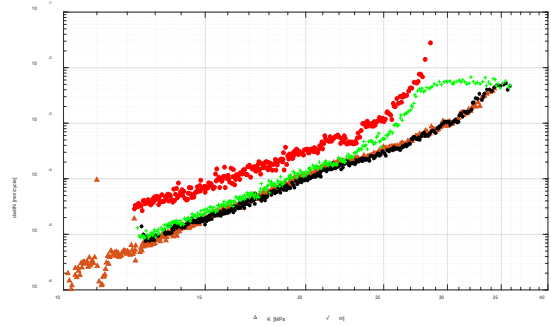


Figure 3. Comparison of  $da/dN$  vs  $\Delta K$  curves (CTS #1A, #2A, #3A and #1B). Source: Own elaboration

### 3.2 Crescent K crack growth tests

As mentioned in section 2.3.1, "Investigation of crack propagation behavior in nodular cast iron based on its microstructure," in this part of the tests, a constant loading range with increasing K was applied to each of the four CTSs tested (CTS #1A, #2A, #3A, and #1B). Utilizing the "MTS Fatigue Crack Growth Test Ware" software of the MTS 810 machine, parameter values of the  $da/dN$  versus  $\Delta K$  curves for each CTS, especially for stages II and III of the curves, were obtained. All curves obtained in this part of the tests are depicted in Fig.3.

Sample CTS #1A exhibits a curve that differs from the others obtained in this type of test due to its slope and higher crack propagation rate. Despite being part of the same batch as CTS #2A, #3A, and #1B samples, it's important to note that its direction and position in the original block differ (see Fig.1 a). Therefore, there's a possibility that the influence of graphite distribution in the crack direction may be more pronounced in CTS #1A than in the others. This could explain why the CTS #1A sample exhibited conditions conducive to greater crack growth acceleration with fewer cycles performed. With the CTS #2A specimen, the curve behavior was tested by decreasing the applied load by approximately 20%, from 7.94kN to 6.55kN, in order to provide a longer representation of the  $da/dN$  curve and a greater number of cycles. Despite the load decrease while maintaining the loading ratio (R) at 0.1, the curve's behavior remained largely unchanged compared to the others. A very similar behavior for the curves obtained in CTS samples #2A, #3A, and #1B can be observed. There is no significant dispersion in the points forming the curves or a large variation in their tendency, indicating that factors such as graphite nodules distribution did not significantly influence crack propagation acceleration or change in crack direction.

Table 2.  
Results of increasing K tests.

CTS	$N_f$	$a_c$	$\Delta K_c$	$C \times 10^{-12}$	$m$
CTS#1	456783	27,76	28,58	190,6	4,76
CTS#2A	288647	35,47	34,32	0,7994	6,27
CTS#3A	824411	34,47	35,87	6,259	5,52
CTS#1B	809397	32,78	35,89	4,609	5,73

Source: Own elaboration

Some slightly scattered points regarding CTS #2A and #1B may be observed due to possible clip gauge displacements when the MTS 810 machine starts executing the cycles during the tests (see Fig. 4). Additionally, the similarity between the curves obtained for CTS #3A and CTS #1B is notable, forming practically one single curve. By checking Figure 1a, it can be seen that both specimens were taken from the bottom of the block but at opposite positions. From each generated curve, parameters related to stages II and III were calculated, allowing for the determination of critical stress intensity factor differential ( $\Delta K_c$ ), crack length ( $a_c$ ), and constants of the Paris equation ( $C$  and  $m$ ), as well as fatigue life calculation ( $N_f - \text{cycles}$ ) for each CTS. Table 2 presents the results of the evaluated parameters  $a_c(mm)$ ,  $\Delta K_c(MPa\sqrt{m})$ ,  $C(mm/cycle/MPa\sqrt{m}^m)$  and  $m$ , for each curve.

The parameters  $a_c$ ,  $\Delta K_c$ ,  $C$  and  $m$  for samples CTS #2A, #3A, and #1B are very close to each other, with the values of  $C$  and  $m$  being closest to those reported in the literature. It is worth noting that the values for  $C$  and  $m$  parameters are characteristic of each material, and for the evaluated NCI, there is no clearly defined range. Therefore, the analysis of these parameters, in this case, is primarily based on the proximity of the results, which are satisfactorily consistent. The results of CTS #1A deviate significantly from most of the results obtained with the other specimens, as mentioned in the explanation of Fig. 1a. According to Table 4, sample CTS #1A exhibits a much smaller number of final cycles ( $N_f$ ) compared to the other samples, resulting in smaller values of  $a_c$  and  $\Delta K_c$ . However, similar to the other samples, the value for  $\Delta K_c$  is very close to the value of  $\Delta K_{IC}$  of 30  $MPa\sqrt{m}$  indicated by the DIN EN 1563 standard for an NCI GGG-40.

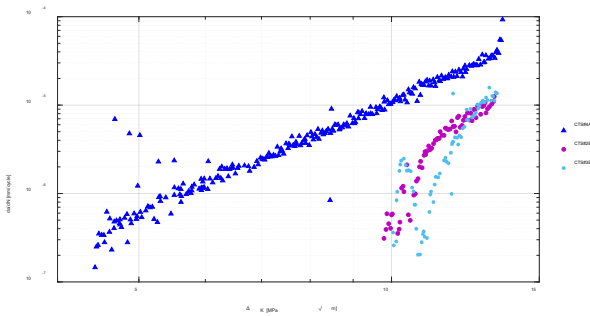


Figure 4.  $da/dN$  vs  $\Delta K$  curve for CTS #4A, #2B and #3B.  
Source: Own elaboration

### 3.3 Decreasing K crack growth tests for stages II and III

For this part of the tests, the procedure outlined in section 2.3.2, "Decreasing K test," was followed. The tests were conducted on three specimens, namely CTS #4A, #2B, and #3B. Utilizing the "MTS Fatigue Crack Growth Test Ware" software of the MTS 810 machine, parameter values of  $da/dN$  versus  $\Delta K$  curves for each CTS at Stage I were obtained, as depicted in Fig.5.

In Fig. 4, it can be observed that the curve for the CTS #4A sample exhibits a steeper slope compared to those of the CTS #2B and #3B samples. In this scenario, it is probable that a similar phenomenon to that observed in the CTS #1A sample during the increasing K tests occurred, where despite having the same loading conditions as the other samples, there is a potential difference in the distribution of graphite nodules concerning the direction of crack growth. Such compositional disparity renders the behavior of the specimen more fragile than others, resulting in increased crack growth and a substantial decrease in  $K$  to a very small  $\Delta K_{th}$  compared to other values obtained. The curves for the CTS #2B and #3B samples exhibit similar slopes and very close crack propagation rates. Conversely, the curve obtained for the CTS #4A sample indicates a lower crack propagation rate and a larger  $\Delta K_{th}$  closer to the values found in the literature. These curves depict the anticipated behavior for a GGG-40 NCI with a more homogeneous distribution of graphite nodules and a structure characterized by a ferritic-pearlitic matrix. By comparing the three curves (CTS #4A, #2B, and #3B) shown in Fig. 5, the behavior of crack growth rates for each sample in Stage I can be observed more clearly. The results obtained for parameters such as the stress intensity factor threshold ( $\Delta K_{th}$ ), corresponding to Stage I of the  $da/dN$  versus  $\Delta K$  curve, are presented in Table 3.

The results presented in Table 3 confirm the observations from Fig. 4. The discrepancy in cycle numbers can be attributed to the control method employed in the test, where each test was conducted until minimal or almost zero crack size variation was detected. Notably, crack propagation stabilized more rapidly in the CTS #3B sample. The crack sizes ( $a$ ) were very similar for the CTS #2B and CTS #3B samples, indicating a closely matched behavior in terms of crack growth rates and corresponding  $\Delta K_{th}$  values. This aligns with values suggested in the literature by some authors such as [39,40]. However, in the case of CTS #4A, a larger crack size ( $a$ ) and a significantly smaller  $\Delta K_{th}$  compared to the others are observed. Although this  $\Delta K_{th}$  value is not drastically different from values reported by authors such as [41]. By examining the graphs obtained (Fig. 4 and Fig. 5), it was possible to combine and compare the different curves to observe the complete curve with all stages (I, II, and III) and obtain more comprehensive information about the general behavior of the material, as evaluated according to the parameters defined for each test. Fig. 6 presents the graphs obtained after comparing the  $da/dN$  versus  $\Delta K$  curves for stages I, II, and III of each specimen.

Table 3.  
Results of decreasing K tests.

CTS	$N_f$ (Ciclos)	$a$ (mm)	$\Delta K_{th}$ ( $MPa\sqrt{m}$ )
CTS #4A	9.229.601	26,37	4,35
CTS #2B	11.669.033	17,21	10,03
CTS #3B	3.807.131	17,37	11,68

Source: Own elaboration

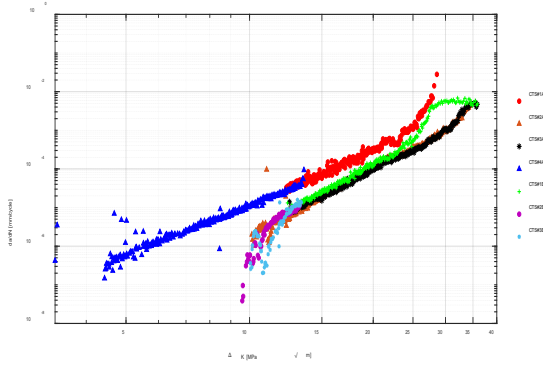


Figure 5. Comparison of complete da/dN vs ΔK curves.  
Source: Own elaboration

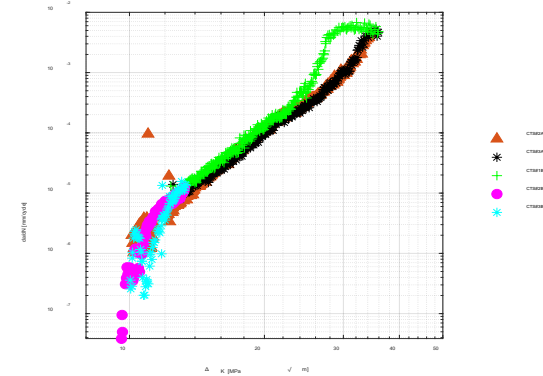


Figure 6. da/dN vs ΔK curve for CTS #2A, #3A, #1B, #2B and #3B.  
Source: Own elaboration

From Fig.5, two sets of curves are discernible. The first set combines results from increasing K tests for specimens CTS #2A, #3A, #1B, and decreasing K for CTS #2B and #3B, exhibiting similar trends. These curves are presented in more detail in Fig. 6. The second set includes results for specimens CTS #1A (rising K) and CTS #4A (decreasing K), demonstrating a different tendency and slope compared to most of the CTS tested. This set is further discussed with the assistance of Fig. 8. Fig 7, displays curves with ΔK values consistent with theoretical values found in the literature (Section 2.2.2), where there is an average value of  $\Delta K_{th} = 10,85 \text{ MPa}\sqrt{\text{m}}$  and an average value of  $\Delta K_c = 34,24 \text{ MPa}\sqrt{\text{m}}$ . These curves best depict the expected behavior for the chosen NCI in the tests' development.

On the other hand, the curve shown in Fig. 8 displays ΔK values that are not entirely characteristic of NCI. While the value of  $\Delta K_c = 28,58 \text{ MPa}\sqrt{\text{m}}$  falls within parameters found in the literature, the value of  $\Delta K_{th} = 4,35 \text{ MPa}\sqrt{\text{m}}$  is excessively low and does not align with characteristic values of the tested material. This suggests increased brittleness in a material that typically exhibits slightly more ductile behavior regarding crack growth, indicating a potential influence of graphite nodules specifically on these samples in accelerating crack propagation.

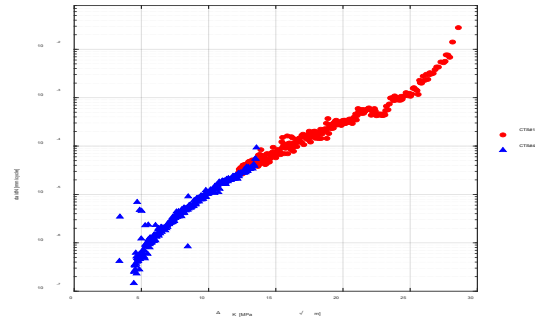


Figure 7. da/dN vs ΔK curve for CTS #1A, #4A.  
Source: Own elaboration

Table 4.

The chemical composition of NCI (wt. %).

C	Mg	Si	P	S	Cr	Mn	Ni	Cu	Fe
3.6	0.08	2.52	0.06	0.02	0.07	0.41	0.31	0.06	92.87

Source: Own elaboration

### 3.4 Results and discussion of SEM analysis

The chemical compounds were measured by SEM-EDX equipment (JEOL JSM 6610 SEM-EDX, Musashino, Tokyo, Japan) and the results are presented in Table 4.

The present chemical composition aligns with the percentages reported by other authors [14,34,42]. The most significant elements (Fe, Si, and C), measured using SEM-EDX equipment, also demonstrate good agreement with the information provided by the casting company from which the samples were procured. In the casting process, additional elements such as silicon and magnesium are essential for modifying the solidification mechanism, while chromium contributes to enhancing tensile strength. According to [21], silicon stabilizes graphite, and magnesium facilitates nodule formation. The morphology and distribution of graphite nodules in nodular cast irons largely determine the mechanical response of the composite microstructures. The high carbon content is responsible for nodular graphite formation, with any remaining carbon contributing to the formation of lamellar perlite during nucleation. The difference observed in the da/dN versus ΔK curve for CTS #1A compared to the others prompted SEM analysis to investigate the morphology of graphite nodules and fracture appearance. The CTS #1A sample, sourced from the top of the NCI block, exhibited a more pronounced influence of graphite nodules on crack propagation, as indicated by the corresponding curve in Fig. 6. During the cooling process, graphite tends to float and nucleate near the top of the block, explaining the steeper slope and higher crack growth rate observed in the da/dN versus ΔK curve, which significantly differs from the other curves. Fig. 8 illustrates the regions where SEM images were captured. In this instance, images were taken at positions correlated with Stages II and III of the da/dN versus ΔK curves for CTS #1A and CTS #2A to facilitate comparison.



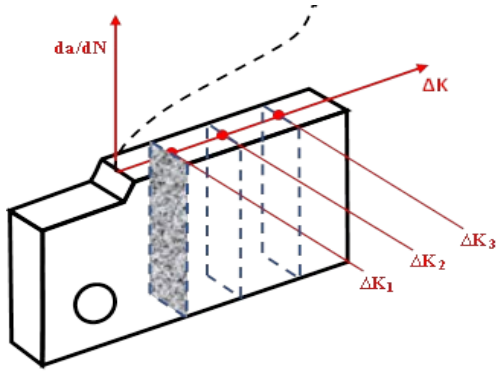


Figure 8. Scheme presenting the position where the images were taken by using SEM.

Source: Own elaboration

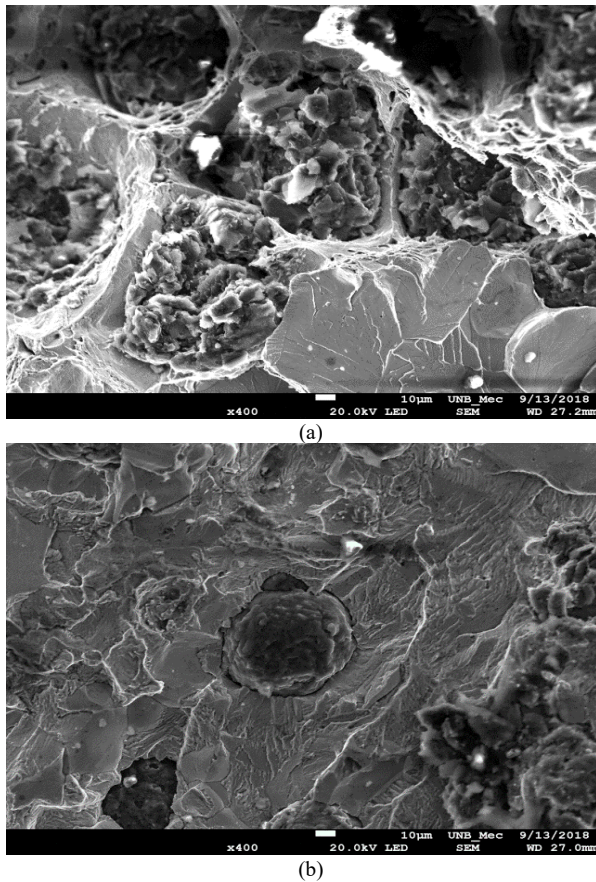


Figure 9. Sample CTS #1A, a) fracture as stage II and b) fracture at stage III.

Source: Own elaboration

### 3.4.1 Sample CTS #1A

Comparing the images obtained in Stage II (Fig. 9 a) and Stage III (Fig. 9 b) for CTS #1A at  $\times 400$  magnification, both ductile and brittle fracture mechanisms are observable. In Fig 9a), intercrystalline cleavage with the presence of coalescence is evident. Microvoids, resulting from plastic deformation induced by cyclic loading (microplasticity), are generally observed, highlighting ductile fracture characteristics. According to [7],

portions of the matrix, particularly those surrounding graphite inclusions, undergo plastic deformation during ductile fracture. In contrast, Stage III (Fig 9b) displays transgranular cleavage, with the absence of coalescence and graphite nodules maintaining their complete shape. Transgranular cleavage fracture entails rapid crack propagation along specific crystallographic planes [43]. These planes typically exhibit the lowest packing density, requiring fewer bond breakages and greater spacing between planes. For many engineering metals, especially ferritic-pearlitic steels, cleavage represents the predominant mechanism of brittle failure, aligning well with the findings presented herein.

### 3.4.2 Sample CTS #2A

The morphology of the CTS #2A sample is depicted in Fig. 10. In Fig. 10 a), intergranular cleavage marks and some incomplete graphite nodules are visible, likely resulting from wear during the crack propagation process. This image also shows a significant presence of microvoids, indicating coalescence. The presence of coalescences is attributed to the ferritic-pearlitic composition of the microstructure, which facilitates intercrystalline cleavage and the formation of microvoids near the graphite nodules. Fig. 10.b) illustrates the flat surface (brittle fracture) where transgranular fracture mechanisms are evident. In this case, transgranular cleavage occurs, accompanied by nodules approximately  $50\mu\text{m}$  in size, and there is an absence of the coalescence process.

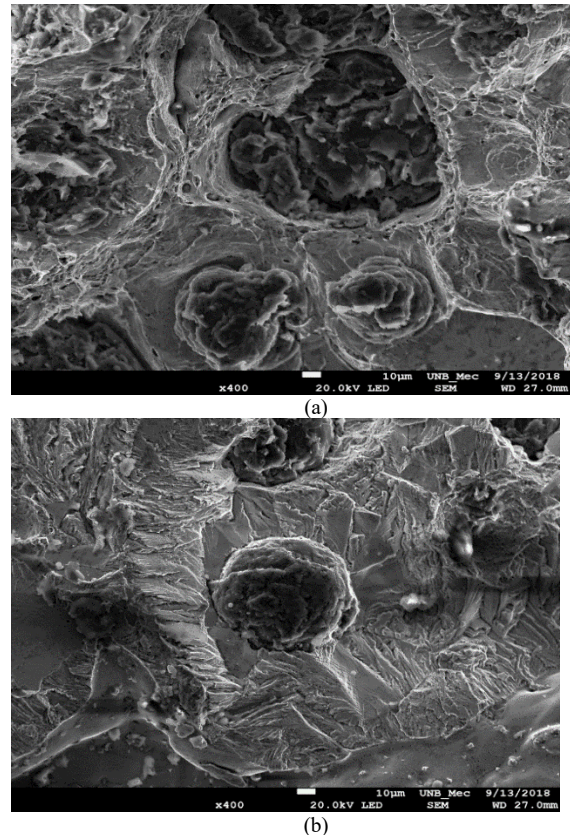


Figure 10. Sample CTS #2A: a) ductile fracture zone. b) brittle fracture zone.

Source: Own elaboration Micrographic Analysis

A micrographic analysis was conducted to characterize the morphology and distribution of graphite nodules on the samples. This analysis utilized an optical microscope with 40x magnification equipped with a 5-megapixel camera. The aspect ratio (AR) was determined using Equation (1).

$$AR = \frac{\text{major axis}}{\text{minor axis}} \quad (1)$$

The roundness (Rd) is given by equation (2),

$$Rd = \frac{4A}{\pi L_m^2} \quad (2)$$

Where A is the area of the graphite and  $L_m$  is the Max feret of the graphite feature. The nodularity (Nd) is determined according to equation (3).

$$Nd = \left( \frac{\sum A_{nodular} + 0,5 \sum A_{intermed}}{\sum A_{all}} \right) \times 100 \quad (3)$$

According to the ISO 16112:2006 standard, graphite nodules are classified based on their Rd. Nodules with Rd below 0.525 are categorized as graphite compacted, those falling within the range of 0.525 to 0.625 are classified as intermediate, and nodules with Rd values exceeding 0.625 are considered nodular. The results of the micrographic analysis are summarized in Table 5.

According to Table 5, CTS #1A exhibited a significantly higher fraction of graphite compared to the remaining samples. Additionally, it is evident that CTS #1A also had a lower quantity of nodules per unit of area, particularly noticeable in the ductile zone. This phenomenon can be attributed to the timing of nucleation and growth of graphite nodules. As noted by [21], magnesium acts as nuclei for graphite, initiating and facilitating its growth into spheroids. Nodules typically begin nucleating at around 1130°C, and the cooling rate during solidification controls their growth size. Higher cooling rates tend to result in smaller graphite growth compared to lower cooling rates. In the case of CTS #1A, the cooling rate may have accelerated graphite growth compared to the other CTS samples (CTS #2A, CTS #3A, and CTS #1B). Considering that all CTS samples originate from the same batch, it is reasonable to associate the position of each CTS within the block with irregularities in grain growth. The sensitivity of cooling speed during graphite nucleation in the

NCI manufacturing process is underscored by the findings presented here. Additionally, apart from graphite solidification, several factors contribute to poor aspect ratios and nodularity observed in the graphite nodules of CTS #1A. These factors may include low residual magnesium, ineffective post-inoculation due to silicon excess, presence of high levels of tramp elements, or carbonaceous residues leading to the deterioration of spheroidal graphite. Numerous studies have indicated that nodularity reductions, even within ferritic, pearlitic, or ferritic-pearlitic matrices, result in decreased tensile and impact properties. The mechanical properties are inversely proportional to nodularity levels, with decreasing nodularity correlating with reduced fatigue strength and affecting crack propagation. Finally, the present findings align well with the work of [24], where they asserted that an increase in non-spheroidal graphite content in pearlitic or ferritic steel leads to a progressive decrease in fatigue limit.

#### 4. Final conclusions

Due to their appealing properties, nodular cast irons (NCIs) are widely employed in various components across industries such as automotive, aerospace, and energy. The present study aims to deepen the understanding of a specific batch of NCI by incorporating fatigue crack growth investigations into a series of previously conducted tests and studies. This research endeavors to explore potential correlations between crack propagation behavior and microstructural morphology, particularly focusing on the NCI alloy GGG40. Preliminary conclusions drawn from the crack propagation tests and microstructural analysis are outlined herein. The microstructural examination confirms the typical morphology observed in NCI alloys, characterized by graphite spheroids or nodules dispersed within a ferritic matrix. The distribution and size of these graphite nodules in the NCI microstructure align with the mechanical properties observed in the tested samples. It is widely acknowledged that NCI materials exhibit a broad range of mechanical properties, attributed to the distribution and morphology of graphite nodules. Notably, even specimens sourced from the same NCI block demonstrate discernible differences in crack propagation properties, highlighting the significant influence of graphite nodule distribution. Specimens extracted from the top of the NCI block exhibited higher crack propagation rates. For comprehensive analysis, the fractured specimens were categorized into brittle and ductile regions on their surfaces. Subsequent SEM analysis was conducted on each region to examine fracture patterns and morphology. In specimens originating from the top of the NCI block, the influence of nodular graphite was observed, attributed to the flotation mechanism. Micrographic analysis was employed to determine the size, roundness, shape, and distribution of graphite nodules. Previous research has indicated that graphite nodule flotation occurs due to excessive growth of certain nodules, which absorb carbon directly from the liquid phase. Due to their lower density, these graphite nodules tend to migrate towards the surface. This phenomenon likely explains the variation in fracture behavior observed based on the specimen's position within the NCI block. Further

Table 5.

Experimental results obtained from the micrographics analysis.

CTS#	Zone	qd	%área	Nod.size	AR	Rd	Nd
1A	II	31,40	24,98	63,66	1,479	0,726	85,48
2A		20,40	13,35	57,72	1,525	0,714	79,34
3A		43,60	9,29	32,94	1,779	0,727	90,96
1B		38,00	9,82	36,28	1,495	0,728	85,56
1A	III	20,00	23,84	77,92	1,648	0,673	89,24
2A		42,60	13,60	40,33	1,564	0,705	85,89
3A		30,80	8,35	37,15	1,602	0,703	88,86
1B		44,20	8,35	31,01	1,597	0,697	83,09

Source: Own elaboration

investigation is warranted to validate these preliminary findings and advance understanding of fatigue and fracture behavior in the specific NCI alloy examined in this study. Specifically, exploring the influence of stress ratio (R), the presence of overloads in variable amplitude loading histories, and delving into more detailed fracture mechanisms would be fruitful avenues for future research.

## Acknowledgments

This research was supported by FAPDF (Research Foundation of Federal District) project number 0193.001554/2017 and CNPq (National Council for Scientific and Technological Development) project number 408551/2016-0 and 314602/2021-6. The first author expresses gratitude to the National Council for Scientific and Technological Development (CNPq) for providing the fellowship grant with reference number 314602/2021-6. The first also thank to the Foundation for Research Support of the Federal District (FAPDF), Process No. 00193-00002184/2023-91.

## Bibliography

- [1] Labrecque, C., and Gagné, M., Ductile Iron: fifty years of continuous development, *Can. Metall. Q.* 37(5), pp. 343–378, 1998. DOI: <https://doi.org/10.1179/cmqr.1998.37.5.343>.
- [2] Hervas, I., Ben-Bettaieb, M., Thuault, A., and Hug, E., Graphite nodule morphology as an indicator of the local complex strain state in ductile cast iron, *Materials & Design*, 52, pp. 524–532, 2013. DOI: <https://doi.org/10.1016/j.matdes.2013.05.078>
- [3] Di-Cocco, V., Iacoviello, F., Rossi, A., and Ecarla, F., Mechanical properties gradient in graphite nodules: influence on ferritic DCI damaging micromechanisms, 2013, pp. 222–230.
- [4] Iacoviello, F., Di-Bartolomeo O., Di-Cocco, V. and Piacente, V., Damaging micromechanisms in ferritic-pearlitic ductile cast irons, *Mater. Sci. Eng. A*, 478(1–2), pp. 181–186, 2008. DOI: <https://doi.org/10.1016/j.msea.2007.05.110>.
- [5] Bonora N., and Ruggiero, A., Micromechanical modeling of ductile cast iron incorporating damage. part I: ferritic ductile cast iron, *Int. J. Solids Struct.*, 42(5–6), pp. 1401–1424, 2005. DOI: <https://doi.org/10.1016/j.jislsolstr.2004.07.025>.
- [6] Lacaze, J., Solidification of spheroidal graphite cast irons: III. Microsegregation related effects, *Acta Mater.*, 47(14), pp. 3779–3792, 1999. DOI: [https://doi.org/10.1016/S1359-6454\(99\)00233-5](https://doi.org/10.1016/S1359-6454(99)00233-5).
- [7] Ferdinando, D.O., and Boeri, R., Study of the fracture of ferritic ductile cast iron under different loading conditions, *Fatigue Fract. Eng. Mater. Struct.*, 38(5), pp. 610–620, 2015. DOI: <https://doi.org/10.1111/ffe.12266>.
- [8] Ceschini, L., Morri, A., and Morri, A., Effects of casting size on microstructure and mechanical properties of spheroidal and compacted graphite cast irons: experimental results and comparison with international standards, *J. Mater. Eng. Perform.*, 26(6), pp. 2583–2592, 2017. DOI: <https://doi.org/10.1007/s11665-017-2714-7>.
- [9] Queirós, R., Domeij, B., and Diószegi, A., Unraveling compacted and nodular cast iron porosity: case studies approach, *Inter Metalcast.*, 18, pp. 1811–1830, 2024. DOI: <https://doi.org/10.1007/s40962-023-01149-9>
- [10] Xu, M.S., and Shi, J.L., Fracture analysis of nodular cast iron crankshaft, *Metalurgija*, 59(4), pp. 517–520, 2020.
- [11] Betancur, A., Anflor, C., Pereira, A., and Leiderman, R., Determination of the effective elastic modulus for nodular cast iron using the boundary element method, *Metals (Basel)*, 8(8), art. 641, 2018. DOI: <https://doi.org/10.3390/met8080641>.
- [12] Hütter, G., Zybelle, L., and Kuna, M., Micromechanisms of fracture in nodular cast iron: From experimental findings towards modeling strategies. A review, *Eng. Fract. Mech.*, 144(6), pp. 118–141, 2015. DOI: <https://doi.org/10.1016/j.engfracmech.2015.06.042>.
- [13] Iacoviello, F., Di-Cocco, V., Rossi, A., and Cavallini, M., Ferritic-pearlitic ductile cast irons: Is  $\Delta K$  a useful parameter? 13<sup>th</sup> Int. Conf. Fract. 2013, ICF 2013, 2, 2013, pp. 998–1006.
- [14] Vaško, A., and Chalupová, M., The micro-mechanisms of failure of nodular cast iron, *Prod. Eng. Arch.*, 5(4), pp. 31–35, 2014.
- [15] Hütter, G., Zybelle, L., and Kuna, M., Micromechanisms of fracture in nodular cast iron: From experimental findings towards modeling strategies - A review, *Eng. Fract. Mech.*, 144, pp. 118–141, 2015. DOI: <https://doi.org/10.1016/j.engfracmech.2015.06.042>.
- [16] Gonzaga, R.A., Influence of ferrite and pearlite content on mechanical properties of ductile cast irons, *Mater. Sci. Eng. A*, 567, pp. 1–8, 2013. DOI: <https://doi.org/10.1016/j.msea.2012.12.089>.
- [17] Costa, N., Machado, N., and Silva, F.S., A new method for prediction of nodular cast iron fatigue limit, *Int. J. Fatigue*, 32(7), pp. 988–995, 2010. DOI: <https://doi.org/10.1016/j.ijfatigue.2009.11.005>.
- [18] Čanžar, P., Tonkovich, Z., and Kodvanj, J., Microstructure influence on fatigue behaviour of nodular cast iron, *Mater. Sci. Eng. A*, 556, pp. 88–99, 2012. DOI: <https://doi.org/10.1016/j.msea.2012.06.062>.
- [19] Ferro, P., Lazzarin, P., and Berto, F., Fatigue properties of ductile cast iron containing chunky graphite, *Mater. Sci. Eng. A*, 554, pp. 122–128, 2012. DOI: <https://doi.org/10.1016/j.msea.2012.06.024>.
- [20] Nan, L., Shu ming, X., and Pei-wei, B., Microstructure and mechanical properties of nodular cast iron produced by melted metal die forging process. *J. Iron Steel Res. Int.*, 20(6), pp. 58–62, 2013. DOI: [https://doi.org/10.1016/S1006-706X\(13\)60112-0](https://doi.org/10.1016/S1006-706X(13)60112-0)
- [21] Azeem, M.A., Bjerre, M.K.R., Atwood, C., Tiedje, N., and P.D. Lee, Synchrotron quantification of graphite nodule evolution during the solidification of cast iron, *Acta Mater.*, 155, pp. 393–401, 2018. DOI: <https://doi.org/10.1016/j.actamat.2018.06.007>.
- [22] Escobar, A., Celentano, D., Cruchaga, M., and Schulz, B., On the effect of pouring temperature on spheroidal graphite cast iron solidification, *Metals (Basel)*, 5(2), pp. 628–647, 2015. DOI: <https://doi.org/10.3390/met5020628>.
- [23] Lucas, L., Boneti, T.M., Hupalo, S.F., Junior, V., and Rosário, A.M., Influence of casting heterogeneities on microstructure and mechanical properties of austempered ductile iron (ADI), No. Stage II, 2017.
- [24] Voigt R.C., and Loper, C.R., Austempered ductile iron - process control and quality assurance, *J. Mater. Eng. Perform.*, 22(10), pp. 2776–2794, 2013. DOI: <https://doi.org/10.1007/s11665-013-0712-y>.
- [25] Dong, M.J., Prioul, C., and Francois, D., Damage effect on the fracture toughness of nodular cast iron: Part I. Damage characterization and plastic flow stress modeling, *Metall. Mater. Trans. A Phys. Metall. Mater. Sci.*, 28(11), pp. 2245–2254, 1997. DOI: <https://doi.org/10.1007/s11661-997-0182-7>
- [26] Berdin, C., Dong, M.J., and Prioul, C., Local approach of damage and fracture toughness for nodular cast iron, *Engineering Fracture Mechanics*, 68(9), pp. 1107–1117, 2001. DOI: [https://doi.org/10.1016/S0013-7944\(01\)00010-8](https://doi.org/10.1016/S0013-7944(01)00010-8)
- [27] Vaško, A., Hortalová, L., Uhrčík, M., and Tillová, E., Fatigue of nodular cast iron at high frequency loading, *Materwiss. Werksttech.*, 47(5–6), pp. 436–443, 2016. DOI: <https://doi.org/10.1002/mawe.201600519>
- [28] Ulewicz R., and Tomski, P.S., The effect of high-frequencies loading on the fatigue cracking of nodular cast iron, 2019, pp. 5–7.
- [29] Seleš, K., Tomić, Z., and Tonković, Z., Microcrack propagation under monotonic and cyclic loading conditions using generalised phase-field formulation, *Eng. Fract. Mech.*, 255, art. 107973, 2021. DOI: <https://doi.org/10.1016/j.engfracmech.2021.107973>.
- [30] D’Agostino, L., De-Santis, A., Di-Cocco, V., Iacoviello, D., and Iacoviello, F., Fatigue crack propagation in Ductile Cast Irons: an Artificial Neural Networks based model, *Procedia Struct. Integr.*, 3, pp. 291–298, 2017. DOI: <https://doi.org/10.1016/j.prostr.2017.04.048>
- [31] Di-Cocco, V., Iacoviello, F., and Cavallini, M., Damaging micromechanisms characterization of a ferritic ductile cast iron, *Eng. Fract. Mech.*, 77(11), pp. 2016–2023, 2010. DOI: <https://doi.org/10.1016/j.engfracmech.2010.03.037>
- [32] Iacoviello, F., and Di-Cocco, V., Ductile cast irons: microstructure influence on fatigue crack propagation resistance, *Frat. Ed Integrità Strutt.*, 13(13), pp. 3–16, 2010. DOI: <https://doi.org/10.3221/IGF-ESIS.13.01>



- [33] Di-Cocco, V., Iacoviello, F., Rossi, A., Cavallini, M., and Natali, S., Graphite nodules and fatigue crack propagation micromechanisms in a ferritic ductile cast iron, *Fatigue Fract. Eng. Mater. Struct.*, 36(9), pp. 893–902, 2013. DOI: <https://doi.org/10.1111/ffe.12056>
- [34] Iacoviello F., and Di Cocco, V., Influence of the graphite elements morphology on the fatigue crack propagation mechanisms in a ferritic ductile cast iron, *Eng. Fract. Mech.*, 167, pp. 248–258, 2016. DOI: <https://doi.org/10.1016/j.engfracmech.2016.03.041>
- [35] Limodin N., et al., Influence of closure on the 3D propagation of fatigue cracks in a nodular cast iron investigated by X-ray tomography and 3D volume correlation, *Acta Mater.*, 58(8), pp. 2957–2967, 2010. DOI: <https://doi.org/10.1016/j.actamat.2010.01.024>
- [36] Betancur A., and Anflor, C.T.M., Multi-Scaling homogenization process for nodular cast iron using BEM, *J. Multiscale Model.*, 08(03n04), art. 1740005, 2017. DOI: <https://doi.org/10.1142/s1756973717400054>
- [37] Pereira, A., Costa, M., Anflor, C., Pardal, J., and Leiderman, R., Estimating the effective elastic parameters of nodular cast iron from micro-tomographic imaging and multiscale finite elements: comparison between numerical and experimental results, *Metals*, 8(9), art. 695, 2018. DOI: <https://doi.org/10.3390/met8090695>
- [38] Fernandino, D.O., Cisilino, A.P., and Boeri, R.E., Determination of effective elastic properties of ferritic ductile cast iron by computational homogenization, micrographs and microindentation tests, *Mech. Mater.*, 83, pp. 110–121, 2015. DOI: <https://doi.org/10.1016/j.mechmat.2015.01.002>
- [39] Mottischka, T., Pusch, G., Biermann, H., Zymbell, L., and Kuna, M., Influence of overloads on the fatigue crack growth in nodular cast iron: Experiments and numerical simulation, *Procedia Eng.* 2(1), pp. 1557–1567, 2010. DOI: <https://doi.org/10.1016/j.proeng.2010.03.168>
- [40] Dahlberg, M., Fatigue crack propagation in nodular graphite cast iron. *International Journal of Cast Metals Research*, 17(1), pp. 29–37, 2004. DOI: <https://doi.org/10.1179/136404604225012398>
- [41] Wasén, J., and Heier, E., Fatigue crack growth thresholds - The influence of Young's modulus and fracture surface roughness, *Int. J. Fatigue*, 20(10), pp. 737–742, 1998. DOI: [https://doi.org/10.1016/S0142-1123\(98\)00034-6](https://doi.org/10.1016/S0142-1123(98)00034-6)
- [42] de Sousa, J.A.G., Sales, W.F., Guesser, W.L., and Machado, Á.R., Machinability of rectangular bars of nodular cast iron produced by continuous casting, *Int. J. Adv. Manuf. Technol.*, 98(9–12), pp. 2505–2517, 2018. DOI: <https://doi.org/10.1007/s00170-018-2387-x>.
- [43] Anderson, T.L., *Fracture Mechanics: Fundamental and Applications*. 2017.

**C.T.M. Anflor**, holds a BSc. Eng. in Mechanical Engineering in 2000, from the University of Passo Fundo. MSc. in Mechanical Engineering in 2003, from the Federal University of Rio Grande do Sul, and a PhD. in Mechanical Engineering in 2007, from the same university, with further doctoral research at Brunel University London, UK in 2013. She is currently a professor of Automotive Engineering at the University of Brasília. Her expertise includes mechanical vibrations, boundary element methods, and solid mechanics. Anflor is the leader of the Experimental and Computational Mechanics Group (GMEC) at the University of Brasília. ORCID: 0000-0003-3941-8335

**J. Hurtado-Águalimpia**, holds a BSc. Eng. in Civil Engineering in 2013, from the University of Antioquia, Colombia. MSc. in Engineering Materials Integrity. His research experience focuses on mechanical testing and the fracture/fatigue mechanics of engineering materials. ORCID:0009-0001-1759-7881

**A.A. Betancur-Arroyave**, received his PhD. in Mechanical Sciences in 2017, from the University of Brasília and his MSc. in Chemical Engineering in 2012, from the Facultad de Minas, at the Universidad Nacional de Colombia. He is currently an instructor at SENAI-Brasília and active member of the Group of Experimental and Computational Mechanics (GMEC) at the University of Brasília. His research interests include materials science and computational mechanics. ORCID: 0000-0002-6687-1197

**S.H.S. Carneiro**, holds a BSc. Eng. in Mechanical-Aeronautical Engineering in 1987, from the Instituto Tecnológico de Aeronáutica (ITA). MSc. in Aeronautical and Mechanical Engineering in 1993, with a focus on Structures, from ITA, and a PhD. in Engineering Mechanics in 2000 from the Virginia Polytechnic Institute and State University. He is currently an associate professor in the Aerospace Engineering program and active member of the Group of Experimental and Computational Mechanics (GMEC) at the University of Brasília. ORCID: 0000-0001-6669-2255

**J.N.V. Goulart**, holds a BSc. Eng. in Civil Engineering in 1999, from the University of Passo Fundo, and both a MSc. and PhD. in Mechanical Engineering from the Federal University of Rio Grande do Sul, with a focus on transport phenomena and solid mechanics. He is currently a professor in the Energy Engineering program at the University of Brasília. He is also an affiliated faculty member of the Graduate Program in Engineering Materials Integrity (PPGIntegridade) and an active member of the Group of Experimental and Computational Mechanics (GMEC) at the University of Brasília. ORCID: 0000-0002-3045-1975



# Structural performance of composite beams using advanced modeling for nonlinear analysis

Mazin M. Sarhan <sup>a</sup> & Faiq M. S. Al-Zwainy <sup>b</sup>

<sup>a</sup> Department of Civil Engineering, College of Engineering, Mustansiriyah University, Iraq. [mazin.m@uomustansiriyah.edu.iq](mailto:mazin.m@uomustansiriyah.edu.iq)

<sup>b</sup> Department of Civil Engineering, College of Engineering, Al-Nahrain University, Iraq. [faiq.m.al-zwainy@nahrainuniv.edu.iq](mailto:faiq.m.al-zwainy@nahrainuniv.edu.iq)

Received: March 28<sup>th</sup>, 2025. Received in revised form: July 24<sup>th</sup>, 2025. Accepted: August 1<sup>th</sup>, 2025.

## Abstract

A few studies used full-embedded steel sections in composite beams to reduce their cross sections. This paper presents the behavior of normal and high-strength composite beams having various heights of full-embedded steel sections. The stirrups and compression reinforcement details of the beams were the same. The finite element method was adopted in the 3D nonlinear analysis of the presented study. Full-scale composite models were investigated and tested under four-point bending. The load-deflection behavior including the elastic and post-cracking stages was monitored in this paper. Furthermore, the stress distribution of embedded steel sections, crack patterns, and modes of failure of the composite beams were investigated and studied. The results showed that the implemented analytical models were accurate, in which the error percentage was only 1.3%. The high-strength concrete composite beams showed more strength and ductile failure than those with normal strength. Also, the full-embedded steel sections have fully or partially yielded.

**Keywords:** concrete; composite beam; reinforcement; crack; finite elements.

# Rendimiento estructural de vigas compuestas mediante modelado avanzado para análisis no lineal

## Resumen

Algunos estudios utilizaron secciones de acero completamente embebidas en vigas compuestas para reducir sus secciones transversales. Este artículo presenta el comportamiento de vigas compuestas normales y de alta resistencia con varias alturas de secciones de acero completamente embebidas. Los detalles de los estribos y el refuerzo de compresión de las vigas fueron los mismos. El método de elementos finitos se adoptó en el análisis no lineal 3D del estudio presentado. Se investigaron y probaron modelos compuestos a escala real bajo flexión en cuatro puntos. En este artículo se monitoreó el comportamiento de carga-deflexión, incluyendo las etapas elásticas y post-fisuración. Además, se investigó y estudió la distribución de tensiones de las secciones de acero embebidas, los patrones de fisuración y los modos de fallo de las vigas compuestas. Los resultados mostraron que los modelos analíticos implementados fueron precisos, en los que el porcentaje de error fue de solo 1.3%. Las vigas compuestas de hormigón de alta resistencia mostraron mayor resistencia y fallo dúctil que aquellas con resistencia normal. Además, las secciones de acero completamente embebidas han cedido total o parcialmente.

**Palabras clave:** hormigón; viga compuesta; reforzamiento; grieta; elementos finitos.

## 1. Introduction

Composite reinforced concrete beams represent a pivotal advancement in structural engineering, offering enhanced strength, durability, and versatility in construction practices. This innovative approach integrates the benefits of both concrete and reinforcing materials to create robust and

efficient structural elements. Key to the efficacy of composite reinforced concrete beams is their ability to distribute loads effectively, harnessing the tensile strength of reinforcing materials to complement the compressive strength of concrete. This synergy enhances structural integrity, mitigates the onset of cracks, and minimizes the propagation of failure mechanisms, thereby ensuring prolonged service

**How to cite:** Sarhan, M.M.S., and Al-Zwainy, F.M.S., Structural performance of composite beams using advanced modeling for nonlinear analysis DYNA, (92)238, pp. 103-110, July - September, 2025.



life and reduced maintenance costs. Moreover, composite reinforced concrete beams facilitate the realization of ambitious architectural visions, enabling the construction of slender and lightweight structural elements characterized by intricate geometries and striking aesthetics.

The performance of beams reinforced with encased sections relies on the bond strength between the section and the concrete. This bond ensures the stability and overall performance of the beam under various loading conditions. The bond allows for the effective transfer of loads between the two materials. A strong bond ensures that the forces acting on the beam are efficiently transmitted from the concrete to the reinforcing steel and vice versa [1-4]. Proper bonding also helps control cracking within the concrete, distributing the stresses effectively, and minimizing the formation and propagation of cracks [5-6]. Furthermore, adequate bond strength contributes to the long-term durability of the reinforced beam [7-8]. It helps prevent debonding, which can lead to structural failure over time due to corrosion, fatigue, or other environmental factors. Engineers may employ mechanical bonding techniques to ensure the integrity and strength of reinforced concrete structures. On the other hand, the behavior of reinforced concrete beams is experimentally monitored at only specific locations due to restrictions in the cost of testing equipment and accessories; therefore, enormous researchers have used Finite Element Modeling (FEM) in their investigations.

Finite Element Methods (FEM) plays a crucial role in analyzing the behavior of composite beams. FEM enables engineers to model complex interactions between different materials, accurately predicting the structural response of composite beams under various loads and conditions. This methodology allows for detailed analysis and optimization of composite beam designs, contributing to the development of more efficient and reliable structural systems in engineering practice. Buyukozturk (1977) [9] stands out as among the earliest researchers to pioneer a methodology aimed at incorporating the influence of reinforcements into the finite element analysis of concrete structures. Subsequently, multiple mathematical models, such as those proposed by Bergan and Holand in 1979 [10] and Vecchio in 1989 [11], were further developed to encompass the simulation of material characteristics and interactive behaviors, which serve as the origins of nonlinearities within concrete structures for Finite Element Method (FEM) analysis. Through the expansion of these methodologies, additional strategies incorporating considerations for the influences of plastic stiffness degradation were assessed in nonlinear finite element analysis, as explored by Oller et al. in 1990 [12]. Thereafter, several researchers used the simulations in beams investigation, for instance, Damian et al. (2001) [13], Wolanski (2004) [14], Hoque (2006) [15], Saifullah et al. (2011) [16], Gilbert (2012) [17], El-Mogy et al. (2013) [18], Peng and Liu (2013) [19], Tsavdaridis et al. (2013) [20], Satasivam and Bai (2014) [21].

Investigations into the behavior of structural elements demand a trustworthy finite element model. It is imperative to possess an in-depth comprehension of the appropriate elements for precise modeling, thereby guaranteeing the accuracy of response estimation. Determining an appropriate

finite element model capable of accurately predicting and computing the exact responses of reinforced concrete members is highly challenging due to the complexity inherent in their behavior and nature. Various factors influence the analysis outcomes of an RC member, including yielding strain, reinforcement material's hardening effects, concrete's crack and crush behavior, material properties, section specifications, and the type of loading applied to the member. In recent years, various scholars have introduced numerous models and methodologies concerning the numerical analysis of reinforced concrete beams, for example, Hazelwood et al. (2015) [22], Qu et al. (2016) [23], and Tong et al. (2017) [24].

This study emphasizes finite element analysis modeling as a dependable and user-friendly approach for conducting nonlinear analysis on composite beams using normal-strength concrete (NSC) and high-strength concrete (HSC). The specimens were modeled and analyzed as full-scale composite beams by using ANSYS software package.

## 2. Research significance

The use of composite beams is a way to reduce the cross sections and increase the ultimate strength of the structure. Most previous studies used composite beams with externally connected sections, while only a few of them used encased sections due to the difficulty of implementation. Therefore, this study focused on concrete beams with fully embedded sections. In addition, according to previous studies, there is complexity and difficulty in modeling the plastic behavior of reinforced concrete using the finite element method; so, this study was intended to cover this gap as well.

## 3. Modeling and analysis of composite beams

The modeling process typically consumes about 40-60% of the total solution time. It holds significant importance in finite element analysis, as unexpected errors may arise during the solution phase due to improper modeling. Considerable reductions in solution time and computer memory requirements can be achieved by appropriately idealizing the structure's geometry.

Ten stages were conducted to model the investigated composite beams. The first stage involved selecting the analysis type, where structural analysis was utilized in this study. The second stage entailed selecting the element type for each material used in the beams. The third stage involved specifying the real constants of the materials, wherein the cross-section of steel bars was defined. The fourth stage entailed assigning the material properties of the element types, and defining the linearity and nonlinearity of materials. The fifth stage encompassed modeling the geometry of the beam. The sixth stage involved meshing, dividing the geometry into specific elements. The seventh stage entailed applying the loads and boundary conditions. In the current study, the loads were applied as displacement, and the boundary conditions comprised hinges and roller supports. The eighth stage involved identifying the options for nonlinear analysis. Static analysis, geometry nonlinear, displacement solution control, and the Newton-Raphson

method were employed in this step. The ninth stage was the solution. The last stage involved viewing the solution results, which included load-deflection behavior, cracks, and stresses.

#### 4. Types of elements used in the reinforced concrete modeling

In finite element analysis, the selection of appropriate element types is a significant criterion. Table 1 displays the types of elements used in reinforced concrete modeling. The concrete was modeled using the SOLID65 element, designed especially for concrete. The treatment of nonlinear material properties is considered the most significant characteristic of this element. The SOLID65 element can be cracked in tension in three orthogonal directions, crush in compression, deform plastically, and exhibit creep behavior. The steel bars were modeled using the LINK180 element, capable of elasticity, accommodating large strains, deflections, plasticity, rotations, and creep. The steel sections were modeled using the SOLID185 element, which features stress stiffening, large strain and deflection capabilities, and plasticity.

The elements utilized in the modeling process necessitate fundamental information concerning their properties, referred to as real constants. In the case of the SOLID65 element, the real constant for the crushed stiffness factor (CSTIF) was employed either through a cracked face or for a crushed element. For the LINK180 element, the cross-sectional area of the reinforcing bars was defined as a real constant. Notably, the real constant of the SOLID185 element did not require definition.

#### 5. Material properties

##### 5.1 Concrete

The material properties play a significant role in structural modeling. Developing concrete behavior in finite element modeling is considered a challenging task. In this study, linear (elastic) and multi-linear (plastic) isotropic material properties were used in the SOLID65 element to model concrete behavior. The modulus of elasticity of concrete ( $E_c$ ) and Poisson's ratio ( $\nu$ ) were defined in the linear isotropic material properties. The modulus of elasticity of concrete ( $E_c$ ) was calculated from eq. (1), and Poisson's ratio ( $\nu$ ) was assumed to be equal to 0.2 for all the models.

$$E_c = 4700 \sqrt{f'_c} \text{ (MPa)} \quad (1)$$

Table 1.  
Types of elements used in the reinforced concrete models.

No.	Modelled Material	Element Type
1	Concrete	SOLID65
2	Steel bars, stirrups	LINK180
3	Steel sections, loaded steel pieces and studs	SOLID185

Source: The authors.

In the nonlinear part, compressive uniaxial stress-strain behavior for concrete was defined. For normal-strength concrete, the stress-strain behavior was adopted based on the model proposed by Desayi and Krishnan (1964) [25], as shown in eqs. (2 and 3), along with eq. (4) proposed by Gere and Timoshenko (1997) [26].

$$f_c = \frac{E_c \varepsilon}{1 + \left(\frac{\varepsilon}{\varepsilon_o}\right)^2} \quad (2)$$

$$\varepsilon_o = \frac{2f'_c}{E_c} \quad (3)$$

$$E_c = \frac{f_c}{\varepsilon} \quad (4)$$

where:

$f_c$  = stress at any strain ( $\varepsilon$ ),

$\varepsilon_o$  = strain at the ultimate compressive strength of concrete ( $f'_c$ ).

For high strength concrete, the stress-strain behavior was adopted based on the model proposed by Thorenfeldt (1987) [27], as shown below:

$$f_c = [((\varepsilon_c/x)^y + y - 1)^{-1}] y f'_c (\varepsilon_c/x) \quad (5)$$

where:

$$y = (0.0588 f'_c) + 0.8 \quad (6)$$

$$x = [y/(y - 1)](f'_c/E_c) \quad (7)$$

$$E_c = 3320 (\sqrt{f'_c} + 2.0784) \quad (\text{N/mm}^2) \quad (8)$$

$$g = \begin{cases} 1 & , \text{when } (\varepsilon_c/x) \leq 1 \\ ((0.0161 f'_c) + 0.67) & , \text{when } (\varepsilon_c/x) > 1 \end{cases} \quad (9)$$

The tension behavior of concrete was simulated using a linear-elastic model prior to cracking. The uniaxial tensile cracking stress was defined depending on the modulus of rupture ( $f_r$ ), as shown in eq. (10).

$$f_r = 0.7 \sqrt{f'_c} \quad (10)$$

##### 5.2 Reinforcement

Steel is a homogeneous material assumed to transfer axial force only. This behavior is assumed to be identical in compression and tension. Steel reinforcement can be modeled as either a bilinear isotropic hardening plasticity material or a multilinear isotropic hardening plasticity material. The von Mises yield criterion is used in both models.

In modeling the bilinear isotropic hardening plasticity material, the modulus of elasticity of steel and Poisson's ratio were assumed to be equal to 200,000 MPa and 0.3, respectively. The strain hardening modulus (ET) was utilized to prevent convergence problems during the solution. In modeling the multilinear isotropic hardening plasticity

material, the uniaxial stress-strain behavior of steel reinforcement was defined. In the current study, compression reinforcement and stirrups were modeled using bilinear isotropic hardening plasticity materials, while tension reinforcement was modeled using multilinear isotropic hardening plasticity material.

## 6. Modeling and mesh generation

In the current study, the concrete and reinforcement were modeled as volumes, which were then meshed by dividing the model into finite elements. To select the best mesh, four full-scale beams (without reinforcement) were modeled in this study; the number of elements ranged between 6180 and 15720 elements. Fig. 1 shows the relationship between the failure load and the number of elements of the models.

The few elements may lead to inaccurate results, while an excessive number of elements requires significant time for the solution and a large memory area, potentially leading to convergence problems before failure. Therefore, selecting the

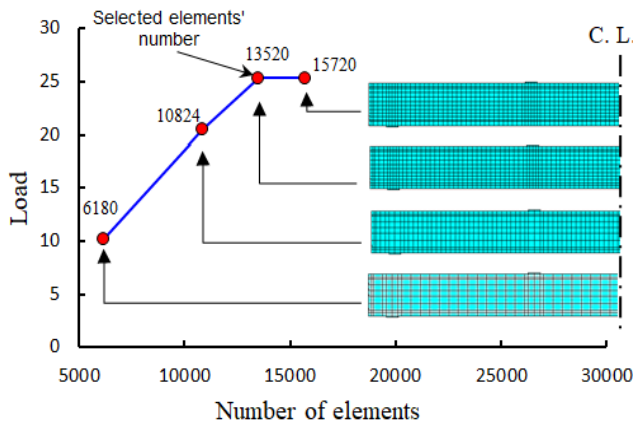


Figure 1. Mesh of concrete model.  
Source: The authors.

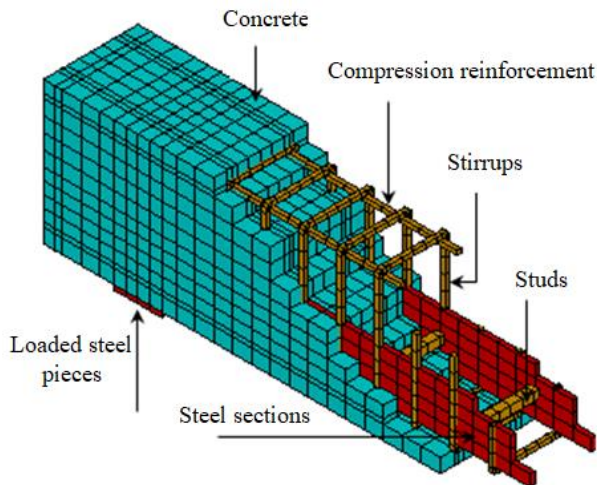


Figure 2. Models' details of a Specimen.  
Source: The authors

ideal number of elements leads to reliable and accurate results. In the current study, the model with 13520 elements was selected. Details of a tested model are presented in Fig. 2.

## 7. Application of boundary conditions and loads

The beams' bending test of this study was performed using a 4-point bending setup in accordance of ASTM C78/C78M. Simply supports (hinge and roller) were used as boundary conditions for the models in the current study. In the hinge support, the nodes were constrained in x and y-directions. In the roller support, the nodes were constrained in y-directions. Both the supports were constrained in the z-direction to prevent the motion in the z-direction. The boundary conditions were applied across the centerline of the loaded pieces (on the bottom nodes). Fig. 3 shows the boundary conditions used in the models.

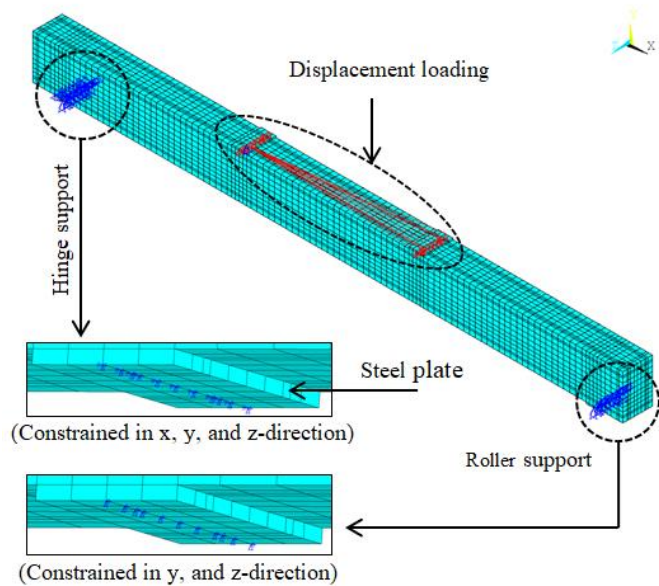


Figure 3. Boundary conditions and displacement application.  
Source: The authors.

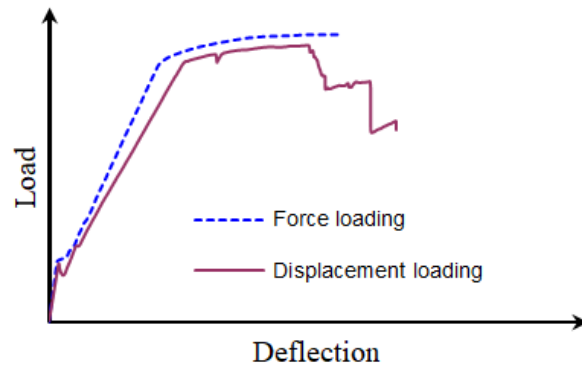


Figure 4. Methods of loads' application.  
Source: The authors

Table 2.  
Parametric test matrix.

Beams ID	Concrete compressive strength (MPa)	Height of steel sections (mm)
B1-C-35	35	100
B2-C-42	42	
B3-C-55	55	
B4-C-70	70	
B5-S-H1	42	50
B6-S-H2		75
B7-S-H3		100
B8-S-H4		131

Source: The authors.

The load can be applied by using the force or the displacement. In the case of application of the force, the force is applied on the nodes; every node takes a specific amount of the force. In the case of the application of the displacement, the couple DOFs (coupled degrees of freedom) option was used. Here, the top centreline nodes of loaded pieces were coupled in one node by using the couple DOFs option, and then a displacement was applied to this node.

Fig. 4 shows the difference between the use of force and displacement loading as was investigated in the current study. It can be clearly seen that the application of displacement is more accurate and reflect the actual behavior of models; thus, it was adopted in the investigations of this study.

## 8. Test matrix

Eight full-scale models were adopted to investigate the structural behavior of composite beams. The models were designed with the dimensions of 0.2 m width x 0.3 m height x 4 m length. The stirrups and compression reinforcement details of the beams were the same. The main reinforcement comprised two steel sections (with rectangular cross-sections) placed at a 90-degree angle; the thickness of the steel sections was 0.1 m, and their yield strength was 370 MPa. To enhance the cohesion between the reinforcement and concrete, the steel sections were provided with twenty steel rods equally spaced along the sections.

The test matrix was divided into two groups. The first group included four models designed with a specific concrete compressive strength for each beam, covering the normal and high-strength ranges. The second group included four models designed with a specific cross-section size of embedded reinforced sections for each beam. Table 2 illustrates the test matrix of this study.

## 9. Results and discussion

### 9.1 Behaviour of composite beams having NSC and HSC

The results include the load-deflection behavior, ultimate loads, deflection along the span, and crack patterns of the tested full-scale models. The composite beams exhibited different ultimate loads depending on the type of concrete strength (NSC or HSC). In general, and for all the beams, the ultimate loads increased with the increase in compressive

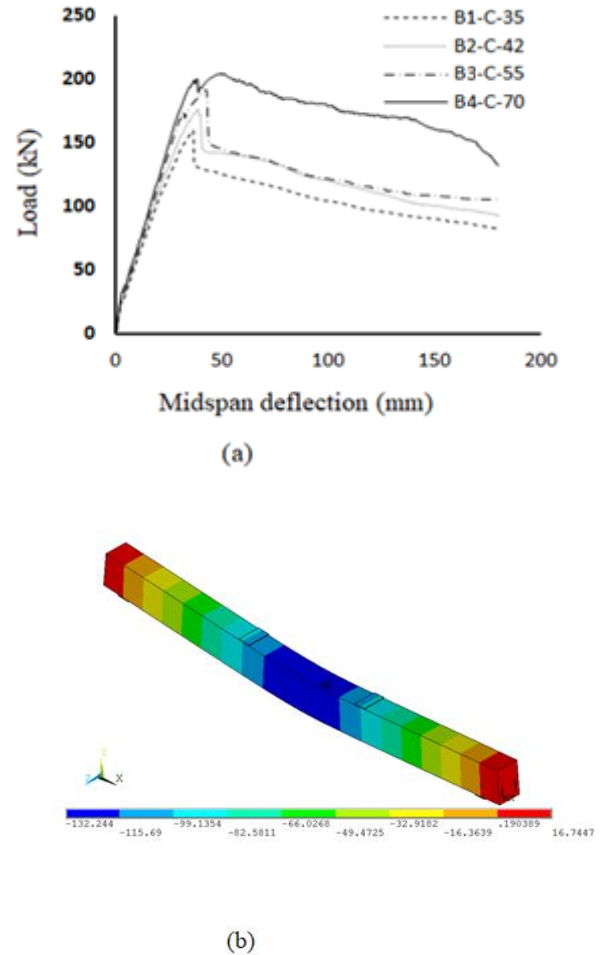


Figure 5. Behaviour of composite beams: (a) load-midspan deflection, (b) deflection along the span.  
Source: The authors

strength, as shown in Fig. 5-a. The ultimate load increased by 22% when the concrete changed from NSC (35 MPa) to HSC (70 MPa). HSC exhibited lower linear elastic behavior than NSC. The concrete crush occurred before a 40 mm deflection for the beam with NSC and before a 50 mm deflection for the beam with HSC. Fig. 5-b shows the deflection along the modeled beams, with maximum deflections at the middle and minimum deflections at the ends. According to Fig. 5-a, the ductility of the tested beams enhanced when the concrete switched from NSC to HSC; however, Fig. 5-b did not present a clear enhancement trend.

During the modeling stage, it's important to consider factors such as material properties, loading conditions, boundary conditions, and structural analysis methods to predict and interpret crack patterns accurately. ANSYS program is capable of recording cracks at each loading substep. Fig. 6 shows the crack patterns of NSC and HSC beams at failure loads. Flexural cracks were caused by bending stresses in the beam and were observed along the bottom of the beam's cross-section in the vicinity of the neutral axis. Additionally, crushing cracks occurred due to high compressive forces, resulting in localized crushing or spalling of the concrete. The failure mode of all beams was flexure.



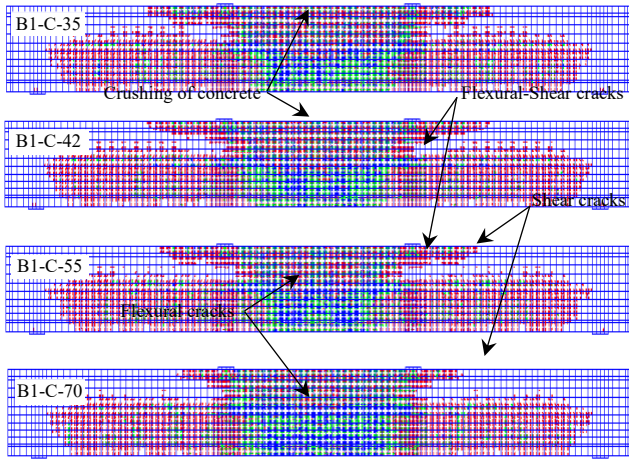


Figure 6. Cracks patterns for the modelled beams at failure.  
Source: The authors

## 9.2 Behavior of composite beams having different heights of steel sections

Fig. 7 illustrates the midspan deflection of composite beams under load. Among the beams, Beam B5-S-H1 exhibited the lowest ultimate load compared to the others. There was only a slight difference in ultimate loads between Beams B6-S-H2, B7-S-H3, and B8-S-H4. Specifically, the ultimate load of Beam B5-S-H1 differed from that of Beam B6-S-H2 by 22%. From the analysis, it can be concluded that increasing the height of steel sections from 50 mm to 75 mm resulted in a 28% increase in the load-carrying capacity. Moreover, the load-carrying capacity was marginally improved when the height of steel sections increased by 57%.

The results also showed that the steel sections have fully or partially yielded depending on the height of the steel section. Fig. 8 depicts the state of yielding for different heights of steel sections of beams. According to Fig. 8-a, the steel sections with a height of 50 mm have fully yielded. However, the steel sections with heights of 75-131 mm have partially yielded, as shown in Fig. 8-(b-d). The maximum

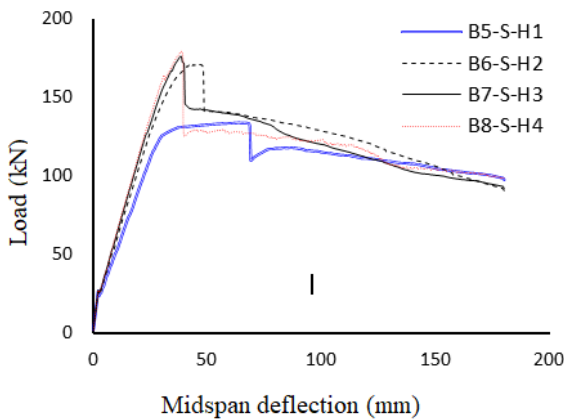
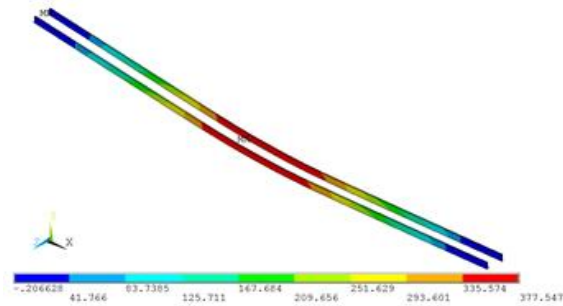
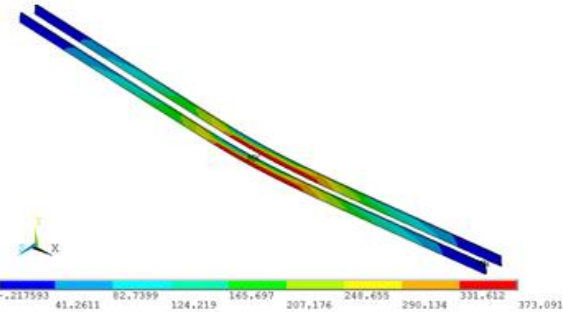


Figure 7. Load-midspan deflection curve of models of Group B.  
Source: The authors

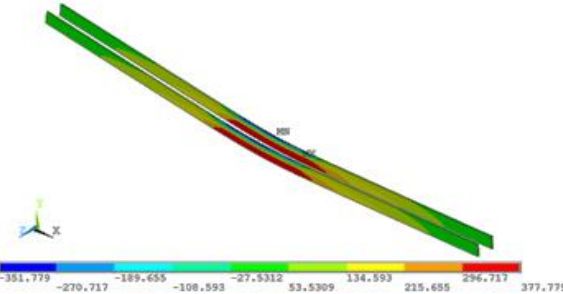
stresses of steel sections with heights of 50 mm, 75 mm, 100 mm, and 131 mm were 378 kN, 373 kN, 378 kN, and 385 kN, respectively. It can also be noticed that the maximum stresses were concentrated at the mid-span of steel plates for all the beams. Thus, the failure modes of all beams were flexure.



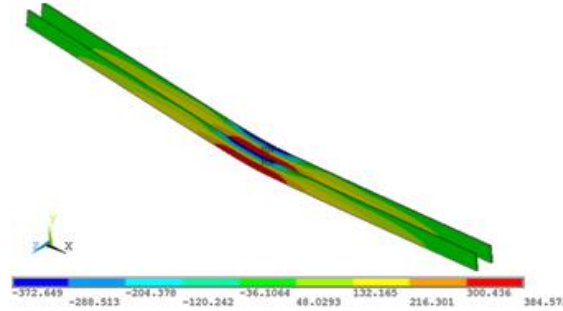
a- (Beam B5-S-H1)



b- (Beam B6-S-H2)



c- (Beam B7-S-H3)



d- (B8-S-H4)

Figure 8. Stresses of steel plates with the height of: (a) 50 mm (Beam B5-S-H1); (b) 75 mm (Beam B6-S-H2); (c) 100 mm (Beam B7-S-H3); (d) 131.25 mm (Beam B8-S-H4).  
Source: The authors

## 10. Conclusions

This research conducts nonlinear finite element analysis on NSC and HSC composite beams employing diverse steel sections. The examination of these composite beams was performed under four-point loading conditions. From the findings of this investigation, the following conclusions can be drawn:

1. There was a good agreement between the tested beams and finite element models, the difference in ultimate load was 1.3% or less. Also, the structural behavior obtained by the finite element modeling, represented by the load-deflection curves, showed good similarity with the experimentally tested beams.
2. The ductility of tested beams increased when the concrete compressive strength increased. Also, the ultimate load increased by 22% when the concrete compressive strength increased from 35 MPa to 70 MPa.
3. The steel sections have fully or partially yielded depending on the height of the steel section; the maximum stresses were concentrated at the bottom mid-span of steel sections for all the beams.
4. The use of steel sections with the heights of 50 mm to 75 mm increased the load-carrying capacity by approximately 28%, approximately. However, the use of steel sections with heights of 75 mm to 131 mm did not significantly improve the load-carrying capacity of beams.
5. The best-performing tested beam was B4-C-70 in terms of ductility, strength and general structural behaviour.
6. The finite element models accurately predicted that the beams failed in flexure according to the appearance of cracks.

## Acknowledgments

The authors would like to thank Mustansiriyah University ([www.uomustansiriyah.edu.iq](http://www.uomustansiriyah.edu.iq)) Baghdad - Iraq, for its support in the present work. Also, the authors would like to thank Al-Nahrain University ([www.nahrainuniv.edu.iq](http://www.nahrainuniv.edu.iq)) Baghdad - Iraq, for its help in the current work.

## Conflicts of Interest

The authors declare no conflict of interest.

## References

- [1] Munoz, M.B., Study of bond behaviour between FRP reinforcement and concrete, PhD. Thesis, Departament d'Enginyeria mecànica i de la construcció industrial, Universitat de Girona, Girona, Spain, 2011.
- [2] Saikali, E.R., Palermo, D., and Pantazopoulou S., Bond behaviour of steel reinforcing bars embedded in ultra-high-performance steel fiber reinforced concrete, Proceedings of CSCE Annual Conference (CSCE), 2019.
- [3] Basaran, B., and Kalkan, I., Investigation on variables affecting bond strength between FRP reinforcing bar and concrete by modified hinged beam tests. *Composite Structures*, 242, art. 112185, 2020. DOI: <https://doi.org/10.1016/j.compstruct.2020.112185>.
- [4] Wang, X., Liu, Y., and Xin, H., Bond strength prediction of concrete-encased steel structures using hybrid machine learning method. *Structures*, 32, pp. 2279-2292, 2021. DOI: <https://doi.org/10.1016/j.istruc.2021.04.018>.
- [5] Wang, L., He, T., Zhou, Y., Tang, S., Tan, J., Liu, Z. and Su, J., The influence of fiber type and length on the cracking resistance, durability and pore structure of face slab concrete. *Construction and building materials*, 282(2), art. 122706, 2021. DOI: <https://doi.org/10.1016/j.conbuildmat.2021.122706>.
- [6] Niu, Y., Wei, J., and Jiao, C., Crack propagation behavior of ultra-high-performance concrete (UHPC) reinforced with hybrid steel fibers under flexural loading. *Construction and Building Materials*, 294(10), art. 123510, 2021. DOI: <https://doi.org/10.1016/j.conbuildmat.2021.123510>.
- [7] Yan, F., and Lin, Z., Bond durability assessment and long-term degradation prediction for GFRP bars to fiber-reinforced concrete under saline solutions. *Composite Structures*, 161, pp. 393–406, art. 55, 2017. DOI: <https://doi.org/10.1016/j.compstruct.2016.11.055>.
- [8] Lin, H., Zhao, Y., Feng, P., Ye, H., Ozbolt, J., Jiang, C. and Yang, J.-Q. State-of-the-art review on the bond properties of corroded reinforcing steel bar. *Construction and Building Materials*, 213(1), pp. 216–233, 2019. DOI: <https://doi.org/10.1016/j.conbuildmat.2019.04.077>.
- [9] Buyukozturk, O., Nonlinear analysis of reinforced concrete structures. *Computers and Structures*, 7(1), pp. 149–156, 1977. DOI: [https://doi.org/10.1016/0045-7949\(77\)90069-4](https://doi.org/10.1016/0045-7949(77)90069-4).
- [10] Bergan, P.G., and Holand, I., Nonlinear finite element analysis of concrete structures. *Computer Methods in Applied Mechanics and Engineering*, 2(17-18), pp. 443–467, 1979. DOI: [https://doi.org/10.1016/0045-7825\(79\)90027-6](https://doi.org/10.1016/0045-7825(79)90027-6).
- [11] Vecchio, F.J., Nonlinear finite element analysis of reinforced concrete membranes. *ACI Structural Journal*, 86(1), pp. 26–35, 1989. DOI: <https://doi.org/10.14359/2620>.
- [12] Oller, S., Oñate, E., Oliver, J., and Lubliner, J., Finite element nonlinear analysis of concrete structures using a “plastic-damage model”. *Engineering Fracture Mechanics*, 35(1–3), pp. 219–231, 1990. DOI: [https://doi.org/10.1016/0013-7944\(90\)90200-Z](https://doi.org/10.1016/0013-7944(90)90200-Z).
- [13] Damian, K., Thomas, M., Solomon, Y., Kasidit, C., and Tanarat, P., Finite element modeling of reinforced concrete structures strengthened with FRP laminates. Report for Oregon Department of Transportation, Salem, 2001.
- [14] Wolanski, A.J., Flexural behavior of reinforced and prestressed concrete beams using finite element analysis, MSc. Thesis, Department of Civil and Environmental Engineering, Marquette University, Wisconsin, USA, 2004.
- [15] Hoque, M., Rattanawangcharoen, N., Shah, A.H., and Desai, Y.M., 3D nonlinear mixed finite-element analysis of RC beams and plates with and without FRP reinforcement. *Computers and Concrete*, 4(2), pp. 135-156, 2007. DOI: <https://doi.org/10.12989/cac.2007.4.2.135>.
- [16] Saifullah, I., Nasir-uz-zaman, M., Uddin, S.M.K., Hossain, M.A., and Rashid, M.H., Experimental and analytical investigation of flexural behavior of reinforced concrete beam, *International. Journal of Engineering and Technology*, 11(1), pp. 188-196, [online]. 2011. Available at: <https://shorturl.at/9MWyu>.
- [17] Gilbert, A.M., Validation of a laboratory method for accelerated fatigue testing of bridge deck panels with a rolling wheel load, MSc. Thesis, Department of Civil Engineering, Montana State University, Bozeman, USA, 2012.
- [18] El-Mogy, M., El-Ragaby, A., and El-Salakawy, E., Experimental testing and finite element modeling on continuous concrete beams reinforced with fibre reinforced polymer bars and stirrups. *Canadian Journal of Civil Engineering*, 40(11), pp. 1091–1102, 2013. DOI: <https://doi.org/10.1139/cjce-2012-0509>.
- [19] Peng, Q., and Liu, W., Inverse analysis of related parameters in calculation of concrete drying shrinkage based on ANSYS design optimization. *Journal of materials in civil engineering*, 25(6), pp. 683–692, 2013. DOI: [https://doi.org/10.1061/\(ASCE\)MT.1943-5533.0000635](https://doi.org/10.1061/(ASCE)MT.1943-5533.0000635).
- [20] Tsavdaridis, K.D., Mello, C.D., and Huo, B.Y., Experimental and computational study of the vertical shear behaviour of partially encased perforated steel beams. *Engineering structures*, 56, pp. 805–822, 2013. DOI: <https://doi.org/10.1016/j.engstruct.2013.04.025>.
- [21] Satasivam, S., and Bai, Y., Mechanical performance of bolted modular GFRP composite sandwich structures using standard and

- blind bolts. *Composite Structures*, 117, pp. 59–70, 2014. DOI: <https://doi.org/10.1016/j.compstruct.2014.06.011>.
- [22] Hazelwood, T., Jefferson, A.D., Lark, R.J., and Gardner, D.R., Numerical simulation of the long-term behaviour of a self-healing concrete beam vs standard reinforced concrete. *Engineering Structures*, 102, pp. 176–188, 2015. DOI: <https://doi.org/10.1016/j.engstruct.2015.07.056>.
- [23] Qu, Y., Li, X., Kong, X., Zhang, W., and Wang, X., Numerical simulation on dynamic behavior of reinforced concrete beam with initial cracks subjected to air blast loading. *Engineering Structures*, 128, pp. 96–110, 2016. DOI: <https://doi.org/10.1016/j.engstruct.2016.09.032>.
- [24] Tong, L., Liu, B. and Zhao, X.-L. Numerical study of fatigue behaviour of steel reinforced concrete (SRC) beams. *Engineering Fracture Mechanics*, 178, pp. 477–496, 2017. DOI: <https://doi.org/10.1016/j.engfracmech.2017.02.017>.
- [25] Desayi, P., and Krishnan, S., Equation for the stress-strain curve of concrete. *International Concrete Abstracts Portal*, 61(3), pp. 345-350, 1964. DOI: <https://doi.org/10.14359/7785>.
- [26] Gere, J.M., and Timoshenko, S.P., *Mechanics of Materials*. ed, Boston, MA: PWS, 1997.
- [27] Thorenfeldt, E., Tomaszewicz, A., Jensen, J.J., Mechanical properties of high-strength concrete and applications in design. In *Proceedings of the Symposium on Utilization of High-Strength Concrete*, Stavanger, Norway, 1987.

**M.M. Sarhan**, received the BSc. Eng in Civil Engineering from the Mustansiriyah University (Iraq) in 2006, the MSc. Eng in Civil Engineering from the Mustansiriyah University (Iraq) in 2009, and PhD from Wollongong University (Australia) in 2019. He is an inventor and got his patent in engineering field from Australia. He teaches courses for undergraduate programs in the fields of civil engineering. ORCID: 0000-0003-2190-0342

**F.M.S. Al-Zwainy**, received his PhD from the Baghdad University (Iraq) in 2009. After a stint as an independent consultant in industry, when he worked on projects with local government as well as international firms, he has since held academic positions both at ISRA University (Jordan) and Al-Nahrain University (Iraq). He is an inventor and got his patent in engineering field from Australia. He teaches courses for undergraduate and postgraduate programs in the fields of applied statistics and construction project management. He is an active editor and reviewer for the KSCE Journal of Civil Engineering (Springer) and the International Journal of Engineering Sciences and Research Technology (IJESRT, open access); he is also a member of the editorial board of Civil Engineering and Urban Planning: An International Journal (AIRCC Publishing Corporation) and a member of the Project Management Institute. ORCID: 0000-0002-9948-6594



# Flexible electrode for spinal cord electrostimulation

Juan José Melo-Portilla, Luisa Fernanda Puentes-Alzate, Karen Daniela Valencia-Poveda  
& Angelica María Ramírez-Martínez

*Facultad de ingeniería biomédica Universidad Militar Nueva Granada, Cajicá, Colombia. est.juan.melo@unimilitar.edu.co, est.luisa.puentes@unimilitar.edu.co, est.karen.valencia@unimilitar.edu.co, angelica.ramirez@unimilitar.edu.co*

Received: January 20<sup>th</sup>, 2025. Received in revised form: May 30<sup>th</sup>, 2025. Accepted: July 31<sup>st</sup>, 2025.

## Abstract

This study focuses on the development and evaluation of flexible electrodes designed for the electrostimulation of the lumbosacral region of the spinal cord. The research encompasses the design and fabrication phases of three distinct prototypes, as well as the assessment of their electrical properties. The electrodes were physically fabricated using a structure composed of PET/ITO sheets and silver ink, after conducting specific tests with different solutes to optimize the composition of the conductive ink. A systematic classification of the prototypes was carried out based on specific manufacturing parameters, followed by an analysis of their electrical conductivity under different configurations. The study includes a characterization of the potential and electric field behavior generated, both in the isolated electrode and at the electrode-spinal cord interface. This research aims to contribute to the field of neurostimulation by developing more efficient and safer flexible electrodes for medical applications.

**Keywords:** flexible electrode; channels; electro-stimulation; current; spinal cord; spin-coating; conduction.

# Electrodo flexible para electroestimulación medular

## Resumen

Este estudio se centra en el desarrollo y evaluación de electrodos flexibles diseñados para la electroestimulación de la región lumbosacra de la médula espinal. La investigación abarca desde la fase de diseño y fabricación de tres prototipos distintos, hasta la evaluación de sus propiedades eléctricas. Los electrodos fueron fabricados físicamente utilizando una estructura compuesta por láminas de PET/ITO y tinta de plata, realizando previamente pruebas específicas con diferentes solutos para optimizar la composición de la tinta conductora. Se realiza una clasificación sistemática de los prototipos basada en parámetros específicos de fabricación, seguida de un análisis de su conductividad eléctrica bajo diferentes configuraciones. El estudio incluye una caracterización del comportamiento del potencial y campo eléctricos generados, tanto en el electrodo de manera aislada como en la interfaz electrodo-médula. Esta investigación busca contribuir al campo de la neuroestimulación mediante el desarrollo de electrodos flexibles más eficientes y seguros para aplicaciones médicas.

**Palabras clave:** electrodo flexible; canales; electroestimulación; corriente; médula espinal; spin-coating; conducción.

## 1. Introducción

La lesión medular es una afección que provoca trastornos en la movilidad, la sensibilidad o las funciones autónomas del cuerpo. Tiene diversas repercusiones psicológicas y sociales tanto para la persona afectada como para su familia [1]. Como resultado, genera importantes procesos de discapacidad en la vida de quienes la padecen. De acuerdo con las estadísticas de la organización Mundial de la salud, se estima que alrededor de 250.000 y 500.000 personas se ven afectadas anualmente por una lesión en la médula

ocasionado por traumatismos (caídas y accidentes de tráfico), o por causas no traumáticas (por ejemplo, tumores o enfermedades degenerativas) [2].

Aunque para Colombia no se cuenta con estadísticas detalladas de la incidencia de esta enfermedad, se reporta que el conflicto armado colombiano y los accidentes de tránsito son las principales causas de lesiones medulares [3].

Para el tratamiento de este tipo de patología se han investigado diferentes soluciones como terapias físicas, hidroterapias, electroestimulación medular y el uso de células madre. Sin embargo, se ha evidenciado que la terapia física y

**How to cite:** Melo-Portilla, J.J., Puentes-Alzate, L.F., Valencia-Poveda, K.D., and Ramírez-Martínez, A.M., Electrodo flexible para electroestimulación medular DYNA, (92)238, pp. 111-119, July - September, 2025.



la hidroterapia además de ser costosas y extensas, no brindan una recuperación completa al paciente, si no que se emplea como un tratamiento a largo plazo para el manejo del dolor [4,5]. Por otra parte, el uso de células madre se emplea para la regeneración neuronal y ha dado resultados prometedores, en cuanto a la diferenciación de las células en neuronas y astrocitos mejorando la función motora de las extremidades inferiores [6,7]. Aun así, estos estudios no han sido probados in vivo en sujetos humanos.

Dentro de estas propuestas la más destacada en los últimos años ha sido la estimulación medular. Esta técnica consiste en aplicar corrientes eléctricas a través de electrodos, que pueden colocarse sobre la piel o implantarse quirúrgicamente cerca de la médula espinal. Ésta ha demostrado tener los mejores resultados en comparación a los métodos mencionados anteriormente debido a que promueve la creación de nuevas raíces nerviosas, posibilitando la recuperación de la función de la marcha sin necesidad de tener el estímulo activado y así dotando de autonomía a la persona afectada [8]. La rehabilitación a través de electroestimulación presenta altos costos, debido a que se emplean materiales como el oro [9] y se desarrollan estudios especializados lo cual no lo hace accesible para todas las personas; Por lo tanto, se hace necesario la implementación de estrategias más eficientes y económicas que permitan generar una recuperación accesible para toda la comunidad y rápida para todas las personas que presentan este tipo de patología, en países que no cuentan con los recursos necesarios, principalmente en Colombia. Es por esto que este estudio busca diseñar un electrodo implantable que dé alcance a las raíces nerviosas involucradas en los movimientos de miembros inferiores, para recuperar en el paciente movimientos como la marcha, manufacturado con materiales que permitan un precio más accesible.

Ante tal pretensión, este estudio se enfoca en el diseño y la fabricación de prototipos de electrodos flexibles destinados a la estimulación medular teniendo en cuenta la anatomía de la médula espinal. En primera instancia, se lleva a cabo la clasificación de los prototipos desarrollados, evaluando su cumplimiento con parámetros clave establecidos durante la etapa de fabricación. Posteriormente, se realiza una caracterización detallada de la conductividad eléctrica en los canales de cada electrodo, con el propósito de asegurar un desempeño eficiente y consistente bajo condiciones operativas. Finalmente, se efectúa un análisis del comportamiento del potencial eléctrico y del campo generado, considerando tanto el electrodo de manera aislada como su interacción con el tejido medular, a través del software Comsol multiphysics. Estas etapas integradas buscan garantizar la viabilidad técnica y funcional del dispositivo, promoviendo soluciones tecnológicamente avanzadas y accesibles que contribuyan a la rehabilitación motora de pacientes con lesión medular.

## 2. Metodología

La metodología de la investigación se segmenta en tres partes fundamentales. Primero se proponen diversas geometrías de electrodo basada en la literatura existente, esto con el fin que los contactos que se diseñaron en el

electrodo faciliten o logren activar las regiones necesarias en la médula espinal; luego se presenta la manufactura del electrodo, donde se evalúan los materiales y métodos que se seleccionaron para asegurar la eficacia del diseño seleccionado y por último se

realiza un estudio del campo eléctrico y potencia producida por el diseño del electrodo. Esto facilitara la evaluación de la efectividad y mejorar el rendimiento.

### 2.1 Parámetros de diseño del electrodo

Para realizar las propuestas de electrodos que se desarrollan, es importante conocer anatómicamente la región de la médula que se busca estimular; La médula espinal, es el centro principal de los movimientos reflejos y funciona como la vía de comunicación del encéfalo con los órganos sensoriales y motores del cuerpo humano. Sin embargo, es necesario tener en cuenta que la médula espinal se encuentra protegida por diferentes capas como la piamadre, aracnoides, y duramadre; siendo esta última en donde realmente se situaría el electrodo. Ahora bien, la médula espinal es un cordón de tejido nervioso con aspecto cilíndrico situado al interior de la columna vertebral con una longitud media de 40-50cm y diámetro aproximado de 1-2cm, que puede variar dependiendo del sexo de la persona [10]. Así mismo, está compuesta por nervios y raíces espinales de calibre aproximado de 0.5mm, en donde cada nervio está conformado por dos grupos de raíces espinales denominadas anteriores y posteriores, es decir, las raíces motoras emergentes de la médula espinal y las raíces sensitivas aferentes.

Cada par de nervios espinales se designan y enumeran según la región y nivel donde emergen de la columna vertebral. Para el desarrollo del electrodo se define como región primordial de estudio aquella comprendida entre L1-S2, debido a que en esta sección se encuentran contenidos los nervios espinales encargados de la estimulación de los músculos responsables de la marcha, entre los cuales se incluyen las iliopsoas, vasto lateral recto femoral, tibial anterior, semitendinoso, gastrocnemio, extensor largo común de los dedos, soleos, bíceps femoral y glúteo mayor. En la Tabla 1 se puede ver la relación del nervio espinal según el músculo.

Tabla 1.  
Relación entre nervios espinales y músculos para estimulación.

Región medular	Músculo inervado
Iliopsoas	L1-L3
Vasto Lateral y Recto Femoral	L2-L4
Tibial Anterior	L3-L4
Semitendinoso	L4-S1
Gastrocnemio	L5-S1
Extensor Larco común de los dedos	L5-S1
Soleo	S1-S2
Bíceps Femoral	S1-S2
Gluteo Mayor	S1-S2

Fuente: Elaboración propia [8].



A partir de esto, se define que por pierna es necesario la activación de mínimo 7 nervios espinales para poder lograr la marcha, es decir, la paleta o matriz a realizar debe contener al menos 14 electrodos. Una matriz que contenga 8 electrodos también puede ser capaz de lograr 4 movimientos mínimos para la marcha humana que implican flexión de cadera, extensión de rodilla, flexión y extensión del tobillo.[8]

Basándose en los antecedentes anatómicos y de la literatura, se realizaron cuatro diseños de paletas electrodo por medio del Software SolidWorks, con el fin de determinar el mejor diseño en base a la activación muscular necesaria para la marcha humana; todos los diseños con el tamaño estándar establecido de 2x6cm. Adicionalmente estos se diseñan a través de la variación de parámetros como cantidad de electrodos, músculos a estimular y tamaño de canales.

## 2.2 Manufactura del prototipo

La fabricación del electrodo cuenta con un análisis de materiales donde se busca que las propiedades de los materiales cuenten con buena conducción, resistencia, flexibilidad y biocompatibilidad. Además de tomar en cuenta características como materiales de fácil acceso y bajo costo, se seleccionan los materiales principales de fabricación; primero se encuentra al PET/ITO que es el sustrato y la tinta de plata para el recubrimiento de los canales y contactos del electrodo. [11]

El PET/ITO está compuesto por PET “polietileno tereftalato” es un plástico utilizado comúnmente en envases y botellas debido a su densidad más baja que la de un plástico normal. En diversos estudios evalúan el comportamiento al agregar un recubrimiento de ITO [8], el ITO es “óxido de indio y estaño”. Esta modificación en el material permite que sea altamente biocompatible, conductor, resistente y flexible.

La tinta de plata es altamente conductiva, utilizada en construcciones de circuitos flexibles. No es tóxica. Además, está basada en soluciones de agua, que aseguran su biocompatibilidad, como ha sido estudiada y comprobada en diversos estudios [12], por lo que es apta para la manufactura del electrodo.

### 2.2.1 Proceso de fabricación

Se evalúa la lámina de PET/ITO buscando la capa conductora. Para ello se mide la resistencia sobre ambas caras del PET/ITO con ayuda de un multímetro FLUKE. La cara de la lámina que marca  $0\ \Omega$  es la capa no conductora y la capa que arroja una resistencia mayor a  $1,074\ K\ \Omega$  se marca para reconocer la capa del PET/ITO es conductora. Se prepara la solución para el ataque químico; este proceso permite que la cara conductora de PET/ITO se adece, debido a que modifica la superficie de la lámina de forma controlada para poder realizar el recubrimiento de los canales y la adherencia sea mayor en la respectiva configuración de canales. Según la guía de laboratorio “Aplicación de litografía y Spin Coating para elaboración de electrodos interdigitado basados en ITO/PET con contactos de plata, utilizados en los MEMS” [11], se determinan las cantidades de los químicos empleados



Figura 1. Proceso – Ataque químico.

Fuente: Elaboración propia.

en el ataque químico. Se mezclan 13,47 g de agua desionizada, 0,33 g de  $\text{NHO}_3$  y 8,19 g de  $\text{HCl}$  (concentración por peso), se realiza la solución de los diferentes químicos en un beaker que previamente se lava y seca para evitar agentes externos que afecten el ataque químico. Se emplea una placa de Petri y se vierte la solución del ataque químico para sumergir la lámina de PET/ITO, la duración del ataque químico es de 2.10 minutos; tiempo que se determina en la guía de laboratorio

[11]. En la Fig. 1 se explica el proceso por medio de un diagrama de flujo.

Terminado el ataque químico se introduce la lámina de PET/ITO en un beaker con 30 ml de agua destilada, proceso que se realiza dos veces; el propósito es eliminar los residuos de la solución del ataque químico. Se emplea una plancha de secado DLAB para secar la lámina y realizar ahora el proceso de recubrimiento de canales por medio de Spin Coating. Antes de realizar dicho proceso se prepara la tinta de plata, es decir, se mezcla con un solvente para lograr una consistencia óptima para crear la película en el electrodo, es mezcla se compone de 0.5 gramos de pasta de plata y se diluye en 1 ml de acetona. El Spin Coating permitirá generar una película delgada y uniforme sobre la lámina por medio de centrifugación; con este método se genera el recubrimiento en los canales del electrodo; se emplea el EZ4 Spin Coater y se configura con los parámetros expuestos en la Fig. 2, se fija el electrodo en el porta sustratos con cinta dobles faz con el fin de que al realizar la centrifugación este no se desacomode; se configura los parámetros de rotación en el menú y paralelamente se prepara la plancha DLAB a  $120\ ^\circ\text{C}$ .

Se sitúa por medio de un gotero la solución de tinta de plata sobre el sustrato, se cierra la tapa y se inicia la rotación. Se debe contabilizar aproximadamente 10 segundos y se adiciona una segunda gota. Una vez finaliza el tiempo de rotación programado, se retira el sustrato y se lleva a la plancha DLAB durante 3 minutos para secar y adherir el recubrimiento de tinta de plata.



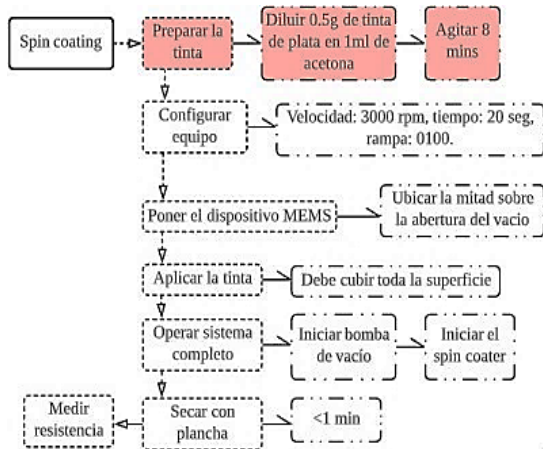


Figura 2. Proceso – Spin Coating.  
Fuente: Elaboración propia.

### 2.2.2 Evaluación de solventes

Se compara tres tipos de solventes para determinar cuál de ellos presenta un mejor comportamiento al desarrollar el recubrimiento en los canales del electrodo. En la primera prueba de solvente, se toman 0.5 g de pasta de plata y se diluyen en 1 ml de acetona. Esta solución se prepara, se observa su consistencia y comportamiento durante el proceso de Spin Coating; para la segunda prueba, se toman 0.5 g de plata y se diluyen en una solución compuesta por 1 ml de acetona al 95% y 5% de acetato de butilo. Esta mezcla de solventes ofrece una viscosidad diferente y, por lo tanto, un rendimiento distinto durante el proceso de recubrimiento. En la tercera prueba, se elabora la solución con 1 ml de acetona al 97 % y 3 % de acetato de butilo, en la que se diluyen 0.5 g de plata. Este proceso de evaluación de diferentes soluciones diluyentes tiene como objetivo determinar cuál de los diferentes solventes proporciona la mejor consistencia y comportamiento de la tinta de plata durante el proceso de Spin Coating. La viscosidad adecuada de la tinta es crucial para obtener un recubrimiento uniforme y de alta calidad sobre los contactos del electrodo.

### 2.3 Modelo de elementos finitos del campo eléctrico y potencia del electrodo

Se desarrolla una simulación en COMSOL con el fin de observar el campo eléctrico y la potencia que se genera en el electrodo. Se configura un estudio estacionario para modelar el flujo de corriente eléctrica, el campo generado y la distribución del potencial eléctrico.

La primera fase de esta metodología consistió en cargar el diseño del electrodo de 8 canales en COMSOL Multiphysics en formato STL para su análisis. El diseño, previamente elaborado en SolidWorks, se exportó en este formato debido a su compatibilidad con el simulador.

Tras cargar correctamente el diseño del electrodo en COMSOL, se asignaron las propiedades físicas y eléctricas de los materiales correspondientes a cada componente del modelo: la base de PET/ITO y los canales de tinta de plata (Ag). El material PET/ITO fue seleccionado debido a sus

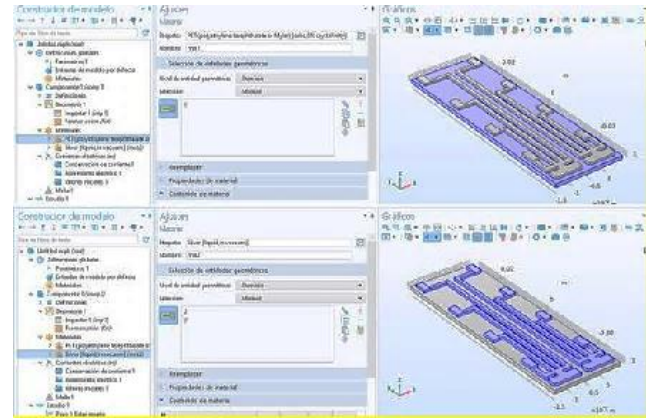


Figura 3. Asignación de Propiedades de los Materiales al Electrodo.  
Fuente: Elaboración propia.

propiedades intrínsecas, como su flexibilidad, biocompatibilidad y resistencia mecánica. Este material presenta una conductividad eléctrica extremadamente baja, de  $1 \times 10^{-18}$  S/m (Siemens metro), y una resistividad de  $1 \times 10^{16} \Omega \cdot m$  (Ohmio metro), lo que lo hace adecuado como sustrato dieléctrico. Por otro lado, los canales del electrodo fueron fabricados con tinta de plata (Ag), un material que destaca por su alta conductividad eléctrica de  $6.30 \times 10^7$  S/m y una resistividad de  $1.6 \times 10^{-8} \Omega \cdot m$ , lo que garantiza una eficiente transmisión eléctrica. En la Fig. 3 se ilustra la asignación de los materiales al modelo del electrodo en COMSOL Multiphysics.

Tras la asignación de las propiedades de los materiales, se realizó un análisis de convergencia empleando un mallado de la geometría compuesto por elementos tetraédricos, lo cual es fundamental para garantizar la precisión de las simulaciones. El mallado seleccionado constó de 33,394 elementos, distribuidos en 8,042 vértices, 14,245 triángulos, 2,967 elementos de arista y 242 elementos de vértice.

Las estadísticas del dominio reflejan la calidad del mallado:

- Calidad mínima del elemento: 0.04149
- Calidad media del elemento: 0.5396
- Ratio de volumen del elemento:  $4.03 \times 10^{-4}$
- Volumen total de la malla:  $1.455 \times 10^{-6} \text{ m}^2$

Este nivel de detalle nos asegura que el modelo cuenta con una resolución óptima para llevar a cabo simulaciones precisas en el análisis de electroestimulación.

#### 2.3.1 Condiciones de contorno

Para continuar con el análisis del electrodo, se definieron los puntos principales del contacto eléctrico, en el módulo de corriente eléctrica; Se establecieron los dos puntos de contacto eléctrico, es decir el terminal positivo y tierra que representara el terminal negativo. Estos contactos se variaron tres veces así:

**Primera configuración:** Terminal positivo, ubicado en el canal superior izquierdo del electrodo y tierra, ubicada en el canal inferior izquierdo del electrodo.

**Segunda configuración:** Terminal positivo, ubicado en el canal superior izquierdo del electrodo y tierra, ubicada en el canal inferior derecho del electrodo.

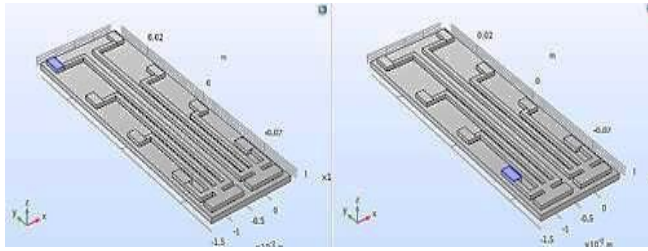


Figura 4. Selección de contactos eléctricos, a. Terminal positiva y b. tierra.  
Fuente: Elaboración propia.

Se asigna una corriente de entrada de 40 mA [13], Esta corriente es suficiente para activar eficazmente las fibras nerviosas, teniendo en cuenta las características de la señal de estimulación. En la Fig. 4 se muestran los contactos de los electrodos.

### 2.3.2 Modelo de Elementos finitos del campo eléctrico y potencia del electrodo sobre la médula espinal

Se realiza un modelo en 3D que simula la médula espinal y un electrodo con los contactos de la segunda configuración que se mencionó anteriormente sobre los contactos eléctricos. De esta forma se buscó observar cómo se transfiere el campo eléctrico del electrodo a la médula.

El procedimiento realizado fue similar al descrito anteriormente, con la inclusión de las condiciones específicas de la médula y el electrodo. Para modelar con precisión los efectos del potencial eléctrico en la zona de interés, se asignaron valores específicos a las propiedades eléctricas de ambos componentes. En el caso de la médula espinal, se emplearon parámetros como una permitividad relativa de 5,000, una conductividad eléctrica de 0.1 S/m y una permeabilidad relativa de aproximadamente 1, de acuerdo con los datos reportados en estudios previos sobre tejidos nerviosos [14]. La configuración del modelo de la médula espinal se presenta en la Fig. 5.

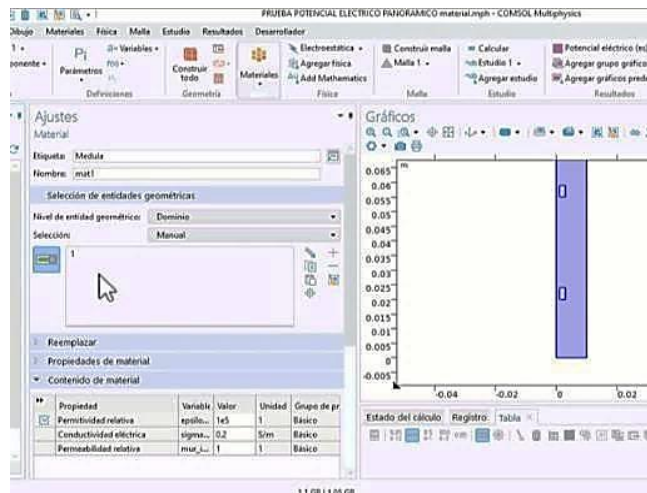


Figura 5. Modelo de la médula espinal con electrodo en el análisis de campo eléctrico.

Fuente: Elaboración propia.

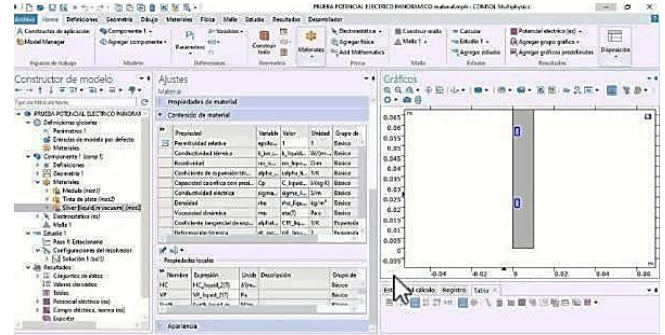


Figura 6. Configuración contactos eléctricos, Tinta Ag.  
Fuente: Elaboración propia.

Por otro lado, el electrodo se modeló utilizando el material “Silver (in vacuum)” disponible en la biblioteca de materiales de COMSOL Multiphysics, que asigna una conductividad eléctrica de S/m y una permeabilidad relativa de 1, y una permitividad relativa de 1. Estos valores fueron corroborados con literatura previa sobre las propiedades de la plata en estado sólido, permitiendo validar su uso como aproximación para la tinta de plata curada utilizada en el diseño experimental, en la Fig. 6 al igual que para la médula se muestra la configuración de los contactos de tinta de plata.

La integración de estas propiedades en las simulaciones permitió observar el potencial eléctrico generado por los canales del electrodo y su interacción con el tejido circundante, lo que facilitó el análisis de la efectividad de la estimulación medular.

## 3. Resultados

A continuación, se exponen los resultados obtenidos en las distintas fases del desarrollo del estudio, incluyendo el diseño y la fabricación de los prototipos, así como los hallazgos derivados de la simulación del campo eléctrico y la potencia generada por el electrodo.

### 3.1 Diseño

La Fig. 7 presenta los resultados correspondientes a los cuatro diseños de electrodos desarrollados, destacando las variaciones en la distribución de los canales en cada uno de ellos.

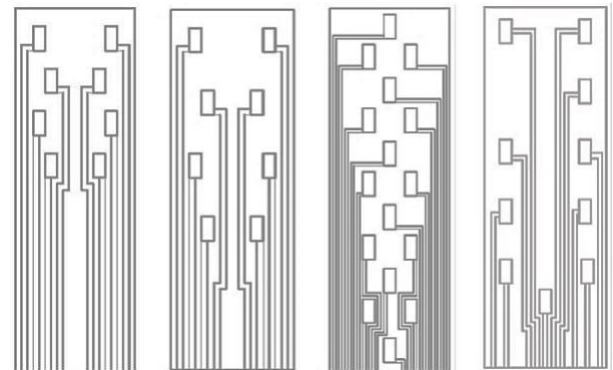


Figura 7. Prototipos de electrodos. a. electrodo 8 canales, b electrodo 8 canales, c electrodo 16 canales y d electrodo de 10 canales. De izquierda a derecha respectivamente.

Fuente: Elaboración propia.



Figura 8. a. Electrodo de 8 canales. b. Electrodo de 10 canales.  
Fuente: Elaboración propia.

Para elegir cual fue el electrodo que favorezca mejores condiciones de manufactura se plasmaron los 4 diseños en lámina adhesiva de vinilo por medio de una técnica de corte laser la cual permite tener una alta precisión en el corte de los canales y contactos. Los diseños que lograron plasmarse sin comprometer la integridad de los canales fueron los modelos B y D, como se muestra en la Fig. 7. En contraste, los modelos A y C presentaron dificultades debido a la separación entre canales, inferior a 1 mm, lo que provocó rupturas en la lámina adhesiva de vinilo durante el proceso.

### 3.2 Manufactura

Como se desarrolla en la metodología, la litografía por ataque químico y el Spin Coating se obtienen 2 resultados (Electrodos), el primer electrodo que se realiza consta de 8 canales unidos de manera paralela, con cuatro en la sección derecha y cuatro en la sección izquierda; el segundo electrodo que se realiza consta de 10 canales unidos de manera paralela, con cuatro en la sección derecha, cinco en la sección izquierda y uno en el centro. En la Fig. 8 se presentan los electrodos fabricados.

Cada contacto y canal de los electrodos que se fabricaron, se observaron en un estereoscopio como se muestra en la Fig. 9. Con este análisis visual se descarta el segundo electrodo fabricado de 10 canales, debido a que el electrodo no presenta las condiciones mínimas para su aprobación. Es decir, que los canales y contactos del electrodo presentan varias irregularidades en el recubrimiento de canal como, por ejemplo, no es uniforme y presenta grietas. Se determina que las irregularidades ocasionan que el funcionamiento del electrodo no sea óptimo debido a que los canales del electrodo no presentan continuidad a lo largo de los mismos. Así mismo se aprecia que la mayoría de los canales y contactos del segundo electrodo no salieron completos.

Se descarta el electrodo de 10 canales por la dificultad de generar los canales a través de este método de fabricación. Se realiza la prueba de impedancia en el electrodo de 8 canales, con ayuda del multímetro digital, tomando 6 medidas para cada canal. En los resultados que se presentan en la tabla 2, se aprecia en las filas el canal que se estudia y en las columnas la repetición de cada medida. A partir de estos resultados se observa que a mayor distancia del canal mayor

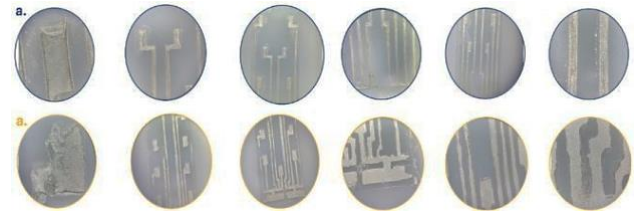


Figura 9. Análisis con estereoscopio. Resultado 8 canales. b. Resultado 10 canales.

Fuente: Elaboración propia.

Tabla 2.  
Datos De Impedancia Electrodo.

Canal	# 1	# 2	# 3	# 4	# 5	# 6
1	0	0	0	0	0	0
2	59.7	57.4	56.2	55.7	56.5	55.5
3	40.1	41.6	40.7	41.2	42.6	43.2
4	82.5	81.3	82.5	82.3	83.3	83.1
5	81.1	80.2	80.1	81.4	80.2	79.9
6	41.8	41.6	41.3	41.5	43.2	41.9
7	63.2	63.6	62.7	61.8	63.6	63.8
8	154.2	154.5	153.5	152	153	151.7

Fuente: Elaboración propia.

Tabla 3.  
Análisis De Repetibilidad y Reproducibilidad Medidas de los electrodos.

Canal	1	2	3	4	5	6	7	8
Media	0	56.35	41.4	82.8	80.2	41.7	63.4	153.25
Promedio	0.00	1.56	1.16	0.76	0.61	0.68	0.75	1.14

Fuente: Elaboración propia.

resistencia va a presentar frente a la estimulación, es decir, que existe una relación directamente proporcional entre la distancia del contacto del canal con el valor de la resistencia. Por lo tanto, el contacto del canal de menor distancia presenta una resistencia de 0  $\Omega$  y el de máxima e 83.3  $\Omega$ .

Con el resultado resistivo de los 8 canales se realiza un análisis estadístico de repetibilidad y reproducibilidad para calcular así el error absoluto de las mediciones, anexo en la tabla 3. El error absoluto ayuda a determinar la precisión de las medidas tomadas; ya que un error absoluto de "0" sería una predicción perfecta; pero en este caso se tiene un error absoluto máximo de 2,56 % en los canales 2 y 3 del electrodo, indicando una imprecisión en la toma de medidas causada por varios factores como mayor recubriendo en ambos canales, presencia de grieta o superficie irregular en el canal o error humano al realizar la medición de resistencia.

Así como se describe en la metodología, aunque se realizaron cambios en los solventes utilizados durante la fabricación de los electrodos, no fue posible completar el proceso para llevar a cabo el análisis de resistividad. Por esta razón, se citan resultados previos como referencia, dejando esta



etapa abierta para futuras evaluaciones. Cabe destacar que la proporción de 1 ml de acetona al 95 % y 5 % de acetato de butilo mostró la mejor adherencia al sustrato PET/ITO y generó una superficie uniforme sin irregularidades visibles. Este comportamiento sugiere que dicha proporción podría ofrecer un desempeño resistivo óptimo en pruebas posteriores.

### 3.3 Modelo de elementos finitos del campo eléctrico y potencia del electrodo

La simulación realizada en COMSOL muestra en la Fig. 10 la distribución del campo eléctrico generado por el electrodo con contactos eléctricos ubicados en la parte superior izquierda e inferior izquierda. La imagen revela que el campo eléctrico alcanza su mayor intensidad en el contacto eléctrico propuesto, lo que indica una estimulación focalizada en esa región, dirigiéndose con mayor precisión hacia las raíces nerviosas.

Las áreas representadas con colores fríos, como azul, verde o morado muestran un gradiente suave en la transmisión del campo eléctrico. Esto es beneficioso, ya que en las regiones donde no se busca estimular, se minimiza el riesgo de generar efectos adversos en tejidos sensibles.

Además del análisis de campo eléctrico, en la Fig. 11 se presenta el comportamiento que tiene el potencial eléctrico el electrodo. Se observa una variación del potencial en el electrodo donde las zonas rojas presentan el mayor valor de potencial eléctrico con un valor de  $4.75 \times 10^{-6}$  V; esto corrobora que la potencia de entrada del electrodo fue de 0.04 A esto genera un gradiente que va a dar lugar al campo eléctrico como se vio en la Fig. 11.

El campo electromagnético en la configuración de contactos eléctricos cruzados que se observan en la Fig. 12 permite determinar que el gradiente de potencial que se concentra de altas a bajas potencias presenta un camino diagonal. Al generar este cruce de contactos se altera la trayectoria del campo eléctrico y esto representa una desviación significativa ya que la mayoría de las veces los campos tienden a ser verticales u horizontales. Existe la posibilidad que ese cambio de trayecto permita estimular terminales nerviosas difíciles de acceder o con mayor probabilidad que se sobre estimulen o no se logren estimular las fibras nerviosas deseadas.

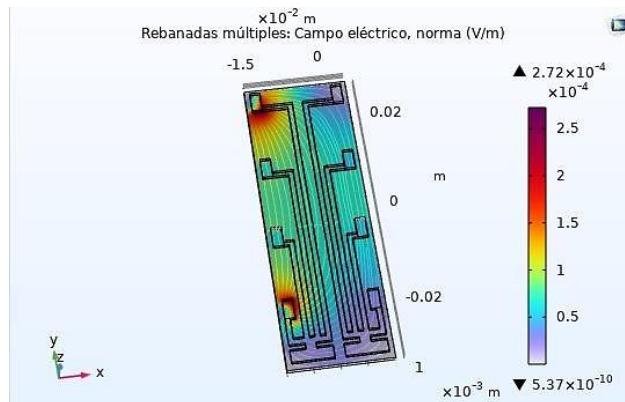


Figura 10. Distribución de campo eléctrico en electrodo con contactos eléctricos en la parte izquierda.  
Fuente: Elaboración propia.

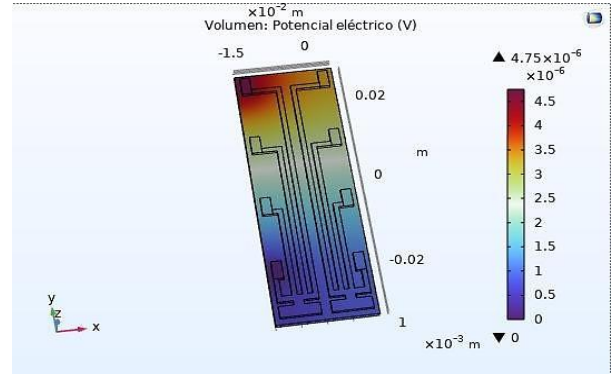


Figura 11. Distribución de potencial eléctrico en electrodo con contactos eléctricos en parte izquierda.  
Fuente: Elaboración propia.

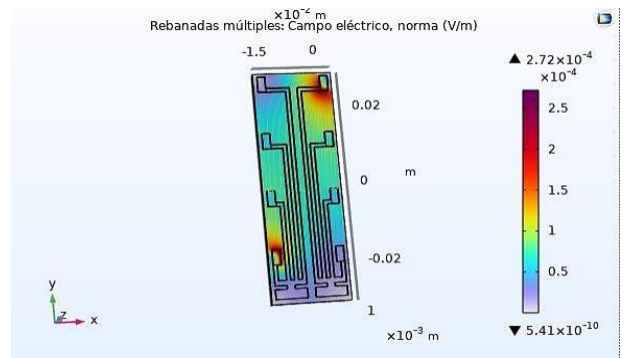


Figura 12. Distribución de campo eléctrico en electrodo con contactos eléctricos cruzados.  
Fuente: Elaboración propia.

La configuración cruzada de los contactos eléctricos, como se observa en la Fig. 13, puede generar un flujo de potencial eléctrico que recorre una mayor longitud a lo largo del electrodo, desplazándose de esquina a esquina. Esta distancia adicional podría incrementar la resistencia del sistema, ya que, en comparación con las configuraciones previas de contactos eléctricos, la línea directa entre los puntos de estimulación es más extensa. Este desplazamiento podría dar lugar a áreas de baja estimulación debido a la mayor distancia entre los contactos.

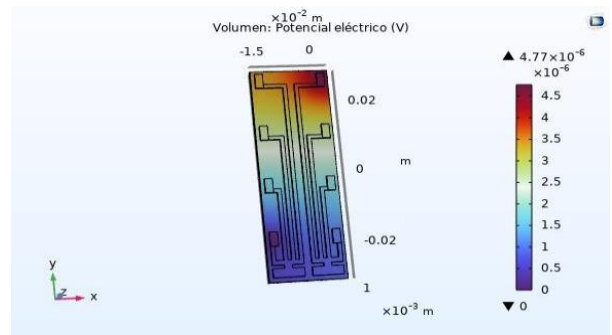


Figura 13. Distribución de potencial eléctrico en electrodo con contactos eléctricos en contactos cruzados.  
Elaboración propia.

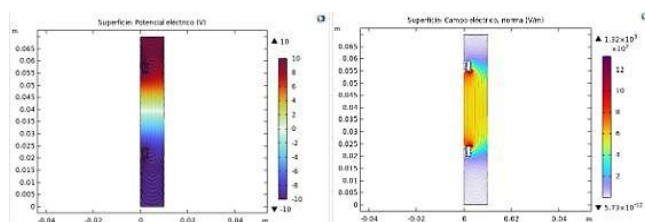


Figura 14. Dominio rectangular de Electrodo-médula espinal Potencial eléctrico y campo eléctrico.

Fuente: Elaboración propia.

Los resultados obtenidos de las simulaciones revelan una distribución del potencial eléctrico y del campo eléctrico generados por los electrodos de estimulación en la médula espinal (Fig. 14). En el primer gráfico, que muestra el potencial eléctrico, se observa un gradiente definido, con una mayor concentración en las cercanías de los electrodos. Este comportamiento es crucial para asegurar que la estimulación se enfoque en áreas específicas de la médula espinal.

En el segundo gráfico, que representa el campo eléctrico, se destacan variaciones en la intensidad de la estimulación a lo largo de la médula espinal. Las zonas cercanas a los electrodos presentan una mayor intensidad (coloreadas en tonos rojos y morados), lo que indica que el campo eléctrico es lo suficientemente fuerte como para generar una estimulación eficaz. Estos resultados demuestran que el diseño del electrodo favorece la estimulación selectiva de las fibras nerviosas, optimizando la eficiencia del tratamiento y minimizando los efectos adversos.

#### 4. Discusión

En este trabajo se presenta el diseño, fabricación y evaluación de electrodos para estimulación de la médula espinal. Durante el proceso de fabricación de los electrodos se identificó la necesidad de incorporar una sección adicional en la parte inferior del electrodo para permitir la conexión con el electro estimulador, lo que requirió una modificación del modelo original. Con este modelo se manufacturaron con éxito 2 modelos de electrodos. Durante la fabricación se identifica una oportunidad de mejora en el recubrimiento y uniformidad de la tinta de plata sobre los canales con el fin de que dichos electrodos tengan un mejor comportamiento; por esta razón se evalúan soluciones de solventes diferentes a la acetona para la disolución de la tinta de plata. La razón radica en que al realizar el proceso de spin Coating la densidad de la disolución era muy variada debido a que la acetona se evapora en tiempos cortos: en el orden de los segundos, debido a su presión de vapor; es por esto que se continúa trabajando actualmente en una solución de acetona y acetato de butilo en proporciones variadas y lograr un solvente que permita disolver la tinta de plata con una densidad uniforme y genere mayor tiempo para terminar el proceso de fabricación.

Las medidas de resistencia del electrodo de 8 canales se realizan bajo los mismos parámetros de superficie, lugar, temperatura, distancia de medida (de la parte más posterior a más inferior del canal) y tiempo (como en todos los estudios analizados). Sin embargo, el primer canal no arroja una medida, ya que en la construcción se genera un error en la fabricación y

se parte a la mitad el canal, por lo que la medida sobre este es imposible de realizar. Pese a esto, los otros 7 canales sí generan una medida satisfactoria y estable, en la que se observa que la distancia de los canales era directamente proporcional a la resistencia presentada en el electrodo.

A partir de las medidas que se adquieren de resistencia, se realiza una prueba de repetibilidad y reproducibilidad para demostrar y garantizar que los resultados medidos 6 veces logran dar un valor similar y que esto no afecte las futuras pruebas a las que se someterá el electrodo. Es así como el comportamiento estadístico de las medidas arroja un error absoluto menor al 3%, valor aceptable ya que, comparándolo con resultados de la literatura estudiada, los valores oscilan en un rango entre un 2% – 5%.

Los resultados obtenidos a través de las simulaciones en COMSOL destacan la efectividad del diseño del electrodo para lograr una estimulación focalizada y controlada en la médula espinal, concentrando la mayor intensidad del campo eléctrico en las zonas cercanas a los contactos eléctricos. Esta distribución permite una estimulación eficiente de las fibras nerviosas, minimizando el riesgo de efectos adversos en tejidos circundantes. En contraste, la configuración con contactos cruzados genera una trayectoria diagonal del campo eléctrico, lo que podría permitir acceder a fibras difíciles de estimular, pero también introduce un aumento en la resistencia y zonas de baja estimulación. Estos hallazgos indican que la configuración lineal de los contactos es la más eficiente para este propósito, y aunque la configuración cruzada puede ser útil en investigaciones adicionales, no representa la opción óptima para la estimulación de las fibras nerviosas.

#### 5. Conclusión

El desarrollo y evaluación de electrodos flexibles para la electroestimulación de la región lumbosacra de la médula espinal presentado en este trabajo demuestra un avance significativo en la búsqueda de soluciones eficientes y accesibles en el campo de la neuroestimulación. A través de un enfoque integrado que incluyó el diseño, la fabricación física de cuatro prototipos y su evaluación eléctrica, se logró optimizar tanto la composición de la tinta de plata como los parámetros de fabricación mediante pruebas experimentales y simulaciones. Los resultados evidencian que los electrodos fabricados ofrecen una distribución uniforme del campo eléctrico y un comportamiento adecuado del potencial eléctrico en la interfaz electrodo-médula, lo que valida su potencial para aplicaciones médicas. Este estudio no solo proporciona una base sólida para futuros desarrollos en neuroestimulación, sino que también resalta la importancia de combinar simulaciones y pruebas experimentales para mejorar la eficacia y seguridad de las tecnologías biomédicas.

#### Agradecimientos

Este trabajo ha sido realizado bajo el proyecto PIC-ING-3897 financiado por la Vicerrectoría de Investigación de la Universidad Militar nueva Granada. Este trabajo es la continuación de estudios anteriores del Semillero de investigación INMED realizado por los estudiantes Leydy Vanessa Rodríguez, Efraín Zapata y Juan David Villa. También se agradece a la profesora Diana Marulanda.

## Referencias

- [1] World Health Organization. Lesión de la médula espinal, [en línea]. 2024. Disponible en: <https://www.who.int/es/news-room/fact-sheets/detail/spinal-cord-injury>.
  - [2] A.E., d.-Ruz, Lesión medular traumática: valoración y manejo integral. Medicina. Programa de Formación Médica Continuada Acreditado, 12(75), pp. 4387–4400, 2019. DOI: <https://doi.org/10.1016/j.med.2019.03.020>
  - [3] Ferrin-Bolaños, C.D., and Loaiza-Correa, H., Interfaz cerebro-computador multimodal para procesos de neurorrehabilitación de miembros superiores en pacientes con lesiones de médula espinal: una revisión. Revista Ingeniería Biomédica, 12(24). art. 1222, 2018. DOI: <https://doi.org/10.24050/19099762.n24.2018.1222>
  - [4] Sato, G., Osumi, M., Mikami, R., and Morioka, S., Long-term physical therapy for neuropathic pain after cervical spinal cord injury and resting state electroencephalography: a case report. Spinal Cord Series and Cases, 8(1), art. 510-0, 2022. DOI: <https://doi.org/10.1038/s41394-022-00510-0>
  - [5] Palladino, L., Ruotolo, I., Berardi, A., Carlizza, A. and Galeoto, G., Efficacy of aquatic therapy in people with spinal cord injury: a systematic review and meta-analysis. Spinal Cord., art. 00892-4, 2023. DOI: <https://doi.org/10.1038/s41393-023-00892-4>
  - [6] Xu, L., et al., The application of stem cell sheets for neuronal regeneration after spinal cord injury: a systematic review of pre-clinical studies. Systematic Reviews, 12(1), art. 02390-3, 2023. DOI: <https://doi.org/10.1186/s13643-023-02390-3>.
  - [7] Zheng, Y., et al. Transplantation of human induced pluripotent stem cell-derived neural progenitor cells promotes forelimb functional recovery after cervical spinal cord injury. Cells, 11(17), art. 2765. 2022. DOI: <https://doi.org/10.3390/cells11172765>
  - [8] Wagner, F.B., Mignardot, J.B., Le-Goff-Mignardot, C.G., et al., Targeted neurotechnology restores walking in humans with spinal cord injury. Nature, 563, pp. 65–71, 2018. DOI: <https://doi.org/10.1038/s41586-018-0649-2>
  - [9] Ahani, A., Saadati-Fard, L., Sodagar, A.M., and Boroumad, F.A., Flexible PET/ITO electrode array for implantable biomedical applications. Annual International Conference of the IEEE Engineering in Medicine and Biology Society, pp. 2878–2881, 2011. DOI: <https://doi.org/10.1109/IEMBS.2011.6090794>
  - [10] Frostell, A., Hakim, R., Thelin, E.P., Mattsson, P., and Svensson, M., A review of the segmental diameter of the healthy human spinal cord. Frontiers in Neurology, 7, art. 0238, 2016. DOI: <https://doi.org/10.3389/fneur.2016.00238>
  - [11] Paez-Sierra, B. and Marulanda, D., Luminescence tuning of MEH-PPV for organic electronic applications. Acta Physica Polonica A, 129(6), pp. 1187–1190, 2016. DOI: <https://doi.org/10.12693/APhysPolA.129.1187>.
  - [12] Garcia, Á.M., Sistema Estimulador Integrado [en línea]. Disponible en: <https://www.tdx.cat/bitstream/handle/10803/5336/maum4de4.pdf>
  - [13] Gabriel, S. et al., The dielectric properties of biological tissues: III. Parametric models for the dielectric spectrum of tissues. Physics in Medicine and Biology, 41(11), art. 003, 1996. DOI: <https://doi.org/10.1088/0031-9155/41/11/003>
- J.J. Melo-Portilla**, recibió el grado de Ing. Biomédico en 2025 de la Universidad Militar nueva Granada, Bogotá, Colombia. Actualmente trabaja como Ingeniero Biomédico, con experiencia en mantenimiento preventivo y correctivo de equipos médicos, procesos de calibración y reparación electrónica. Su interés profesional y de investigación incluye la estimulación de la médula espinal, procesamiento de señales e innovación en dispositivos médicos.  
ORCID: 0009-0002-4143-1483
- L.F. Puentes-Alzate**, recibió el grado de Ing. Biomédica en 2025 de la Universidad Militar nueva Granada, Bogotá, Colombia. Actualmente trabaja en el campo del servicio de ingeniería en la empresa Boston Scientific Colombia. Su interés profesional y de investigación incluye estimulación en la médula espinal, automatización de procesos y medicina regenerativa.  
ORCID:0009-0008-8186-1166
- K.D. Valencia-Poveda**, recibió el grado de Ing. Biomédica en 2025 de la Universidad Militar nueva Granada, Bogotá, Colombia. Actualmente trabaja como Ingeniera Biomédica en la empresa PRO, con experiencia en el manejo de tecnologías médicas, soporte clínico e investigación biomédica. Su interés de investigación y profesional incluye el análisis de señales biomédicas, seguridad del paciente e innovación en tecnologías de salud.  
ORCID: 0009-0009-1122-7124
- A.M. Ramírez-Martínez**, recibió el grado de Ing. Mecánica en el 2004 de la Universidad Nacional de Colombia y Dra. en Ingeniería Biomédica de la Universidad de Zaragoza, España en el 2011. Actualmente, es profesora asociada del Departamento de Ingeniería Biomédica de la Universidad Militar Nueva Granada, Bogotá, Colombia. Su interés en investigación incluye modelado, simulación y experimentación en problemas de neurorrehabilitación. Ella se enfoca en el entendimiento multiescala y multimodal de los sistemas nervioso y muscular, así como en el diseño de dispositivos para rehabilitación.  
ORCID: 0000-0002-9186-5848





# Technological characterization of the generation and distribution of electric power in Colombia at the beginning of the 20<sup>th</sup> century: case Manizales

Carolina Salazar-Marulanda <sup>a</sup>, Javier Herrera-Murcia <sup>b</sup> & Camilo Younes-Velosa <sup>c</sup>

<sup>a</sup> Universidad Nacional de Colombia, sede Medellín, Facultad de Arquitectura, Medellín, Colombia. csalazarma@unal.edu.co

<sup>b</sup> Universidad Nacional de Colombia, sede Medellín, Facultad de Minas, Medellín, Colombia. jherreram@unal.edu.co

<sup>c</sup> Universidad Nacional de Colombia, sede Manizales, Facultad de Ingeniería y Arquitectura, Manizales, Colombia. cyounesv@unal.edu.co

Received: April 23<sup>rd</sup>, 2024. Received in revised form: October 26<sup>th</sup>, 2024. Accepted: November 8<sup>th</sup>, 2024.

## Abstract

This paper presents a characterization and description of the technical development that residential and industrial electrical installations underwent in Colombia at the beginning of the 20th century. The analysis focuses on the city of Manizales – Caldas, given its prominence in the region due to the coffee trade and its role as a commercial hub within the country. Through the examination of historical documents, it was possible to reconstruct the context of the development and expansion of generation plants and transmission and distribution networks, meeting the energy demand driven by the region's commercial growth. Among these elements, the article illustrates the evolution of installation technology, as well as safety and maintenance aspects that, by the end of the century, led to the proposal and approval of laws that merged the experience of foreign professionals with the adaptation of knowledge to the local environment.

**Keywords:** electrical installations; residential and industrial installations; engineering history; urban history.

## Caracterización tecnológica de la generación y distribución de energía eléctrica en Colombia en los inicios del siglo XX: caso Manizales

### Resumen

Este artículo muestra una caracterización y descripción del desarrollo técnico que tuvieron las instalaciones eléctricas residenciales e industriales en Colombia al inicio del siglo XX. El análisis se centra en la ciudad de Manizales – Caldas dado su protagonismo en la región por el comercio del café y por constituir un punto de relación comercial dentro del país. A partir del análisis de documentos históricos, fue posible reconstruir el contexto en que se desarrolló la instalación y expansión de plantas de generación y redes de transmisión y distribución, respondiendo a la demanda de energía impuesta por el crecimiento comercial de la región. Dentro de estos elementos, se muestra la evolución que tuvo la tecnología de las instalaciones, así como aspectos de seguridad y mantenimiento que llevaron a consolidar, al final del mismo siglo, la propuesta y aprobación de leyes que conjugaban la experiencia de profesionales extranjeros y la adaptación del conocimiento al medio local.

**Palabras clave:** Instalaciones eléctricas; instalaciones residenciales e industriales; historia de la ingeniería; historia urbana.

### 1. Introducción

Los últimos años del siglo XIX y las primeras décadas del siglo XX se caracterizaron por la conformación de una sociedad científica en el país que introdujo el pensamiento positivista, generando una transformación cultural cimentada

en principios de orden, higiene, estética y progreso que devino en la construcción de sistemas industrializados, por medio de los cuales se buscaba alcanzar eficiencia, rapidez, seguridad y comodidad en las ciudades.

Esta transición desde procesos artesanales que usaban métodos tradicionales hacia la introducción de técnicas

**How to cite:** Salazar-Marulanda, C., Herrera-Murcia, J., and Younes-Velosa, C., Caracterización tecnológica de la generación y distribución de energía eléctrica en Colombia en los inicios del siglo XX: caso Manizales. DYNA, (92)238, pp. 120-128, July - September, 2025.



avanzadas que se basaban en la estandarización de los procedimientos, fue posible gracias a los planes estatales que buscaban invertir en la modernización de las ciudades mediante la construcción de obras de saneamiento e infraestructura, con el fin de alcanzar el mejoramiento de las condiciones de vida de los habitantes, el desarrollo del comercio y la internacionalización de los mercados [1].

En esta tendencia modernizadora, la implementación de servicios públicos fue la obra de mayor impacto en las principales ciudades colombianas, pues por medio de las redes se garantizaba la regularización, modernización y ampliación de las estructuras urbanas. Tanto para acueductos y alcantarillados como para la generación y distribución de energía eléctrica, se aprovecharon los adelantos de la técnica para producir escenarios seguros y eficientes que llevaban a resolver las problemáticas higienistas inherentes al crecimiento y la densificación. Sin embargo, aunque las redes de agua garantizaban la habitabilidad de los espacios, fue la llegada de la energía eléctrica la que mayores expectativas de transformación cultural suscitó [2], pues condujo a la utilización de dispositivos que permitieron alcanzar en muy corto tiempo la sistematización y automatización de procesos, convirtiéndose en un privilegio que representaba bienestar, confort y salud para quienes tenían acceso a ella [3].

En este sentido, la implementación de la energía eléctrica en los primeros años del siglo XX fue más un espectáculo que una realidad doméstica [2] ya que su llegada introdujo modas y prácticas culturales que desencadenaron la aparición de escenarios para el ocio, la recreación y la cultura, permitiendo extender a la noche las actividades urbanas y dinamizar las calles mediante la aparición de lámparas, avisos luminosos y la decoración de las vitrinas en los almacenes [1].

Sin embargo, la literatura sobre el tema es escasa y no brinda un panorama nacional sobre las características de la implementación y extensión de las redes en el país. Algunos trabajos historiográficos han abordado la importancia de la luz eléctrica en Colombia desde la historia económica y empresarial [4]. *De la vela al apagón. 100 años del servicio eléctrico en Colombia* [5]; *Una aproximación a la lógica espacial del surgimiento y desarrollo del sector eléctrico en Colombia* [6]; *La electrificación en Colombia* [7]; *Historia de la energía en Colombia 1537-1930* [8], proponen un marco de análisis desde lo económico, la lógica del determinismo tecnológico y el impacto social de las redes eléctricas. Así mismo, otros trabajos como *Desarrollo y crisis del sector eléctrico colombiano 1890-1993* [9] dejan entrever los altibajos del sector en la industria nacional. Otras investigaciones se centran en la implementación de energía eléctrica en Bogotá y Medellín por ser las ciudades pioneras en servicios públicos a nivel nacional, mientras que el registro de redes de suministro de electricidad en ciudades como Manizales, no se ha desarrollado a profundidad a pesar de la trascendencia de estas instalaciones en la región cafetera, tema que pretende abordar este trabajo desde la consulta del Archivo Histórico de Manizales.

Así, pudimos encontrar que en los últimos años del siglo XIX y primeros del siglo XX las ciudades se iluminaron mediante la instalación de plantas generadoras de electricidad que en su mayoría obedecían a empresas privadas. En Bogotá, la primera empresa se denominó *Bogotá Electric*

*Light Co*, propiedad de los hermanos Ospina de Medellín y la familia Carrizosa de Bogotá que entró en funcionamiento en 1890 con aproximadamente 100 lámparas de arco [8]. Por su parte, Medellín constituyó en 1895 la Compañía Antioqueña de Instalaciones Eléctricas con un capital mixto entre el municipio, el departamento y particulares y entró en servicio en 1897 con 150 lámparas de arco para espacios públicos, 3.000 lámparas domésticas y una planta generadora de AC a 2.3kV alimentada por aguas de la quebrada Santa Helena [7]. Otras ciudades continuaron iluminándose: Barranquilla en 1892, Cartagena en 1893, Manizales en 1905 y posteriormente Cali en 1910 [7], siendo uno de los casos más representativos la ciudad de Manizales que para ese momento no alcanzaba los 25.000 habitantes.

Manizales se destacó en las postrimerías del siglo XIX por ser la ciudad intermedia entre las rutas comerciales que unían Bogotá, Medellín y Cali, y así mismo, por tener comunicación directa con los puertos de Barranquilla y Buenaventura, lo cual le daba acceso tanto al comercio nacional como internacional. Además de su posición geográfica, el poder económico relacionado con el comercio del café, le valió la implementación de procesos de tecnificación avanzados para la época, lo que devino en un rápido perfeccionamiento de los sistemas para la comercialización y transporte del grano, y por consiguiente, en la aparición de todo tipo de entidades que facilitaban las negociaciones. Varias empresas extranjeras abrieron sucursales en la ciudad, como el *Banco de Londres y América del Sur* que tenía oficinas en Bogotá, Medellín, Barranquilla y Cali pero debido a la importancia de las negociaciones de exportación de café, abrió en 1925 una oficina en Manizales [10]; o el *Banco Mercantil Americano* que tenía oficinas en la ciudad desde 1921 y que al ser filial de la *Compañía Mercantil de Ultramar*, favoreció la comercialización de todo tipo de mercancías en la ciudad. Así mismo, aparecieron otras infraestructuras como trilladoras, tostadoras, empaquetadoras y fábricas que gracias al crecimiento de la industria cafetera favorecieron el desarrollo de la ciudad.

En este sentido es importante analizar el caso de Manizales desde la construcción de redes de servicios y específicamente de las de energía eléctrica, ya que condujeron a la implementación de avances significativos como: sistemas de transporte como el cable aéreo y el ferrocarril, intercambio comercial con importantes casas extranjeras que le dieron acceso a materiales y maquinarias de última tecnología, y asesoramiento de profesionales extranjeros que instalaron de manera técnica y científica el sistema, sentando las bases para el desarrollo urbano, social y económico de la ciudad, implementando en muy corto tiempo un servicio de vanguardia que se desarrolló hasta producir una de las hidroeléctricas más representativas del centro del país.

Este artículo pretende exponer las características técnicas para la creación y evolución de la *Empresa Municipal de Energía*, puesta en funcionamiento en 1916 según estándares de calidad internacionales, bajo la dirección de ingenieros extranjeros y con materiales importados desde la casa General Electric de Nueva York, con el fin de caracterizar la tecnología implementada, las características del servicio, las falencias de funcionamiento y seguridad, la evolución de la

empresa hasta la constitución de la Central Hidroeléctrica de Caldas, y el impacto generado por la llegada de la luz a la ciudad en los primeros años del siglo XX.

2. Metodología

Este trabajo aborda las obras realizadas para la puesta en funcionamiento de la Empresa Municipal de Energía Eléctrica en la ciudad de Manizales a través del análisis del saber aplicado desde la ingeniería, lo que permitió establecer las condiciones particulares para la creación, desarrollo y servicio ofrecido por la empresa.

La caracterización de esta investigación cualitativa se basa fundamentalmente en la consulta, registro y análisis de fuentes documentales que reposan en el Archivo Histórico de Manizales, las cuales están constituidas principalmente por actas, Acuerdos del Concejo Municipal, contratos y correspondencia entre los años 1907 y 1944. De estos se extrajo la información técnica, se rastreó la toma de decisiones y la cronología de los eventos que llevaron a la evolución de la empresa hasta la consolidación a mediados del siglo XX de la Central Hidroeléctrica de Caldas - CHEC. Desafortunadamente dentro de los archivos no se encontró información gráfica relacionada con planos de las obras, fotografías o imágenes que permitieran ilustrar este artículo, a pesar de que todos los documentos consultados referían la entrega de material gráfico relativo a los proyectos realizados. Las imágenes presentadas en el texto corresponden a fuentes secundarias.

Se consultaron también archivos de prensa en el periódico La Patria y La voz de Caldas con el fin de resaltar el impacto urbano, social y económico de las redes de energía eléctrica y su representatividad en la construcción de infraestructura para el crecimiento y desarrollo de la ciudad. Así mismo, se indagaron fuentes secundarias que llevaron a la construcción del pensamiento positivista y progresista de los primeros años del siglo XX, el cual enmarcó la incorporación de avances técnicos para la realización de obras públicas como factor de modernización en Colombia, y así mismo, permitieron identificar los ideales civilizatorios de la elite local para la transformación de la estructura urbana.

3. Evolución de la generación y distribución de energía eléctrica 1900 – 1930

3.1 La primera planta eléctrica

La llegada de la energía eléctrica a la ciudad de Manizales en 1907 se dio de la mano de la compañía llamada *Crédito Antioqueño*, empresa que realizó el montaje y puesta en operación de la primera unidad de generación de energía eléctrica para iluminar el espacio público y proporcionar la instalación de las primeras lámparas de uso residencial. Las condiciones para la puesta en funcionamiento del nuevo sistema de generación de energía incluían declarar la empresa de utilidad pública para hacer viable la expropiación de terrenos, servidumbres y acequias; legislar sobre la propiedad privada para permitir el uso de paredes y tejados para la fijación de cables; y normatizar

el espacio público para la instalación de postes y transformadores en las calles que hasta el momento no existían (ver Fig. 1). Ya que se trataba de una planta de generación hidráulica, las llamadas acequias o canales de suministro de agua para la producción de la energía, debían ser entregadas por el municipio.

Esta transformación cultural que suponía dejar atrás las lámparas de petróleo para acoger el servicio prestado por la empresa, impuso a los usuarios la obligatoriedad de pagar por el servicio y acoger las directrices técnicas para el funcionamiento de las redes, lo que significó una nueva legislación urbana para normatizar las instalaciones. El uso principal de la energía eléctrica fue el de alumbrado público que se prestaba entre las seis de la tarde y las cinco de la mañana, para lo cual, el *Crédito Antioqueño* realizó la instalación de 200 focos de luz incandescente. El contrato también contemplaba la instalación de las primeras 50 lámparas de uso residencial, la alimentación de motores y la generación de calor, lo que promovió el desarrollo de fábricas y la llegada de los primeros electrodomésticos a la ciudad. Las tarifas incluían un costo por instalación de \$15 COP para usuarios residenciales y de \$12 COP para el municipio, y una mensualidad por consumo de acuerdo con una capacidad instalada entre 4 y 16 bujías (Tabla 1), siendo una bujía al parecer la intensidad de luz equivalente a la de una vela.

El contrato firmado entre el municipio y la empresa privada para proporcionar luz, fuerza y calor por 30 años, implicó de parte del municipio, otorgar la exención del pago de derechos de aduana para la importación de maquinaria y materiales requeridos en el montaje del sistema, ceder el uso



Figura 1. Aspecto de las calles antes de la instalación de redes eléctricas (1900).

Fuente: Tomada de [11].

Tabla 1. Tarifas de la compañía Crédito Antioqueño, 1908.

Usuario	Servicio	Tarifa mensual (COP)			
		4 Bj	8 Bj	10 Bj	16 Bj
Residencial	Lámparas	0,30	0,40	0,50	0,60
Municipio					0,50

Bj: Bujías.

Fuente: Elaboración propia

de aguas públicas para la generación de energía y evitar la instalación de otras plantas productoras de energía eléctrica en la ciudad [12]. Sin embargo, hacia 1910 la calidad del alumbrado ofrecido por la empresa se deterioró debido a las frecuentes y prolongadas interrupciones, a la demora de la compañía para hacer reparaciones y a la obligatoriedad del pago por parte de los usuarios aunque no recibieran el servicio. Esta situación, sumada a las altas tarifas impuestas por la empresa *Crédito Antioqueño*, llevó a que en 1913 el municipio rescindiera el contrato y se iniciara el montaje de su propia planta para la producción de energía eléctrica en la ciudad.

### 3.2 Empresa Municipal de Energía Eléctrica

A partir del fracaso anterior y mediante el Acuerdo N° 60 de 1915 del Concejo Municipal se dispuso la construcción de una planta eléctrica para Manizales, no solo para devolver a la ciudad la iluminación perdida, sino por la necesidad de adelantar dos proyectos urbanos que dependían de la generación de energía eléctrica. El primer proyecto tenía que ver con el suministro de agua, ya que las partes altas de la ciudad requerían la instalación de bombas para garantizar la distribución de agua potable; y, un segundo proyecto relacionado con la puesta en funcionamiento de trenes eléctricos que facilitarían el movimiento de las cargas y agilizarían los procesos de comercialización de productos agrícolas como el café [13].

El proyecto para esta nueva planta estaba planteado para ser una hidroeléctrica que se abastecía con aguas del río Chinchiná. Su operación se realizaría a través de la nueva Empresa Municipal de Energía Eléctrica, contaría con un presupuesto de \$40.000 COP para su construcción y estaría dirigida por una Junta Autónoma, la cual, además de los compromisos legales y administrativos, debía fijar las tarifas a pagar por concepto de alumbrado, fuerza, calor e instalaciones, y definir la distribución de las lámparas que el municipio ubicaría en los lugares públicos [14].

El contrato firmado por Gabriel Sanín Villa en representación de la *Casa Cock de Medellín* para la realización del proyecto, requería por parte de la compañía la elaboración de un plano del acueducto, otro del edificio para el montaje de la planta eléctrica con una capacidad de hasta 10.000 kW, y un plano de distribución de luz y fuerza en la ciudad. Debía también entregar el presupuesto para el montaje inmediato de 250 kW, las especificaciones de la maquinaria que debía comprarse en Estados Unidos, la rasante del acueducto en por lo menos diez mojones y los diseños de toma y desarenadores en la bocatoma. Este contrato debía estar ejecutado en un plazo de sesenta días [15].

Una vez finalizado el proyecto por Sanín Villa, la Junta de la Empresa de Energía Eléctrica firmó un contrato con el señor John H. Wisner, ciudadano norteamericano representante de la casa *Wesselhoft & Wisner* domiciliada en Nueva York, Bogotá y Barranquilla, para la realización de las obras conducentes a montar la planta eléctrica y suministrar la maquinaria y equipos requeridos, los cuales debían ser específicamente fabricados por General Electric & Co., puestos en Puerto Colombia (Barranquilla) en un plazo

máximo de ocho meses, exentos de derechos de aduana y asegurados contra todo riesgo hasta su llegada a Manizales [16].

Dada la casi completa inexistencia de materiales de alta calidad en el mercado nacional, la importación de estos materiales fue de grandes proporciones. Además de la turbina y el generador de 250 kW, de sus accesorios de medida, control y de protección, la importación incluyó para el montaje de la red los transformadores de distribución con potencias entre 15 a 3 kW refrigerados en aceite, los conductores a utilizar, aisladores triple falda para una tensión nominal de 25kV en húmedo y 60kV en seco, sus soportes y herrajes. Para las instalaciones residenciales se importaron todos los materiales, desde los conductores, tuberías y los soportes aislantes, hasta accesorios para las acometidas y una gran cantidad de luminarias de diferentes *bujías* junto con sus respectivos portalámparas. Para las instalaciones industriales, se importaron también las bombas de agua junto con sus accesorios de instalación, medida, control y protección.

Las labores de mantenimiento fueron tenidas en cuenta a partir de la importación de aceites de reserva para transformadores y máquinas rotativas, equipos de medición y soldadura portátiles, y elementos hoy tan comunes como alicates, martillos y limas, entre muchos otros. Desafortunadamente, en los documentos consultados no existe información acerca del tipo de generador utilizado y de la tensión nominal del sistema. Sin embargo, por los datos recolectados lo más probable es que se haya tratado de un generador AC y de un sistema de distribución trifásico en el cual las cargas de iluminación y de tracción eran del mismo tipo.

### 3.3 El montaje de la planta de energía

En la misma fecha y con el señor John H. Wisner, se firmó otro contrato para la construcción del edificio en donde se instalarían la turbina, el generador -o dínamo como era llamado en su momento- y los tableros de la planta de producción de energía eléctrica. Este edificio sería de características sencillas, construido en mampostería, cubierto con teja de barro, con ventanas sin vidrios y bases para el montaje de los equipos realizadas con cemento Portland. Debajo del edificio se construyeron los canales para el paso de la tubería y los desagües, y al interior, se instalaron todos los equipos, tuberías y pararrayos de manera técnicamente adecuada o científica, como era conocida en su momento, al igual que el término *pararrayos* que actualmente se refiere a un descargador de sobretensiones.

El montaje de las redes de distribución o *canalizaciones* de transmisión desde la planta hasta Manizales estaba conformado por tres hilos de alambre desnudo, soportados por postes de madera apropiada para la humedad, con una altura de 4 metros (libres) carbonizados en su base, dispuestos a una distancia de 40 metros entre sí y con aisladores para alta tensión (prueba húmeda 10kV, prueba en seco 35kV) que se aseguraban mediante soportes de hierro galvanizado. En estos mismos postes, se disponía de un circuito metálico de dos alambres para uso telefónico, provisto de protectores para evitar el peligro que representaba

su cercanía con las líneas de alta tensión. Los materiales para la instalación de la planta eléctrica ascendieron a un valor de \$30.884 oro americano y los necesarios para la construcción del edificio a \$13.308 oro americano [16].

Todos los permisos para el paso de la red de distribución y la colocación de postes debían ser tramitados por la Junta con los dueños de los terrenos, mientras que el contratista se comprometía a realizar todos los trabajos de acarreo, montaje e instalación de la planta hasta entregarla funcionando correctamente, con excepción de la acequia que debía ser construida por el municipio para suministrar el agua necesaria para la generación de energía eléctrica. Los materiales llegaban a Puerto Colombia (Barranquilla) procedentes de Nueva York (EEUU), se embarcaban en vapores que navegaban por el río Magdalena hasta el puerto de La Dorada (Caldas), desde donde eran transportados por el ferrocarril hasta Mariquita (Tolima) y embalados finalmente en el cable aéreo, que comunicaba desde 1922, con Manizales (Caldas). El trámite para conseguir la exención del pago de derechos fluviales estaba a cargo de la Junta, mientras que para el transporte hasta Manizales, la compañía *The Dorada Extension Railway Limited* otorgó un descuento del 25% en el valor de los fletes en el trayecto de La Dorada hasta la ciudad [17].

Adicionalmente, el señor Wisner se comprometía a dejar un encargado y capacitar a los empleados del municipio que estarían al frente del manejo de la planta, además de entregar toda la obra en el menor tiempo posible, o al menos sin exceder el plazo máximo de 16 meses. Con el fin de disminuir este tiempo, la Junta ofreció a la compañía un pago de \$10 COP por cada día de anticipo para la entrega de la obra terminada [16]. Finalmente, la unidad hidroeléctrica estuvo terminada en 1918, produciendo suficiente energía trifásica para alimentar lámparas, planchas, calentadores y motores en la ciudad [18].

### 3.4 Expansión de la cobertura

El incremento de servicios que requerían energía eléctrica y el aumento de solicitudes para instalaciones residenciales e industriales llevó al montaje en la ciudad de otras tres plantas de energía eléctrica: Empresa Eléctrica de Manizales (1925) sucesora del pleito con la compañía Crédito Antioqueño de 1905; Planta Eléctrica de Sancancio (1926), creada para alimentar la fábrica de Hilados y Tejidos de Caldas (Ver Fig. 2); y, Planta Eléctrica de Guacaica (1927) que proveía 1.000 kW para movilizar el cable aéreo hacia el norte del departamento y el Chocó.

Para el año 1922 mediante el Acuerdo N°67 se definió una legislación precisa sobre los recorridos de las redes de distribución en la ciudad o *canalizaciones*, la cual buscaba imponer respeto por las instalaciones realizadas por cada compañía presente en la ciudad. En este sentido, el gerente de la Empresa Eléctrica de Manizales sugirió dividir la ciudad en tres sectores para que cada empresa estuviera a cargo de sus redes y del suministro y cobro de la energía eléctrica correspondientes a cada sector, y no se generaran inconvenientes con la mezcla de instalaciones. Sin embargo, esta medida resultaba inconveniente para la Empresa Municipal de Energía, pues para la época, tenía una gran

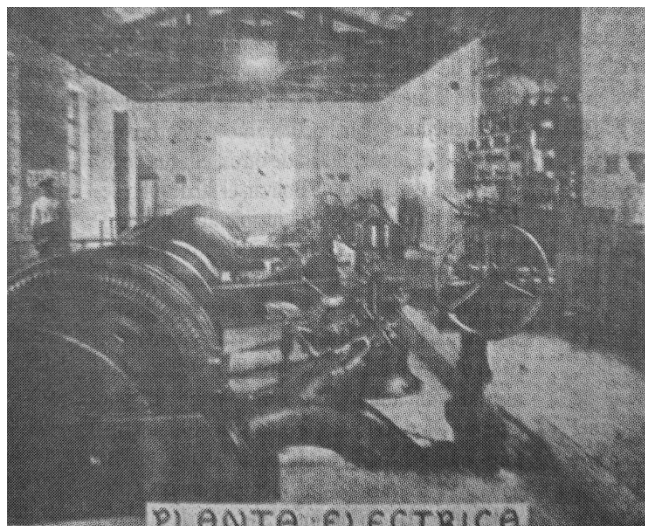


Figura 2. Instalación de la planta eléctrica de Sancancio.

Fuente: Tomada de [20]

extensión de redes de distribución por toda la ciudad y restringir la prestación de su servicio a un solo sector le generaría grandes pérdidas, por lo que esta medida no llegó a implementarse [19].

Otras disposiciones para controlar la competencia de las tres compañías en la prestación del servicio se direccionaban a: la exigencia de realizar de manera técnicamente adecuada o científica las instalaciones bajo la asesoría técnica de un profesional, sin afectar las de las otras compañías, unificar las tarifas y crear una caja de tesorería en cada compañía para la implementación del pago por el servicio con el fin de registrar todas las entradas de dinero. Igualmente, se debía incrementar la vigilancia en la ciudad para controlar el fraude en las instalaciones, lo que se había hecho común y provocaba accidentes frecuentes y deterioro de las redes [21].

### 3.5 Legislación para la seguridad de las redes

Apenas con algunos años de operación de estas redes eléctricas, Manizales sufrió en 1925 y 1926 dos incendios que destruyeron el centro de la ciudad, por lo que la normativa se orientó a tratar de disminuir los riesgos y cumplir con las exigencias de las compañías aseguradoras, ya que se señalaban las instalaciones eléctricas -mal realizadas- como causales de las conflagraciones. Para la renovación de las pólizas de seguro con la empresa Liverpool & Globe London, la Empresa Municipal de Energía debió asumir además del incremento en las ratas de seguro, condiciones precisas para prevenir la destrucción por un nuevo incendio. En este sentido se solicitaba: realizar instalaciones eléctricas con materiales de buena calidad (Fig. 3) y bajo supervisión profesional; prohibir al interior de las viviendas y locales la utilización de aparatos de combustión a base de petróleo y gasolina; utilizar para las construcciones materiales incombustibles como el concreto; procurar la ampliación o ensanche de las calles; y eliminar los aleros de los edificios. Además, era necesario instalar un sistema contra incendios, para lo cual, se negociaron hidrantes con



**Acaba de llegar:**  
 Pantallas estilos ultramodernos para negocios.  
 Pantallas y lámparas muy bonitas para la casa.  
 Material para toda clase de instalaciones eléctricas.  
 Bombillos de 2 y media a 1000 bujías.

**Ferretería Electra**  
 TELEFONO 3-2-9 y 7-3-5.  
**VISITENOS! LE CONVIENE!**

Figura 3. Comercialización de productos para instalaciones eléctricas.  
 Fuente: Tomada del Periódico La Voz de Caldas, 12 de abril de 1931.

Portalámparas (socket) para prueba de bobillas	\$2,00/mes
Traslado de una lámpara de un local a otro	\$1,50
Traslado de una lámpara en el mismo edificio	\$1,00
Planchas y calentadores uso doméstico de hasta 550 watos	\$4,00/mes
Planchas y calentadores uso doméstico de más de 550 watos	\$4,00 + 0,50 amperio/mes
Planchas y calentadores industriales	\$1,00 amperio/mes
Motores de un caballo de fuerza	\$4,00/mes
Motores (pago los primeros días del mes)	\$3,50/caballo
Motores de 6:00 de la tarde a 12:00 de la noche	\$7,00/caballo
Motores de 6:00 de la tarde a 12:00 de la noche (pago primeros días el mes)	\$6,00/caballo

Fuente: Elaboración propia.

compañías como *Bopp & Reuther de Waldhoff de Alemania* por valor de US\$45 cada aparato [22].

Otra situación sobre la seguridad de las redes se dio en mayo de 1929 cuando se presentó una queja al comandante del Cuerpo Oficial de Bomberos relativa a las bajas condiciones de seguridad que presentaba la subestación de la Empresa Eléctrica de Manizales. Las características del edificio donde se encontraba instalada la subestación no eran adecuadas, ya que estaba construido con paredes de recallosa, piso de madera y vigas de madera expuestas. Los pararrayos se encontraban en el interior del edificio. Las líneas de alta tensión estaban instaladas sobre postes de madera y los brazos salientes no estaban suficientemente alejados de los tejados. Debido a los materiales usados y a la presencia de dispositivos dentro del edificio que presentaban riesgo de explosión, se solicitaba trasladar la subestación a un edificio construido con concreto u otro material incombustible, reemplazar los postes por estructuras metálicas y elevar sus brazos 50 centímetros por encima de los aleros; así mismo cambiar los alambres por calibre #6 B.S. (#6 Brown and Sharpe – B.S., o AWG) y ubicar los soportes entre 24 y 30 metros de distancia. Para fortalecer estas medidas de seguridad, se determinó desde este momento que la línea de mayor tensión siempre debía ir ubicada en la parte más alta y las secundarias mínimo un metro por debajo de estas [23], disposiciones que se conservan en las instalaciones actuales.

### 3.6 El valor de la energía

Desde el punto de vista tarifario, mediante el Acuerdo N°72 de 1927 se estableció un estándar inicial de cobro por parte de la Empresa Municipal de Energía, a partir del establecimiento del limitador de corriente para el alumbrado, que determinó varias categorías para la prestación del servicio (Tabla 2).

Tabla 2.  
 Tarifas de la Empresa Municipal de Energía, 1927.

Concepto	Valor dispositivo (COP)
Alumbrado watio nocturno	\$0,02
Alumbrado diurno y nocturno	\$0,02 + 25%
Alumbrado avisos luminosos y vitrinas watio nocturno	\$0,01
Alumbrado exterior (focos al frente del edificio) watio nocturno	\$0,01

Todas las cuentas por concepto de luz y calefacción tenían un descuento del 25% del valor total si se pagaban durante los diez primeros días del mes. Se prestaba el servicio de arrendamiento de lámparas, las cuales debían ser de mínimo 30 W y de al menos 60 W para negocios. El valor del traslado de las lámparas estaba calculado para la zona central de la ciudad y por fuera de este perímetro tendría un incremento de \$0,50 COP por cada lámpara. Este mismo recargo se estipulaba para el traslado a edificios construidos en concreto. La instalación de lámparas solo podría ser solicitada por los propietarios del edificio. El consumo mínimo liquidado para el servicio de motores sería de 1 H.P.

El servicio se suspendía si no se realizaba el pago en los primeros días del mes siguiente al cobro y no se admitía la ausencia de los habitantes como excusa para no realizar el pago por el servicio. La reconexión del servicio tenía un valor de \$0,50 COP [24]. Todo lo cual llevó a un incremento en la oferta de productos para realizar instalaciones seguras, eficientes y estéticas dentro de los edificios (Ver Fig. 4).

**La luz es barata**

si Vd. emplea siempre lámparas Osram - D.  
 Con lámparas Osram - D en todas partes, la corriente eléctrica le dará el máximo de luz.

**OSRAM**

Compre pues siempre **LAMPARAS OSRAM-D**

Figura 4. Aviso publicitario para incrementar la comercialización de lámparas.

Fuente: Tomada del periódico La Patria, 4 de agosto de 1940.



Tabla 3.

Tarifas de la Empresa Municipal de Energía, 1928.

Servicio	Tarifa (COP)	Cobro mínimo
Alumbrado particular	\$0,30 kWh	\$4,00 COP
Teatros (iluminación)	\$0,30 kWh	
Planchas y calentadores	\$0,15 kWh	\$2,00 COP/plancha
Motores 5:00 am - 5:00 pm		\$5,00 COP/H.P.*
Motores 12:00 m - 5:00 pm		50% más sobre la tarifa

\*: Durante los 10 primeros días del mes o \$6,00 COP/H.P. pasado este plazo.

Fuente: Elaboración propia

Otras disposiciones importantes se dieron en 1928 cuando se empezó a realizar el cobro de la energía por medio de contadores de energía instalados en los lugares de consumo, promoviendo el uso racional de esta. Una de las medidas más importantes fue restringir el uso de motores industriales entre las 5:00 de la tarde y las 12:00 de la noche para beneficiar el alumbrado. También se reglamentó el acceso a los contadores, los cuales, estarían sellados y únicamente podrían ser manejados por los técnicos de la empresa, ocasionando la rotura de los sellos una penalización con la suspensión del servicio. Todos los usuarios debían pagar por los materiales y la instalación de los contadores y el suministro se cobraría a \$0,15 COP/kWh. Igualmente, las industrias que tuvieran un consumo superior a 7 H.P. debían asumir el costo del transformador, así como el valor de los materiales y su instalación [25]. Las tarifas se diferenciarían tal como se muestra en la Tabla 3.

### 3.7 La ampliación de la Empresa Municipal de Energía

Con el fin de realizar la construcción del tranvía municipal, en enero de 1928 se dictaron las disposiciones para la ampliación o para la época, el *ensanche* de la Empresa Municipal de Energía bajo la dirección de los ingenieros electricistas de la secretaría de obras públicas, para lo cual, se creó el cargo de interventor del municipio a cargo de: verificar el desarrollo de las obras, licitaciones, contratos, compra y calidad de materiales y maquinarias, así como el transporte y negociaciones relacionadas con la colocación de postes y alambrados; vigilar la calidad de las obras; inspeccionar los trabajos y proponer soluciones técnicas [26]. La importación de los materiales para el ensanche de la planta eléctrica se haría por medio de licitación, asegurando que el proveedor cumpliera con las especificaciones de calidad requeridas. El municipio solamente asumiría los costos de los materiales importados, ya que tanto los materiales nacionales como el costo de la mano de obra debía ser asumido por el contratista.

De esta manera, se aprobó el ensanche de la planta eléctrica para aumentar la capacidad existente de 700 kW a 10.000 kW, lo cual permitiría poner en funcionamiento el tranvía (1.200 kW); abaratar las tarifas de iluminación y fuerza; generar un excedente que permitiría cubrir la demanda futura; y atender las necesidades de algunos de los municipios cercanos. La propuesta buscaba implementar un sistema progresivo, en el cual, se irían montando unidades de 2.000 kW hasta completar los 10.000 kW [27].

La firma de Medellín Tulio Ospina & Co. fue la encargada de realizar los estudios para la ampliación de la planta eléctrica. Para esta época, Medellín había ganado protagonismo en el sector eléctrico debido a que había implementado un modelo de propiedad y dirección de las empresas de energía del Estado a través del poder municipal [8]. El contratista hizo entrega el 4 de junio de 1928 de un plano general de la obra, un plano de la acequia, un plano de la bocatoma, un plano de la tubería, tanques y edificios y las siguientes recomendaciones: sobre la bocatoma y el *desarenadero* decidieron no realizar modificaciones porque ya estaba adelantada su construcción, así que se acogieron a las especificaciones que presentaba [28].

La acequia fue calculada para una capacidad de 2.200 litros/segundo con una pendiente promedio de 1/1.000. La tubería debía recorrer 170 metros de longitud y una caída de 78 metros para lo cual se proponía un diámetro de 35" y 1/4" de espesor. La instalación completa estaría conformada por dos unidades generadores de 850 H.P cada una compuestas por la siguiente maquinaria:

- 2 turbinas tipo Pelton de 850 H.P. cada una para trabajar a 260 rpm, completas con sus cubiertas, válvulas, boquillas, reguladores automáticos de aceite a presión, chumaceras de lubricación automática y acoplamiento adecuado para los generadores.
- 2 generadores trifásicos de corriente alterna de 710 KVA cada uno para trabajar a 260 rpm y 4kV a 60 Hz, con sus respectivos excitadores.
- 2 tableros de distribución completos con sus aparatos de medida, voltímetros, amperímetros, interruptor automático con tanque de aceite y clavijas de conexión.

Todos estos aparatos lo mismo que sus mecanismos de operación deberán venir montados en placas de pizarra con aislamiento para 4kV, con transformador de corriente y potencial para medición. El peso aproximado de todo el equipo fue de 63.000 libras.

- 4 equipos de pararrayos de película de óxido especial para 5kV, equipos estos de alta protección, completos con sus bobinas de reacción y soportes de pararrayos. El peso de estos cuatro equipos es de 1.300 libras.

Las líneas de transmisión de estas nuevas plantas debían ir soportadas por postes metálicos clavados en el suelo y provistos de una cruceta metálica de 2 metros de ancho ubicada a una altura de 8 metros sobre el piso. La cruceta debía tener seis aisladores para 10kV situados a una distancia de 38 centímetros entre ellos. El circuito de tres cables estaría conformado en toda su extensión por alambres de aluminio #00 B.S. (2/0 Brown and Sharpe – B.S., o AWG), mientras el otro circuito estaría conformado en su parte inicial de 800 metros de cable de cobre #4 B.S. y de este punto en adelante por cables de aluminio #00 B.S. La única reforma que se exigía para la línea de transmisión de energía generada por las dos unidades de 710 kVA era reemplazar los 800 metros de alambre de cobre #4 B.S. por alambre de aluminio #00 B.S. y de esta manera cada uno de los circuitos serviría para transportar la energía de cada uno de los generadores. En caso de daño de uno de los generadores de 710 kVA la línea se utilizaría para transportar la energía producida por los dos generadores existentes de 350 kVA. El valor de todos estos equipos y su montaje era de \$99.319 COP y el valor del kVA

equivalía a \$69,94 COP [28]. En julio de 1929 se firmó otro contrato con Gregorio Mejía Ruiz para realizar los estudios definitivos a partir del proyecto de Tulio Ospina, elevando el presupuesto a \$144.870 COP [29].

La licitación para la compra de los materiales se abrió el 2 de septiembre de 1929 y se recibieron propuestas hasta el 12 de diciembre de 1929. Los dos generadores de corriente alterna solicitados debían ser fabricados por la casa *General Electric Co. o Westinghouse Electric Co.* Los transformadores debían ser de refrigeración por aceite y sistema de radiadores, cada uno con capacidad de 1.000 KVA, el voltaje primario de 4kV y el secundario de 15kV, la tensión nominal del sistema. Los motores hidráulicos que se solicitaban debían ser del sistema Pelton [30].

Durante la década de 1930 se continuaron desarrollando mejoras y ampliaciones a la planta generadora como el contrato con Helmer Hallberg, súbdito sueco y gerente de la Compañía Sudamericana *SKF*, que ganó la licitación por un valor de 6.400 libras esterlinas para la compra de un equipo hidroeléctrico [31]; el contrato con SKF para el suministro de la nueva unidad eléctrica para la planta municipal [32] y la renovación del contrato con Eolo A. Faulin, súbdito italiano, para la prestación de servicios profesionales [33], entre otras negociaciones. Finalmente, en 1939 el municipio adquirió la *Empresa Eléctrica de Sancancio* y arrendó la planta hidroeléctrica de Guacaica al ferrocarril de Caldas, adquiriendo el monopolio para la generación y distribución de energía eléctrica en la ciudad, lo que devino en el surgimiento de la *Central Hidroeléctrica de Caldas* - CHEC en 1943 [34].

#### 4. Conclusiones

La llegada de la electricidad permitió ampliar la vida urbana hacia diversos horarios y actividades que fomentaron la aparición de oficios, servicios, industrias e infraestructuras que implicaron una culturización de los ciudadanos en dos sentidos. De una parte, pudieron disfrutar de la luz en horas nocturnas y con ello, tener acceso a innovadores artefactos que llegaban desde el extranjero para brindar bienestar y comodidad en las actividades cotidianas; y de otra, debieron adaptarse al cumplimiento de normativas que regulaban la prestación y el pago por el servicio, así como a la modificación del paisaje urbano con la instalación de todo tipo de artefactos que permitían el funcionamiento de las redes de energía eléctrica en la ciudad.

La necesidad de avanzar en la legislación, normatividad y en los aspectos tarifarios del consumo de energía eléctrica en la ciudad dio inicio a una serie de cambio constante en las regulaciones que permitieron afrontar problemáticas puntuales inherentes a la instalación o prestación del servicio, pero que no respondían a disposiciones regladas por estamentos especializados para formular un marco de actuación eficiente y seguro como el propuesto hasta los inicios del siglo XXI con el RETIE [35] que surge tardíamente como una medida para reglamentar las instalaciones, incluir normas de seguridad al sistema, garantizar un servicio adecuado y promover la disminución de accidentes de origen eléctrico.

Las altas especificaciones de los materiales importados, la estandarización de los procesos, el diseño de las redes

dirigido por expertos y la capacitación de técnicos locales para el mantenimiento y operación del sistema, fueron elementos que desde la llegada de la energía eléctrica a la ciudad marcaron el camino para avanzar hacia una industria de vanguardia que desde mediados del siglo XX consiguió suministrar energía a cinco municipios del departamento de Caldas y convirtió a Manizales en escenario del Congreso Nacional de Electrificación en 1955 [36].

Finalmente, el desarrollo de la generación, transporte y distribución de energía eléctrica en Manizales y en Colombia siguió un proceso similar al de muchas otras áreas tecnológicas. Desde la adopción inicial de técnicas y estrategias extranjeras por la ausencia de conocimiento local, a la generación progresiva de conocimiento y adaptación a las condiciones y experiencias locales representadas fundamentalmente en la creación de normas y reglamentos técnicos que fueron perfeccionándose hasta la actualidad.

#### Agradecimientos

Los Autores agradecen a la Universidad Nacional de Colombia – Sede Medellín y a la Universidad Nacional de Colombia – Sede Manizales por el apoyo para la realización de este trabajo.

#### Referencias

- [1] Salazar-Marulanda, C., La ciudad iluminada: tecnificación como ideal de progreso en Manizales, 1905-1949. Medellín: Universidad Nacional de Colombia, 2023.
- [2] Arango-Cardinal, S., Ciudad y arquitectura: seis generaciones que construyeron la América Latina moderna. Fondo de Cultura Económica, Bogotá, 2014.
- [3] Capel, H., y Casals, V., Capitalismo e historia de la electrificación, 1890-1930: capital, técnica y organización del negocio eléctrico en España y México. Ediciones del Serbal, Barcelona, 2013.
- [4] Herazo-Berdugo, E., Electrificando a Colombia, una historia social y cultural de la tecnología 1800-1950. Universidad de Los Andes, tesis Doctorado Historia, Bogotá 2019. DOI: <https://doi.org/10.57784/1992/41229>
- [5] Cuervo-González, L.M., De la vela al apagón. 100 años de servicio eléctrico en Colombia. CINEP, Santa Fe de Bogotá, 1992.
- [6] Simbaqueva, E., Una Aproximación a la lógica espacial del surgimiento y desarrollo del sector eléctrico en Colombia. 1889-1945, tesis Maestría Economía Universidad de los Andes, Bogotá, 1988.
- [7] Poveda-Ramos, G., La electrificación en Colombia. Universidad de Medellín, Medellín, 1993.
- [8] De-la-Pedraja, T.R., Historia de la Energía en Colombia 1537-1930. el Áncora Editores, Bogotá, 1985.
- [9] Sanclemente, C., Desarrollo y crisis del sector eléctrico Colombiano 1890-1993. Empresa Editorial Universidad Nacional, Santa Fé de Bogotá, 1993.
- [10] Londoño, L., Manizales. Hoyos Editores, Manizales, 2017.
- [11] Gutiérrez, E., Banco de Caldas, Corporación Financiera de Caldas y Fondo Cultural Cafetero, Eds., Manizales de ayer: álbum de fotografías. Fondo Cultural Cafetero, Bogotá, 1987.
- [12] Archivo Histórico de Manizales, 18 de diciembre de 1907, caja 61, Libro 221, Folios 372-377.
- [13] Archivo Histórico de Manizales, 19 de noviembre de 1915, caja 94, libro 356, folios 4-5.
- [14] Archivo Histórico de Manizales, Acuerdo No17 de 22 de febrero de 1916, caja 94, libro 356, folios 95-96.
- [15] Archivo Histórico de Manizales, Acuerdo No12, 11 de noviembre de 1915, caja 94, libro 356, folios 85-87.
- [16] Archivo Histórico de Manizales, Acuerdo No21, 9 de marzo de 1916, caja 94, libro 356, folios 109-119.

- [17] Archivo Histórico de Manizales, 11 de agosto de 1925, caja 129, libro 507, folio 347.
- [18] Gaviria-Toro, J. Monografías de Manizales. Manizales: Blanco y Negro, 1924.
- [19] Archivo Histórico de Manizales, 30 de octubre de 1925, caja 130, libro 515, folios 357-358.
- [20] Arboleda-González, C. “Los servicios públicos. Redes que hablan”. En Manizales 150 años. Manizales: Editorial La Patria, 1999.
- [21] Archivo Histórico de Manizales, 23 de junio de 1925, caja 130, libro 515, folios 162-164.
- [22] Archivo Histórico de Manizales, 7 de diciembre de 1925, caja 129, libro 507.
- [23] Archivo Histórico de Manizales, 28 de mayo de 1929, caja 151, libro 628, folio 267.
- [24] Archivo Histórico de Manizales, 7 de junio de 1927, caja 146, libro 598, folios 85-86.
- [25] Archivo Histórico de Manizales, 5 de septiembre de 1928, caja 144, libro 593, folio 340.
- [26] Archivo Histórico de Manizales, 3 de enero de 1928, caja 144, libro 593, folios 33-34.
- [27] Archivo Histórico de Manizales, 10 de noviembre de 1927, caja 129, libro 507.
- [28] Archivo Histórico de Manizales, 4 de junio de 1928, caja 151, libro 628, folios 217-224.
- [29] Archivo Histórico de Manizales, 4 de junio de 1928, caja 151, libro 628, folios 264-265.
- [30] Archivo Histórico de Manizales, 6 de agosto de 1929, caja 151, libro 628, folios 242-244.
- [31] Histórico de Manizales, 8 de octubre de 1934, caja 183, libro 792, folios 214-221.
- [32] Archivo Histórico de Manizales, 22 de octubre de 1935, caja 188, libro 814, folios 225-231.
- [33] Archivo Histórico de Manizales, 16 de agosto de 1937, caja 198, libro 870, folio 160.
- [34] Archivo Histórico de Manizales, 16 de septiembre de 1943, caja 250, libro 1022, folios 245-256.
- [35] C.M., de M. y Energía, Reglamento técnico de instalaciones eléctricas - RETIE: Ministerio de Minas y Energía, Bogotá, 2004.
- [36] Hurtado-Hidalgo, J., Cronología del sector eléctrico colombiano. En Revista Santander, 9, pp. 56–77, 2014.

**C. Salazar-Marulanda**, Arquitecta de la Universidad Nacional de Colombia, Sede Manizales. MSc. en Historia de la Arquitectura de la Universidad Nacional de Colombia, Sede Bogotá y PhD en Historia de la Universidad Nacional de Colombia, Sede Medellín. Profesora Asociada Escuela de Arquitectura de la Universidad Nacional de Colombia, Sede Medellín. Sus intereses de investigación están relacionados con la historia urbana y la historia de la técnica.  
ORCID: 0000-0003-4088-8780.

**J.G. Herrera-Murcia**, Ingeniero Electricista de la Universidad Nacional de Colombia. MSc. y Dr. de la misma universidad. Profesor Asociado en la Universidad Nacional de Colombia – Sede Medellín. Sus intereses de investigación están relacionados con el diseño y la simulación de sistemas de energía eléctrica.  
ORCID: 0000-0001-5993-296X

**C. Younes-Velosa**, Ingeniero Electricista, Abogado, MSc. en Ingeniería Eléctrica con énfasis en Ingeniería de Alto Voltaje, MSc. en Regulación Energética y PhD en el área de Ingeniería eléctrica. Más de 20 años de experiencia en docencia e investigación en compatibilidad electromagnética, protección contra rayos y Política Energética.  
ORCID: 0000-0002-9685-8196

# Entregando lo mejor de los **colombianos**



Línea de atención al Cliente Nacional: 01 8000 111 210

Línea de atención al Cliente Bogotá: (57-1) 472 2000

» [www.4-72.com.co](http://www.4-72.com.co)

## DYNA

DYNA 92 (238), July - September, 2025  
is an edition consisting of 100 printed issues  
which was finished printing in the month of September of 2025  
in Todograficas Ltda. Medellín - Colombia

The cover was printed on Propalcote C1S 250 g,  
the interior pages on Propal Beige 90 g.  
The fonts used are Times New Roman, Imprint MT Shadow



## Loquax

- Research on airport reservation bus scheduling.
- Enhancing urban E-commerce efficiency: a fleet composition benchmark.
- Integration of AI, RPA and Big Data in strategic accounting management and consulting: perspectives and challenges.
- Implementation of Google App script for automatic generation of pre-registration form.
- A framework for environmental performance evaluation in resource-constrained air navigation services: a Cuban case study.
- Classification of pothole distress severity in asphalt pavements using YOLOv8.
- Agent-Based models for integrated water resource management: quantifying land use changes by integrating economic and social incentives. Case study: Vista Hermosa (Meta).
- The adoption of cutting software in small furniture manufacturers: a survey in Brazil.
- Cost analysis of climate change and prevention measures in the Chancay-Lambayeque Valley, Perú.
- Analysis of the infrastructure works on accessibility using graph theory: case study “la Línea” tunnel.
- Microstructure influence on crack propagation behavior of nodular cast iron.
- Structural performance of composite beams using advanced modeling for nonlinear analysis.
- Flexible electrode for spinal cord electrostimulation.
- Technological characterization of the generation and distribution of electric power in Colombia at the beginning of the 20th century: case Manizales.
- Investigación sobre la programación de autobuses de reserva en aeropuertos.
- Mejorando la eficiencia del comercio electrónico urbano: una referencia para la composición de flotas.
- Integración de IA, RPA y Big Data en la gestión y consultoría estratégica contable: perspectivas y desafíos.
- Implementación de Google app script para la generación automática de la ficha de pre-matricula.
- Evaluación del desempeño ambiental en navegación aérea con recursos limitados: estudio de caso en Cuba.
- Clasificación de la severidad del deterioro tipo bache en pavimentos asfálticos utilizando YOLOv8.
- Modelo basado en agentes para la gestión integral del recurso hídrico: cuantificación de los cambios en el uso del suelo mediante la integración de incentivos económicos y sociales. Estudio de caso: Vista Hermosa (Meta).
- Adopción de software de corte en pequeños fabricantes de muebles: una encuesta en Brasil.
- Análisis de costos de cambio climático y medidas de prevención en el valle de Chancay-Lambayeque, Perú.
- Análisis del impacto de obras de infraestructura sobre accesibilidad mediante teoría de grafos: estudio de caso túnel de la Línea.
- Influencia de la microestructura en el comportamiento de propagación de grietas en fundición nodular.
- Rendimiento estructural de vigas compuestas mediante modelado avanzado para análisis no lineal.
- Electrodo flexible para electroestimulación medular.
- Caracterización tecnológica de la generación y distribución de energía eléctrica en Colombia en los inicios del siglo XX: caso Manizales.